

General Disclaimer

One or more of the Following Statements may affect this Document

- This document has been reproduced from the best copy furnished by the organizational source. It is being released in the interest of making available as much information as possible.
- This document may contain data, which exceeds the sheet parameters. It was furnished in this condition by the organizational source and is the best copy available.
- This document may contain tone-on-tone or color graphs, charts and/or pictures, which have been reproduced in black and white.
- This document is paginated as submitted by the original source.
- Portions of this document are not fully legible due to the historical nature of some of the material. However, it is the best reproduction available from the original submission.

Massachusetts Institute of Technology
Research Laboratory of Electronics
Cambridge, Massachusetts 02139

(NASA-CR-146315) THEORY OF PASSIVE REMOTE
SENSING WITH MICROWAVES Final Report
(Massachusetts Inst. of Tech.) 301 p HC
\$9.75 CSCL 14E

N76-18629

Unclas
G3/43 18427

Final Report

on

California Institute of Technology
Jet Propulsion Laboratory
Contract No. 953524

Submitted by: J. A. Kong
Principal Investigator

July 15, 1975

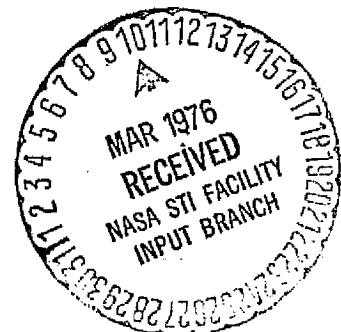


Table of Contents

	page
Theory of Passive Remote Sensing with Microwaves	1
Appendix I. Studies of the Model for Microwave Remote Sensing of Ice and Snow	27
Appendix II. Machine Inversion of Remote Sensing Data	63
Appendix III. Passive Microwave Remote Sensing of Moisture in Sandlike Soils	92
Appendix IV. The Brightness Temperature of a Half-Space Random Medium with Nonuniform Temperature Profile	182
Appendix V. Microwave Remote Sensing of a Two-Layer Random Medium	218
Appendix VI. Microwave Thermal Emission from a Stratified Medium with Nonuniform Temperature Distribution	264

Theory of Passive Remote Sensing with Microwaves

Contents

1. Introduction
2. Accomplished work of the past and proposed work for the future
3. Stratified media with uniform temperature distribution
4. Half-space random media with nonuniform temperature distribution
5. Two layer random media with uniform temperature distribution
6. Stratified media with nonuniform temperature distribution
7. References

The following publications in the reference section are performed under the JPL/Caltech Contract 953524:

Papers: 52, 56-58, 68
Theses: 53-54, 69-70
Reports: 60-67

I. Introduction

In remote sensing of the Earth with microwaves, we are interested in surface and subsurface geophysical features rather than atmospheric effects. Researches are being performed on ocean surfaces¹⁻³⁵ as well as in land areas.³⁶⁻⁴⁵ The articles by Staelin⁴⁶ and Tomiyasu⁴⁷ provide a comprehensive review on atmospheric and surface observations, passive and active sensing, and their implications and applications.

Our interest is directed toward land areas; especially snow and ice covered land or water, and deserts. The objective is to develop theoretical models that are practical and useful in data interpretation.

We now briefly review the relevant theories that are of direct interest to us. Gurvich, Kalinin, and Matveyev⁴⁸ derived expressions for the brightness temperature of a half-space random medium with laminar structure and used to interpret Kosmos 243 data for Antarctic areas. Assuming a half-space containing random distributed scatterers embedded in a low loss dielectric, England⁴⁹ examined emission darkening caused by scatterers with a radiative transfer approach. Stogryn examined the brightness temperature of a vertically structured medium with no scattering.⁵⁰ He also studied scattering by random dielectric constant fluctuations in the low frequency limit using a perturbation approach.⁵¹

II. Accomplishments of the Past and Proposed Work for the Future

The dominant factors that determined remote sensing measurements are absorption, layering, anisotropy, submerged scattering centers, nonuniform temperature distributions, and surface roughness. Assuming uniform temperature distribution, the first three factors are accounted for in the composite model,⁵² which also extends the half-space model of Gurvich et al to treat layered media. The composite model was used to match⁵³⁻⁵⁴ (Appendices 1, 2) spacecraft data with ground truth measurements.⁵⁵ Satellite data were also studied with a stratified model.⁷⁰ (Appendix 3) Gurvich et al assumed uniform temperature distributions. We solve the problem of microwave thermal emission from a half-space random medium with nonuniform temperature distributions.⁵⁶ (Appendix 4) The observed data for slab medium exhibit coherent effects. We developed modified radiative transfer equations and solved for the reflectivities of a two layer random medium.⁵⁷ (Appendix 5) The results are applicable to active sensing as well as passive sensing. For a stratified medium with a nonuniform distribution, we use the fluctuation-dissipation theorem and solved for the brightness temperature.⁵⁸ (Appendix 6) All these results are easily used. They are summarized in the subsequent sections.

The task is, however, by no means completed. We have concentrated on structures that are laminar. Three dimensional scattering needs to be considered. Surface roughness has so far been neglected.

Its effect should be included. Our final goal is a composite model which accounts for all the determining factors. We would like to be able to identify the effect of each individual factor on the observed data. The theoretical models should be used to interpret all available data. Only through data match can a useful and practical theory be developed.

III. Stratified Media with Uniform Temperature Distribution

The emissivity e is related to the reflectivity r by

$$e = 1 - r. \quad (1)$$

The reflectivity is equal to the square of the reflection coefficient R ,

$$r = 1 - R^2. \quad (2)$$

For the stratified medium as shown in Figure 1, R is calculated in the form of continuous fractions⁵⁹

$$\begin{aligned}
 R = & \frac{1}{R_{01}} + \cfrac{\left[1 - \frac{1}{R_{01}^2}\right] e^{-i2k_1 x d_1}}{\frac{1}{R_{01}} e^{-i2k_1 x d_1}} + \frac{1}{R_{12}} \\
 & + \cfrac{\left[1 - \frac{1}{R_{12}^2}\right] e^{-i2k_2 x (d_2 - d_1)}}{\frac{1}{R_{12}} e^{-i2k_2 x (d_2 - d_1)}} + \dots \\
 & + \frac{1}{R_{(n-1)n}} + \cfrac{\left[1 - \frac{1}{R_{(n-1)n}^2}\right] e^{-i2k_{nx} (d_n - d_{n-1})}}{\frac{1}{R_{(n-1)n}} e^{-i2k_{nx} (d_n - d_{n-1})}} + R_{nt} \quad (3)
 \end{aligned}$$

REPRODUCIBILITY OF THE
ORIGINAL PAGE IS POOR

where for horizontal polarization

$$R_{\ell(\ell+1)} = \frac{1 - \epsilon_{\ell} k_{(\ell+1)} x^{\epsilon_{(\ell+1)}} k_{\ell x}}{1 + \epsilon_{\ell} k_{(\ell+1)} x^{\epsilon_{(\ell+1)}} k_{\ell x}} \quad (4)$$

and for vertical polarization

$$R_{\ell(\ell+1)} = \frac{1 - \mu_{\ell} k_{(\ell+1)} x^{\mu_{(\ell+1)}} k_{\ell x}}{1 + \mu_{\ell} k_{(\ell+1)} x^{\mu_{(\ell+1)}} k_{\ell x}} \quad (5)$$

The above result is exact. Absorption is taken into account by the imaginary parts of μ and ϵ .

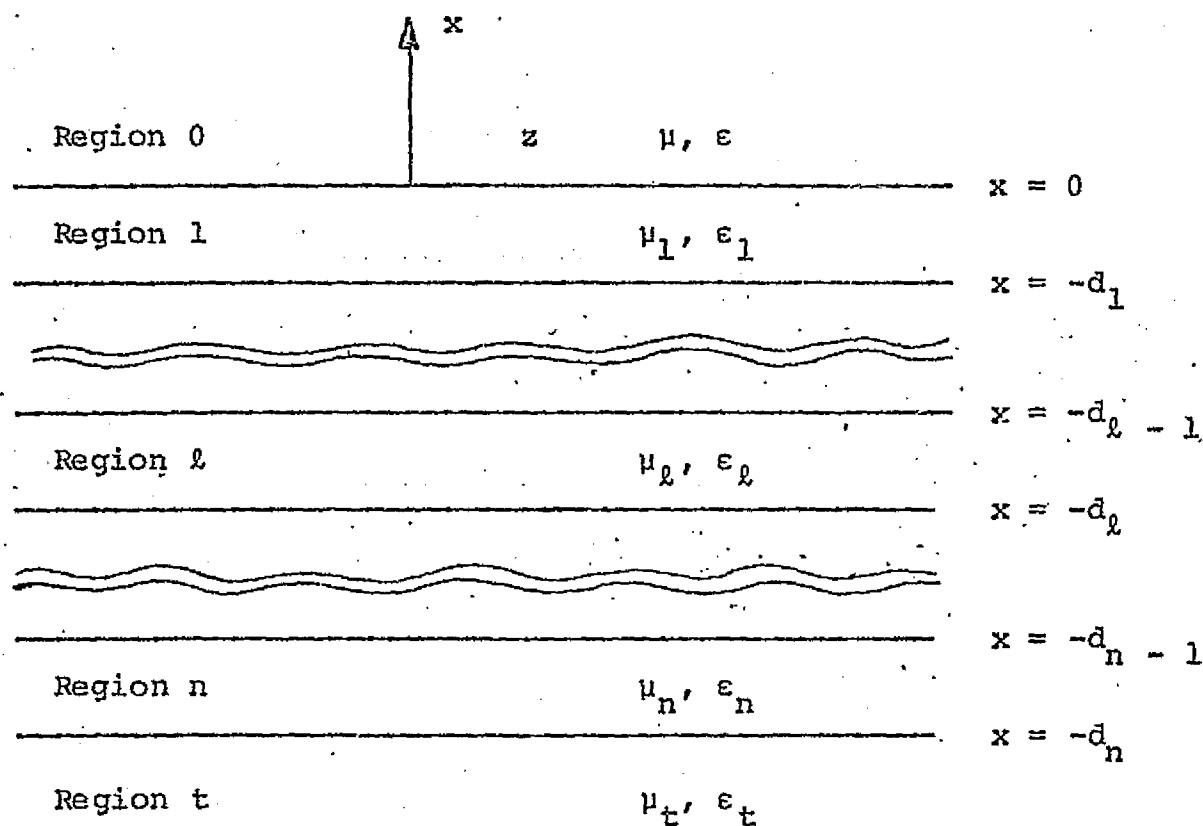


Figure 1. Stratified medium with uniform temperature distribution.

IV. Half-Space Random Media with Nonuniform Temperature Distribution

For a half-space medium with constant absorption and scattering coefficients, the brightness temperature is determined by the following simple closed-form formula⁵⁶

$$T_B = \frac{2\kappa_a(1 - r_{ot})}{(\alpha + \kappa_a) - r_{ot}(\alpha - \kappa_a)} \left\{ T_O + \frac{\alpha}{\alpha + \gamma \cos \theta} T_h \right\}, \quad (6)$$

where we assume that the temperature distribution has the profile

$$T(z) = T_O + T_h e^{\gamma z}. \quad (7)$$

In (6) r_{ot} is the reflectivity of the medium, θ the observation angle, κ_a the absorption coefficient, and

$$\alpha = (\kappa_a + \kappa_s) \sqrt{(1 - \tilde{\omega}) \left[1 - \frac{\tilde{\omega}^2}{2} p_f + \frac{\tilde{\omega}^2}{2} p_b \right]}. \quad (8)$$

In (8) κ_s is the scattering coefficient, p_f the forward-scattering function, p_b the backward-scattering function, and the scattering albedo is

$$\tilde{\omega} = \frac{\kappa_s}{\kappa_a + \kappa_s}. \quad (9)$$

For a medium with no scattering, $\kappa_s = \tilde{\omega} = 0$. Thus

$$T_B = (1 - r_{ot}) \left(T_o + \frac{\kappa_a T_h}{\kappa_a + \gamma \cos \theta} \right). \quad (10)$$

For a medium with scattering and uniform temperature distribution, $T_h = 0$. Thus,

$$T_B = \frac{2\kappa_a (1 - r_{ot})}{(\alpha + \kappa_a) - r_{ot}(\alpha - \kappa_a)} T_o. \quad (11)$$

For uniform temperature distribution and small scattering albedo, we expand (11) to first order in $\tilde{\omega}$ and obtain

$$T_B = (1 - r_{ot}) \left(1 - \frac{(1 - r_{ot}) k_m^2 \Delta \ell}{8k_m'' \cos \theta (1 + 4k_m^2 \ell^2 \cos^2 \theta)} \right) T_o. \quad (12)$$

Numerical results are given in Fig. 2 to compare brightness temperature for TE and TM waves as a function of radiometer viewing angle θ_o , with temperature profile $T(z) = 222 + 34 \exp[0.81z]$. Clearly, scattering lowers the brightness temperature at all viewing angles.

Figure 2.

Frequency = 20 GHz

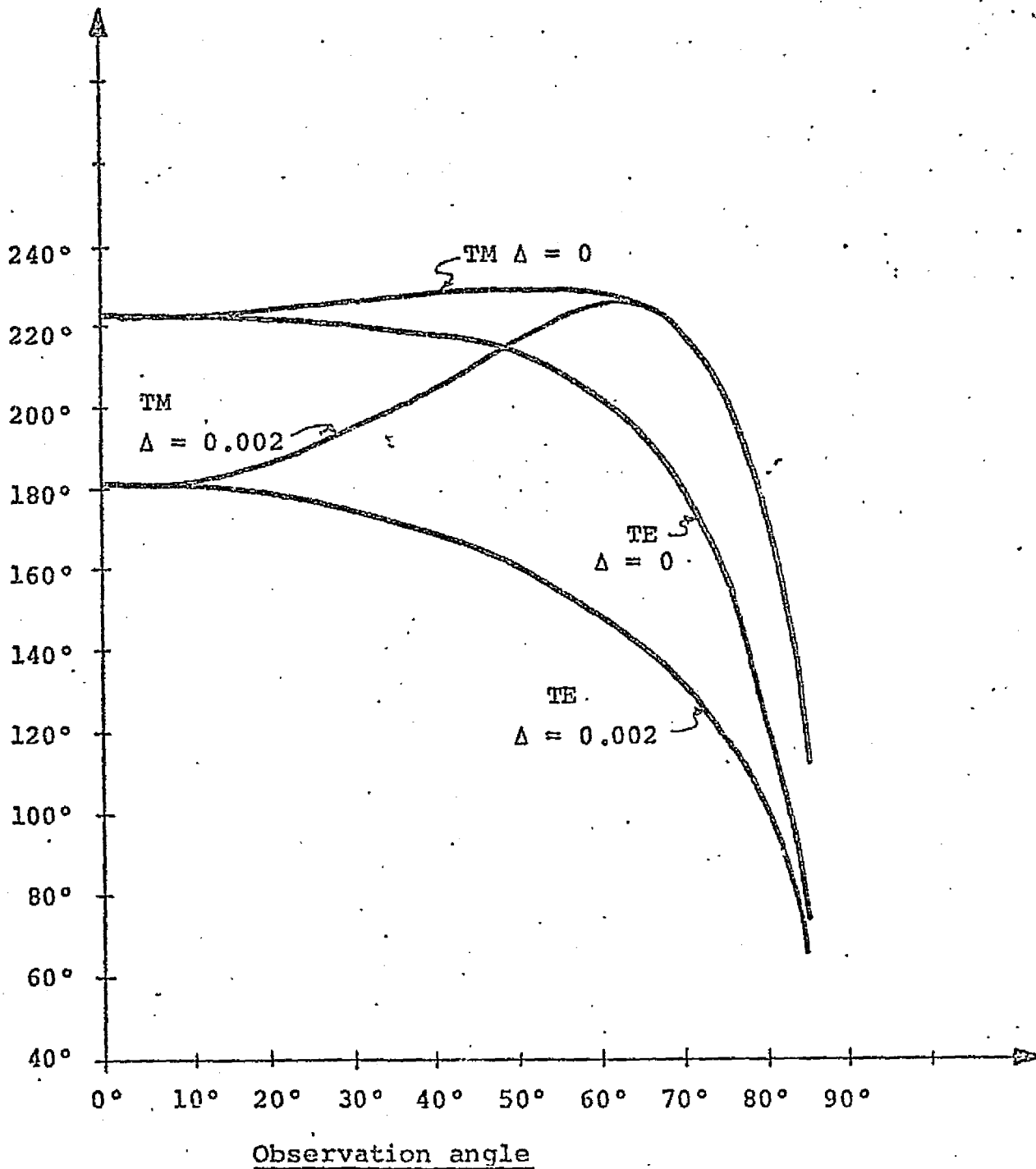
$$\epsilon_m' = 1.8$$

$$\epsilon_m'' = 0.00054$$

$$\lambda = 2 \text{ mm.}$$

Brightness Temperature

$$T = T_1(z)$$



V. Two Layer Random Media with Uniform Temperature Distribution

Consider a slab of random medium of thickness d . A plane wave is normally incident upon the slab. The reflectivity r is solved from the modified radiative transfer (MRT) equations, which include coherent effects due to the two boundaries.⁵⁷

$$r = \frac{|R_{01} + R_{12} e^{i(\eta_1 + \eta_2)d}|^2}{|D|^2} + \frac{t_{01}^2}{|D|^2}$$

$$\left. \begin{aligned} &1 - f_2 r_{12} (f_2 - r_{12} e^{-(\kappa_1 + \kappa_2)d}) - (f_2 - r_{12})(1 - f_2 r_{12} e^{-(\kappa_1 + \kappa_2)d}) e^{-2\alpha d} \\ &(1 - f_2 r_{01})(1 - f_2 r_{12}) - (f_2 - r_{01})(f_2 - r_{01}) e^{-2\alpha d} \end{aligned} \right\}$$

where

$$t_{01} = 1 - r_{01}$$

$$\eta_1 - \eta_2 = i \frac{\kappa_s}{2}$$

REPRODUCIBILITY OF THE
ORIGINAL PAGE IS POOR

$$\eta_1 + \eta_2 = 2k_{1m} + \frac{i \delta \ell k_{1m}^2}{2(1 - R_{01} R_{12} e^{i(\eta_1 + \eta_2)d})}$$

$$\left\{ \frac{3 - i4k_{1m}\ell}{1 - i2k_{1m}\ell} + R_{01} R_{12} \left(\frac{3 + i4k_{1m}\ell}{1 + i2k_{1m}\ell} \right) e^{i(\eta_1 + \eta_2)d} \right\}$$

$$f_2 = \frac{2(\kappa_e - \alpha) - K_s p_f}{K_s p_b}$$

$$\alpha = \kappa_e (1 - \omega)^{1/2} \left(1 - \frac{\omega}{2} p_f + \frac{\omega}{2} p_b \right)^{1/2}$$

$$p_f = \frac{1 + 4k_{1m}^2 \ell^2}{1 + 2k_{1m}^2 \ell^2}$$

$$K_s = \frac{D_1}{|D|^2} \frac{\kappa_s (1 + 2k_{1m}^2 \ell^2)}{1 + 4k_{1m}^2 \ell^2}$$

$$\kappa_e = \kappa_a + K_s$$

$$\kappa_1 = 2\eta_1'' = \kappa_a + \frac{\kappa_s}{2} + \frac{\kappa_s}{2} \frac{D_1}{|D|^2} \frac{(3 + 8k_{1m}^2 \ell^2)}{(1 + 4k_{1m}^2 \ell^2)}$$

$$p_b = \frac{1}{1 + 2k_{1m}^2 \ell^2}$$

$$\kappa_2 = 2\eta_2'' = \kappa_a - \frac{\kappa_s}{2} + \frac{\kappa_s}{2} \frac{D_1}{|D|^2} \frac{(3 + 8k_{1m}^2 \ell^2)}{(1 + 4k_{1m}^2 \ell^2)}$$

$$D = 1 + R_{01} R_{12} e^{i(\eta_1 + \eta_2)d}$$

$$D_1 = 1 - r_{01} r_{12} e^{-(\kappa_1 + \kappa_2)d}$$

For a half-space random medium, we let $d \rightarrow \infty$,

$$r = r_{01} + \frac{t_{01}^2 f_2}{1 - r_{01} f_2}$$

which is identical to previous results. When the second layer is a perfect conductor, $R_{12} = -1$, $r_{12} = 1$ and we have

$$r = \left| \frac{R_{01}^2 - e^{i(\eta_1 + \eta_2)d}}{1 - R_{01} e^{i(\eta_1 + \eta_2)d}} \right|^2 + \frac{t_{01}^2 \{f_2 - e^{-(\kappa_1 + \kappa_2)d} + (1 - f_2 e^{-(\kappa_1 + \kappa_2)d}) e^{-2\alpha d}\}}{\{1 - f_2 r_{01} + (f_2 - r_{01}) e^{-2\alpha d}\} |1 - R_{01} e^{i(\eta_1 + \eta_2)d}|^2}$$

It is interesting to note that as $\tilde{\omega} \rightarrow 1$, we have $\alpha \rightarrow 0$, $f_2 \rightarrow 1$. Thus $r \rightarrow 1$ and all the incident power is reflected. In Fig. 3 we illustrate the emissivity for a slab random medium. We see that

Figure 3.

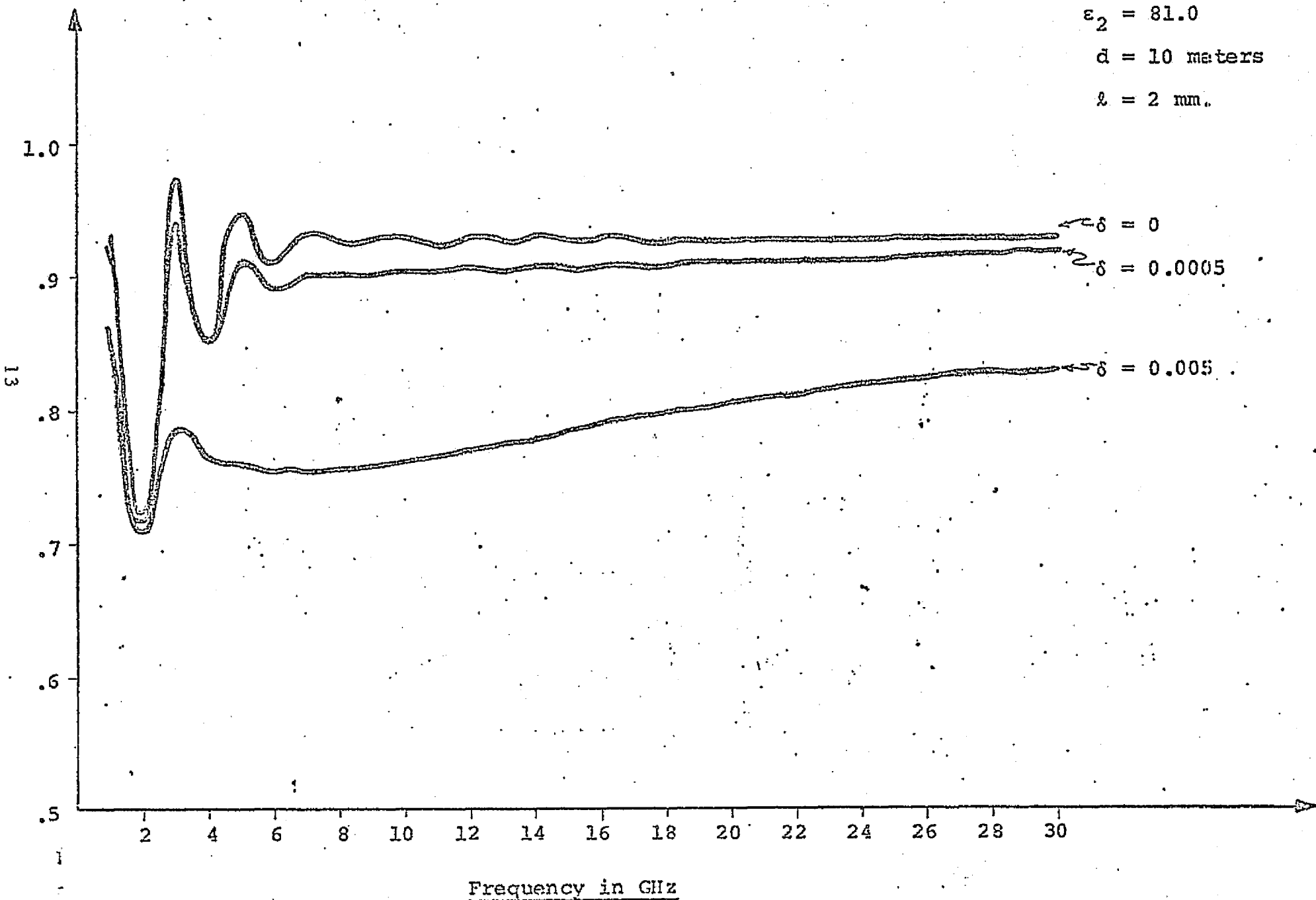
$$\epsilon_{1m} = 3.0(1 + i.001)$$

$$\epsilon_2 = 81.0$$

$$d = 10 \text{ meters}$$

$$l = 2 \text{ mm.}$$

Emissivity



scattering dampens the interference pattern and decreases emissivity in general. The existence of the interference patterns depends on the location of the subsurface and the extinction loss of the random medium.

The brightness temperature of a stratified medium with nonuniform temperature distribution is calculated in the following form⁵⁸

VI. Stratified Media with Nonuniform Temperature Distribution

The brightness temperature of a stratified medium with nonuniform temperature distribution is calculated in the following form⁵⁸

$$T_B(\vec{k}, \omega) = k^3 \cos \theta \sum_{\ell=1}^t \frac{\epsilon_{\ell}''}{\epsilon_0} \int_{-d_{\ell}}^{-d_{\ell}-1} dz' T_{\ell}(z')$$

$$\left\{ \left| \frac{1}{k_z} \hat{e}(k_z) [A_{\ell} \hat{e}_{\ell}(-k_{\ell z}) e^{ik_{\ell z} z'} + B_{\ell} \hat{e}_{\ell}(k_{\ell z}) e^{-ik_{\ell z} z'}] \right|^2 \right.$$

$$\left. + \left| \frac{1}{k_z} \hat{h}(k_z) [C_{\ell} \hat{h}_{\ell}(-k_{\ell z}) e^{ik_{\ell z} z'} + D_{\ell} \hat{h}_{\ell}(k_{\ell z}) e^{-ik_{\ell z} z'}] \right|^2 \right\},$$

where

$$\hat{e}_{\ell}(k_z) = \frac{1}{(k_x^2 + k_y^2)^{1/2}} \{\hat{x} k_y - \hat{y} k_x\},$$

$$\hat{h}_{\ell}(k_z) = \frac{1}{k_{\ell}} \{\hat{e}_{\ell} \times \vec{k}_{\ell}\}.$$

Here is the observation angle, ϵ_{ℓ}'' is the imaginary part of the permittivity in layer ℓ , $T_{\ell}(z')$ is the temperature distribution.

in layer l , and A_l , B_l , C_l and D_l are wave amplitudes in region l that are related to those in other regions by propagation matrices.⁵⁹

References

1. V. W. Pidgeon, "Bistatic cross section of the sea," IEEE Trans. on Ant. Prop., AP-14, pp. 405-406, May 1966.
2. N. Levanon, "Averaged pulse-shape measurements of radar sea return at near-vertical incidence," IEEE Trans. Geosci. Elec., GE-9, pp. 233-241, Oct. 1971.
3. R. K. Moore and W. J. Pierson, Jr., "Worldwide oceanic wind and wave predictions using a satellite radar-radiometer," J. Hydronautics, 5, pp. 52-60, April 1971.
4. C. Cox and W. Munk, "Statistics of the sea surface derived from sun glitter," J. Marine Res., 13, no. 2, pp. 198-227, 1954.
5. C. Cox and W. Munk, "Measurement of the roughness of the sea surface from photographs of the sun's glitter," J. Opt. Soc. Amer., 44, pp. 838-850, Nov. 1954.
6. W. H. Munk, "High frequency spectrum of ocean waves," J. Marine Res., 14, pp. 302-314, 1955.
7. C. S. Cox, "Measurements of slopes of high-frequency wind waves," J. Marine Res., 16, pp. 199-230, Oct. 15, 1958.

8. J. A. Ewing, "A note on wavelength and period in confused seas," J. Geophys. Res., 74, pp. 1406-1408, Mar. 15, 1969.
9. D. Stilwell, Jr., "Directional energy spectra of the sea from photographs," J. Geophys. Res., 74, pp. 1974-1986, April 15, 1969.
10. A. Stogryn, "The apparent temperature of the sea at microwave frequencies," IEEE Trans. Ant. Prop., AP-15, pp. 278-286, March 1967.
11. W. Nordberg, J. Conaway, and P. Thaddeus, "Microwave observations of sea state from aircraft," Quart. J. Roy. Meteorol. Soc., 95, pp. 408-413, April 1969.
12. D. B. Ross, V. J. Cardone, and J. W. Conaway, Jr., "Laser and microwave observations of sea-surface condition for fetch-limited 17- to 25-m/s winds," IEEE Trans. Geosci. Electron., GE-8, pp. 326-336, Oct. 1970.
13. J. P. Hollinger, "Passive microwave measurements of sea surface roughness," IEEE Trans. Geosci. Electron., GE-9, pp. 165-169, July 1971.
14. E. C. Monahan, "Oceanic whitecaps," J. Phys. Oceanography, 1, pp. 139-144, April 1971.

15. J. D. Dippleman, "Apparent microwave emissivity of sea foam," J. Geophys. Res., 75, pp. 696-698, Jan. 20, 1970.
16. W. Nordberg, J. Conaway, D. B. Ross, and T. Wilheit, "Measurements of microwave emission from a foam-covered, wind-driven sea," J. Atmos. Sci., 28, pp. 429-435, April 1971.
17. D. C. Blanchard, "Whitecaps at sea," J. Atmos. Sci., 28, p. 645, May 1971.
18. G. F. Williams, Jr., "Microwave emissivity measurements of bubbles and foam," IEEE Trans. Geosci. Electron., GE-9, pp. 221-224, Oct. 1971.
19. P. W. Rosenkranz and D. H. Staelin, "Microwave emissivity of ocean foam and its effect on nadiral radiometric measurements," J. Geophys. Res., 77, pp. 6528-6538, Nov. 20, 1972.
20. S. F. Singer and G. F. Williams, Jr., "Microwave detection of precipitation over the surface of the ocean," J. Geophys. Res., 73, pp. 3324-3327, May 15, 1968.
21. A. H. Schooley, "Upwind-downwind ratio of radar return calculated from facet size statistics of a wind-disturbed water surface," Proc. IRE, 50, pp. 456-461, April 1962.

22. J. K. Parks, "Toward a simple mathematical model for micro-wave backscatter from the sea surface at near-vertical incidence," IEEE Trans. Ant. Prop., AP-12, pp. 590-605, Sept. 1964.
23. N. W. Guinard and J. C. Daley, "An experimental study of a sea clutter model," Proc. IEEE, 58, pp. 543-550, April 1970.
24. N. W. Guinard, J. T. Ransone, Jr., and J. C. Daley, "Variation of the NRCS of the sea with increasing roughness," J. Geophys. Res., 76, pp. 1525-1538, Feb. 20, 1971.
25. R. W. Newton and J. W. Rouse, Jr., "Experimental measurements of 2.25-cm backscatter from sea surfaces," IEEE Trans. Geosci. Electron., GE-10, pp. 2-7, Jan. 1972.
26. V. W. Pidgeon, "Doppler dependence on radar sea return," J. Geophys. Res., 73, pp. 1333-1341, Feb. 15, 1968.
27. J. W. Wright, "A new model for sea clutter," IEEE Trans. Ant. Prop., AP-16, pp. 217-223, March 1968.
28. A. K. Fung and H. L. Chan, "On the integral for backscattering from a randomly rough surface," Proc. IEEE (Lett.), 59, pp. 1280-1281, Aug. 1971.

29. B. S. Yaplee, A. Shapiro, D. L. Hammond, B. D. Au, and E. A. Uliana, "Nanosceond radar observations of the ocean surface from a stable platform," IEEE Trans. Geosci. Electron., GE-9, pp. 170-174, July 1971.
30. K. Tomiyasu, "Short pulse wide-band scatterometer ocean surface signature," IEEE Trans. Geosci. Electron., GE-9, pp. 175-177, July 1971.
31. D. E. Weissman, "Two frequency radar interferometry applied to the measurement of ocean wave height," IEEE Trans. Ant. Prop., AP-21, pp. 649-656, Sept. 1973.
32. A. Stogryn, "Equations for calculating the dielectric constant of saline water," IEEE Trans. Mic. Theory Tech., MTT-19, pp. 733-736, Aug. 1971.
33. T. Wilheit, W. Nordberg, J. Blinn, W. Campbell, and A. Edgerton, "Aircraft measurements of microwave emission from Arctic sea ice," Remote Sensing of Environment, 2, pp. 129-139, Oct. 1972.
34. I. Katz, "Utilization of a radar altimeter for determination of ocean roughness," Proc. Electronics and Aerospace Systems Conv., (Washington, DC, Oct. 1970), pp. 266-269.

35. T. Berger, "Satellite altimetry using ocean backscatter," IEEE Trans. Ant. Prop., AP-20, pp. 295-309, May 1972.
36. E. G. Wermund, "Remote sensors for hydrogeologic prospecting in arid terrains," IEEE Trans. Geosci. Electron., GE-9, pp. 120-130, July 1971.
37. J. C. Blinn, III., J. E. Conel, and J. G. Quade, "Microwave emission from geological materials: Observations of interference effects," J. Geophys. Res., 77, pp. 4366-4378, Aug. 1972.
38. W. P. Waite and H. C. MacDonald, "'Vegetation penetration' with K-band imaging radars," IEEE Trans. Geosci. Electron., GE-9, pp. 147-155, July 1971.
39. J. W. Rouse, Jr., "Arctic ice type identification by radar," Proc. IEEE, 57, pp. 605-611, April 1969.
40. C. R. Grant and B. S. Yaplee, "Back scattering from water and land at centimeter and millimeter wavelengths," Proc. IRE, 45, pp. 976-982, July 1957.
41. J. C. Alishouse, D. R. Baker, E. P. McClain, and H. W. Yates, "Microwave sensing for earth surface measurements," Instrum. Contr. Syst., pp. 105-107, Jan. 1972.

42. T. Wilheit, W. Nordberg, J. Blinn, W. Campbell, A. Edgerton, "Aircraft measurements of microwave emission for Arctic Sea Ice," Rem. Sensing Environ., 2, pp. 129-139, 1972.
43. P. Noekstra and P. Cappillino, "Dielectric properties of sea and sodium chloride ice at UHF and microwave frequencies," J. Geophys. Res., 76, no. 20, pp. 4922-4931, July 1971.
44. R. K. Moore and C. S. Williams, Jr., "Radar terrain return at near-vertical incidence," Proc. IRE, 45, pp. 228-238, Feb. 1957.
45. P. Gloersen, W. Nordberg, T. J. Schmugge, T. T. Wilheit, W. J. Campbell, "Microwave signatures of first-year and multiyear sea ice," J. Geophys. Res., 78, pp. 3564-3572, June 1973.
46. D. H. Staelin, "Passive remote sensing at microwave wavelengths," Proc. IEEE, 57, pp. 427-439, April 1969.
47. K. Tomiyasu, "Remote sensing of the earth by microwaves," Proc. IEEE, 62, pp. 86-92, Jan. 1974.
48. A. S. Gurvich, V. L. Kalnen, and D. T. Matveyev, "Influence of the internal structure of glaciers on their thermal radio emission," Atm. Oceanic Phys. (USSR), 9, no. 12, pp. 713-717, 1973.

49. A. W. England, "Thermal microwave emission from a halfspace containing scatterers, Radio Sci., 9, pp. 447-454, April 1974.
50. A. Stogryn, "The brightness temperature of a vertically structured medium, Radio Sci., 5, pp. 1397-1406, Dec. 1970.
51. A. Stogryn, "Electromagnetic scattering by random dielectric constant fluctuations in a bounded medium," Radio Sci., 5, 1974.
52. J. A. Kong, "Microwave remote sensing of ice and snow,"
) Proceedings of the URSI Commission II Specialist Meeting on Microwave Scattering and Emission from the Earth, pp. 239-244, Bern, Switzerland, Sept. 1974.
53. M. Nagase, "Studies of the model for microwave remote sensing of ice and snow, S. B. Thesis, MIT, 1975.
54. D. Chu, "Machine inversion of remote sensing data, S. B. Thesis, MIT, 1975.
55. Schmugge, Wilheit, Gloersen, Meier, Frank, Dirmhirn, "Microwave signatures of snow and fresh water ice," Interdisciplinary Symposium Advanced Concepts Tech., Goddard Space Center, Nov. 1973.

56. L. Tsang and J. A. Kong, "The brightness temperature of a half-space random medium with nonuniform temperature profile," to be published.
57. L. Tsang and J. A. Kong, "Microwave remote sensing of a two-layer random medium," to be published.
58. L. Tsang, E. Njoku, and J. A. Kong, "Microwave thermal emission from a stratified medium with nonuniform temperature distribution," to be published.
59. J. A. Kong, Theory of Electromagnetic Waves, Wiley-Interscience, New York, 1975.
60. J. A. Kong, "Composite model for microwave remote sensing," RLE Progress Report No. 114, pp. 78-80, 1974.
61. L. Tsang and J. A. Kong, "Effect of surface roughness on emissivity," RLE Progress Report No. 114, pp. 74-75, 1974.
62. J. A. Kong, P. Wong, and D. Pao, "Emissivity and reflection coefficients for stratified earth media," RLE Progress Report No. 109, pp. 70-74, 1973.
63. J. A. Kong, "Probing depth for microwave remote sensing of ice and snow calculated by a seminumerical approach using MACSYMA," RLE Progress Report No. 114, pp. 81-85, 1974.

64. J. A. Kong, "Remote sensing of ice thickness with a radio-meter," RLE Progress Report No. 115, pp. 95-98, 1975.
65. L. Tsang and J. A. Kong, "Effects of scattering and nonuniform temperation distributions on brightness temperature in remote sensing, RLE Progress Report No. 115, 1975.
66. L. Tsang, E. Njoku, and J. A. Kong, "Calculation of the brightness temperature of an inhomogeneous medium with the fluctuation-dissipation approach," RLE Progress Report, 1975.
67. J. A. Kong, "Electromagnetic waves in layered biaxial media," RLE Progress Report No. 110, pp. 34-38, 1973.
68. E. Njoku, "Microwave emission from clouds and rainfall," Electrodynamics Memo No. 41, Dec. 1974.
69. P. S. K. Wong, "Effects of subsurface spherical scatterers on surface emissivity, S. M. Thesis, MIT, 1974.
70. B. Djermakoye, "Passive microwave remote sensing of moisture in sandlike soils," S. B. Thesis, MIT, 1975.

APPENDIX I

STUDIES OF THE MODEL FOR
MICROWAVE REMOTE SENSING OF ICE AND SNOW

by

MASATO NAGASE

SUBMITTED IN PARTIAL FULFILLMENT
OF THE REQUIREMENTS FOR THE
DEGREE OF BACHELOR OF SCIENCE

at the

MASSACHUSETTS INSTITUTE OF TECHNOLOGY

June, 1975

Signature of Author *Masato Nagase*
Department of Electrical Engineering, May 9, 1975
Certified by *Jim C. Hong*
Thesis Supervisor
Accepted by *David Allen*
Chairman, Departmental Committee on Thesis

STUDIES OF THE MODEL FOR
MICROWAVE REMOTE SENSING OF ICE AND SNOW

by

MASATO NAGASE

Submitted to the Department of Electrical Engineering on
May 9, 1975, in partial fulfillment of the requirements
for the Degree of Bachelor of Science.

ABSTRACT

A two layer composite model^[3] is used to match microwave emission data of fresh water ice and snow in order both to test the model and to interpret the data. The magnitude of coherent effects are empirically estimated with the object of explaining features of the emission spectra, and the model is modified to deal with polarization effects and oblique incidence.

Thesis Supervisor: Jin Au Kong

Title: Associate Professor of Electrical Engineering

ACKNOWLEDGEMENT

I wish to thank Professor Jin Au Kong for his patience spending his valuable time with me, and for his guidance and encouragement throughout the preparation of this thesis.

I thank Donald Chu for helping my writing and for his useful suggestions.

Thanks are also due to my parents for the invaluable support they gave me throughout these years. Without their faith in me, all I have accomplished would have been impossible.

TABLE OF CONTENT

Abstract	Page 28
Acknowledgement	29
Table of Content	30
Table of Illustrations	31
I. Introduction	32
II. Data Matching	
The Composite Model	34
Data Matching	35
Summary	40
III. Modification of the Model	
Polarization and Oblique Incidence	42
Coherent Effects	47
IV. Summary and Suggestions for Future Studies	51
Appendix I : Result of the Inversion	53
Appendix II: Emissivities at 37.5GHz for both Polarizations	60
References	61

TABLE OF ILLUSTRATIONS

	<u>Page</u>
Fig. 1 Two Layer Model	34
Fig. 2 Model and Ground Measurement for Bear Lake	36
fig. 3 Model and Ground Measurement for Steamboat Spring	37
Fig. 4 Model and Ground Measurement for South Cascade Lake	38
Fig. 5 Model and Ground Measurement for South Cascade Glaciers	39
Fig. 6 Two Layer Model (Oblique Incidence)	42
Fig. 7 Emissivity as a Function of th Incident Angle	46
Fig. 8 South Cascade Lake Data Matched with Coherence	49
Fig. 9 Emissivities with Different Coherence Factors	50

I. INTRODUCTION

Remote sensing of the earth at microwave frequencies is of great use because of its all weather and day-night operational capability. This is due to high transmission through the atmosphere and cloud. Many factors such as absorption, layering, scattering, polarization, incident angle, anisotropy and medium inhomogeneity affect the radiobrightness spectra. In order to interpret the data, all these effects should be incorporated in a theoretical composite model. Development of such models, combined with the interpretation of the measurements will lead to numerous practical applications. For remote sensing of ice and snow, applications include ice dynamics, climatology, glaciology and navigation etc.

Effects of scattering due to medium inhomogeneity have been accounted for by A.S.Gurvich et al.^[1] The theory enables us to distinguish the spectra of the continental glaciers from those of shelf glaciers. Inversion of the data is performed. The estimated values for the variance of the density fluctuations and the characteristic length of ice crusts agree with the measurements. In order to develop a more complete model, the formulas given in that paper have been extended and combined by J.A.Kong with the stratified model^[2] which also accounts for the effects of layering, absorption and anisotropy.

In the present paper, the model developed by Kong is referred to as the composite model^[3] and is used extensively to match emission data. The problems encountered in the process of matching and inverting the data suggest the presence of additional factors that influence emission properties. With the object of improving the model, the magnitudes of coherent effects are estimated and the two layer composite model is modified to deal with polarization effects and oblique incidence.

II. DATA MATCHING

The Composite Model

The two layer composite model^[3] consists of a layer of snow with depth d and relative complex permittivity $\epsilon_1 = \epsilon_1' + i\epsilon_1''$ on top of ice, water or land.

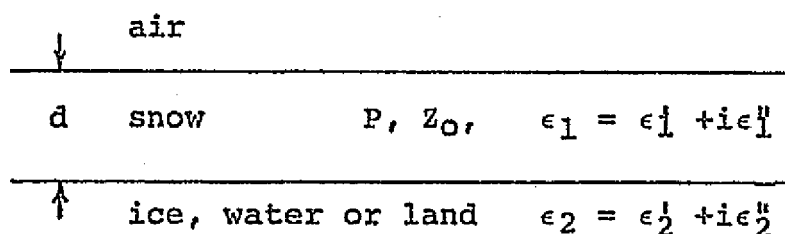


Fig. 1 Two layer model

The reflectivity and scattering factors are calculated separately to give total emissivity e of the structure:

$$e = 1 - r - s \quad (1)$$

where r is the reflectivity of the object and s is the power coefficient of scattering effects. Observations are assumed to be made from nadir. The oscillatory behavior of r and scattering effects due to the substrata are neglected in the model. The emissivity depends on frequency and seven model parameters: $d, \epsilon_1', \epsilon_1'', \epsilon_2', \epsilon_2'', Z_0$ and P . ϵ_1 and ϵ_2 are the relative complex permittivity of a top and a bottom layer respectively. Z_0 is a characteristic correlation depth for

the refractive index. P is a dimensionless scattering parameter and is related to the variance of refractive index fluctuation σ_{no}^2 by $P = \frac{n_1'}{n_1''} \sigma_{no}^2$, where $n_1' + n_1''i = (\epsilon_1' + \epsilon_1''i)^{1/2}$

Data Matching

The model has been tested on the emission data from fresh water ice and snow published by T. Schmugge et al^[4]. The data was taken by microwave radiometers in the frequency range 1.43Ghz to 37.5Ghz during the flights made over dry snow with different substrata: lake ice, wet soil, glacier ice, firn and wet snow. The lowest four of six frequency channels are the nadir views. The 37.5Ghz channel provides vertical and horizontal polarizations with the look angle of 45°. The information on the second highest frequency channel (19.35Ghz) is ambiguous, but the nadir observation is assumed for our purpose of inverting the data. Emissivity as a function of frequency is calculated for each set of different parameter values in order to fit the theoretical curve to the data within the margin of 0.03 in emissivity. We have assumed the constant depth and ground temperature. The calculation is made using the computer language, MACSYMA*

*Project MAC's SYmbolic MANipulation system: developed by the Mathlab Group, Project MAC, MIT, whose work is sponsored by the Advanced Research Project Agency, Department of Defense, under contract number N00014-70-A-0362-0001

The data and the results of inversion are presented in Appendix I, and explained for each site individually in the following paragraphs.

i) Bear Lake ($d = 0.15\text{m}$, altitude 1805m)

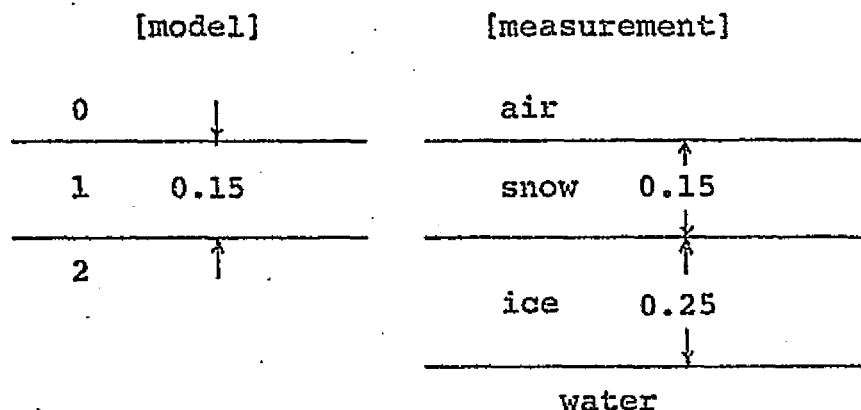


Fig. 2 Model and ground Measurements

The data shows a sharp drop in emissivity at low frequencies. This characteristic is best matched by setting $\epsilon_1^i = 3.2$ and $\epsilon_2 = 80 + 80i$. For such dielectric properties, the penetration depth at 1.43Ghz is about 47.5cm. The sharp drop can thus be accounted for by layering, especially due to the large values of ϵ_2^i and ϵ_2^r . This is in good agreement with the ground measurement which indicates that there is water beneath snow. The modeling is crude because we have ignored a slab of ice between snow and water. The parameter values obtained for snow are very much like those of ice. We believe that the model should be extended to a

three layer model in order to account for the dependence of the data on both snow and ice layers and scattering effects caused by ice.

ii) Steamboat Spring ($d = 0.8\text{m}$, altitude 2070m)

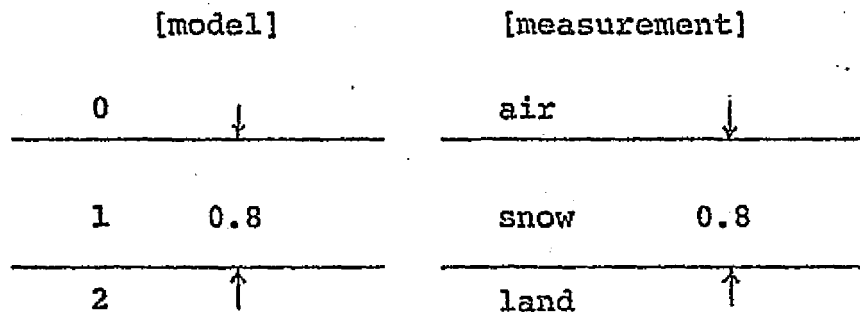


Fig. 3 Model and ground measurement

As mentioned in the Bear Lake case, low emissivity in the data at the lowest frequency channel (1.43GHz) is caused by the substratum. Penetration and probing depth* at 1.43 gigahertz are calculated to be 39.4cm and 5.3m respectively, while d is 0.8m. The values 60-80 and 0-80 for ϵ_2' and ϵ_2'' suggest that wet soil with moisture of greater than 35% appears to be water-like from the radiometers. The value $\epsilon_1 = 2.2 + 0.04i$ is typical for snow. This agrees with the measurement. It should be noted that Z_0 is 0.4mm, the lowest among all six tested. It indicates this snow has fine structure.

*The maximum depth that we can probe depends on sensitivity of radiometer. Assuming the sensitivity of 2°K, we define probing depth as the maximum that can distinguish a two layer medium from a half space case.

iii) South Cascade Lake ($d = 0.5\text{m}$, altitude 1610m)

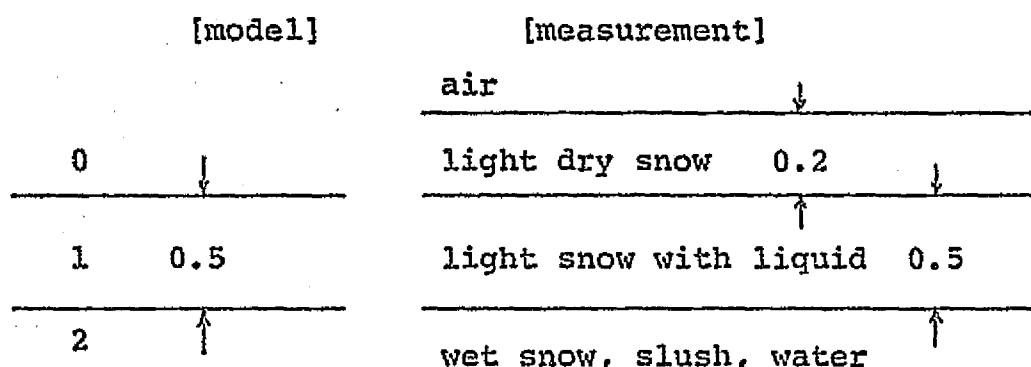


Fig. 4 Model and ground measurement

At this site, the simulation of the real structure is very crude. The largest values for the imaginary part of complex permittivity of snow are obtained. This reflects the presence of liquid within snow as indicated by the ground measurement. We also note that there is very little volume scattering ($P = 0.35$) compared with other sites. This is in agreement with Schmugge's explanation^[4] that scattering effects are washed out by the increased effective loss tangent for snow when liquid water is present.

iv) South Cascade Glaciers

P-0, $d = 4.9\text{m}$, altitude 1610m, below firn line.

P-1, $d = 6.8\text{m}$, altitude 1890m, above firn line.

P-3, $d = 8.4\text{m}$, altitude 2040m.

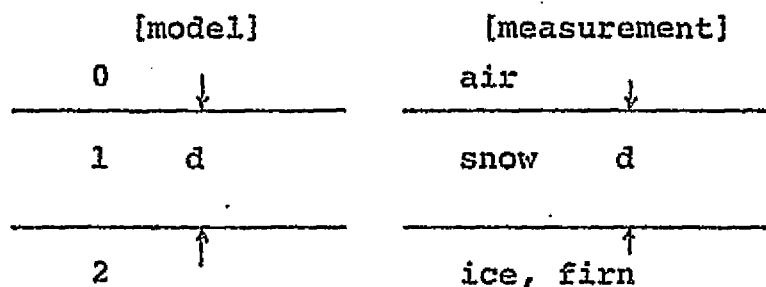


Fig. 5 Model and ground measurement

The parameter values obtained indicate that there is no liquid content in snow. The effects of volume scattering for all three places at this site are relatively large ($P = 1.8-2.3$), and this checks with the past observation^[5] that multi-year ice has lower emissivity at higher frequency channels than new ice. The values for ϵ_2^1 and ϵ_2'' are distinctively different from those of other three sites and this is justified by the fact that there is ice or firn, instead of water or moist land underneath the snow. Because we have ignored the scattering effect caused by the substratum, the model can be modified to deal with such effects.

Summary

The parameter values shown in Appendix I are obtained, as a result of tedious and time-consuming computer manipulation to fit the data within the margin. Emissivities at different frequencies are calculated for a set of parameters and compared with the data by inspection. This procedure is repeated unsystematically until we find a reasonable match. Consistent results cannot be guaranteed because such a method often depends on the person doing the manipulation. D.Chu has written a computer program^[6] to perform such inversions automatically. The program has been tested on the same data. Although it is not as flexible as a human operator (the program approaches the data only from above and below), his method has advantage of providing consistent results in a short time.

The composite model proved to be capable of explaining many features of the emission data. These characteristics can be related to physical parameters by matching the data. The results of the inversion suggest that we are able to determine the dielectric properties of a top and a bottom layer, relative magnitude of liquid content, size of the scattering centers and relative magnitude of scattering effect. We have not tried to invert the thickness, but we believe that we can estimate d in case of ice or snow, provided that d is smaller than 0.5m.

The above mentioned parameter values, for example, can distinguish dry snow from wet snow, first-year ice from multi-year ice, snow or ice with fine structure from that with rough structure and of course, snow and ice from water or land. Although we dealt only with smooth surfaces, the effect of surface roughness can be explained by modifying the reflection coefficient used in the model^[7].

The major difficulty in matching Schmugge's data was caused by his ambiguity about the incident angle of the 19.35 gigahertz channel. This channel provides the horizontal polarization and scanning mode. The abrupt drop in emissivity at this frequency made the matching very difficult. If we assume that the data was obtained by scanning the radiometer from 0° to 45° for example, this sharp drop can be accounted for by the polarization and angle dependence of emissivity.

The present model is limited to only two layer media. For some data, more sophisticated modeling is necessary. In order to explain the data from polarization channels, the model should be modified. This is done in the following part of the paper together with the examination of oscillatory behavior of the reflectivity.

II. MODIFICATION OF THE MODEL

Polarization and Oblique Incidence

Dual polarization and scanning capability of microwave sensors are attractive features which can provide additional information on radio emission. Two of six radiometers used for Schmugge's data have polarization channels: dual at 37.5Ghz and horizontal polarization at 19.35Ghz. The present model, however, is insufficient to account for the measurements on these channels. In order to deal with effects on emissivity of scanning and polarization, we modify the composite model as follows.

We assume the angle of incidence θ_0 and the angle of refraction θ_1 as shown in Fig. 6.

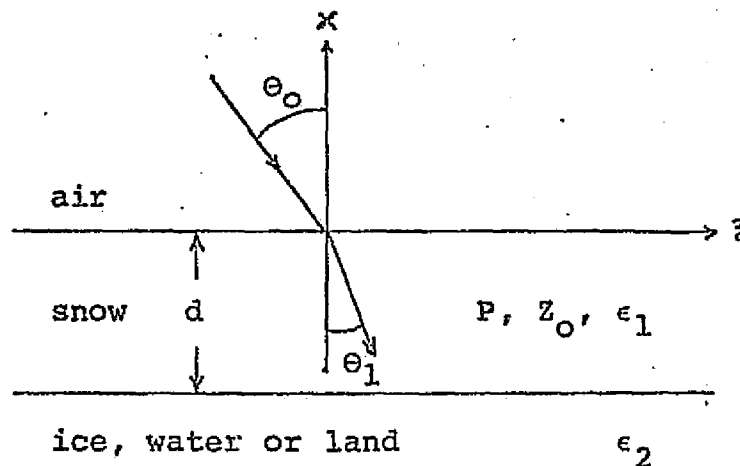


Fig. 6 Two Layer Model (Oblique Incidence)

From the composite model, reflectivity r is given by

$$r \cong \frac{|R_{01}|^2 + |R_{12}|^2 \cdot e^{-4k_{1x}d}}{1 + |R_{01}|^2 \cdot |R_{12}|^2 \cdot e^{-4k_{1x}d}} \quad (2)$$

where $k_{1x} = k_{1x}' + k_{1x}'' i = k_0 (\epsilon_1' + \epsilon_1'' i - \sin^2 \theta_0)^{1/2}$,
and R_{01} and R_{12} are the reflection coefficients of a top and
a bottom interfaces. For the horizontal polarization,

$$R_{01} = \frac{1 - \frac{k_{1x}}{k_{0x}}}{1 + \frac{k_{1x}}{k_{0x}}} \quad (3.a)$$

and

$$R_{12} = \frac{1 - \frac{k_{2x}}{k_{1x}}}{1 + \frac{k_{2x}}{k_{1x}}} \quad (3.b)$$

where $k_{2x} = k_0 (\epsilon_2' + \epsilon_2'' i - \sin^2 \theta_0)^{1/2}$,

and $k_{0x} = k_0 (1 - \sin^2 \theta_0)^{1/2}$.

For the vertical polarization,

$$R_{01} = \frac{\epsilon_1 k_{0x} - k_{1x}}{\epsilon_1 k_{0x} + k_{1x}} \quad (4.a)$$

$$R_{12} = \frac{\epsilon_2 k_{1x} - \epsilon_1 k_{2x}}{\epsilon_2 k_{1x} + \epsilon_1 k_{2x}} \quad (4.b)$$

The polarization dependent power coefficient of the scattering effect due to medium inhomogeneity for an unbounded half space is given by Gurvich et al^[1]. By extending their result to a two layer case, we obtain,

$$s_h = \frac{n_1^4}{2n_1^2} \cdot \sigma_{no}^2 \cdot \frac{n_1^4 \cdot k_o \cdot z_o}{1 + (2n_1^4 k_o z_o \cos \theta_1)^2} \cdot \cos \theta_o$$

$$\times (1 - |R_{01}|^2) \cdot (1 - e^{-4 \cdot k_o n_1 \cdot d / \cos \theta_1}) \quad (5)$$

where s_h is the scattering factor for the horizontal polarization, and

$$s_v = s_h \cdot \cos^2 (2\theta_1) \quad (6)$$

for the vertical polarization where θ_o and θ_1 are related by Snell's law:

$$n_1 \cdot \sin \theta_1 = \sin \theta_o \quad (7)$$

The emissivity for each polarization are,

$$e_h = 1 - r_h - s_h \quad (8.a)$$

and

$$e_v = 1 - r_v - s_v \quad (8.b)$$

where reflectivities r_h and r_v are calculated for polarization from (3) and (4) respectively.

We have used the parameter values matched before (Appendix I) to calculate the emissivities at 37.5Ghz channel for both polarizations. Appendix II lists the results in comparison with the actual data. In Fig. 7, we show the incident angle dependence of emissivity for the two polarizations.

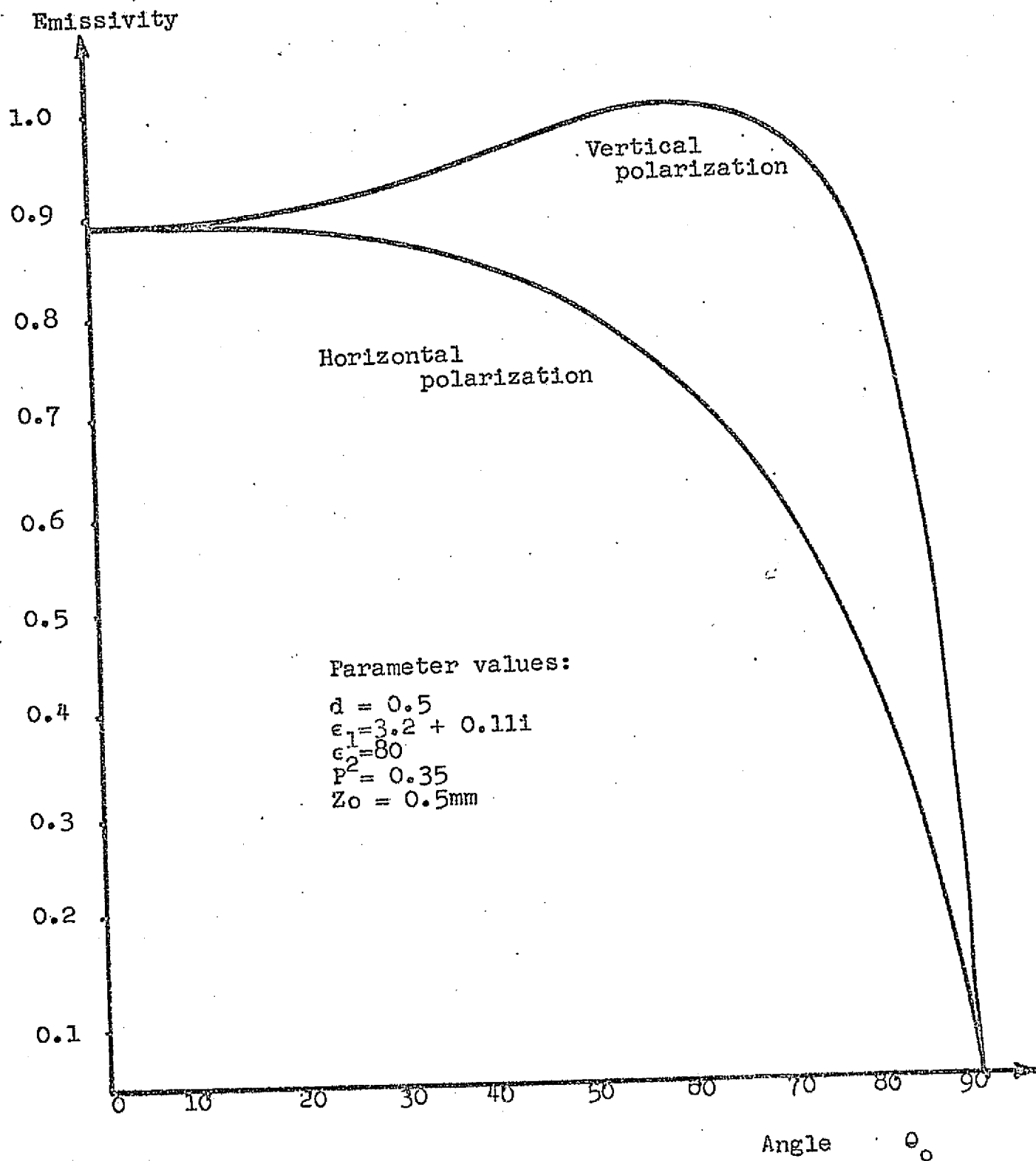


Fig. 7 Emissivities as a Function of Incident Angle

Coherent Effects

The composite model assumes all radiation is rendered incoherent by scattering and medium inhomogeneity. In general scattering and absorption attenuate the coherent wave. In the case of ice or snow, we observe a large scattering effect in the higher frequency channels. Absorption is relatively small for a thin layer medium and at low frequencies. In such situations, we expect the data to show some characteristics of coherent radiation in low frequency channels. Since such characteristics cannot be matched by the present model, we are to remove the assumption of total incoherence from the model in order to come up with better match and to investigate the magnitude of coherent effects.

The exact expression of the reflection coefficient for a two layer medium is,

$$R = \frac{|R_{01}| + |R_{12}| \cdot e^{2i \cdot k_{1x}d}}{1 + |R_{01}||R_{12}| \cdot e^{2i \cdot k_{1x}d}} \quad (9)$$

where R_{01} , R_{12} , k_{1x} are as defined earlier (Fig. 1).

By separating the real and imaginary part of k_{1x} , we find the reflectivity $r = |R|^2$:

$$r = \frac{|R_{01}|^2 + |R_{12}|^2 \cdot e^{-4k_{1x}''d} + 2N \cdot |R_{01}| \cdot |R_{12}| e^{-2k_{1x}''d} \cdot \cos 2k_{1x}'d}{1 + |R_{01}|^2 |R_{12}|^2 \cdot e^{-4k_{1x}''d} + 2N \cdot |R_{01}| \cdot |R_{12}| e^{-2k_{1x}''d} \cdot \cos 2k_{1x}'d} \quad (10)$$

where N characterizes the magnitude of the oscillatory behavior of the reflectivity. If we assume the wave to be incoherent, N is 0. A totally coherent wave in this case corresponds to $N = 1$. By adjusting the coherence factor N , we have matched the data of South Cascade Lake (Appendix I). We have obtained the best result with $N = 0.25$. The imaginary part of k_{1x} accounts for absorption of coherent wave. The scattering loss is neglected because coherence effects are important only at the lowest two frequency channels where there is negligible scattering. The match is improved and the graph is shown in Fig. 8 in comparison with our result before. Fig. 9 shows the emissivities with different values of N .

Although the above procedure accounts for some features in the emission data, the method is purely empirical. The theory that accommodates coherent effects has been investigated by L. Tsang^[8]. In his paper incoherent wave and scattering effects are combined with a coherent wave which suffers scattering loss as well as absorption.

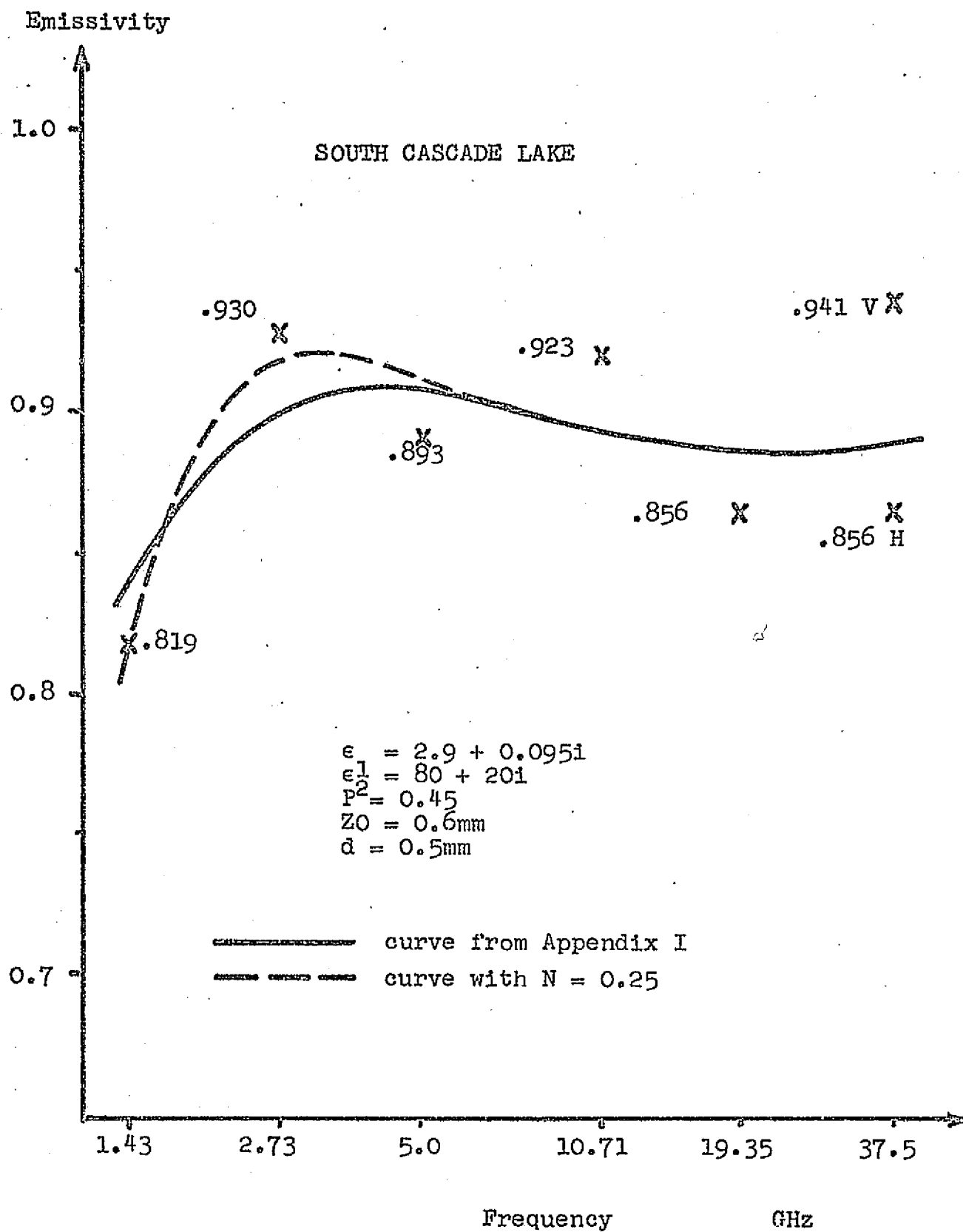


Fig. 8 South Cascade Lake Data Matched with Coherence

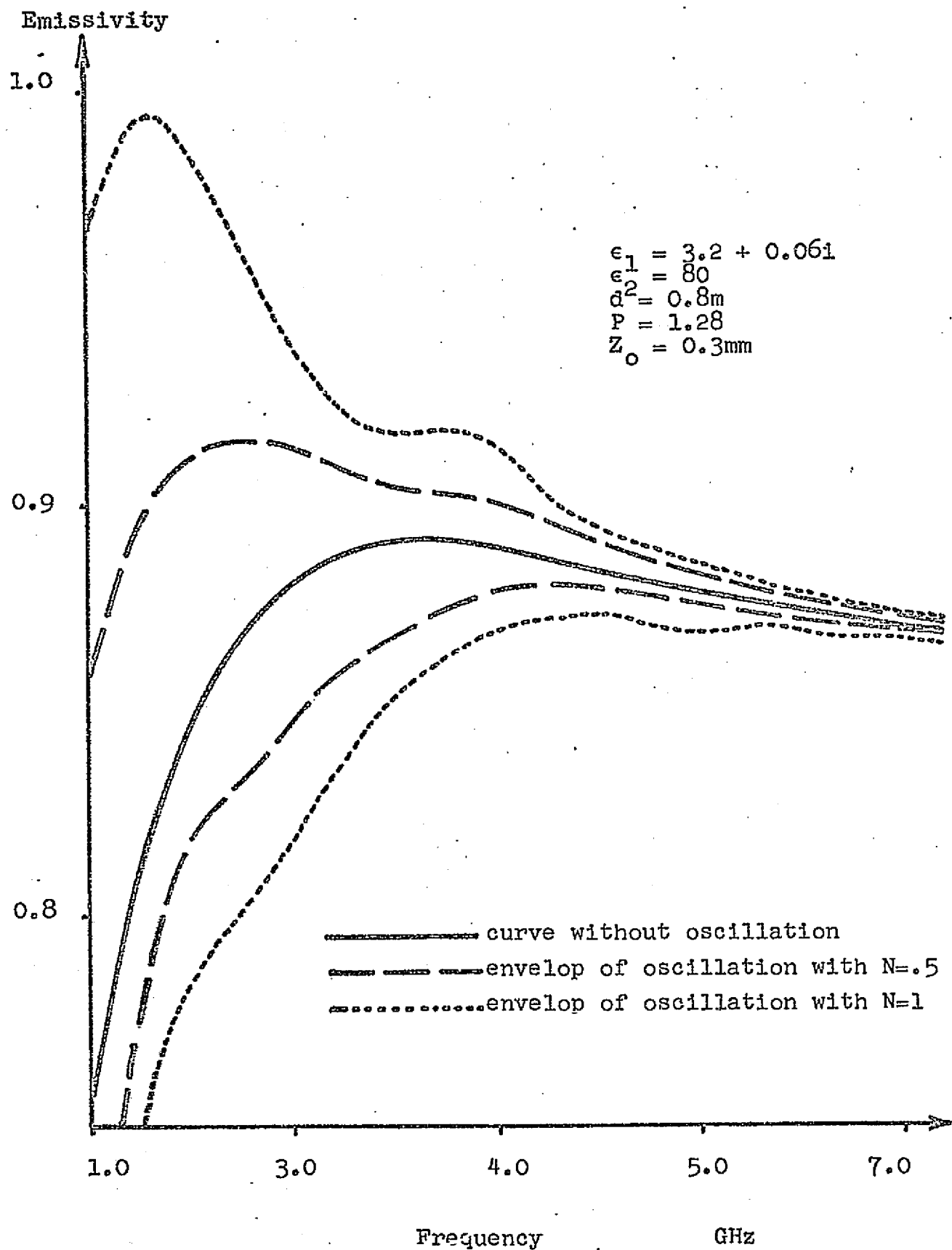


Fig. 9 Emissivities with Different Coherence Factors

IV. SUMMARY AND SUGGESTIONS FOR THE FUTURE STUDIES

We have found that the two layer composite model can provide useful parameter values from emission data. The inversion is a tedious process. The theoretical curve must be matched with the data as closely as possible in order to obtain the reasonable values. The modification to allow some coherent effects in the model has improved the matching. The generalized model which deals with polarization and angle dependence accounts for the additional features of the emission spectra. We need more accurate data, however, in order to perform data inversion using the modified model. Ambiguity about the oscillatory behavior can only be cleared up by probing at many different frequencies. Also if the scanning angle had been given on the 19.35Ghz channel of Schmugge's measurements, the data matching would have been far more successful. Since polarization can provide additional information, it is desirable to equip with dual polarization for all channels. Such a feature is particularly useful when we study surface areas.

It is essential to compare the values obtained using the model with the actual ground measurements. Except for the snow or ice thickness, however, Schmugge's measurements of geophysical parameters are ambiguous. In order to further the study that relates the model's parameters to geophysical parameters, precise ground measurements are

required. Small scale experiments on the detection of radio emission can be set up for such a purpose.

The model can now deal with absorption, anisotropy, layering, polarization, incident angle, scattering and medium inhomogeneity. As for layering, we have only tried a two layer case. Often, a two layer model becomes a crude approximation of a real situation. Because the present model neglects scattering due to the underlying medium, a three layer model should replace the two layer one when the substratum is ice and when the whole structure is more complicated. It should be pointed out that data are expressed in emissivity which assumes the constant ground temperature. This approximation is valid when the length of temperature wave is considerably small compared to the thickness of the layer. In this case temperature variations caused by weather changes in a thin surface layer have little effect on emissivity. For the more general case, the effect of temperature variation with depth can be studied.

APPENDIX I

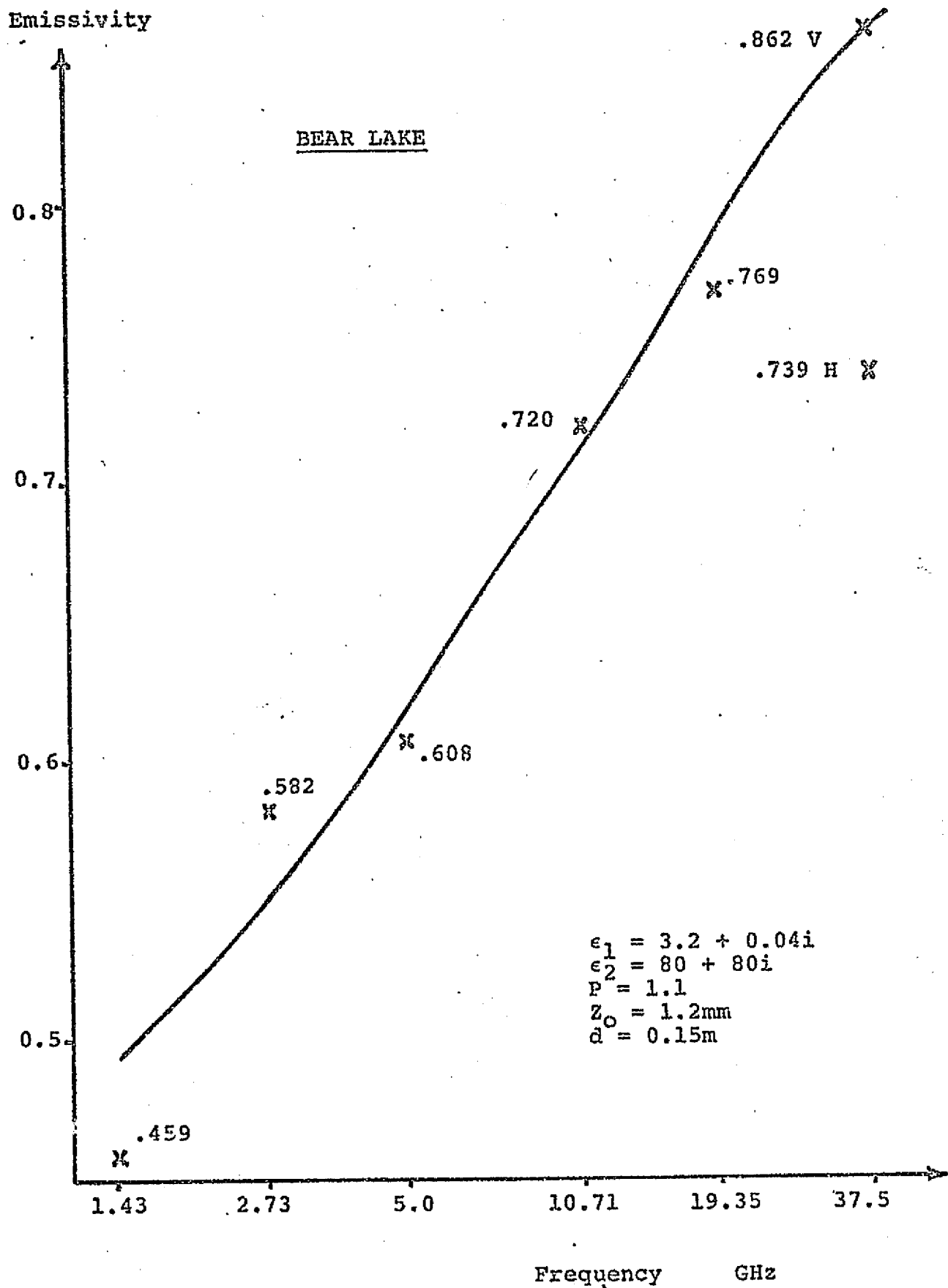
[Results of the Inversion]

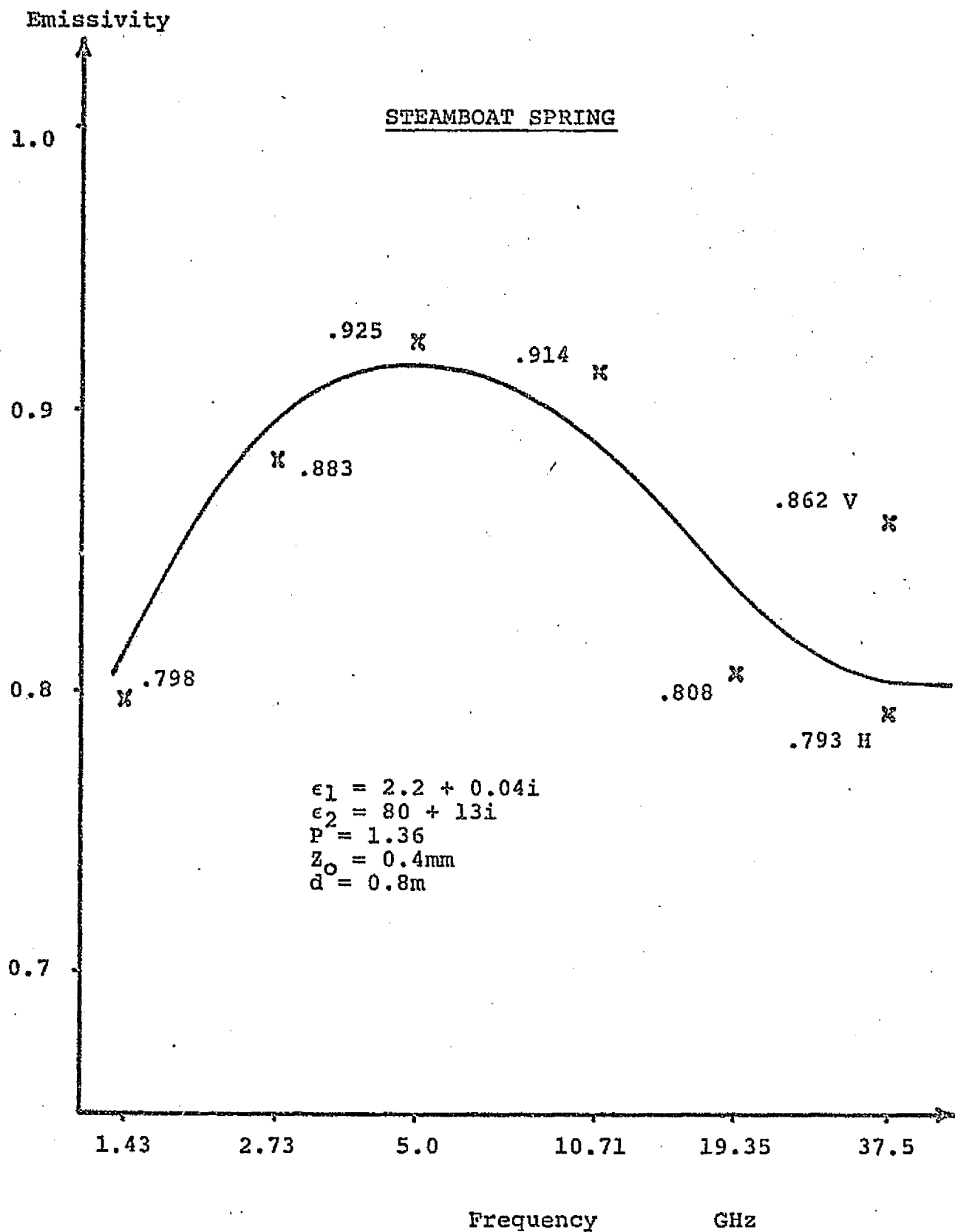
	<u>Bear Lake</u>	<u>Steamboat</u>	<u>S. C. Lake</u>
$d(m)$	0.15	0.8	0.5
ϵ_1^i	3.2	2.2	2.9-3.2
ϵ_1^u	0.04-0.048	0.04	0.095-0.11
ϵ_2^i	80	60-80	70-80
ϵ_2^u	80	0-80	0-20
P	1.1-1.6	1.34-1.38	0.35-0.45
$Z_O(mm)$	0.8-1.2	0.37-0.4	0.5-0.65

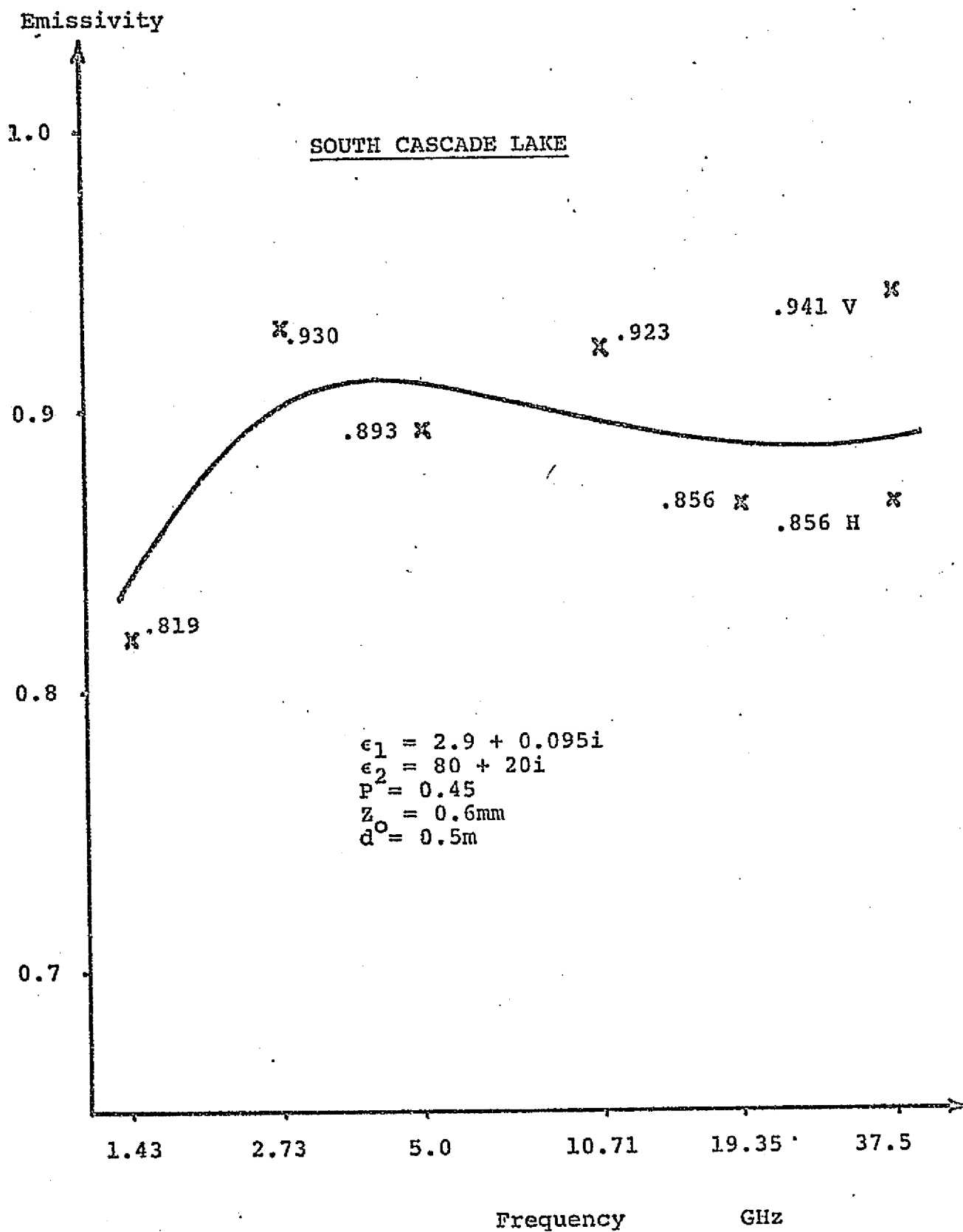
	<u>S.C.G,P-3</u>	<u>S.C.G,P-1</u>	<u>S.C.G,P-0</u>
$d(m)$	8.4	6.8	4.9
ϵ_1^i	3.1	2.7-2.8	2.6-2.7
ϵ_1^u	0-0.0004	0-0.0004	0-0.0008
ϵ_2^i	3.0-3.2	3.1-3.2	3.0-3.2
ϵ_2^u	0.004-0.05	0.004-0.05	0.03-0.05
P	1.8-2.1	1.9-2.0	1.75-2.3
$Z_O(mm)$	0.75-0.9	0.9-0.95	0.5-0.8

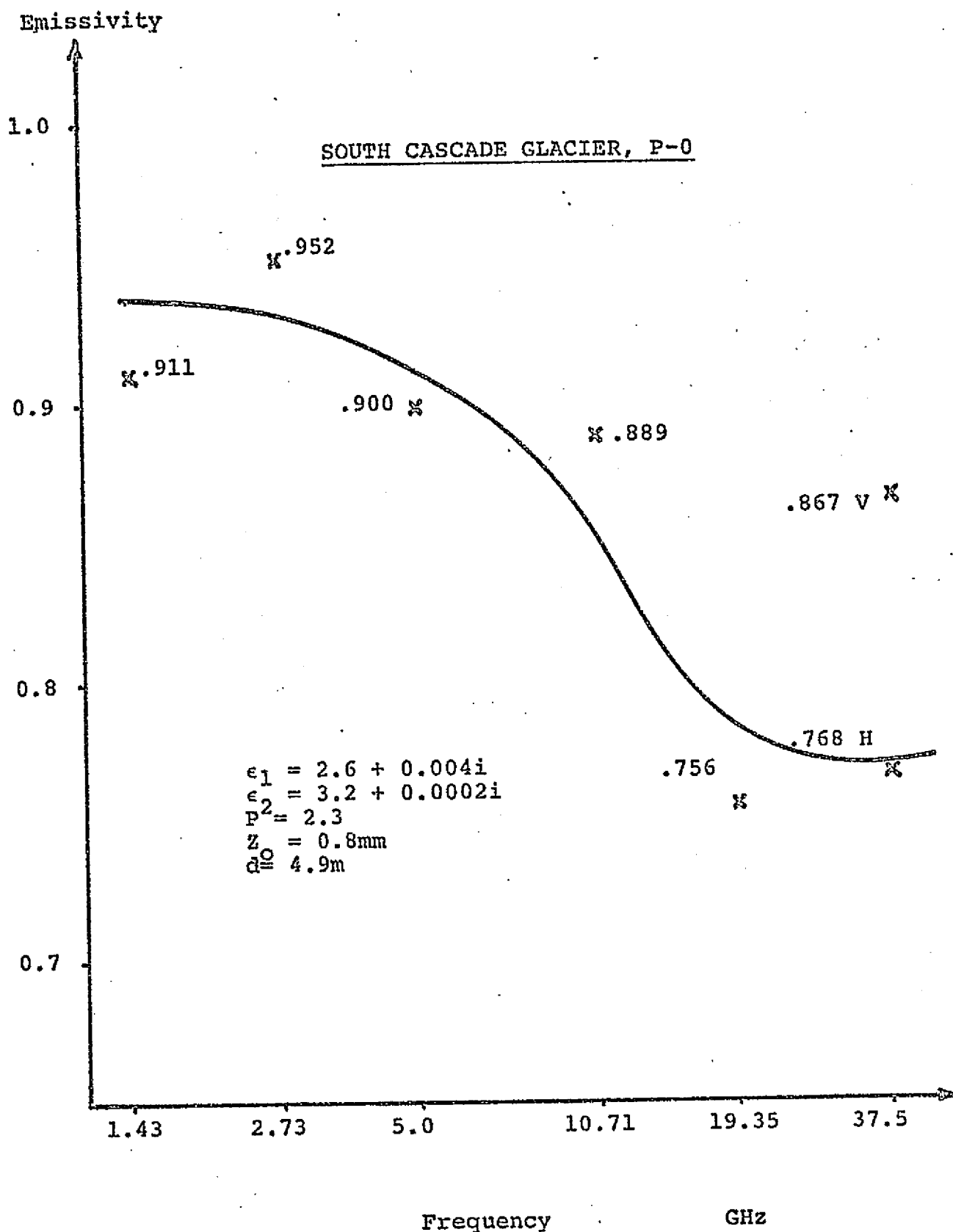
Thickness d is given by the measurements.

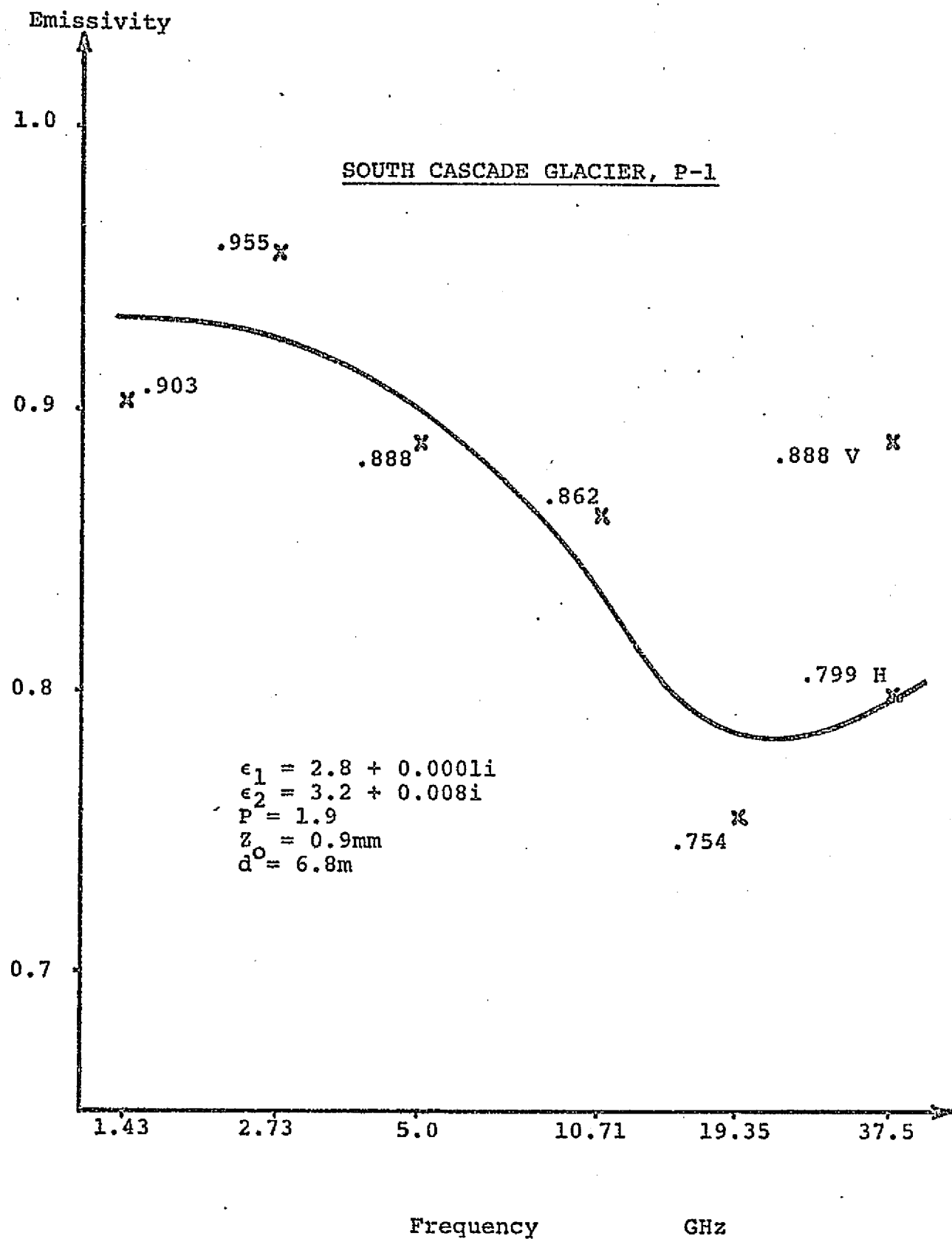
The data and the theoretical curve are plotted in the following pages.

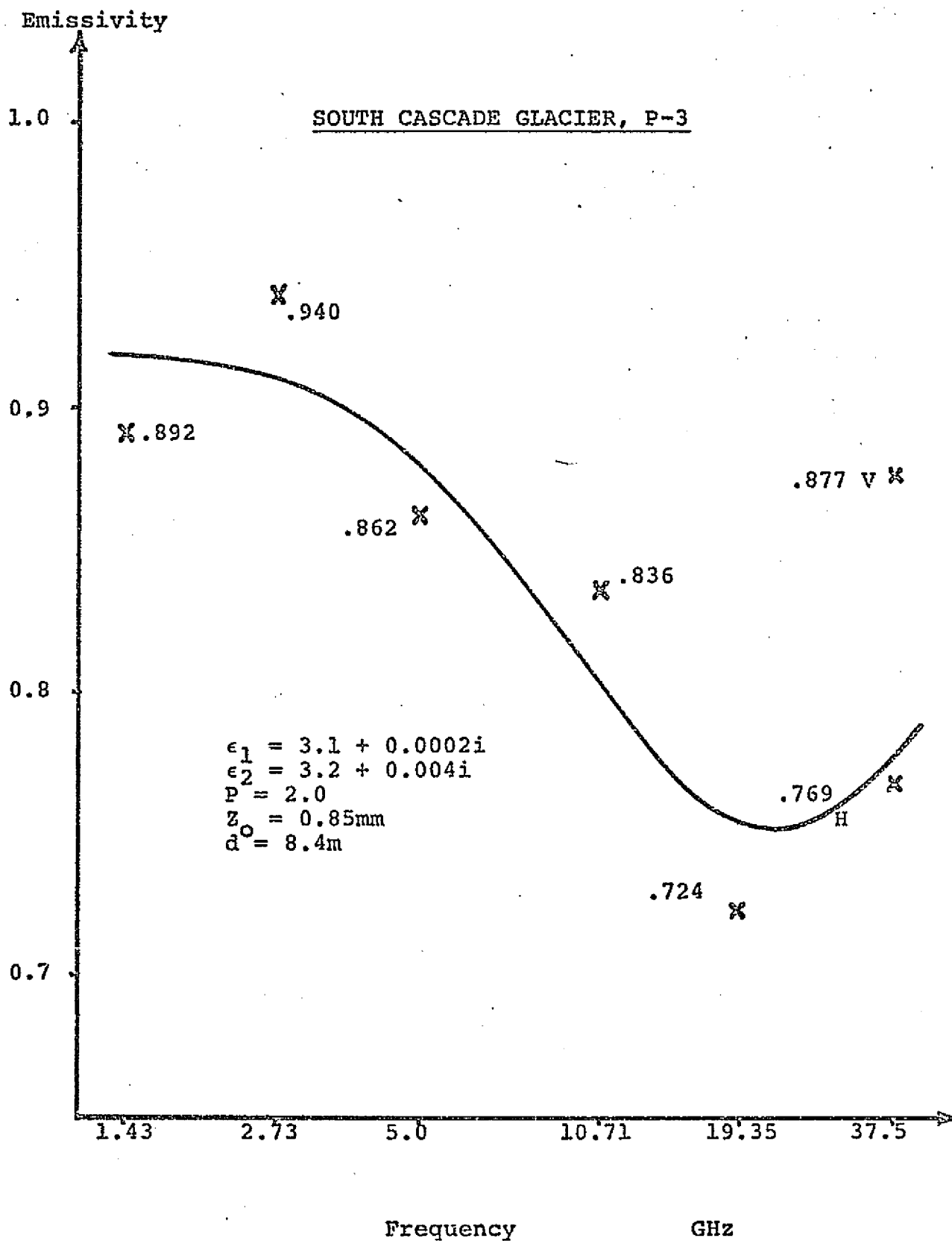












APPENDIX II

[Emissivities at 37.3GHz for both polarizations]

<u>Location</u>	Actual data observed		Figures calculated	
	<u>Horizontal</u>	<u>Vertical</u>	<u>Horizontal</u>	<u>Vertical</u>
South Cascade Lake	.856	.941	.830	.964
Bear Lake	.739	.862	.767	.928
Steamboat Spring	.793	.862	.800	.953
Glacier P-0	.768	.867	.751	.924
Glacier P-1	.799	.888	.767	.929
Glacier P-3	.769	.877	.731	.906

Radiometers are aimed at 45° from nadir.

For the calculation, we have used the results of data
matching given in Appendix I.

References

- [1] A.S.Gurvich, V.I.Kalinin, and D.T.Matveyev, "Influence of the Internal Structure of Glaciers on their Thermal Radio Emission," Izv. Atmospheric and Oceanic Physics, vol. 9, Nov. 12, 1973, pp.1247-56.
- [2] J.A.Kong, "electromagnetic Waves in Layered Biaxial Media," Res.Lab of Electronics QPR, MIT, No. 110, pp. 34-38, July, 1973.
- [3] J.A.Kong, "Microwave Remote Sensing of Ice and Snow," Proceedings of the URSI Commission II, Edited by E.Schanda, Inst. of Applied Physics Univ. of Berne, 1974
- [4] T.Schmugge, T.T.Wilheit, P.Gloersen, M.F.Meier, D.Frank, and I.Dirmhirm, "Microwave Signatures of Snow and Fresh Water Ice," Interdisciplinary Symposium on Advanced Concepts and Techniques in the Study of Snow and Ice Resources, November, 1973.
- [5] Gloersen,P., W.Nordberg, T.J.Schmugge, T.T.Wilheit and W.J.Cambell, "Microwave Signatures of First-year and Multi-year Sea Ice," J. of Geophysics Res. 78:3564, 1973.
- [6] D.Chu, "Machine Inversion of Remote Sensing Data," S.B.Thesis, Department of E.E., June, 1975

- [7] L.Tsang and J.A.Kong, "Effects of Surface Roughness on Microwave Remote Sensing," Res.Lab of Electronics, QPR, MIT, No.114, 1973
- [8] L.Tsang, "Emissivity of a Two Layer Random Medium," presented in QPR on C.I.T/J.P.L. Contract 953524 Covering period Nov. 25, 1974 to Feb. 25, 1975, March, 1975

APPENDIX II

MACHINE INVERSION
of
REMOTE SENSING DATA

by
Donald Chu

Submitted in Partial Fulfillment
of the Requirements for the
Degree of Bachelor of Science

at the

MASSACHUSETTS INSTITUTE OF TECHNOLOGY

June 1975

Signature of Author.....*Donald Chu*.....

Department of Electrical Engineering

May 11, 1975

Certified by.....*Jim Au Kong*.....
Thesis Supervisor

Accepted by.....
Chairman, Departmental Committee on Theses

MACHINE INVERSION

of

REMOTE SENSING DATA

by

Donald Chu

Thesis Advisor.....Jin-Au Kong

Associate Professor of Electrical Engineering

Massachusetts Institute of Technology

ABSTRACT

A computer program is described which interprets data according to a mathematical model. The program begins with a wide range for each of the unknown model parameters and tightens that range about the actual value of the parameter. Examples are presented which demonstrate the successes and the failings of the program. To show the utility of the program, emissivity measurements, published by T. Schmugge, are inverted according to J.A. Kong's Composite Model. The results agree with those obtained after much effort by M. Nagase.

Table of Contents

	page
1. Inversion.....	67
2. Problems and Principles.....	69
3. A Program.....	72
4. Performance.....	77
5. Inversion of Real Data.....	82
6. Summary.....	87
Program Operation	88
Acknowledgments	90
Bibliography	91

Table of Figures

	page
1. Limiting Curves.....	69
2. Error Dependence on ϵ'	70
3. Distinguishing Parameters.....	71
4. Emissivity Dependence on ϵ'	72
5. A Consequence of Nonlinearity.....	73
6. Changing Limits.....	75
7. How to Get the Best Fit.....	75
8. Emissivity versus Log Frequency.....	78
9. Bear Lake.....	84
10. South Cascade Lake.....	85
11. Steamboat Springs.....	86

INVERSION

A mathematical model relates an observed quantity with a set of parameters.

$$\text{observation} = f(\text{parameter}_1, \dots, \text{parameter}_n)$$

If the value of each parameter were known, the observed quantity could be found. In remote sensing, however, observations are made at different values of one parameter, such as frequency. Then the remaining parameters are determined from the observations. Operating a function in reverse this way is called inversion and involves the solution of $(n-1)$ simultaneous equations. Because these implicit equations can be complicated, inversion may be difficult.

The Composite Model was devised by J.A. Kong to interpret the thermal radiation from masses of snow and ice in terms of structural and dielectric properties.¹ Emissivity, the measured quantity, is modeled as a function of five parameters and frequency.

$$\text{emissivity} = f(\epsilon', \epsilon'', p, z_0, d, \omega)^*$$

From measurements at five frequencies, these parameters can, in principle, be determined. Exponential and polynomial expressions in the model, however, make the solution prohibitive.

* ϵ' and ϵ'' are the real and imaginary parts of the dielectric constant. p and z_0 relate to the magnitude and frequency distribution of scattering. d is the thickness of the ice or snow, and ω is the angular frequency.

It would be convenient to have a computer program to perform the inversion. The computer would take any model and a set of data and return values for the model parameters. Such a program would be particularly useful for evaluating models. If the parameters had physical significance, they could be measured independently and compared with the inverted results. A program is described here which uses an iterative process to take a wide range of parameter values and tighten it about an inverted value.

PRINCIPLES and PROBLEMS

The further a parameter is from its true value, the worse the prediction will fit the data. This is the principle behind the program. Two sets of limits, C_1 and C_2 , are chosen to generate curves, one above and one below the measurements. As the range of each parameter is decreased, the limiting curves approach the measured curve. By minimizing the difference between the prediction and the measurements, the program tries to bring each parameter closer to its proper value.

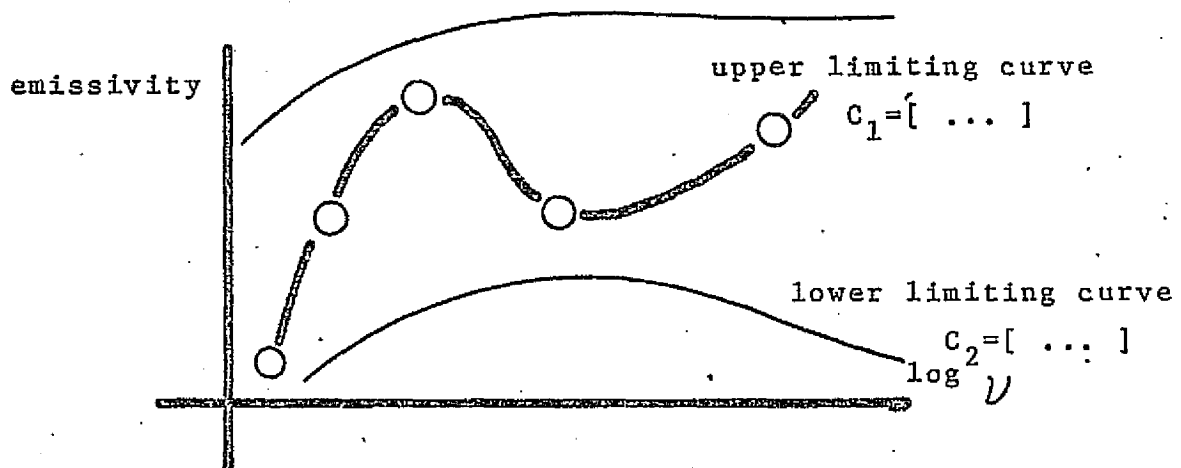


figure 1

There are two problems with this approach. First, a parameter may not yield the minimum error at its true value unless all the other parameters assume their actual values. Second, if changing either of two parameters has the same effect, how can one decide which parameter to change.

If the model were perfect, when all the parameters took on their true values, the variance between the prediction and data would be zero. Then, if one parameter, for instance ϵ' , were allowed to change, the minimum in the error would increase. Were a second parameter allowed to change, the minimum in the error curve would, in general, be shifted from the actual parameter value.

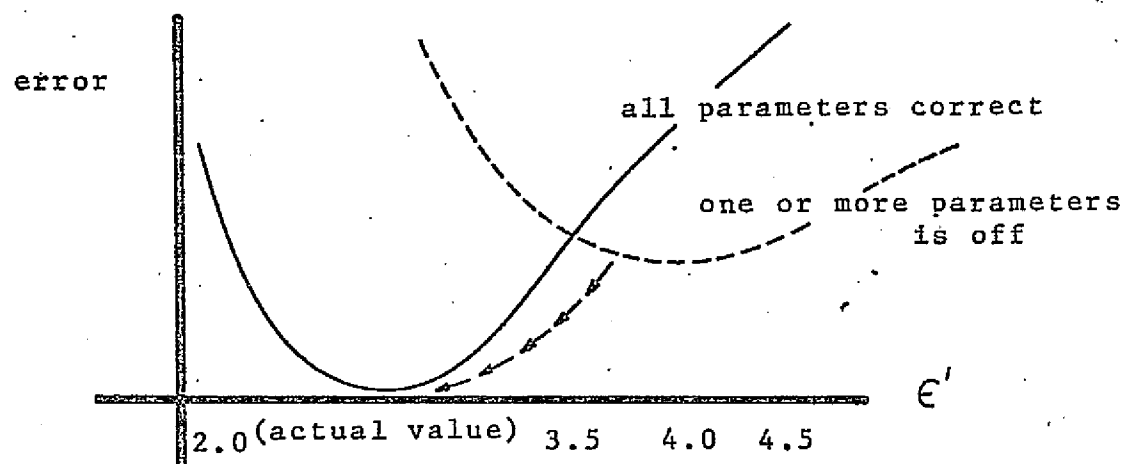


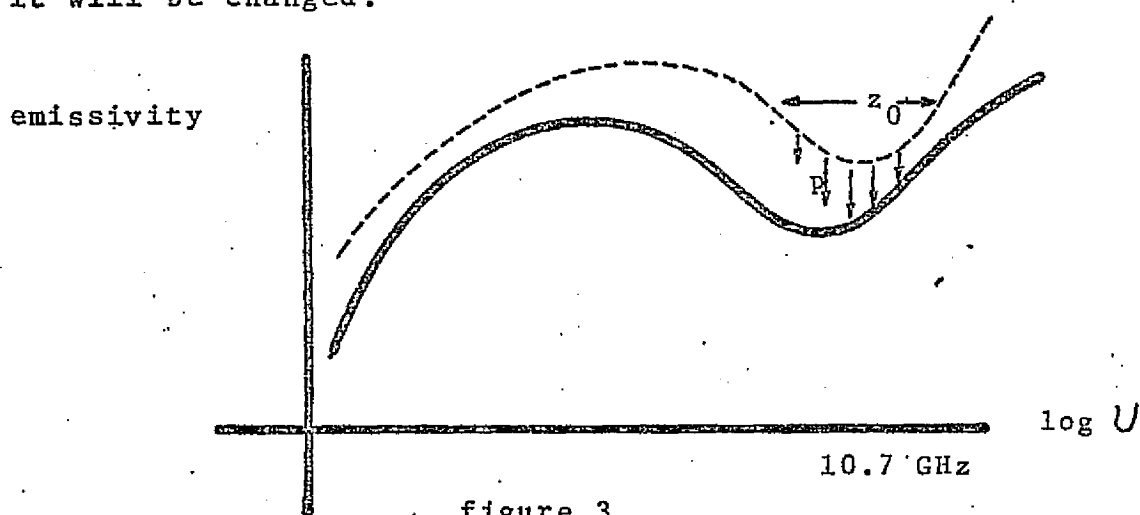
figure 2

During the inversion, none of the five parameter values is known. The error gives only a crude idea of where the parameter lies. Rather than declare the value of ϵ' to be four, the program uses the error to decide which of the limits is nearer the true value of ϵ' . As the parameters converge to their proper values, the minimum in the error curve should approach the true value of ϵ' .

The effects of the parameters generally overlap. For instance, decreasing the emissivity at 10.7 gigahertz may be done by increasing the magnitude of the scattering

curve or by translating it in frequency.² The first choice involves the parameter p while the second involves z_0 . Which should change?

To distinguish between them, the program applies a test. If changing p forces a limiting curve to cross the measured curve, p will not be changed. Then, z_0 is given an opportunity. If z_0 can improve the fit without crossing, it will be changed.



PROGRAM

Before beginning, the program must have the emissivities, their frequencies and any fixed parameters. For each of the remaining parameters, a range must be established. The limits are grouped into two sets which generate the upper and lower limiting curves. These sets of limits must satisfy two requirements. First, these curves may never cross the measurements; the upper curve must be higher than the measured emissivity at any frequency. Second, holding all other parameters constant, a limit from the upper curve, $C_1[j]$, must generate a curve higher than the one generated by its lower curve counterpart, $C_2[j]$; as a parameter varies from the upper curve limit to the lower one, the curve becomes lower.

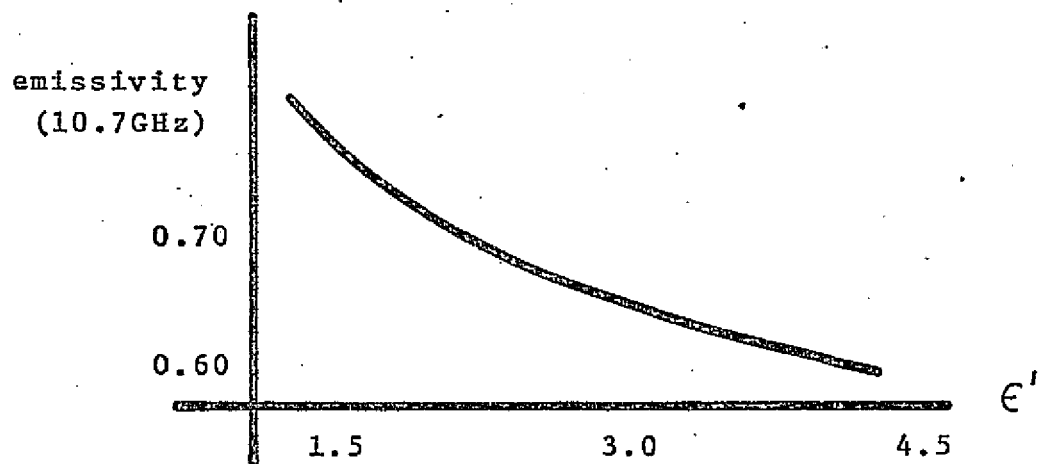


figure 4

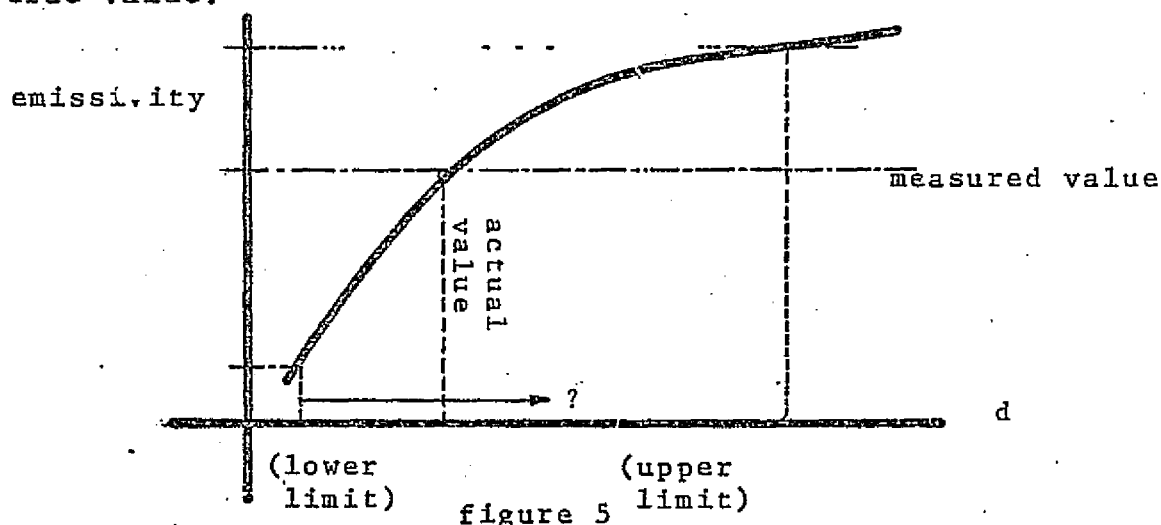
The model operates on both limits of each parameter to decide which better fits the measurements. Meanwhile, the other parameters are held constant midway between

their limits. To determine which limit fits better, the difference between the predicted emissivity, EM1, and the measured emissivity, em, is squared and summed over the five frequencies.

$$\text{VARI} = \sum_{i=1}^5 (\text{EM1}[i] - \text{em}[i])^2$$

The limit with the greater variance is changed. In matching the measurements, the program minimizes the squared error.

How much the limit should change is uncertain. Since emissivity depends nonlinearly upon each parameter, a parameter range cannot be decreased by any set fraction. If, for example, the lower limit of the ice thickness, d, were moved halfway across the range, the actual value of d would be left outside the new range. Each change must be checked to see that the new limit has not overshoot the true value.



A limiting curve should be able to approach the measured curve without ever crossing it. If the curves do cross, it would be because a parameter had bypassed its true value. This is the assumption behind a test to insure that the actual parameter value is still included in the new range. Before the old limit is changed, the proposed limit is tested to see that the curve it generates is everywhere above or below the measurements. If so, the sum of the absolute differences between the predicted and measured emissivities will equal the absolute sum of the differences.

$$\sum_{i=1}^5 |EML[i] - em[i]| = \left| \sum_{i=1}^5 (EML[i] - em[i]) \right|$$

If this crossing condition is met, the new limit is adopted. If not, the proposed limit will be moved back toward its old value.

The tentative limits change by incrementing the index L. If L were one, and the limit did not satisfy the crossing condition, L would become two, and the new limit would be tested.

Often it is not desirable to change the parameter range too drastically. The new limiting curve might be moved so close to the measured curve that subsequent parameters could not change without causing the curves to cross.

The initial value of L is called G and must be specified each time the program is run. When G is high, the limits change gradually, and the last parameter has much the same opportunity to converge to its true value as the first one has. $C_1[j]$ is the j^{th} element in the first set of parameter limits. $C_2[j]$ is its counterpart in the second set.

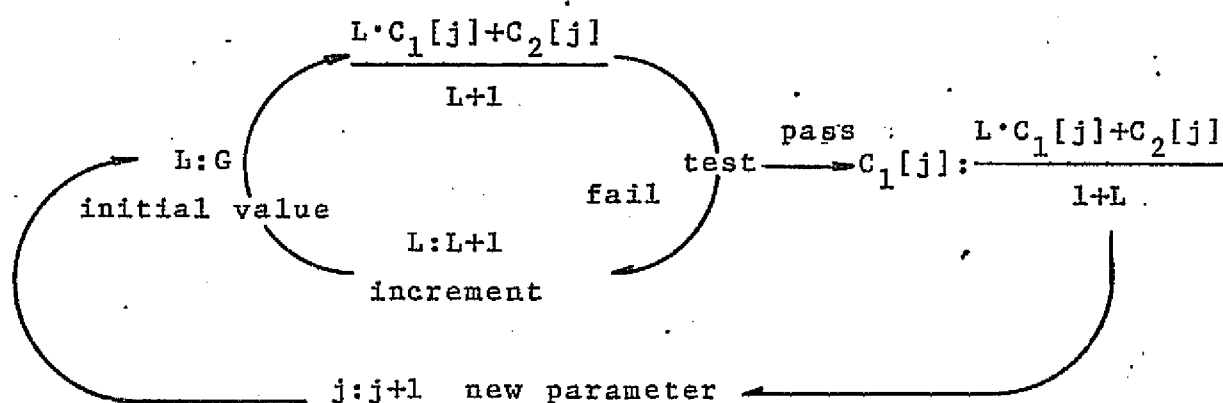


figure 6

The same way an area may be better filled using small squares, a curve may be better fit by approaching the parameter values in small steps.

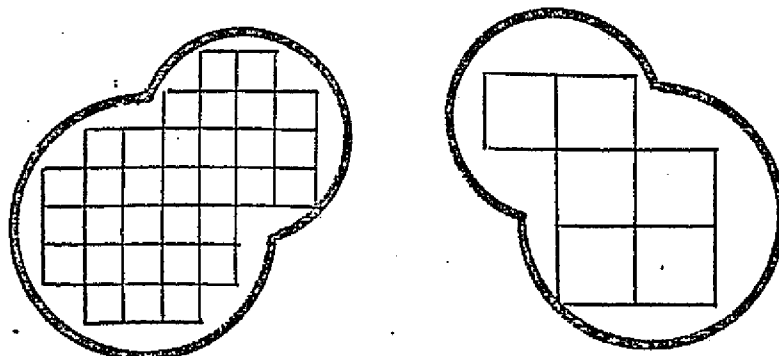
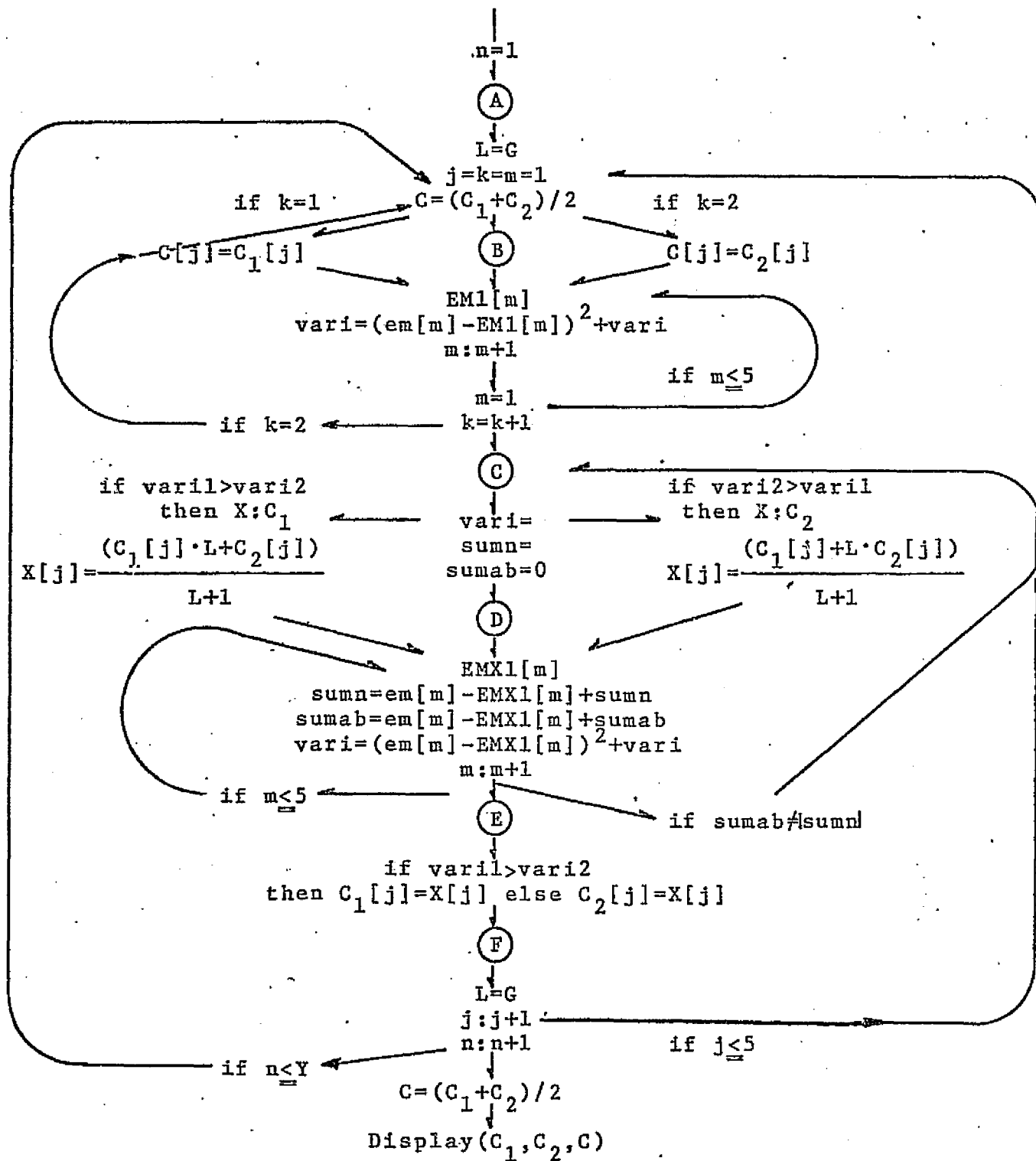


figure 7



FLOW CHART

PERFORMANCE

If this program is to be used with confidence, the inverted values it returns must be unique. No matter what the initial limits are or in what order the parameters change, the final result should be the same.

To examine the effects of the initial limits on the results, three sets of limits are inverted for the same set of emissivities. The first set, A, is symmetrical about the true parameter values. The second set, A', is asymmetrical. The third, A'', is identical to A' except for the range of d, ice thickness. In A'', the true value of the ice thickness is left outside the initial limits.

For the set of parameters

$\epsilon' = 3.0$ $\epsilon'' = 0.05$ $p = 1.0$ $z_0 = 0.1$ $d = 10$,

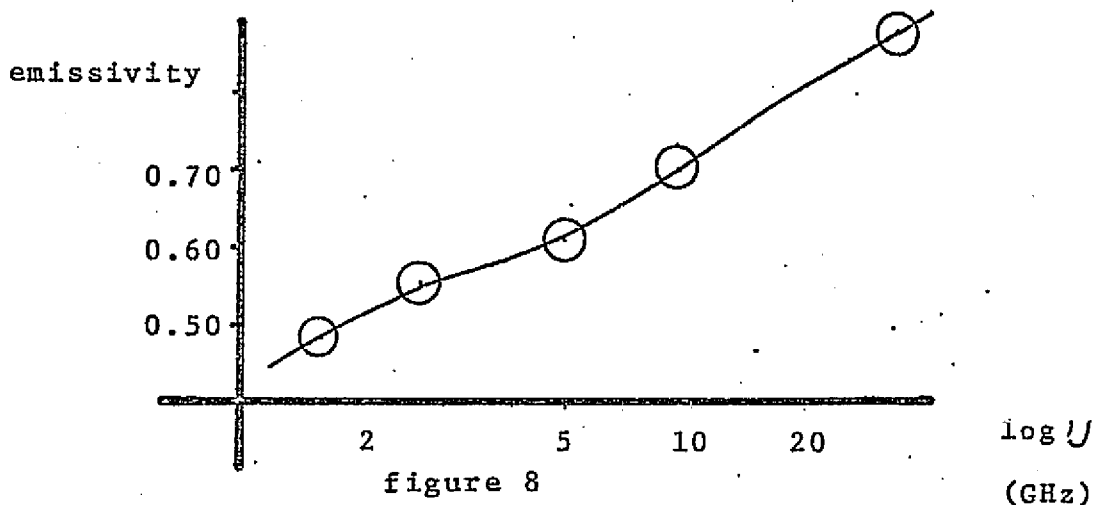
the Composite Model predicts these emissivities

0.483	@	1.4 GHz
0.537	@	2.7 GHz
0.607	@	5.0 GHz
0.705	@	10.7 GHz
0.853	@	37.5 GHz

	<u>Initial Limits</u>	<u>Final Limits*</u>	<u>midpoint</u>
A	2.5 < ϵ' < 3.5	3.21 < ϵ' < 3.33	3.27
	0.1 > ϵ'' > 0.01	0.06 > ϵ'' > 0.05	0.054
	0 < p < 2.0	1.02 < p < 1.27	1.15
	0.05 < z_0 < 0.15	0.13 < z_0 < 0.14	0.14
	20 > d > 1	12 > d > 9.6	10.7
A'	2.0 < ϵ' < 3.5	3.05 < ϵ' < 3.23	3.14
	0.1 > ϵ'' > 0.01	0.06 > ϵ'' > 0.05	0.056
	0.5 < p < 2.0	1.09 < p < 1.27	1.18
	0.09 < z_0 < 0.15	0.13 < z_0 < 0.14	0.14
	15 > d > 1	11 > d > 9.2	10

*Twenty iterations were performed with G equal to nine.

	<u>Initial Limits</u>	<u>Final Limits</u>	<u>midpoint</u>
A''	$2.0 < \epsilon' < 3.5$	$2.78 < \epsilon' < 2.96$	2.87
	$0.1 \approx \epsilon'' \approx 0.04$	$0.07 \approx \epsilon'' \approx 0.06$	0.068
	$0.5 < p < 2.0$	$1.08 < p < 1.27$	1.18
	$0.09 < z_0 < 0.15$	$0.12 < z_0 < 0.12$	0.12
	$9 < d^0 < 1$	$8. < d^0 < 7$	7.6



The final limits of the first two sets, A' and A'', are almost identical. They differ in the value of ϵ' , but the difference is small compared to the wide range across which ϵ' was originally allowed to vary. In this example, the midpoint values of A' are as good as or better than those of A. It seems there is no reason to believe that the initial limits should be symmetrical about the actual parameter values.

Three of the five parameters have been very accurately determined. The midpoints for ϵ'' , p and d are in error by only ten percent of their initial ranges. Values for ϵ' and z_0 , however, are much less accurate. For A, the midpoint of ϵ' is too high by more than twenty-five percent of its

initial range. z_0 is off by forty percent of its original range. For A', the error in the midpoint of ϵ' is only ten percent of the initial range, but z_0 is too high by almost seventy percent of its initial range.

This is the problem referred to earlier. During the inversion, a parameter is assumed equal to the average of its current limits. If this average is very different from the actual parameter value, the minimum error may occur when ϵ' is far from its true value. The program may be tricked into changing the better of the two limits. If the crossing condition then fails to detect the mistake, the new limit may leave the actual value of ϵ' outside the range. For this curve, it is not surprising that ϵ' and z_0 overshoot their true values. ϵ' and z_0 tend to their upper limits in order to match the very low emissivity at low frequency, and there is no point a limiting curve is likely to cross as these two increase.

The final limits for the set A" are quite different because of the incorrect range for d. Among the parameters, only ϵ' has a midpoint value correct to ten percent of its initial range. Low as it was to start with, the upper limit of d still decreased. There is no indication that this limit was improperly set. When establishing initial limits, it is safer to make the ranges broad.

So, for any set of limits that includes the actual value of each parameter, the results are the same. The

inversion should also be independent of the order in which the parameters are changed. The inverted results should be the same whether ϵ' is considered first or last. Starting with the set of initial limits, A' , the same set of emissivities is inverted with the parameters considered in two new orders. Again, twenty iterations are performed with G equal to nine.

The results for the three orders are almost identical. Again ϵ' and z_0 are too high. Again ϵ'' , p and d are very close to their true values. The only difference between the results is in ϵ' . There the difference between the midpoints is still small compared to the initial range. When G is equal to a large number like nine, the parameter order has little effect on the results.

<u>order</u>	<u>Final Limits</u>	<u>midpoint</u>
ϵ'' , p , z_0 , d , ϵ'	$3.07 < \epsilon' < 3.25$ $0.06 > \epsilon'' > 0.05$ $1.09 < p < 1.27$ $0.13 < z_0 < 0.14$ $11 > d > 9$	3.16 0.055 1.18 0.14 10
d , z_0 , p , ϵ'' , ϵ'	$3.25 < \epsilon' < 3.50$ $0.07 > \epsilon'' > 0.04$ $1.04 < p < 1.22$ $0.14 < z_0 < 0.15$ $15 > d > 6.7$	3.37 0.54 1.13 0.14 11
ϵ' , ϵ'' , p , z_0 , d	$3.05 < \epsilon' < 3.23$ $0.06 > \epsilon'' > 0.05$ $1.09 < p < 1.27$ $0.13 < z_0 < 0.14$ $11 > d > 9.2$	3.14 0.056 1.18 0.14 10

In this example, the inversion program determines ϵ'' , p and d very accurately, ϵ' less accurately and fails to determine z_0 . For another curve, the program determines ϵ' , p and z_0 very accurately and ϵ'' and d less accurately.

It seems that how well a particular parameter is determined depends upon the curve. In the first curve, there are very low values of emissivity at 1.4 and 2.7 gigahertz which force ϵ' and z_0 to be large. Because ϵ' and z_0 can increase without causing the limiting curves to cross any measurement, the crossing condition does not restrain them from overshooting their true values. In the second curve, there is a distinct drop in the emissivity at 19.4 gigahertz that pinpoints z_0 . There is nothing, however, to highlight d and ϵ'' . Their inverted values are less accurate.

$\epsilon' = 2.7$ $\epsilon'' = 0.1$ $p = 0.75$ $z_0 = 0.07$ $d = 30$

0.776	@	1.4 GHz
0.863	@	2.7 GHz
0.893	@	5.0 GHz
0.873	@	10.7 GHz
0.858	@	19.4 GHz
0.870	@	37.5 GHz

<u>Initial Limits</u>	<u>Final Limits</u>	<u>midpoint</u>
$3.5 \geq \epsilon' > 2.0$	$2.72 > \epsilon' > 2.54$	2.63
$0.01 < \epsilon'' < 0.1$	$0.07 < \epsilon'' < 0.08$	0.075
$2.0 > p > 0.1$	$0.98 > p > 0.75$	0.86
$0.15 > z_0 > 0.05$	$0.073 > z_0 > 0.061$	0.067
$0.1 < d < 50$	$42 < d < 48$	45

INVERSION of REAL DATA

To test the model itself, emissivity data can be inverted to determine the physical properties of a site. Then the deduced properties can be checked with what is known about the site.

T. Schmugge published an article including both measured emissivities and descriptions of three frozen lakes.³ Masato Nagase inverted this data using the Composite Model and correlated the parameter values he found with the properties of each site.⁴ The inversion process was long and tedious. Using this program, the inversion can be done in minutes.* The results agree closely with Nagase's and generate emissivities that differ from the measurements by less than 0.04 on the emissivity scale of zero to one.

In performing the inversion, the real and imaginary parts of the dielectric constants for the underlying water or moist soil are assumed to be known. The ice thicknesses for the thicker two lakes are also assumed. Emissivity approaches a constant value past a certain depth beyond which the program cannot distinguish different thicknesses. For Bear Lake, the thinnest of the three, the data is inverted for ice thickness. The ice is specified to be between one and fifty centimeters thick. The program narrows this range to thirteen to twenty-four centimeters.

*For five frequencies and five parameters, the time required per iteration is about forty seconds.

The actual thickness measured at the site was fifteen centimeters.

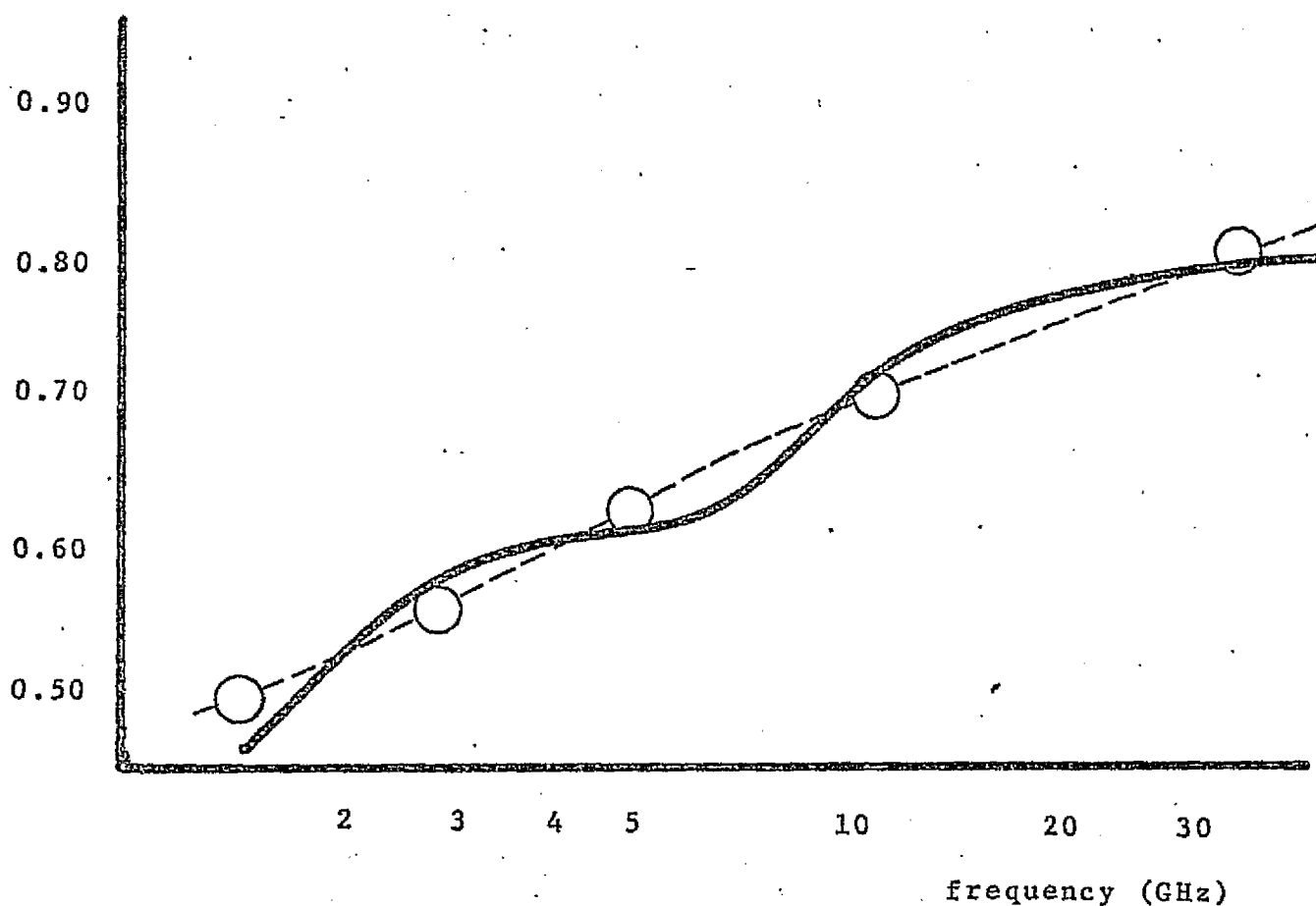
The emissivity data is given for six frequencies between 1.4 and 37.5 gigahertz. The emissivity at 37.5 gigahertz is measured separately for horizontal and vertical polarizations. For the sake of matching, the two points are reduced to one, their average.

Schmugge is unclear as to how the emissivity is measured at 19.4 gigahertz. At one point, he refers to that channel as horizontally polarized and scanning. In another place, he implies that that radiometer views from nadir, directly downward. Because the horizontally polarized emission is less intense than the vertically polarized emission when measured at an angle, the very low emissivity at 19.4 gigahertz suggests that this radiometer does scan. Since the model works only for observations made from nadir, the measurement at 19.4 gigahertz is ignored.

The initial limits assumed here and earlier are chosen to span the range of values found in ice and snow. The dielectric properties are reviewed by S. Evans in the Journal of Glaciology.⁵ The parameters p and z_0 are scattering parameters introduced by Gurvich.⁶ The choice of range for them is based on Nagase's experience which is documented in his thesis.⁷

emissivity

BEAR LAKE

parametermidpointNagase's
resultsEMIem ϵ'

3.16

3.2

0.497

0.459

 ϵ''

0.034

0.04-0.048

0.556

0.582

p

1.39

1.1-1.6

0.624

0.608

 z_0

0.083

0.08-0.12

0.702

0.720

d=15

18

0.813

0.800

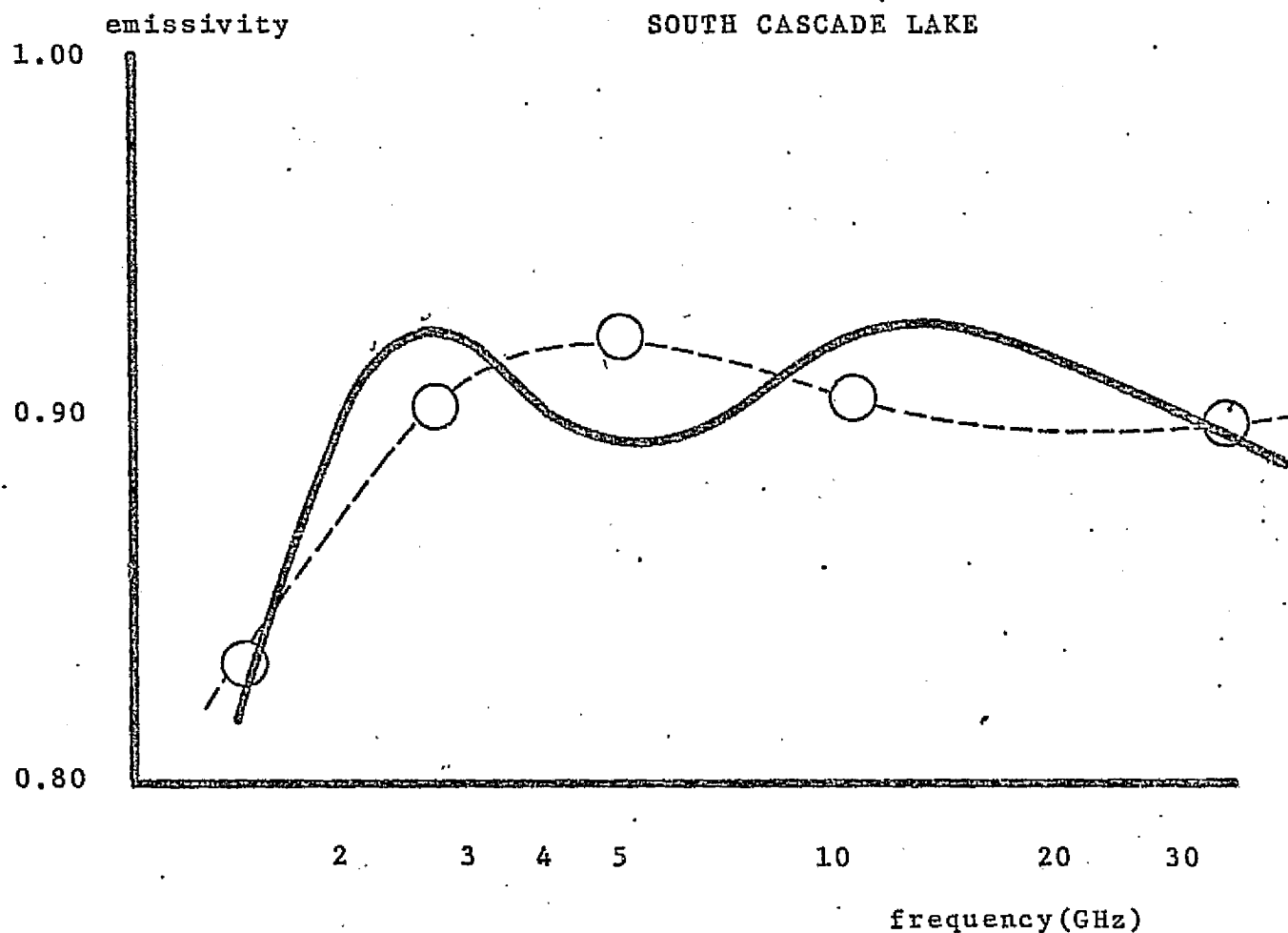
ewp=80

ewpp=80



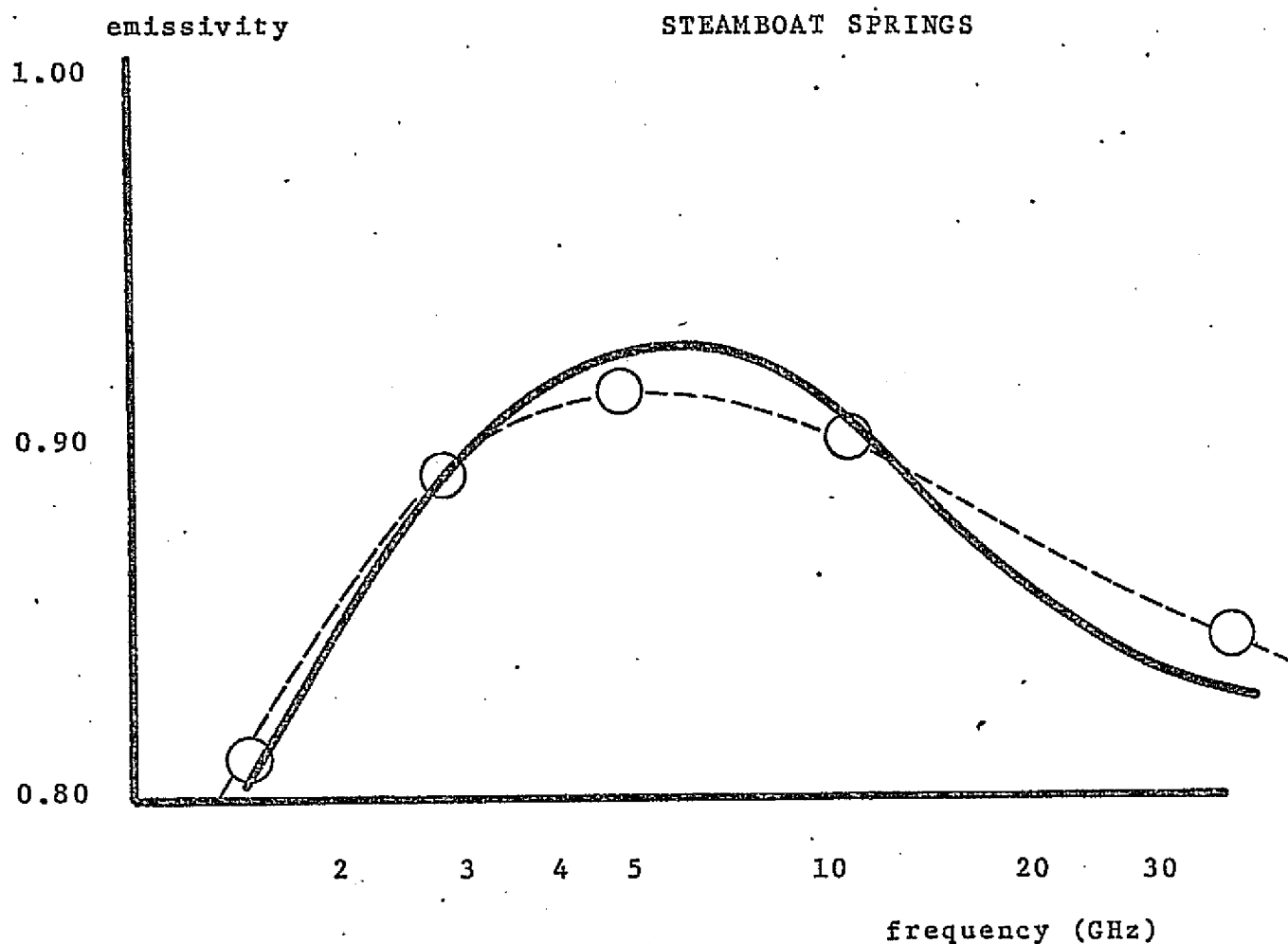
The circles represent the emissivities predicted using the midpoint parameter values.

figure 9



<u>parameter</u>	<u>midpoint</u>	<u>Nagase's results</u>	<u>EM1</u>	<u>em</u>
'	2.7	2.9-3.2	0.833	0.819
"	0.082	0.095-0.11	0.905	0.930
p	0.39	0.35-0.45	0.922	0.893
z_0	0.058	0.05-0.065	0.901	0.923
d=50			0.901	0.899
ewp=75				
ewpp=10				

figure 10



<u>parameter</u>	<u>midpoint</u>	<u>Nagase's results</u>	<u>EM1</u>	<u>em</u>
ϵ'	3.0	2.2	0.808	0.798
ϵ''	0.049	0.04	0.887	0.883
p	0.82	1.34-1.38	0.910	0.925
z_0	0.026	0.037-0.04	0.897	0.914
$d=80$			0.847	0.828
$ewp=70$				
$ewpp=40$				

The initial limits for these three inversions were $2.0 < \epsilon' < 3.5$, $0.1 \times \epsilon'' \times 0.01$, $0 < p < 2.0$, $0.01 < z_0 < 0.1$.

figure 11

SUMMARY

This general inversion scheme uses an iterative approach to tighten initially wide ranges about the actual values of a set of parameters. Limiting curves above and below the measured points are generated by two sets of parameter limits. These sets are made to converge subject to the condition that their limiting curves never cross the measurements. This criterion is intended to insure that the limits do not bypass the true parameter values. Because the parameters are considered sequentially, their order may affect the final results. To minimize this, the limits can be made to change gradually allowing each parameter equal opportunity to converge to its proper value.

The success of the program varies between sets of data. Some are better inverted than others. The quality of the inversion can always be checked by substituting the inverted values into the model and comparing the prediction with the measurements. The result, however good or bad, are consistent for different initial limits and parameter orders. In the final examples, the program demonstrates its utility by successfully repeating three difficult inversions of remote sensing data done by M. Nagase.

(C1) "set any fixed parameters."\$

(C2) ewp:ewpp:80\$

(C3) w:[0.9E5e9, 1.715e10, 3.142e10, 6.729e10, 2.356e11]\$

(C4) "Set the data to be matched.

This set of emissivities was generated by the
Composite Model for $\epsilon_{lp}=2.6$, $\epsilon_{lpp}=0.09$, $p=1.5$, $z_0=0.0005$, $d=0.15$.
Note that the unit of length used is the meter."\$

(C5) em:[0.602, 0.711, 0.802, 0.827, 0.782]\$

(C6) "Here is a key to interpreting the parameter array.

[ϵ_{lp} , ϵ_{lpp} , p , z_0 , d]
Set the initial limits."\$

(C7) c1:[2.0, 0.1, 0, 0.0001, 0.2]\$

(C8) c2:[3.5, 0.01, 2.0, 0.001, 0.01]\$

(C9) "Batch the program."\$

(C10) batch(zchu,20,dsk,kong);

(C11) FIT(G,Y):=BLOCK(KEEPFLOAT:TRUE,

N:1,

ZERO,

L:G,

J:K:M:1,

I,

C:(C1+C2)/2,

IF K=1 THEN C[J]:C1[J] ELSE C[J]:C2[J],

NTP: EV(REALPART(SQRT(EMP+MI*EMPP))), EVAL, NUMBER),

NTPP: EV(IMAGPART(SQRT(EMP+MI*EMPP))), EVAL, NUMBER),

NIP: EV(REALPART(SQRT(C11+MI*C22))), EVAL, NUMBER),

NIPP: EV(IMAGPART(SQRT(C11+MI*C22))), EVAL, NUMBER),

R01: EV(SQRT(((NIP-1)**2+NIPP**2)/

((NIP+1)**2+IP**2))), EVAL, NUMBER),

R12: EV(SQRT(((NIP-NTP)**2+(NIPP-NTPP)**2)/

((NIP+NTP)**2+(NIPP+NTPP)**2))), EVAL, NUMBER),

VARI: 0,

C,

A: EV(R12*EXP(-2*NIPP*C25*MI[I]/3.E8), EVAL, NUMBER),

Q: EV(2*NIP*C24*MI[I]/3.E8, EVAL, NUMBER),

R: EV((C1**2+A**2)/(1+R01*A)**2), EVAL, NUMBER),

S: EV((C2**2+Q/4)*(1-R01**2)**2

(1-EXP(-4*NIPP*C25*MI[I]/3.E8))/(1+Q**2), EVAL, NUMBER),

EN1: EV(1-R-S, EVAL, NUMBER),

DIF: EV(EN1-EN1, EVAL, NUMBER),

SQU: EV(DIF**2, EVAL, NUMBER),

VARI: EV(VARI+SQU, EVAL, NUMBER),

N: N+1,

IF L<=5 THEN GO(B) ELSE K:1,

IF K=1 THEN VARI1:VARI ELSE VARI2:VARI,

K:K+1,

IF K=2 THEN GO(A),

K:1,

C,

IF VARI1>VARI2 THEN X:APPEND(C1,[I]) ELSE X:APPEND(C2,[I]),

IF VARI1>VARI2 THEN C[J]:(L*C1[J]+C2[J])/(L+1)

ELSE C[J]:(C1[J]+L*C2[J])/(L+1),

REPRODUCIBILITY OF THE
ORIGINAL PAGE IS POOR

```

((NIPX+1)**2+NIPX**2)), NUMER),
RX12: EV(SQRT(((NIPX-NTX)**2+(NIPX-NTPP)**2)/
((NIPX+NTX)**2+(NIPX+NTPP)**2))), NUMER),
SUMN: SUMAB:0,

```

D,

```

AX: EV(IX12*EXP(-2*NIPX*X[5]*W[N]/3.E8), NUMER),
QX: EV(7*NIPX*X[4]*W[N]/3.E8, NUMER),
RX: EV((RX01**2+AX**2)/(1+(RX01*AX)**2), NUMER),
SX: EV((X[3]*QX/4)*(1-EXP(C1**2)*
(1-EXP(-4*NIPX*X[5]*W[N]/3.E8)))/(1+QX**2), NUMER),
EMX1: EV(1-RX-SX, NUMER),
DIFX: EV(EMX1-EP[N], NUMER),
SUM : EV(SUM +DIFX, NUMER),
SUMAB: EV(SUMAB+ABS(DIFX), NUMER),
M: M+1,
IF M<=5 THEN GO(D) ELSE M:1,
IF SUMAB=ABS(SUMN) THEN GO(E),
IF L>10 THEN GO(F),
L:L+1,
GO(C),

```

REPRODUCIBILITY OF THIS
ORIGINAL PAGE IS POOR

E,

```

IF VARI1>VARI2 THE C1:Y ELSE C2:X,

```

F,

```

, RENVALUE(VARI, VARI1, VARI2),
L:G,
J:J+1,
IF J<=5 THE GO(A) ELSE J:1,
N:N+1,
IF N<=Y THE GO(ZERO),
C:(C1+C2)/2,
DISPLAY(C1, C2, C))$

```

(D12)

BATCH DO E

(C13) Let the program perform ... Whoops . Excuse me.??

(C13) "I forgot the quotation mark. As I was saying,
Let the program perform five iterations with
the initial value of L equal to one."\$

(C14) "It should return the values of the parameters given in command (

(C15) fit(1,5);

RPART FASL BSK MACSYM BEI G LOADED
LOCAL G DO E

C1 = [2.65625, 0.0859375, 1.5, 2.5E--

C2 = [2.75, 0.083125, 1.5625, 5.5000001

C = [2.703125, 0.08453125, 1.53125, 4.00000

(D15)

DO E

(C16) "The exact value of C is [2.6, 0.09, 1.5, 0.0005, 0.15]."\$

(C17) ^2

5647) .IOT 1,1 :logout

HL ITS 921 CO SOL 7 FREE. 21:00:57

ACKNOWLEDGMENT

I first thank Professor Jin-Au Kong for generously giving his time to advise me in this effort.

I also thank Masato Nagase, who has helped me throughout the work on ice, and Eni Njoku, who pointed out what requirements an inversion program must satisfy.

This program was realized using MACSYMA, the symbolic manipulation system developed by the Mathlab Group of Project MAC, MIT. Their work is sponsored by the Advanced Research Projects Agency, Department of Defense, Office of Naval Research under contract number N00014-70-A-0362-0001.

BIBLIOGRAPHY

1. J.A. Kong, "Microwave Remote Sensing of Ice and Snow", Proceedings of the URSI Commission II, Specialist Meeting on Microwave Scattering and Emission from the Earth, E.Schanda-editor, Institute of Applied Physics, University of Bern, pp. 239-243, 1974.
2. *ibid.*
3. T. Schmugge, T.T. Wilheit, P. Gloersen, M.F. Meier, D. Frank, and I. Dirmhirn, "Microwave Signatures of Snow and Fresh Water Ice", Interdisciplinary Symposium on Advanced Concepts and Techniques in the Study of Snow and Ice Resources, National Academy of Sciences, Washington, D.C., pp. 551, November 1973.
4. M. Nagase, Studies of the Model for Microwave Remote Sensing of Ice and Snow, S.B. thesis, Department of Electrical Engineering, MIT, Cambridge, MA, June 1975.
5. S. Evans, "Dielectric Properties of Ice and Snow-A Review", Journal of Glaciology, Cambridge, England, volume 5, number 42, pp. 773-792, October 1965.
6. A.S. Gurvich, V.I. Kalinin and D.T. Matveyev, "Influence of the Internal Structure of Glaciers on Their Thermal Radio Emission", Izvestia, Atmospheric and Oceanic Physics, volume 9, number 12, pp. 1247-1256, 1973.
7. M. Nagase, *op. cit.*

APPENDIX III

PASSIVE MICROWAVE REMOTE SENSING OF
MOISTURE IN SANDLIKE SOILS

by Boucar Djermakoye

Submitted in partial fulfillment of the requirements
for the degree of
Bachelor of Science

at the

MASSACHUSETTS INSTITUTE OF TECHNOLOGY

June 1975

Signature of Author... *Boucar Djermakoye*
Department of Electrical Engineering June 1975
and Computer Science
Certified by... *John An Kong*
Thesis Supervisor (Academic)
Accepted by.....
Chairman
Departmental Committee on Graduate Students

I dedicate my thesis to my grandfather, the late
Djermakoye SaïDou.

Acknowledgement

I would like to thank Professor J. A. Kong for the constant help and encouragement that he gave me on this thesis.

I also would like to thank E. Njoku and L. Tsang for the helpful discussions which I had with them.

Table of Contents

List of Figures	96
Abstract	98
Introduction.	99
The Dielectric Constant	102
Frequency Dependence	102
Water Content Dependence	106
Temperature Dependence	109
Thermal Emission and Radiation	110
Blackbody Radiation	110
Emission by a Surface	112
Different Approaches to Surface Sensing by Radiative Transfer Equations	115
A Half-Space Model	115
A Generalized Half-Space Model	120
A Skin Depth Approach	123
Proposed Model and Approach	126
Soil Mechanics Considerations	126
Fresnel Reflection Coefficients	133
Computer Results	139
Possible Future Investigation	148
Data from Nimbus 5	152
Data from Nimbus 5	152
Ground Truth Data	153
Conclusion	158
References	178

2
C

List of Figures

- Figure 1. Loss tangent and polarizable dielectric constant vs frequency.
- Figure 2. Dielectric relaxation spectrum of water.
- Figure 3. Behavior of the dielectric constant in wetted soil.
- Figure 4. Reflection of an electromagnetic wave at the boundary of a half-space.
- Figure 5. Variation of the electric field at the air-soil interface.
- Figure 6. Experimental results of the behavior of brightness temperature vs volume percent of water.
- Figure 7. Element of soil in which vertical flow takes place.
- Figure 8. Grain size distribution of experimental sand sample.

Figure 9. Rayleigh probabilistic distribution.

Figure 10. Predicted moisture profile in sandlike soil.

Figure 11. N layer-medium with a characteristic transition region Δx .

Figure 12. Moisture pulse propagation in a sandlike soil medium.

Abstract

Variation of soil characteristics with water content, soil type and its electrical properties are investigated by passive microwave remote sensing. A theoretical model is developed to distinguish the parameters or assess the possibility of distinguishing these parameters from wavelengths ranging from $\lambda = 100$ cm to $\lambda = 1$ cm.

Radiometer measurements are frequency, angle and polarization dependent. The theoretical model consists of an N layer medium on which various types of moisture profiles are mapped simulating surface water distributions in desert areas.

The results are expressed in brightness temperature and are compared with available data from the Nimbus 5 satellite. The validity and limitations of the model are examined as well. It was found that moisture content in soils with sand-like composition was not as easily detectable as the results of controlled experiments showed.

Introduction

The field of passive remote sensing is at the same time very old and very young. Very young if we remember that the first radiometer was acknowledged by R. H. Dicke in 1946 in a science revue entitled "The measurement of thermal radiation at microwave frequencies" in which Dicke explains that the behavior of a microwave switching circuit that compares the thermal radiation power emitted from an object with that emitted from an internal reference source. And yet, a field very old if one takes notion of all the variety of applications, not all fully exhausted, that were derived from it. Without involving ourselves with the whole list we may just mention a few applications of remote sensing such as measurements of ocean surface dynamics, ocean salinity, atmospheric temperature; detection of sea ice, storm cells, agricultural crops and soil moisture content. We shall be interested with the latter feature.

Whereas meteorologists are interested in tracking the moisture content of soil over large areas to learn more about mass and energy exchange at the air-soil interface, and hydrologists in the same behavior to predict runoff, our more modest task is to try to determine its presence in dry areas of mostly sandlike composition.

..

Standing between the almost rainfree Sahara desert and the rain favored regions of the tropical zone, the Sahel region meets the definition of a transition area, and as such, displays many of the characteristics we intend to study.

It seems thus far that we are nowhere limited in the analysis of thermal radiation except within the frequency spectrum. Dicke makes a point of confining himself to microwave frequencies, and yet remote sensing at visible and infrared wavelengths has contributed useful data. However, it was noticed that the surface of the earth could not be observed when obscured by cloud cover, nor could it be observed during nighttime, except perhaps with "cryogenically cooled far-infrared sensors". Hence the "operational utility" of these sensors is limited since most of the earth's surface is covered by clouds or in darkness. In contrast cloud cover is much more transparent at microwave frequencies which make microwave sensors more insensitive to weather or sunlight.

The only possible unattractive feature of microwave sensing is the poor spatial resolution associated with it. The resolution of optical and infrared sensors will generally be better than that of microwave sensors since high resolution can be achieved only with antennas large relative to wavelength. This is not a real problem, however, if the regions of interest are widespread enough such as ours.

But more determining factors are involved in our analysis (as we shall see later) such as the sensitivity of the microwave radiometer, which as given by R. H. Dicke is:

$$\Delta T = 2T_N / \sqrt{B\tau}$$

T_N = absolute system noise temperature

B = RF noise bandwidth

τ = postdetection integration time.

ΔT is the variation in brightness temperature where brightness temperature is related to the surface temperature by $T_B = e T_s$ (e = emissivity at the surface).

An even more important factor is the drainage dynamics of water in sandlike soils. To understand better the phenomena we will resort to concepts in soil mechanics.

Among the various techniques used to determine the brightness temperature or correspondingly the emitted power from the earth, radiative transfer equations are often the ones referred to. However, great care must be taken in applying them, since they are applicable in certain cases only. On the other hand through the Fresnel reflection coefficient approach we find more flexibility and dynamic range. We shall nonetheless investigate the different possible approaches and choose the most appropriate for our particular analysis.

The Dielectric Constant

Since the properties of soils are our major concern, we are thereby inclined to look upon the characteristics of their dielectric constants which depend on frequency, water content, and temperature.

Frequency Dependence

The frequency dependence of the dielectric materials is linked to the way they react to an electric field. The charge carriers within them are capable of being displaced by the latter and give rise to polarization. There are many kinds of polarizations^[1] such as electron polarization α_e , atomic polarization α_a , orientation or (dipole) polarization α_d , space charge or interfacial polarization α , and resonance polarization α_r . We limit ourselves to the effect of the electronic displacement and orientation polarization. The Clausus-Mosotti equations expresses the relationship between the dielectric constant and the polarization as follows:

$$\frac{\epsilon - 1}{\epsilon + 2} = \frac{4\pi}{3} n\alpha$$

where n is the number of molecules, and $\alpha = \alpha_e + \alpha_d$.
 ϵ is the dielectric constant.

REPRODUCIBILITY OF THE
ORIGINAL PAGE IS POOR

When applied to moist soils the dielectric constant is allowed to be complex: $\epsilon = \epsilon' + i \epsilon''$. The imaginary part of the dielectric constant governs the dissipative feature of the soils. In Figure 1, $\tan \delta$ is the loss tangent $\tan \delta = \epsilon''/\epsilon'$ and τ is the relaxation time (in the case of electron displacement alone it can reach the order of $\tau = 10^{-15}$ s).

The dependence of the dielectric constant (soils) on frequency is related to the dielectric relaxation spectrum of the water contained within it.

When comparing the relaxation of water in bulk and moist soil, Figure 2 and Figure 3^[2], we observe similar distributions. The only difference is that "the maximum dielectric loss of relaxation in soils is displaced to lower frequency and the relaxation occurs over a narrower frequency band in soils than in bulk water" as noted by P. Hoesktein and A. Delaney in a paper treating with the dielectric properties of soils^[3].

An analytical expression was found by Cole and Cole (1941) for the relaxation of soil water which is the following.

$$\epsilon(\omega) = \epsilon_{\infty}' + \frac{\epsilon_s' - \epsilon_{\infty}'}{1 + (i\omega\tau)^{1-\alpha}}$$

the subscript ∞ and s refer to values of ϵ at frequencies such that $\omega\tau \gg 1$ and $\omega\tau \ll 1$. τ is the relaxation

$\epsilon, \tan \delta$

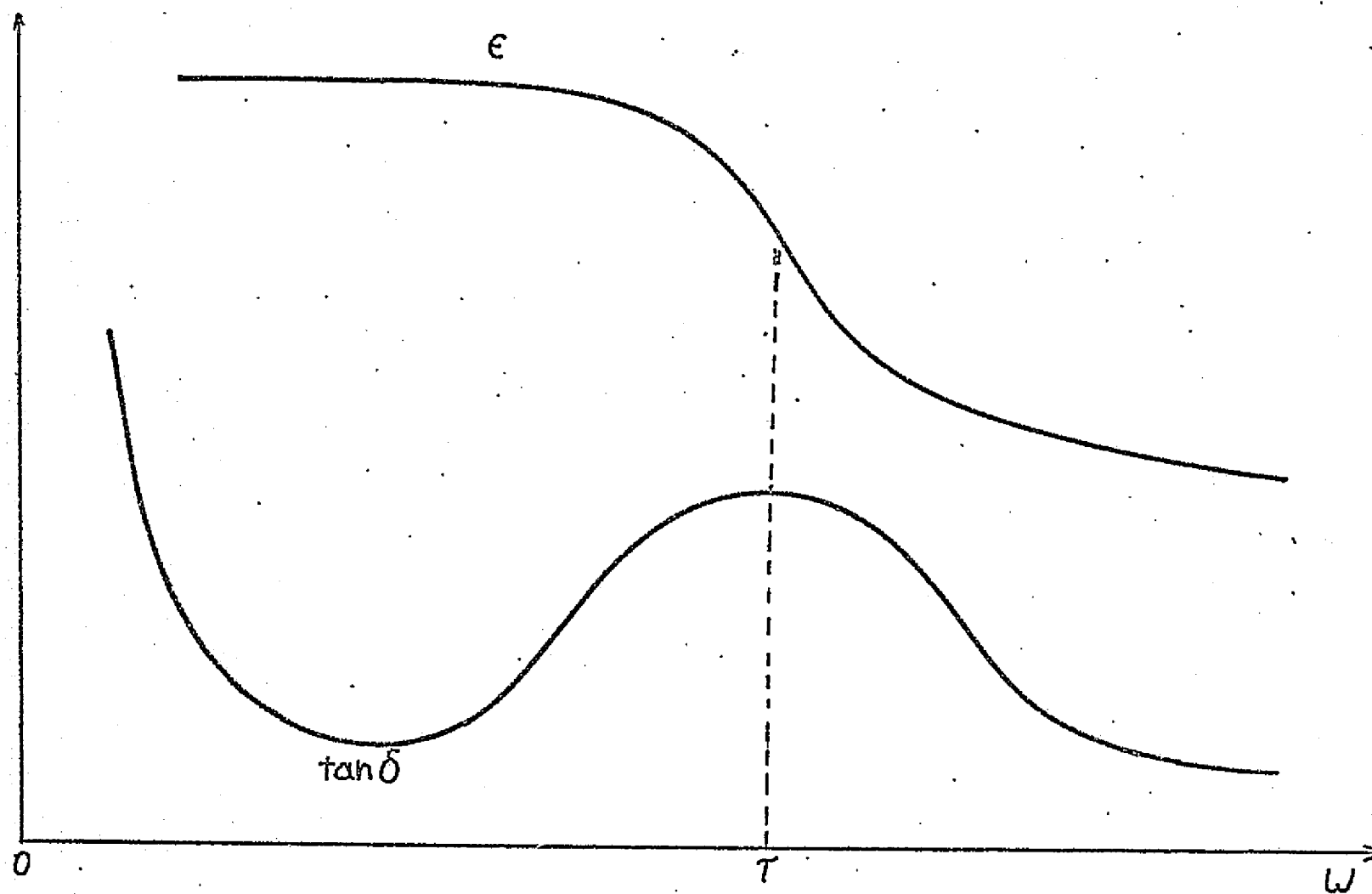


Figure 1.

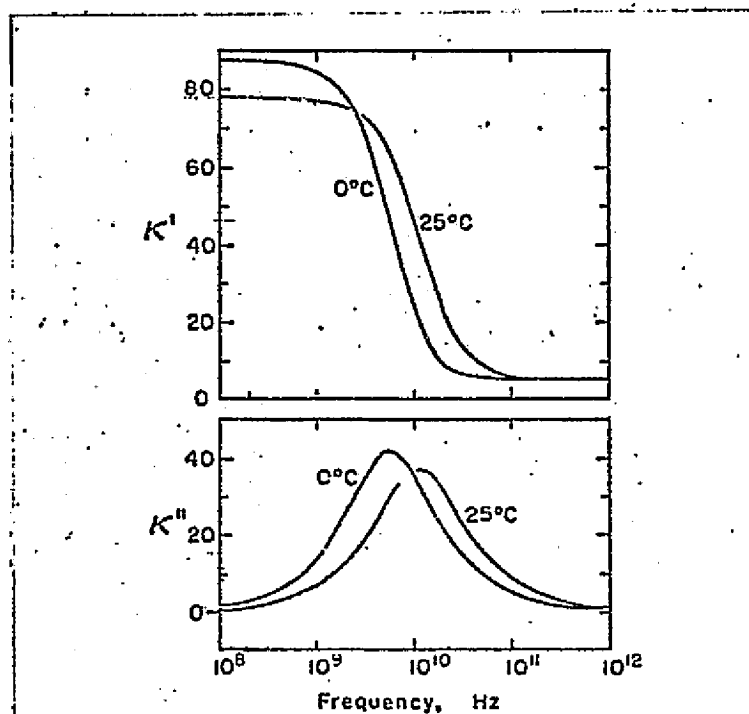


Figure 2.

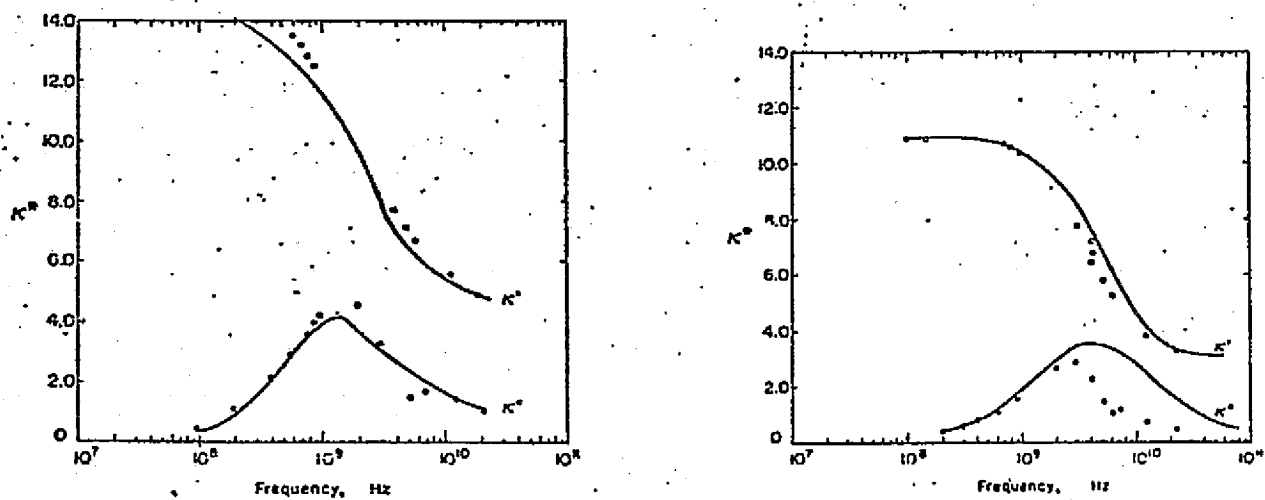


Figure 3.

time. α is a parameter showing the distribution of relaxation times.

When mixing water and soils without previously knowing the resulting value of α , it is easier to assume the separate values of α_w (water) and α_s (soil) and obtain the dielectric constant of the mixture by using

$$\epsilon(w) = \epsilon_{w\infty}' + \frac{\epsilon_{ws}' - \epsilon_{s\infty}'}{1 + (i\omega\tau_w)^{1-\alpha_w}} + \epsilon_{s\infty}' + \frac{\epsilon_{ws}' - \epsilon_{s\infty}'}{1 + (i\omega\tau_s)^{1-\alpha_s}}$$

where τ_w and τ_s are the two different relaxation times, α_w , α_s represent the respective dispersion factor. (Actually for water $\alpha_w = 1$.) This equation suffers the inconvenience of not indicating the proportions in which the dry soil and water might be mixed.

Water Content Dependence

In that respect, mixture formulas are more informative and give us a better gauge on the effect of water content on the dielectric constant. It is useful, however, before reviewing some of these formulas to give ourselves some definitions^[4] regarding the terminology that will be used later. For instance, what is usually meant by moisture content is the ratio of the weight of the water to the weight

of the dry soil: water saturation is the ratio of the volume of water in the pores to the volume of the pores (if we assume sandlike soils then each grain of sand can be considered as having a spherical geometry. Within a configuration of four adjacent spheres the spacing in the middle can be assumed to be a "pore" whose size depends only upon the radius of the spheres). Lastly, volume fraction of water is just the ratio of the volume of water filling the pores to the total volume of the material.

It is hard to find a single mixture formula that one can apply in all circumstances. Each one of them is only valid for either a particular frequency range, or mixtures having more than two components where the difference between the dielectric constant may vary a great deal.

Tarkhov's formula gives an average value of ϵ for water bearing materials.

$$\frac{\epsilon - 1}{\epsilon + 2} = \frac{\epsilon_1 - 1}{\epsilon_1 + 2} \theta_1 + \frac{\epsilon_2 - 1}{\epsilon_2 + 2} \theta_2 + \dots + \frac{\epsilon_n - 1}{\epsilon_n + 2} \theta_n$$

where $\theta_1, \theta_2, \dots, \theta_n$ are the volume fractions of the components ($\theta_1 + \theta_2 + \dots + \theta_n = 1$). $\epsilon_1, \epsilon_2, \dots, \epsilon_n$ are the respective dielectric constants. For large differences between dielectric constants we have Lichtehicker's formula

$$\log \epsilon = \theta_1 \log \epsilon_1 + \theta_2 \log \epsilon_2.$$

For mixtures with only two components (soil, water) at microwave frequencies, we have Pierce's formula

$$\epsilon = \epsilon_w + \frac{f_1 (1 - F)}{1 - f_1 F} (\epsilon_s - \epsilon_w).$$

ϵ_s = soil dielectric constant

ϵ_w = water dielectric constant

f_1 = volume fraction of soil

F = adjustable parameter

But of all the formulas the one that showed the best experimental [5] matching was Wiener's formula

$$\epsilon = \frac{\epsilon_s f_s U + \epsilon_w f_w}{f_s U + f_w} \quad (W)$$

f_s = volume fraction of the two components $f_s + f_w = 1$

f_w = volume fraction of the two components $f_s + f_w = 1$

ϵ_s = dielectric

ϵ_w = dielectric

$$U = \frac{\epsilon_s + F}{\epsilon_w + F} \quad \text{where } F \text{ is an adjustable parameter.}$$

Temperature Dependence

The third parameter, which affects the dielectric constant is temperature. No correlation between the temperature behavior of water in bulk and that in moist soils can be made since in the first case we have $d\epsilon'/dt < 0$ and in the second $d\epsilon'/dt > 0$.

However, a more quantitative relationship between the dielectric constant and temperature resides in the Debye formula [6]:

$$\frac{\epsilon - 1}{\epsilon + 2} \cdot \frac{M}{\rho} = \frac{4}{3} N\pi \left(\alpha_e + \frac{\mu^2}{3kT} \right).$$

M = molecular weight of the material

ρ = density

N = Avogadro's number

α_e = polarizability caused by electron displacement

μ = average dipole moment

T = temperature in Kelvin.

Thermal Emission and Radiation

D. H. Staelin, reports the physics of thermal emission [7] as follows: "All solids, liquids, gases and plasmas are coupled electromagnetically to their surroundings and hence absorb and emit electromagnetic radiation over a spectral region ranging from radio frequencies to optical frequencies and beyond. The emission results primarily from the thermal motion of the charged particles which comprise the material, and depends upon the temperature of the material and upon the degree of coupling between the material and the electromagnetic field".

Blackbody Radiation

If we consider the case of perfect coupling to the electromagnetic field such as a perfect absorber blackbody, then the radiation intensity is given by Planck's radiation law:

$$I = \frac{2hf^3}{c^2 (e^{hf/kT} - 1)} \text{ watts m}^{-2} \text{ Hz}^{-1} \text{ ster}^{-1} \quad (1)$$

where

h = Planck's constant

f = frequency

k = Boltzmann's constant

T = temperature.

Between the radio region and frequencies up to $\sim 10^{11}$ Hz and for temperature greater than 5K (which is our case), equation (1) can be reduced to the Rayleigh-Jeans Law:

$$I \approx \frac{2kT}{\lambda^2} \text{ watts m}^{-2} \text{ Hz}^{-1} \text{ ster}^{-1}$$

λ = wavelength in meter.

From this linear relationship between the intensity and temperature we get a similar relationship between the power P intercepted by an antenna (microwave sensor) and the temperature of a blackbody. We then have

$$P = kT \text{ watts Hz}^{-1}$$

or

$$T_B = P/kB$$

where B is the bandwidth of the frequencies considered.

T_B is called brightness temperature.

Emission by a Surface

We can associate a brightness temperature to a surface (earth, air boundaries). "If the intervening atmosphere between those surfaces and the radiometer is lossy then the radiation emitting from them will be somewhat attenuated and the lossy atmosphere itself will emit thermal radiation. A radiometer would thus yield an apparent absolute temperature T_B given by the radiative transfer equation" [8].

$$T_B = t(e T_O + \Gamma T_R) + (1 - t)T_S \quad (2)$$

t = atmospheric transmissivity $(0 \leq t \leq 1)$

e = emissivity of object $(0 \leq e \leq 1)$

T_O = absolute temperature of the surface

Γ = power reflectivity of surface $(0 \leq \Gamma \leq 1)$

T_R = equivalent absolute radiation temperature
incident on surface

T_S = absolute temperature of lossy atmosphere between
surface and radiometer.

One of the interesting parameters of equation (2) is the emissivity e . By applying the principle of detailed balance [9] we get that: (or reciprocity)

$$E = 1 - r$$

$$r = |R|^2$$

where if we consider a half-space such as in Figure 4 with an incident electromagnetic wave, R is the reflection coefficient and r is the reflectivity. R can be expressed as

$$R = \frac{1 - \left(\frac{\mu_o \epsilon}{\mu_o \epsilon_o} \right)^{1/2}}{1 + \left(\frac{\mu_o \epsilon}{\mu_o \epsilon_o} \right)^{1/2}}$$

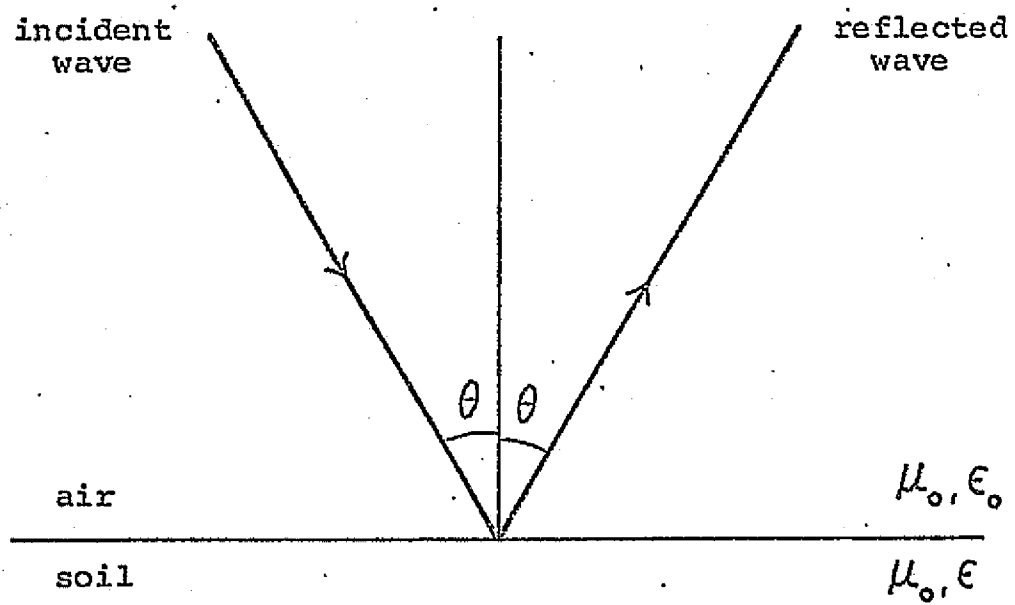


Figure 4.

Different Approaches to Surface Sensing by

Radiative Transfer Equations

As mentioned earlier, the brightness temperature is due to emission of radiation of earth surfaces. However, the word surface is ambiguous. Is the surface the only part that contributes to the emission of the earth? Certainly not since the whole subsurface region adds to the total emission. To determine the depth at which the emission of radiation is negligible we refer to "reciprocity" and examine again the case of an incident electromagnetic wave. The probing depth (or equivalently, the depth just mentioned above) would be the one at which the electromagnetic wave would be totally attenuated.

Half-Space Model

It is through such an approach that K. F. Kunzi modeled the brightness temperature of snow and ice. Hopefully, Kunzi's model for snow and ice^[10] will enlighten us in soil moisture sensing. He uses the radiative transfer equation:

$$T_B(^{\circ}K) = E(\nu) \left(\int_0^{\infty} T(x) \alpha(x, \nu) e^{-\int_0^x \alpha(x', \nu) dx'} dx \right). \quad (3)$$

Here $T(x)$ represents the subsurface temperature, $\alpha(x, \nu)$ is the absorption coefficient (or attenuation coefficient),

x is the depth, ν is frequency, and E is the surface emissivity. We neglect atmospheric losses.

The form of $\alpha(x, \nu)$ can be found, if we consider the electromagnetic fields propagating in the x direction with a dependence of the form $e^{-i(\omega t - k_x x)}$ where k_x is the component of the propagation vector in the z direction. We shall assume normal incidence and take $k_x = k$. We furthermore have that $k = \omega \sqrt{\mu_0 \epsilon}$, since snow and ice have also complex permittivities. k has then a real and imaginary part, which implies that the fields will decay exponentially with depth (Figure 5). The attenuation coefficient α is such that

$$\alpha = \text{Im}(k).$$

Since the half-space considered is inhomogeneous, ϵ is a function of x , and since ϵ is also a function of frequency, $\alpha(x, \nu) = \text{Im}(k)$.

The sursurface temperature on the other hand is approximated by

$$T(x) = T_{10} + \delta e^{-\gamma x}. \quad (4)$$

T_{10} = the temperature at the surface

γ = the thermal decay constant

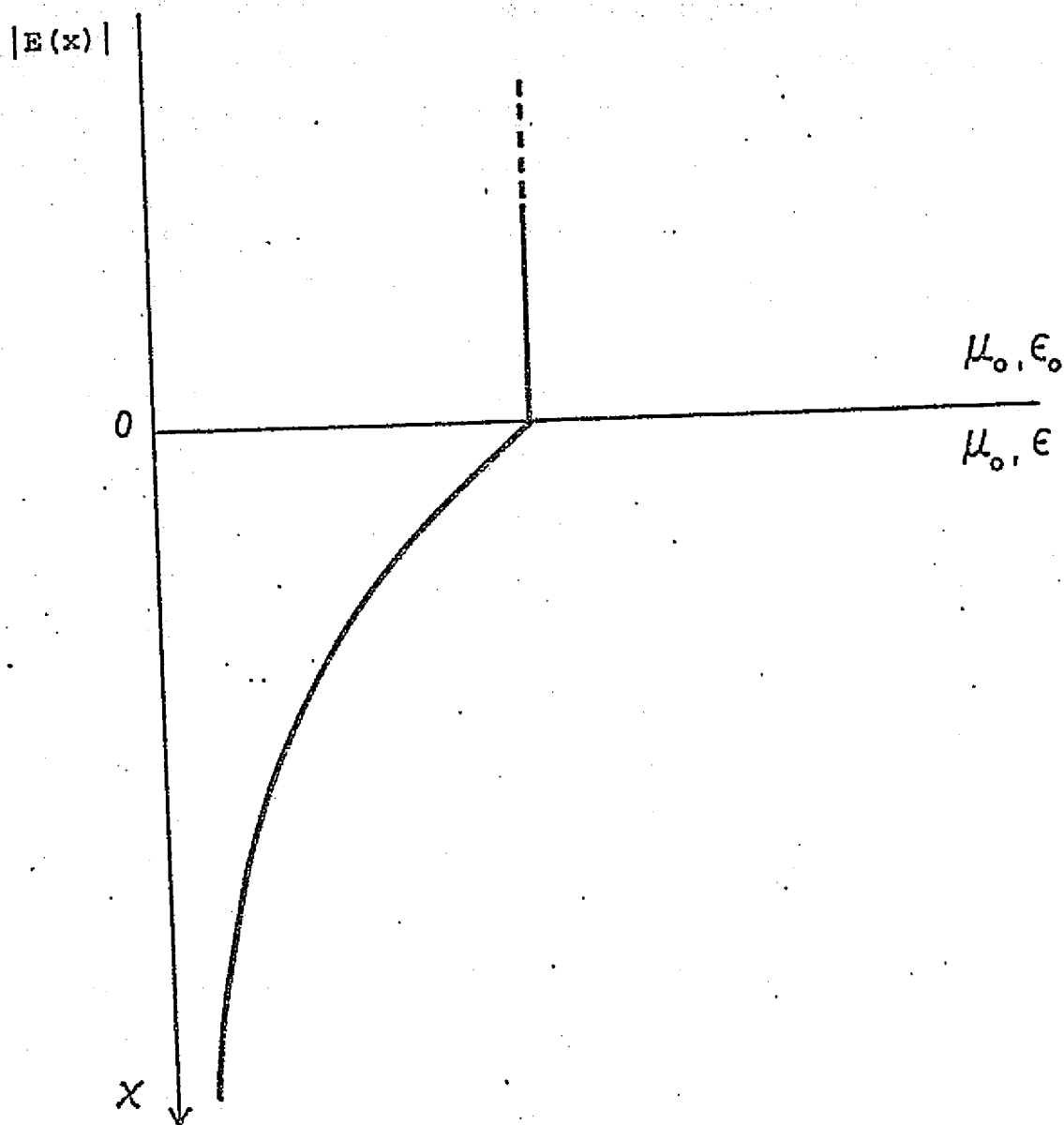


Figure 5.

δ = temperature deviation from T_{10} .

While neglecting scattering, the other assumption being made is that for the dielectric constant, ϵ' is independent of temperature and frequency. It was also found that $\epsilon' \gg \epsilon''$, hence that power absorption coefficient can be approximated by:

$$\alpha \approx \frac{2\pi\nu\epsilon''}{c\sqrt{\epsilon'}}.$$

Integrating equation (3) with α held constant (variation of ϵ'' with temperature and depth are negligible for ice and snow) and using equation (4) we find

$$T_B = T_{10} + \frac{\alpha\delta}{\alpha + \gamma}.$$

Let us then try to apply Kunzi's approach to the case of soil moisture determination. To simplify our task we consider the case of constant temperature throughout the half-space. Equation (3) can be transformed in the following way:

$$T_B = T_S \int_0^{x_1} dx \alpha(x) e^{-\int_0^x \alpha(x') dx} = \int_0^{x_1} -\frac{d}{dx} \left(e^{-\int_0^x \alpha(x') dx} \right) dx$$

$$= -T_S \left(e^{-\int_0^{x_1} \alpha(x') dx} \right) \Big|_0^{x_1} = T_S \left\{ 1 - e^{-\int_0^{x_1} \alpha(x') dx} \right\}. \quad (5)$$

The problem here is to be able to determine the moisture content of the soil given the brightness temperature T_B .

If we want to get a closed form relationship between T_B and the moisture distribution in the soil $f(x)$ we see from equation (5) that $\alpha(x)$ must be integrable for this to be possible.

But what is the dependence of α on $f(x)$. Using Wiener's formula:

$$\epsilon = \frac{\epsilon_w f_w U + \epsilon_s f_s}{f_w U + f_s}$$

where

$$f_w + f_s = 1, \quad U = \frac{\epsilon_s + F}{\epsilon_w + F},$$

identifying $f_w = f(x)$.

ϵ_w = dielectric constant of water

ϵ_s = dielectric constant of soil.

We obtain,

$$\epsilon = \frac{\epsilon_w U f(x) + \epsilon_s (1 - f(x))}{f(x) U + (1 - f(x))}$$

$$\epsilon = \frac{(\epsilon_w \cdot U - \epsilon_s) f(x) + \epsilon_s}{1 + (U - 1) f(x)} = \frac{A f(x) + B}{C f(x) + D}$$

A, B, C, D, are complex. Therefore:

$$\alpha(x) = \frac{\omega}{c} \operatorname{Im} \sqrt{\frac{A f(x) + B}{C f(x) + D}} .$$

Suppose, we are given T_B , T_S , ω , ϵ_w , ϵ_s . We find that we cannot determine ϵ uniquely since there are an infinite number of ways to relate a "real" value of the square root of a complex number.

We could on the other hand postulate the form of $f(x)$ and tentatively (a computer helping) try to approach the given value of T_B , but in doing so we may loose touch ^{with} of the physical reality of the moisture distribution in the soil.

The other deceiving feature of this technique is that the constraints imposed on Kunzi's model make its application to moisture sensing less accurate than what might have been expected. This is due mainly to the fact that the attenuation (moist soil) "was" significant compared to a wavelength, and because the real part of the dielectric constant changes rapidly.

Generalized Half-Space Model

To remedy this, we hope that a more general approach of radiative transfer such as Stogryn's^[11] would be more easily

applicable to our case. The procedure Stogryn uses is still with a half-space model with vertical variations in permittivity and temperature. He finds a radiative transfer equation by solving Maxwell's equations using a randomly fluctuating current density with a known mean value. Since his development is a rather lengthy analytical discussion of Green's function solutions with boundary condition to be satisfied we shall go directly to his results which stand as:

$$T_B = |R|^2 T_{inc} + [1 - |R|^2] \int_{-\infty}^0 dx' T(x') f(x')$$

where

$$f(x') = \frac{\frac{\omega}{2c} \operatorname{Im}[\epsilon(x', \omega)] \left(\frac{\gamma(0)}{\gamma(x')} \right)^2 \exp[-2\operatorname{Im} \int_{-x'}^0 \gamma dx'']}{\operatorname{Re} \{ (\epsilon(0, \omega) - \sin^2 \theta)^{1/2} \}}$$

ϵ = normalized dielectric constant

$$\gamma(x) = (\omega/c) (\epsilon(x, \omega) - \sin^2 \theta)^{1/2}$$

θ = angle of incidence of electromagnetic wave on the half-space (we shall take its value to be zero in our case)

T_{inc} = can be considered as the surface temperature T_s

$T(x')$ = temperature profile in the half-space.

Stogryn's model is very appealing even though the

expression of brightness temperature is long. However, because it is limited by the constraint of a slowly varying dielectric constant (this time real and imaginary parts can vary)

$$\left| \frac{d\varepsilon}{dx} \right| < \left| \frac{\varepsilon}{c} \right|,$$

this would limit in turn our analysis of moisture sensing to slowly varying distribution which may not always be the case.

Skin Depth Approach

Rather than using the radiative transfer approach to the problem, G. Poe and A. T. Edgerton relied on Fresnel Reflection Coefficient^[12] for a half-space as in Figure 4. The model they use to ascertain the moisture content in soil is as follows: "the model originates from the hypothesis that it is the total mass of water per unit area lying between the surface and one electromagnetic skin depth which determines the brightness temperature".

The relation relating the skin depth to the dielectric constant of the half-space, is:

$$\frac{\delta}{\lambda} = \frac{1}{2\pi \operatorname{Im} \sqrt{k}} \quad (6)$$

where δ is the skin depth, λ the wavelength, $k = \epsilon/\epsilon_0$ with the familiar expression of the emissivity

$$e = 1 - r \quad (7)$$

and Wiener's mixture formula (W) they derive a four step procedure to obtain the total mass of water per unit area.

REPRODUCIBILITY OF THE
ORIGINAL PAGE IS POOR

(i) Assuming that the surface temperature T_s is the same throughout the medium, then from measured brightness temperature (corresponding to specified volume percent moisture content) and T_s an effective emissivity $e = T_B/T_s$ is determined.

(ii) From the established emissivity in part (i) and the corresponding volume percent of moisture content, a curve relating e and percent of water in the soil is drawn. (Use equations (7) and (W).)

(iii) Then a curve relating δ to percent of water is determined with equations (6) and (W).

(iv) Finally, the total mass of water per unit area is obtained by just multiplying δ and percent of water. In the result of their analysis it is found that the brightness temperature behaves generally linearly with moisture content. (Figure 6.) This is in accord with some experimental results obtained by T. Schmugge^[13].

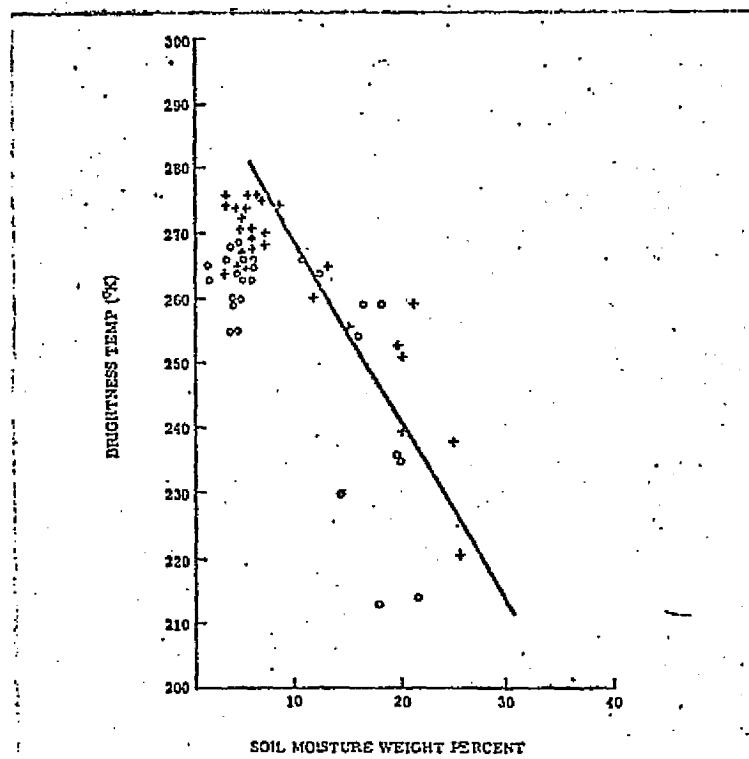


Figure 6.

REPRODUCIBILITY OF THE
ORIGINAL PAGE IS POOR

Proposed Model and Approach

We gave ourselves the task of determining the soil moisture content in the dry region of the Sahel. However, unlike Poe and Edgerton, the emphasis will be made more on determining a moisture profile rather than moisture in bulk. Trying to be more qualitative implies a more thorough knowledge of the dynamics of water flow in sandy soils. The problem at hand consists in evaluating the shape of the water content profile which would simulate the penetration of water after rainfall.

Soil Mechanics Considerations

The drainage mechanics in cohesionless soils has been fully explored by T. W. Lambe^[14]. Hence we shall appeal to his theory for the understanding of water flow in sandlike soils. In a first step we refresh our memory about the general hydrodynamic equation of flow. The assumptions are, as in Figure 7, that flow is vertical and laminar. It will be laminar if we assume that the soil is made of fine sand. We are within that limit if we consider a grain size distribution such as in Figure 8. By using Darcy's Law we obtain the rate of flow r in a soil element such as in Figure 6. We then determine the net rate of flow, Δr by considering the rate of flow both at the bottom and at the top of

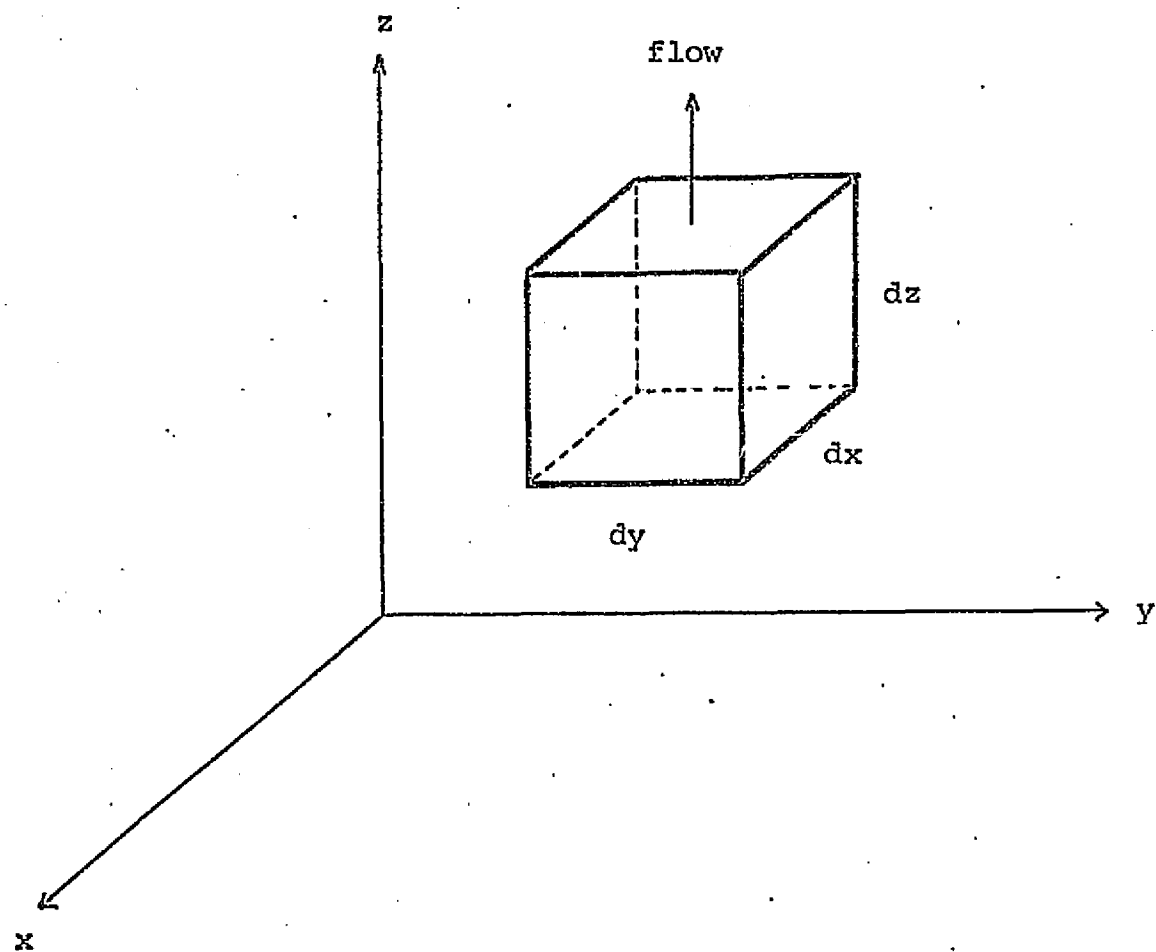


Figure 7.

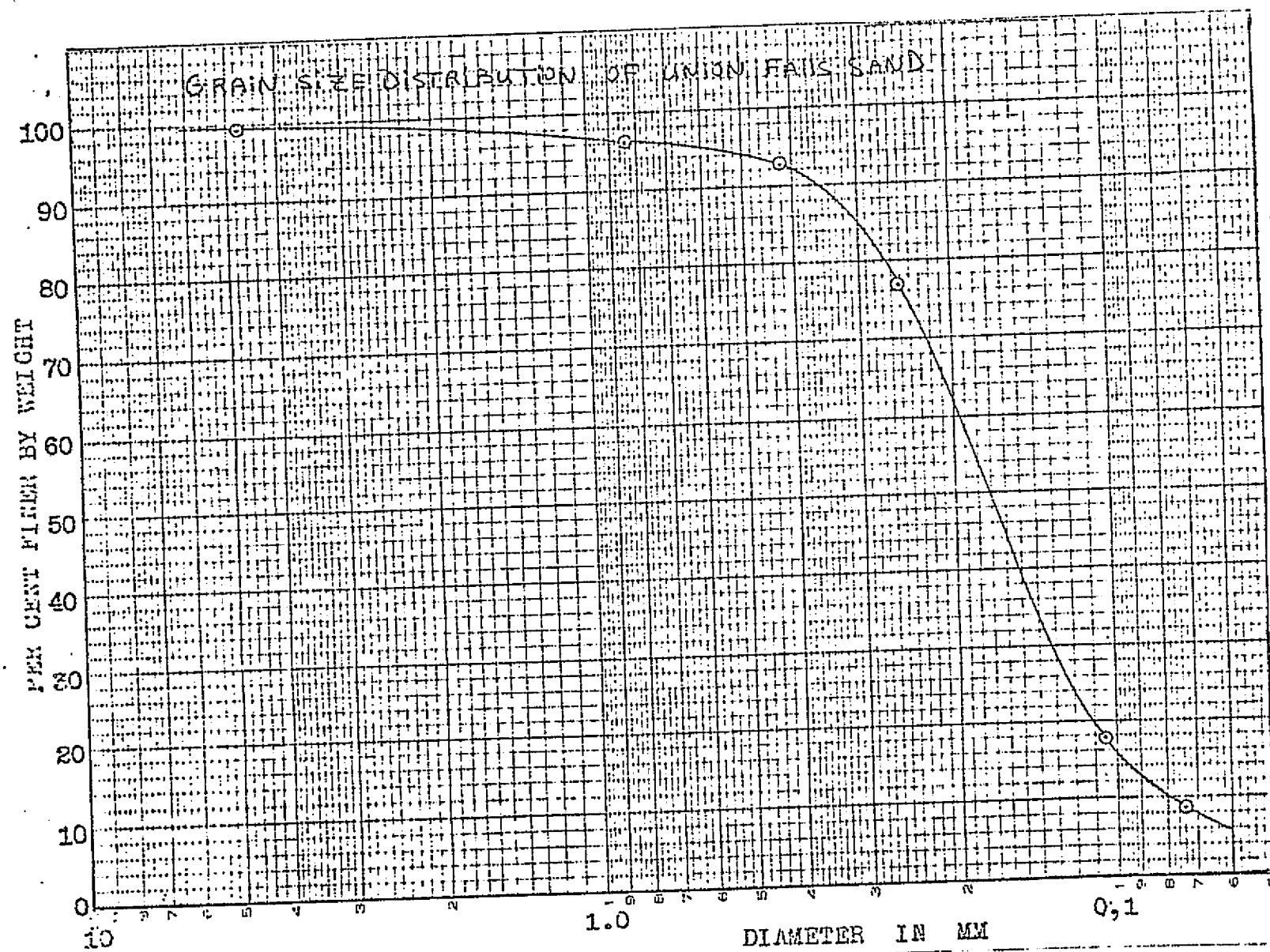


Figure 8.

REPRODUCIBILITY OF THE
ORIGINAL PAGE IS POOR

the soil element (z direction). We then equate Δr with the internal change of water within that element and obtain finally the general hydrodynamic equation for laminar flow in soils which is the following:

$$k_z \frac{\partial^2 h}{\partial z^2} + \frac{\partial k_z}{\partial z} \frac{\partial h}{\partial z} + \frac{\partial k_z}{\partial z} dz \frac{\partial^2 h}{\partial z^2} = \frac{1}{1+e} \left(e \frac{\partial G}{\partial t} + G \frac{\partial e}{\partial t} \right)$$

(8)

where

k_z = permeability in the z direction

h = head

$e = V_v/V_s$ is the void ratio

$G = V_w/V_v$ is percent saturation.

If V is the total volume $dx dy dz$ then,

$V = \text{volume solids} + \text{volume voids} = V_s + V_v$ where

$V_v = \text{volume water} + \text{volume air} = V_w + V_a$.

$$V_v = \frac{e}{1+e} dx dy dz$$

$$V_w = \frac{Ge}{1+e} dx dy dz$$

$$V_s = \frac{dx \, dy \, dz}{1 + e}$$

If in the above equation k is constant, e is constant, G is constant then we get $\partial^2 h / \partial z^2 = 0$ which is the familiar Laplace's equation for one dimensional steady flow.

When considering flow in soils we can generally focus on four groups, they are as follows:

- (i) Flow where G remains constant but e varies.
- (ii) Flow where e and G are both constant or steady flow.
- (iii) Flow where e remains constant and G varies.
- (iv) Flow where both e and G change.

The two first groups have been thoroughly studied and represent no great interest here. Lambe focused on the third category which is no doubt, of greater interest to us.

The important aspect as shown by Lambe is that flow in solids depends upon a total head h , which in turn is made up of several types of head. One type of head which contributes greatly to flow is the capillary head. By head we mean here a cannular path which is used by the water to flow within the soil. When discussing movement of water in soils, we must mention then the effect of capillary pull since there

is a tendency for the water to be held up against gravity.

Lambe experimentally verified this phenoma. The curves that were obtained relating height and corresponding level of saturation agree with the following equation:

$$S(x') = 1 - e^{-1/2 (H_s/x')^2} \quad (9)$$

where $S(x')$ is the saturation percentage from a height x' of total saturation.

H_s = capillary head and is defined as

$$H_s = \frac{2T}{g\rho\sigma}$$

where T is the surface tension, g is gravity, ρ is the density of water, σ is the void radii which will be generally considered as Rayleigh distributed.

What we mean by Rayleigh distribution is a behavior of the probabilistic distribution of the void (pore) radii as in Figure (9). If the probability distribution of void radii r , $P(r)$ is such that,

$$P(r) = \begin{cases} \frac{r}{b} e^{-r^2/2b} & \text{for } r > 0 \\ 0 & \text{otherwise} \end{cases}$$

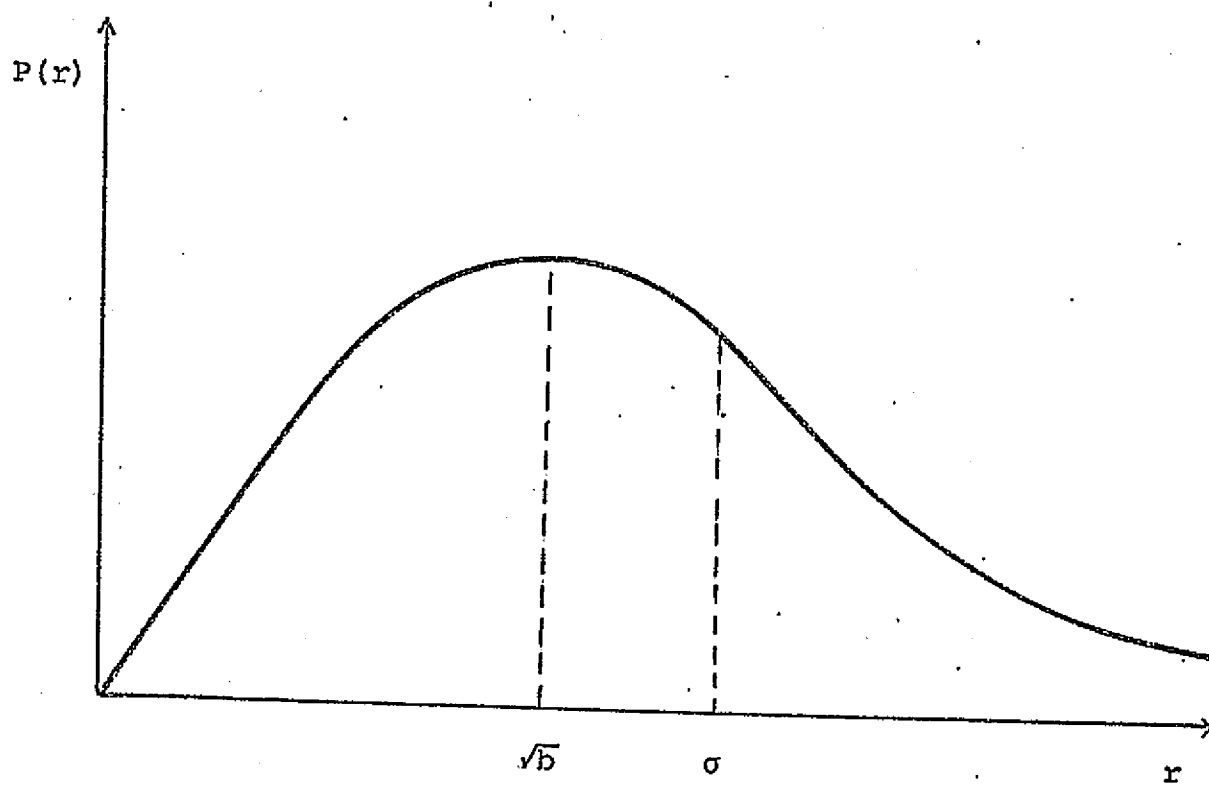


Figure 9.

(where b is a constant and varies with soil type) then the radius associated with the expected value of $P(r)$ can be roughly taken as our σ in the definition of H_S . The expected value of $P(r)$ is taken to be:

$$P(r) = \int_0^{\infty} P(r) dr = \sqrt{\frac{\pi b}{2}}.$$

Fresnel Reflection Coefficients for a N-Layer Media

Now that we have more insight on the soil mechanics aspect of our study we can give ourselves a model that will relate a brightness temperature to a moisture profile conforming to the one just investigated. We shall consider a half-space medium, with constant temperature T_s , with no scattering, non-magnetic which is inhomogeneous in permittivity if we consider the mapping of a moisture profile onto it as in Figure 10. We then partition this half space into N layers of uniform permittivity (calculated through Wiener's formula). We have to then reduce the problem to finding the reflection coefficient of a N layer stratified media. We use Fresnel reflection coefficients as reviewed by J. A. Kong [15] to find the total reflection R at the surface (air, soil boundary).

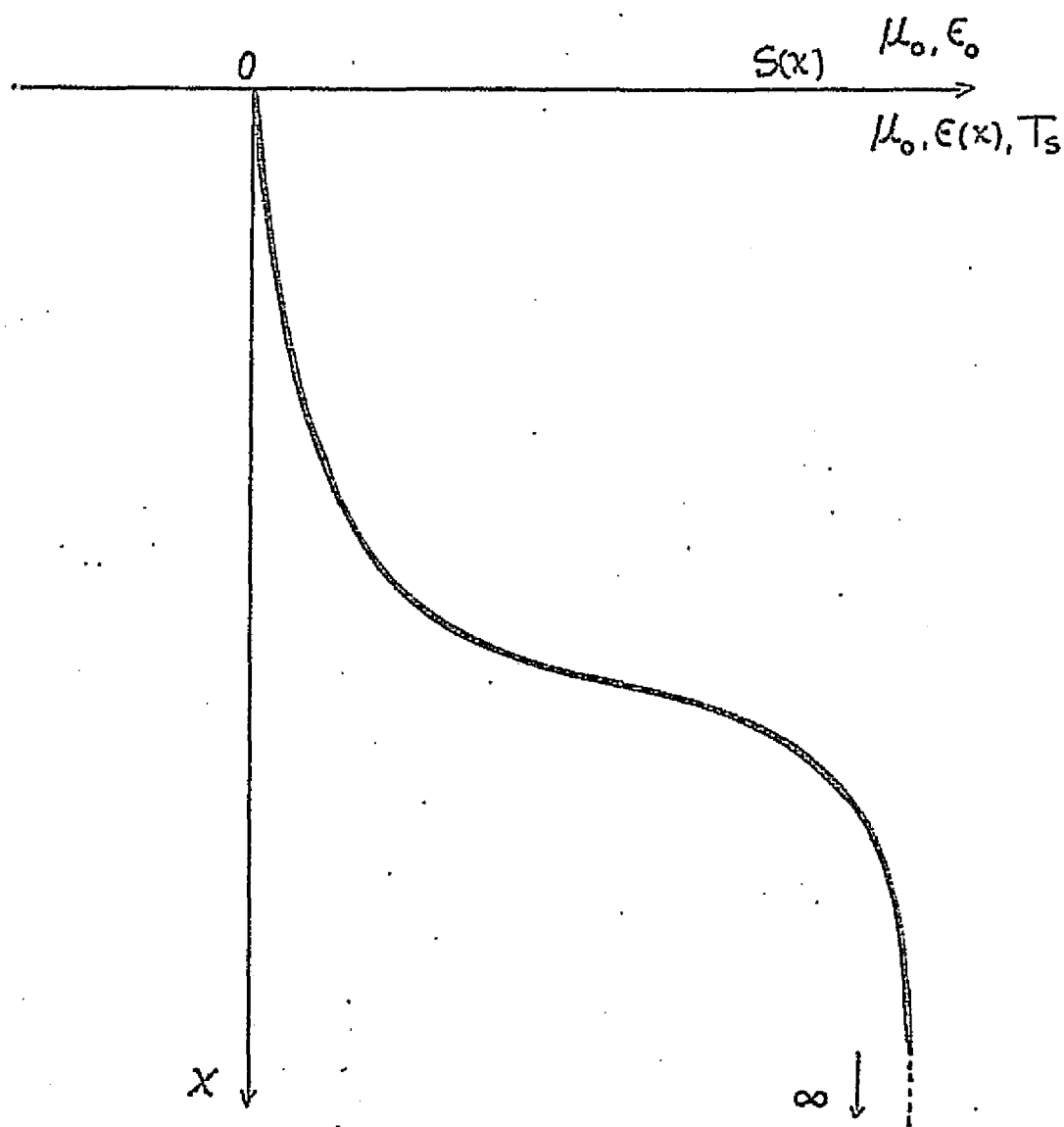


Figure 10.

$$\begin{aligned}
R = & \left\{ \frac{1}{R_{01}} + \sqrt{\frac{R_{01}^2 - 1}{R_{01}}} + R_{01}^2 \exp(i2k_{1x} d_1) \left\{ \frac{1}{R_{12}} + \sqrt{\frac{R_{12}^2 - 1}{R_{12}}} \right. \right. \\
& + R_{12}^2 \exp[i2k_{2x}(d_2 - d_1)] \left. \left\{ \frac{1}{R_{23}} + \sqrt{\frac{R_{23}^2 - 1}{R_{23}}} + \dots \right. \right. \\
& \left. \left. + R_{(n-1)n}^2 \exp[i2k_{nx}(d_n - d_{n-1})] R_{nt} \right\} \dots \right\} .
\end{aligned}$$

(10)

where $R_{(n-1)n}$ is the reflection between two adjacent partitions as we go deeper in the soil.

d_n is the width of each uniform layer; k_{nx} is the propagation vector of the electromagnetic wave in the x direction. (Actually we may just call it k_n since we are considering normal incidence of the E and M waves on the medium.)

To determine the emissivity we recall,

$$E = 1 - |R|^2. \quad (11)$$

With T_s taken to be the temperature of the whole subsurface region, we then obtain the brightness temperature,

$$T_B(^{\circ}k) = E \cdot T_S. \quad (12)$$

Through equations (10), (11), and (12), we can establish curves relating E (and ultimately T_B) to frequency for various heights of the moisture profile (in doing so we test the probing sensitivity of microwave sensing). In view of equation (10), the numerical analysis involved here requires a computer program such as the one listed at the end of these pages. We must however comment on the meaning of some of the characteristic variables used.

H_S , is the capillary height which determines the maximum height of our profile.

K_S , is the value of the dielectric constant of the soil
 $(K_S = 2.55 + i \ 00.015 \text{ at frequencies } \sim 3 \text{ GHz},$
 $K_S = 2.53 + i \ 0.009 \text{ at frequencies above } 3 \text{ GHz}^{[16]}$
 (normalized to ϵ_0),

$FREQ$ is the value of the frequency in each considered frequency range we are interested in (in GHz) between 0.3 GHz and 31.4 GHz. The frequencies considered are successively: 0.3, 1.0, 2.0, 4.0, 10.0, 22.2, 31.4 GHz.

F is the form number used in Wiener's formula. It is

such that for frequencies $< 10 \text{ GHz}$ $F = 32$ and for frequencies $> 10 \text{ GHz}$ $F = 16$.

k_w is the dielectric constant of water.

z is the spacing between each layer of uniform dielectric constant.

E_X , its imaginary part, is the decay or attenuation (of E and M wave) factor.

CF is a proportionality factor which varies with HS to give saturation at the bottom of the head and zero at the top.

We will notice that saturation, in the profile we use is not 100% but 40%. This is due to the fact that in Wiener's formula the water mixture has to be in volume percent. Therefore, if saturation by weight is considered to be 20%, and our type of sand has a specific gravity of 2.66, then the saturation level in volume percent is roughly 40%. Lastly, N , is the number of layers taken in the model. The value should be dependent upon the height of "transition zone" Δx as in Figure 11 where the change in the dielectric constant is the fastest. Another criterion for the choice of

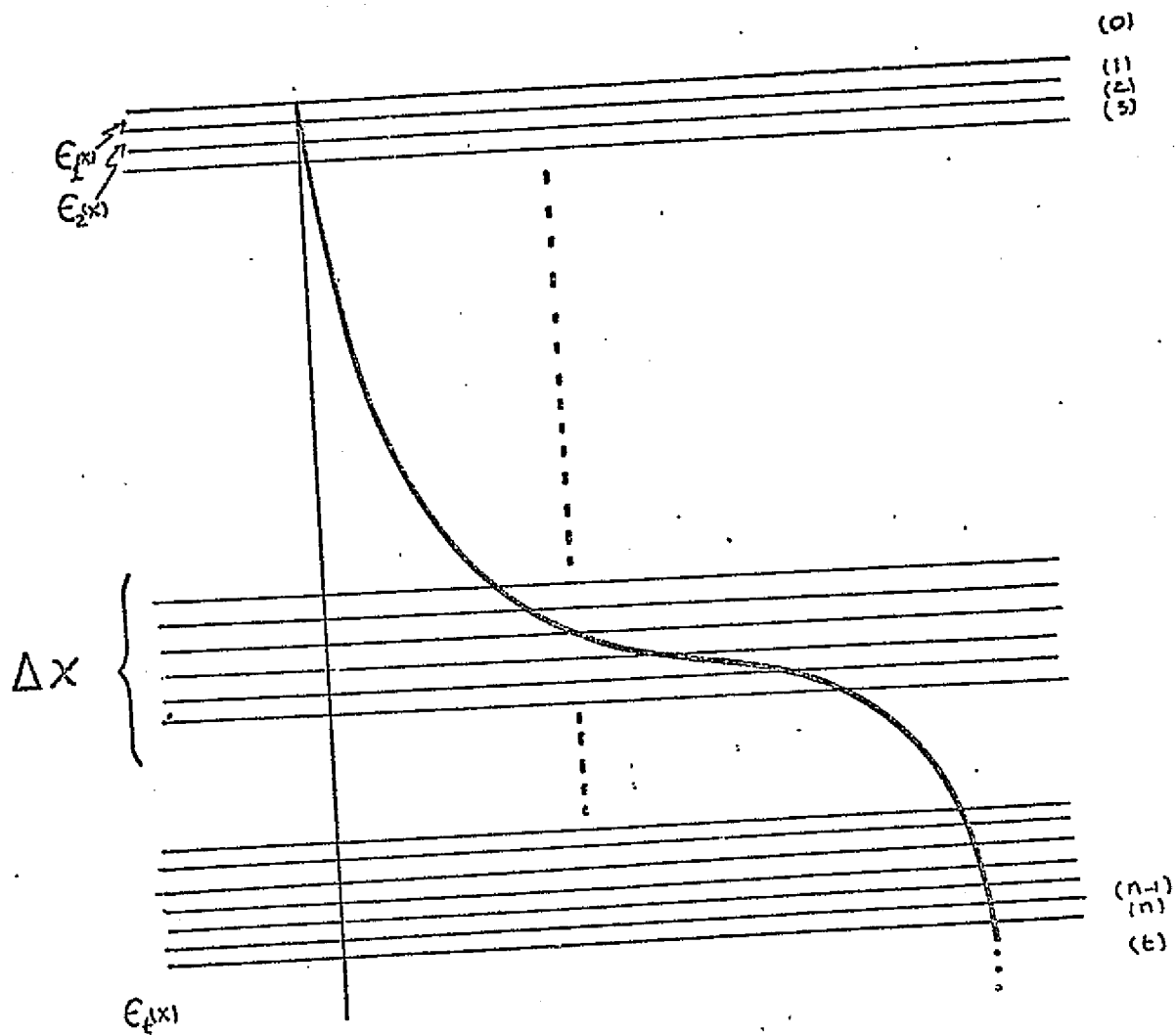


Figure 11.

N is related to the frequency. We assume that N must at least satisfy $N = 10d/3\lambda$ where d is the depth of the profile and λ is the wavelength. Generally, for better sensitivity and accuracy (as to the form of the profile) we take ten to fifteen times the value of N obtain by the above criterion.

There are three distinct ways in which the profile can vary: the height of the profile, the moisture percent at the surface, and the moisture percent at saturation.

Computer Results

We shall first consider variations with height of the moisture profile. The heights examined were successively: $z_1 = 0.7$ cm, $z_2 = 1.5$ cm, $z_3 = 5.9$ cm, $z_4 = 11.0$ cm. Beyond z_4 , the lowest frequency (our reference point since it has the greatest penetration depth) gives invariant results in emissivity ($E = .95$ always). The results in Table A1 show that the most sensitive frequencies are the three lowest ones. However, the amplitude of the emissivity variation is only in the order of 0.04. (This detection process would thus require an emissivity sensitivity in the order of 0.01 at least.)

We now vary the moisture percent at the surface of the soil (hence simulating recent rain). The variations are taken from 0% to 20% as in Tables B2(a) and B2(b). This

Frequencies

0.3 GHz	1 GHz	2 GHz	4 GHz	10 GHz	27.2 GHz	31.4 GHz
(1)	(2)	(3)	(4)	(5)	(6)	(7)

E(n) with $n = 1 \dots 7$ is the corresponding emissivity

z =	0.7 cm	1.5 cm	5.9 cm	11 cm
E(1) =	0.88	0.88	0.89	0.92
E(2) =	0.88	0.89	0.90	0.93
E(3) =	0.88	0.91	0.93	0.94
E(4) =	0.91	0.91	0.94	0.94
E(5) =	0.94	0.94	0.94	0.94
E(6) =	0.94	0.94	0.94	0.94
E(7) =	0.94	0.94	0.94	0.94

Table A1.

Effect of height variations of the moisture profile.

time the whole spectrum of emissivities is affected and furthermore by the same amount ($\Delta E = 0.01$).

However, in one case (Table 2.) the height is z_4 and the moisture variation is from 0 to 20% and in the other the height is $z_3 < z_4$ with a moisture variation from 0 to 10%. This shows better sensitivity at lower depth.

Finally, we vary the moisture percent at saturation. (Actually in the model the saturation level is uniform after a certain depth which we called z_n $n = 1, 2, 3, 4$. It is at that depth that we make the variations in moisture percent.) Varying the volume (what we called moisture) percent at saturation reflects a variation in the specific gravity of the sand that constitutes the soil. We took a saturation percent of 40% which corresponded to a specific gravity of 2.66 for the sand grain. For the purpose of discussion we considered the case of a specific gravity of 4 which corresponds to a saturation volume percent of 50%. (However, as mentioned, the characteristic sand would be considered extremely fine. This may therefore alter the shape of the moisture profile. We are therefore considering a hypothetical situation.) The results are shown in Tables 3a and 3b. Changes are noticeable only in the case of the two lower frequencies. Lastly, we consider the case of simultaneous variations as in Tables 4a and 4b where we varied in both cases all the parameters discussed so far. The variations in emissivity were still bound to $\Delta E = 0.04$ for

Moisture content 0%

$$E(1) = 0.93$$

$$E(2) = 0.94$$

$$E(3) = 0.95$$

$$E(4) = 0.95$$

$$E(5) = 0.95$$

$$E(6) = 0.95$$

$$E(7) = 0.95$$

Moisture content 20%

$$E(1) = 0.92$$

$$E(2) = 0.93$$

$$E(3) = 0.94$$

$$E(4) = 0.94$$

$$E(5) = 0.94$$

$$E(6) = 0.94$$

$$E(7) = 0.94$$

Table 2(a).

Effect of surface moisture variations on emissivity at
 $z = 11$ cm.

Moisture content 0%

$$E(1) = 0.90$$

$$E(2) = 0.90$$

$$E(3) = 0.94$$

$$E(4) = 0.95$$

$$E(5) = 0.95$$

$$E(6) = 0.95$$

$$E(7) = 0.95$$

Moisture content 10%

$$E(1) = 0.89$$

$$E(2) = 0.90$$

$$E(3) = 0.93$$

$$E(4) = 0.94$$

$$E(5) = 0.94$$

$$E(6) = 0.94$$

$$E(7) = 0.94$$

Table 2(b).

Effect of surface moisture variations on emissivity at
 $z = 5.9$ cm.

Moisture content 40%

$$E(1) = 0.93$$

$$E(2) = 0.94$$

$$E(3) = 0.95$$

$$E(4) = 0.95$$

$$E(5) = 0.95$$

$$E(6) = 0.95$$

$$E(7) = 0.95$$

Moisture content 50%

$$E(1) = 0.92$$

$$E(2) = 0.94$$

$$E(3) = 0.95$$

$$E(4) = 0.95$$

$$E(5) = 0.95$$

$$E(6) = 0.95$$

$$E(7) = 0.95$$

Table 3(a).

Effect of bottom saturation level on emissivity at
 $z = 11$ cm.

Moisture content 40%

$$E(1) = 0.90$$

$$E(2) = 0.93$$

$$E(3) = 0.94$$

$$E(4) = 0.95$$

$$E(5) = 0.95$$

$$E(6) = 0.95$$

$$E(7) = 0.95$$

Moisture content 50%

$$E(1) = 0.88$$

$$E(2) = 0.93$$

$$E(3) = 0.94$$

$$E(4) = 0.95$$

$$E(5) = 0.95$$

$$E(6) = 0.95$$

$$E(7) = 0.95$$

Table 3(b).

Effect of bottom saturation level on emissivity at
 $z = 5.9$ cm.

z = 0.7 cm

Surface moisture content 10%
Bottom saturation level 40%

$$E(1) = 0.88$$

$$E(2) = 0.88$$

$$E(3) = 0.88$$

$$E(4) = 0.91$$

$$E(5) = 0.93$$

$$E(6) = 0.94$$

$$E(7) = 0.94$$

z = 11 cm

Surface moisture content 0%
Bottom saturation level 40%

$$E(1) = 0.93$$

$$E(2) = 0.94$$

$$E(3) = 0.95$$

$$E(4) = 0.95$$

$$E(5) = 0.95$$

$$E(6) = 0.95$$

$$E(7) = 0.95$$

Table 4(a).

Simultaneous variations of parameters.

z = 1.5 cm

Surface moisture content 20%
Bottom saturation level 40%

$$E(1) = 0.88$$

$$E(2) = 0.88$$

$$E(3) = 0.91$$

$$E(4) = 0.94$$

$$E(5) = 0.94$$

$$E(6) = 0.94$$

$$E(7) = 0.94$$

z = 5.9 cm

Surface moisture content 0%
Bottom saturation level 40%

$$E(1) = 0.90$$

$$E(2) = 0.93$$

$$E(3) = 0.94$$

$$E(4) = 0.95$$

$$E(5) = 0.95$$

$$E(6) = 0.95$$

$$E(7) = 0.95$$

Table 4(b).

Simultaneous variations of parameters.

most frequencies.

Three major features can be deduced from this analysis. First the probing depth of the detection process is limited to no more than 20 cm. Second the emissivity variations are limited within a small range $\Delta E = 0.04$. Third the emissivity is dependent on the surface moisture.

Possible Future Investigation

If the latter varies with time (after rainfall, water will filter through the soil gradually) then the emissivity will also be a function of time. However, the longer the elapsed time between rainfall and the probing procedure the less likely the moisture content (or distribution) will be distinguishable. W. T. Lambe derived experimentally that the moisture profile (related to the capillary effect) would vary in fact with a characteristic time T where

$$T = \frac{k}{n} \frac{dh}{dG} \frac{t}{L^2}$$

where k is the permeability, h is a head, n is the number of heads, L is their average height, and t is time expressed in minutes.

It was found that for a characteristic value of T (for which the surface moisture content goes from saturation

to 0% water) corresponded to an elapsed time $t = 120$ mn.

Also it was noted by T. Schmugge^[17] that the total moisture content within a particular surface layer does not change readily. He states "Results indicate that, although the surface layer changes rapidly (He means the distribution.), the total moisture in the top 15 cm does not: thus the average soil in the top 15 cm decreases from 20% at 3 days to 16% after 6 days, whereas the surface layer top half-centimeter has dried from 20% to 8.5%".

We see that if we were interested in times in the order of 2 hours instead of 72 hours then the decrease in the top 15 cm would not be nearly as great as 20%. If, furthermore, we used satellites with orbital periods of 2 hours, then we might investigate a moisture pulse propagation in sandlike soils.

It would be reasonable as a first approximation to assume a gaussian distribution of volume percent in the soil as in Figure 12. The purpose would then be to determine v_p the moisture propagation velocity given $T_B(t)$ as a function of time. The moisture profile would be of the form:

$$M(x, t) = M_0 e^{-\frac{(x - v_p t)^2}{2 s_m^2}}$$

where M_0 = magnitude (maximum volume percent)

v_p = propagation velocity

REPRODUCIBILITY OF THE
ORIGINAL PAGE IS POOR

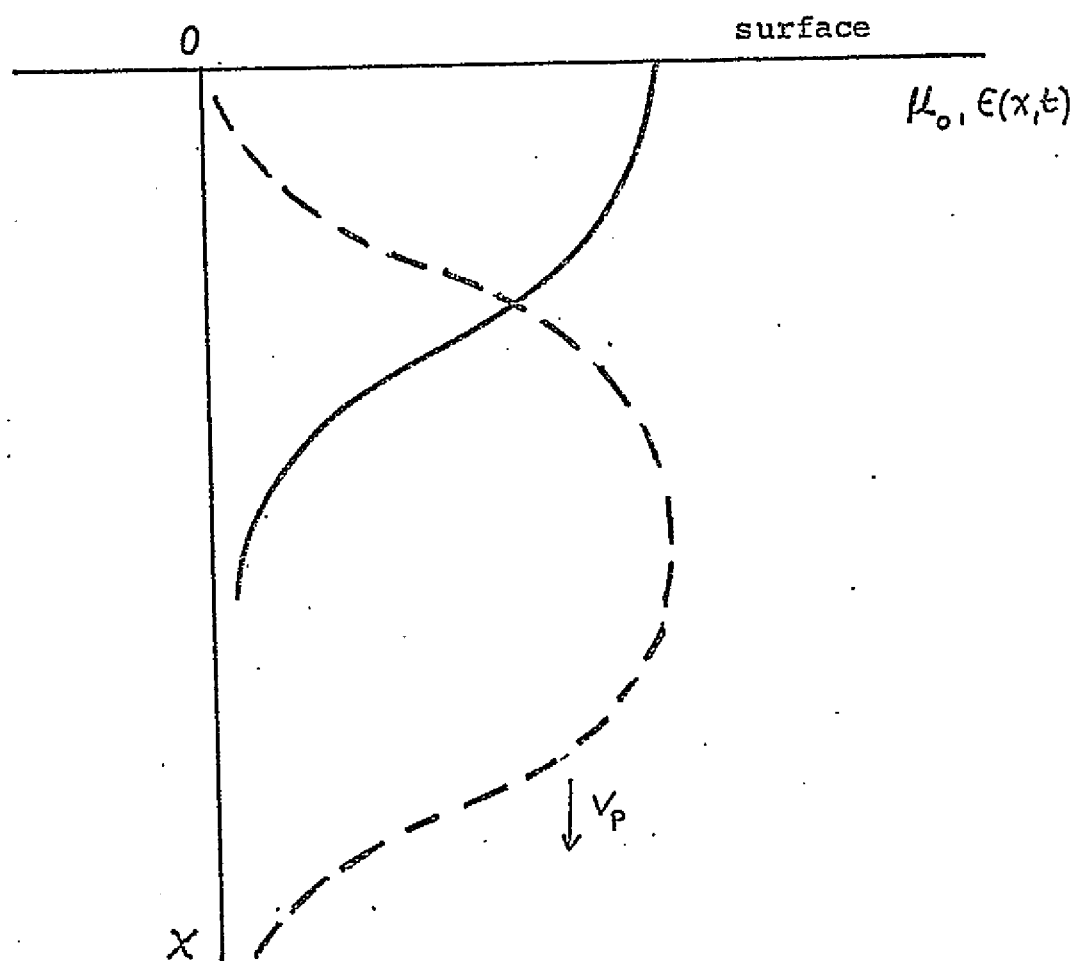


Figure 12.

s_m = smearing constant

x = depth from the surface.

The smearing constant s_m would in fact be a function of porosity, temperature and humidity content. Of course no work has been done in that area and no formula has been given to determine

$s_m(P, t, h)$.

(Figure 12.)

Data from Nimbus 5

Having familiarized ourselves with the problem of moisture sensing it seems that we have a better chance of interpreting the available data related to the Sahel region in Africa. Our task would be somewhat pretentious if we were to consider the whole of the Sahel. We have therefore confined our study to the following geographical sites: 12°W, 4°W, 4°E, 12°E, 20°E of longitude and 17°N of latitude. These sites have the interesting feature of being located at the center of the Sahel belt.

Data from Nimbus 5

The satellite used to record data was the Nimbus 5 which was launched in late 1972. Its microwave sensors were locked on the following resonant frequencies: 22.2, 31.4, 53.6, 54.9 and 58.8 GHz. We shall only be interested in the two lower frequencies since they lie within the water vapor and liquid water emission band respectively. The higher frequencies are much less sensitive to them^[18] (mainly used for probing the atmosphere).

The brightness temperature measurements were generally taken within a time period of seven to eight days at intervals of twenty days. This was motivated by the fact that the flight pattern of the satellite had to overlap on five specific

locations. It should be noted that all the measurements were taken over a period of seven months (from December to June). Some months have been omitted for lack of cataloged data. Furthermore, the readings in Data Set I of location (3) and (4) of the month of December bear the year 1973 instead of 1972. This is due to the launching time of the satellite which created an offset in the space-time correspondence for locations (3) and (4). Consequently, no 1972 data was given for them. To remedy this, readings were taken in December 1973. The locations (or sites) were chosen with at eight longitudinal degree interval to best eliminate any possible overlap of readings that could be caused by the 200 km \times 200 km resolution coverage of the satellite.

Ground Truth Data

However, to have a more complete status on the region covered ground truth data is needed. Table (1) displays such information^[14]. The stations from which the readings were taken are in accord with the locations of interest.

	<u>latitude</u>	<u>longitude</u>
Timbuctu	16°N	5°E
Bilma	18°N	13°E
Faya-Largeau	18°N	19°E
Nema	16°N	7°W
Atar	18°N	13°W

REPRODUCIBILITY OF THE
ORIGINAL PAGE IS POOR

TABLE-(1)

YEAR	REGION	JAN	FEB	MAR	APR	MAY	JUN	JULY	AUG	SEP	OCT	NOV	DEC	
1968	TIMBUCTU	295	298	301	304	307	306	304	301	304	304	301	296	(K)
		0.0	0.0	0.0	0.0	2.5	18	57	80	35	2.5	0.0	0.0	(mm)
1968	BILMA	290	293	294	301	305	306	306	306	304	300	295	290	(K)
		0.0	0.0	0.0	0.0	0.0	0.0	2.5	12	5	2.5	0.0	0.0	(mm)
1972	BILMA	300	303	308	311	315	316	315	313	312	311	306	300	(K)
		0.0	0.0	0.0	0.0	1	1	3	10	5	2	0.0	0.0	(mm)
1972	FAYA-LARGEAU	298	303	307	312	314	315	314	313	312	310	306	301	(K)
1972	NEMA	303	306	310	313	315	315	311	308	310	312	309	304	(K)
		0.0	0.0	1	3	10	30	63	111	55	15	0.0	0.0	(mm)
1972	ATAR	300	302	307	309	311	315	315	314	313	310	306	301	(K)
		1	1	0.0	0.0	1	8	83	33	35	8	10	1	(mm)

	REGION	JAN	FEB	MAR	APR	MAY	JUN	JULY	AUG	SEP	OCT	NOV	DEC
	BILMA	1	1	1	1	1	1	2	2	1	1	1	1
FAYA-LARGEAU		2	2	2	2	2	1	2	3	2	1	2	2
	NEMA	3	3	2	3	4	3	4	5	4	3	3	3
	ATAR	3	2	2	2	3	3	3	3	3	4	4	4

(DEGREE OF CLOUDINESS)

in oktas

(1972)

The temperatures in Table (1) are expressed in Kelvin degrees since they will be used as ground surface temperatures. The assumption here is that the ground and the ambient air are in thermal equilibrium. The difference in the measurements at Bilma between 1968 and 1972 (temperature and rainfall) shows clearly the trend towards a drought. We may specify that all measurements of temperature and rainfall are averages (unfortunately) per month. Cloudiness readings are in oktas, where one okta correspond to a degree of cloudiness where $1/8$ th of the sky is covered by clouds (mostly cumulus). Also, it has been recorded that evaporation was highest during the pre-rainy season. But the mean relative humidity in July is approximately the same as that in December for the latitude considered (the level of humidity is invariant over the year).

As for the geological features of the Sahel, they are mostly uniform. We can give ourselves a sort of typical profile of laterite soils if we examine the region of Sefa, Senegal^[20].

Parent rock:	Sandy-argillaceous sandstone
0 - 12 cm:	Carboniferous surface debris, slight cohesion, porous
12 - 28 cm:	Sandy, medium cohesion, porous
28 - 55 cm:	Hardened, sandy argillaceous, strong to medium cohesion, porous
90 - 120 cm:	Sandy-argillaceous, unhardened concretions
120 < cm:	Transition to argillaceous sandstone.

Of course, this profile will be subject to variations as we go from the Western-most part of the Sahel to the Eastern-most part of it. However, generally we are likely to find sandlike characteristic in the soils.

We have so far mentioned only the existence of a data set I. Actually there are two data sets, I, and II. This is due to the confusion (which may be unexcusable) that arose when we tried to match our locations to the satellite's trajectory. As a result, in the first retrieval of data, three of the five locations gave emissivities which went as low as $E = 0.51$. This being more characteristic of water than dry sand. The drought in the Sahel appeared for a while as a figment of the imagination. Not very long after this, it was found that the data collected referred to the following points: 7.3°W , 0° , 7.3°E , 17.5°E of longitude and 0° of latitude. The three first points very reassuringly were found to lie within the Gulf of Guinea. A second data set was therefore collected and while being more reliable, was also more realistic if we look at the emissivity distribution (Table 5). Comparing the Figures in Table 5 with an emissivity of $E \sim 0.51$, we are then compelled to believe in the seriousness of the drought in the Sahel region.

	<u>loc (1)</u>	<u>loc (2)</u>	<u>loc (3)</u>	<u>loc (4)</u>	<u>loc (5)</u>
December	E = 0.96	E = 0.93	-	-	-
January	E = 0.93	-	E = 0.94	E = 0.92	-
February	E = 0.93	E = 0.91	E = 0.95	E = 0.97	-
April	E = 0.94	-	-	E = 0.95	-
June	-	E = 0.91	E = 0.92	-	-

Table 5.

Computed emissivity for data set II using $T_B = E \cdot T_s$.

Conclusion

The model through which we tried to relate brightness temperature to moisture content is a N layer stratified media with vertical variations in dielectric constant. Soil mechanics considerations predict the type of moisture profile which governs these variations. Results are obtained using a computer program.

Even though we did not include in the model any horizontal variations in the flow equations or temperature variations and restricted observations to nadir, the parameters that were incorporated in it seemed to be the most important ones as to the understanding of remote sensing of moisture in sandlike soils. It would then appear that along with being limited to a probing depth of twenty centimeters, a limiting factor in remote sensing is the sensitivity of the radiometer. The results show that unfortunately no appreciable moisture content can be determined (while land-sea boundaries have been shown to be quite distinct). However, the mixture formulas should be reviewed as well as the correlation between more accurate ground truth data and brightness temperature before any final conclusions can be drawn.

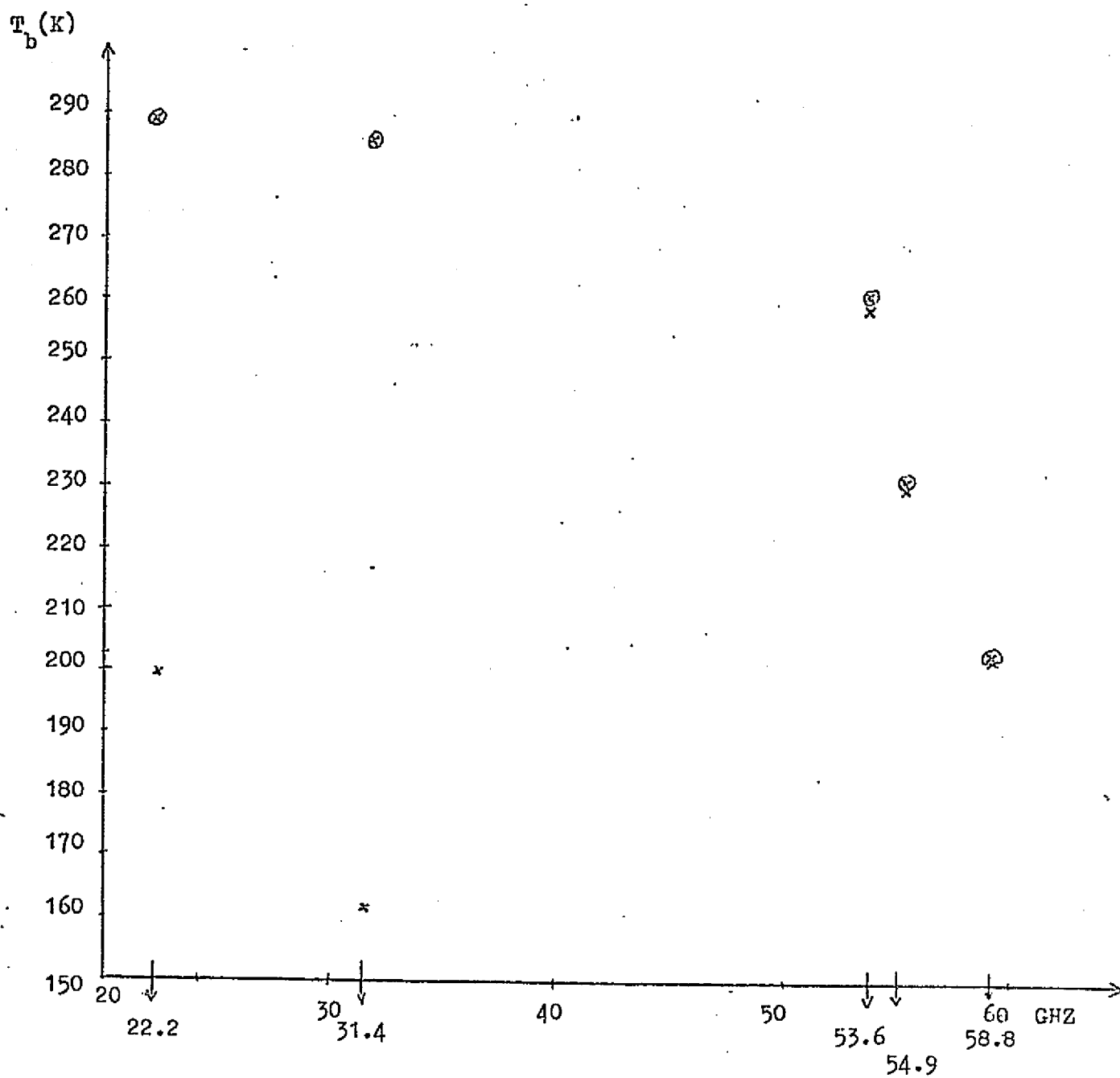
Data Set I.

The five locations considered are:

Latitude: 0° 0° 0° 0° 0°

Longitude: 7.3°W 0° 7.3°E 17.5°E 21°E

Measurements were all taken between 10:00 am and
12:30 pm.

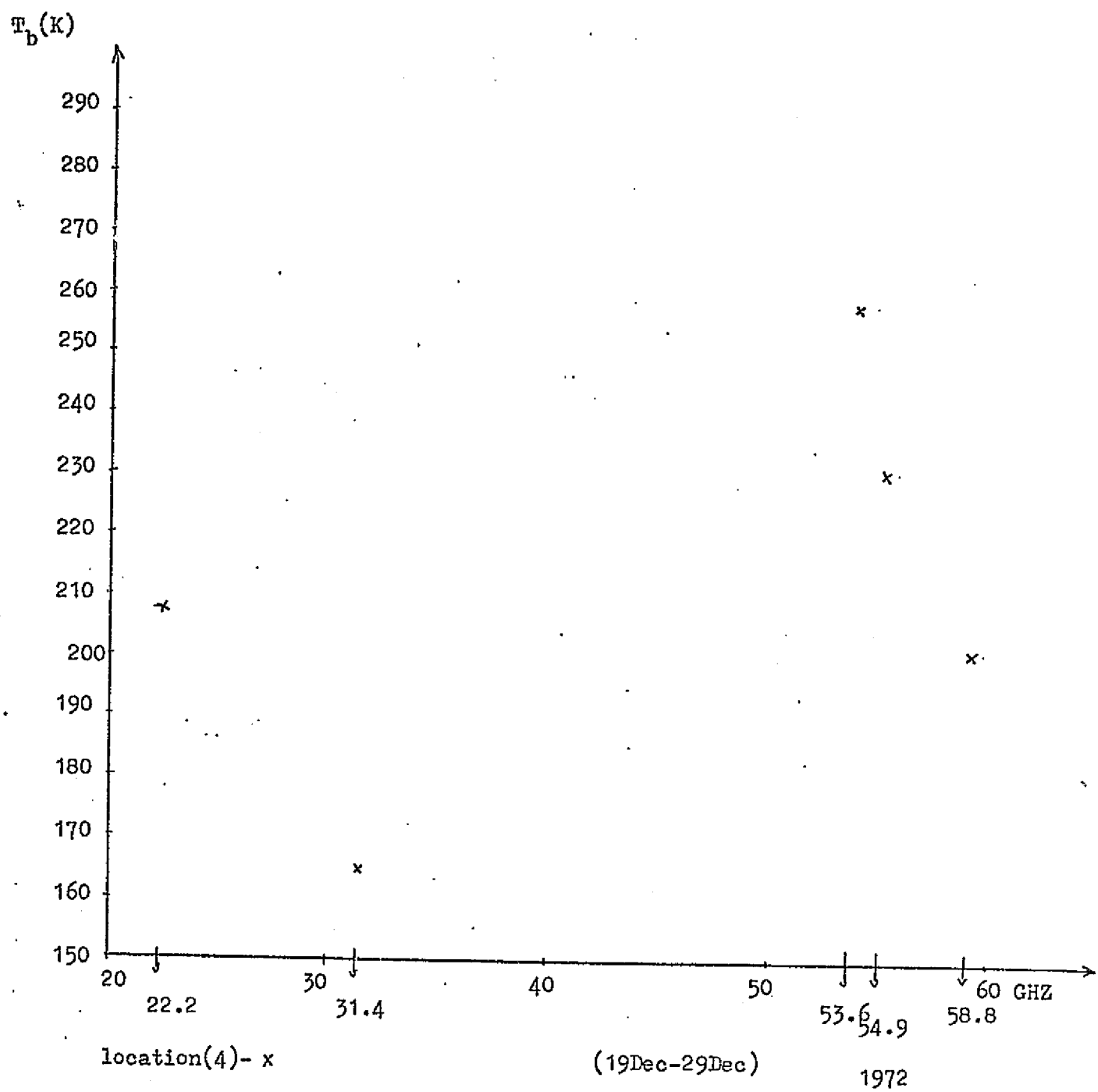


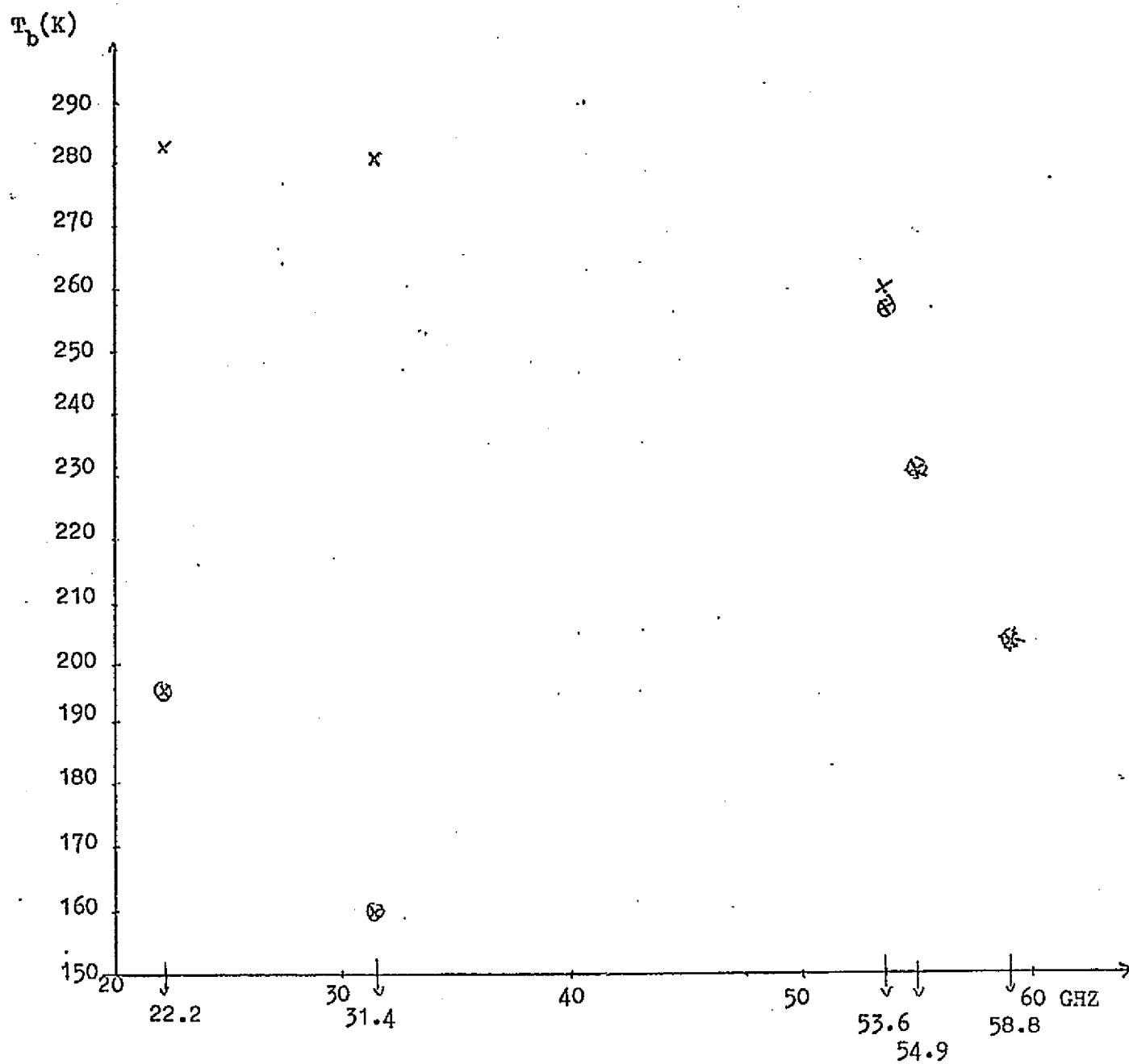
location(1)- \otimes

location(2)- x

(19Dec-29Dec)

1972

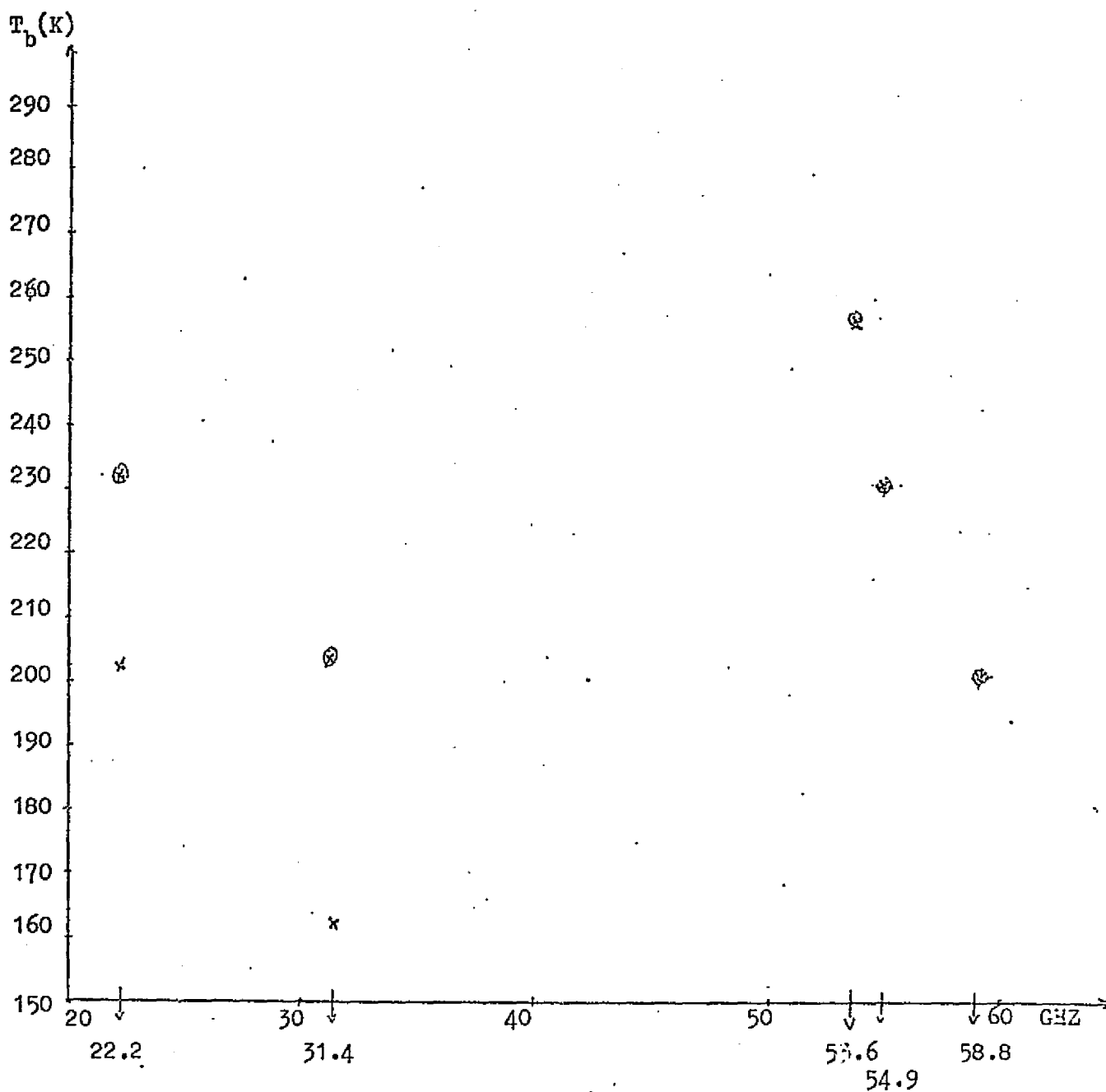




location(3)- ⊗

location(5)- x

(22Dec-23Dec) 1973

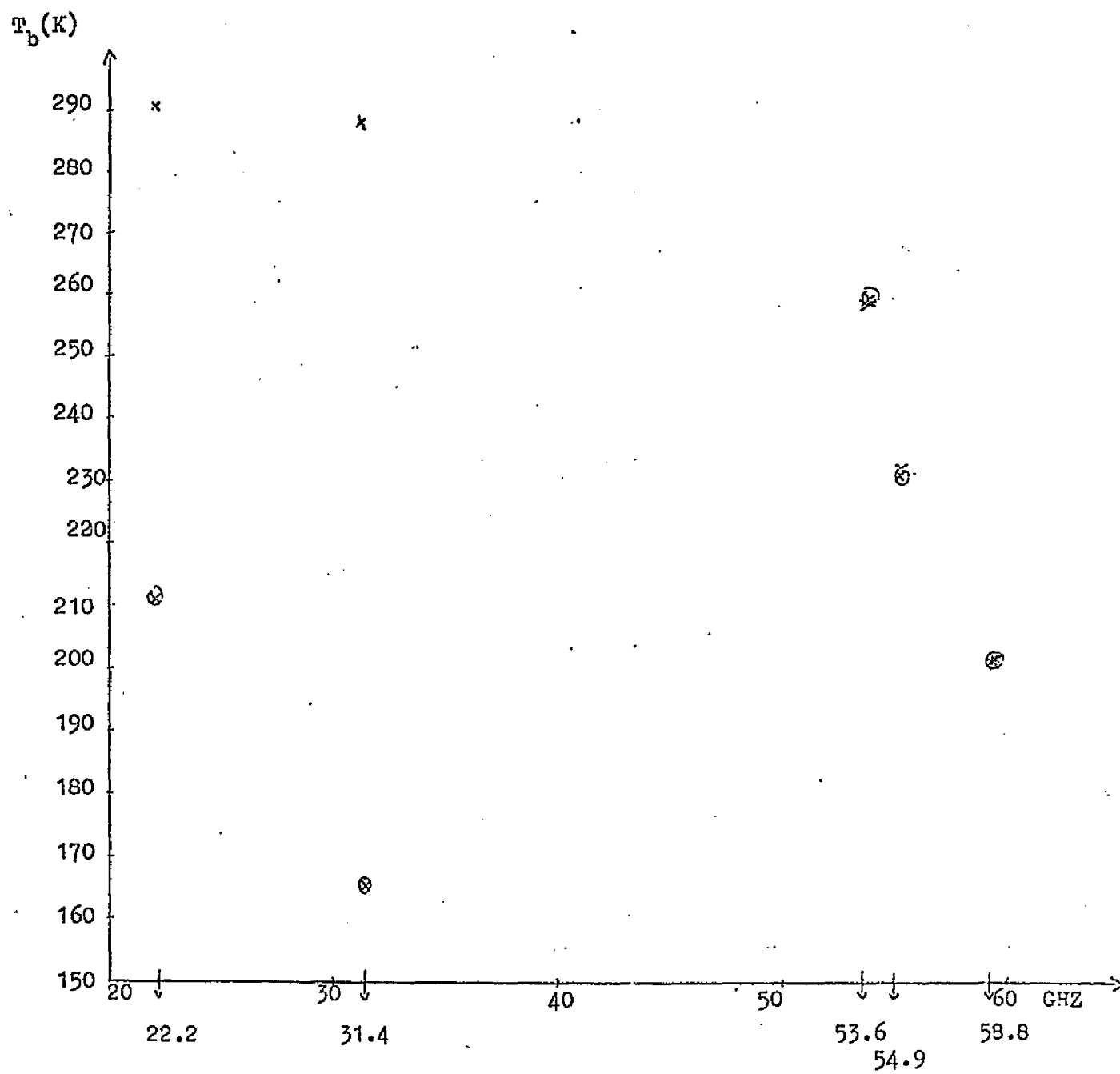


location(2)- ⊗

location(3)- x

(21Jan-30Jan)

1973

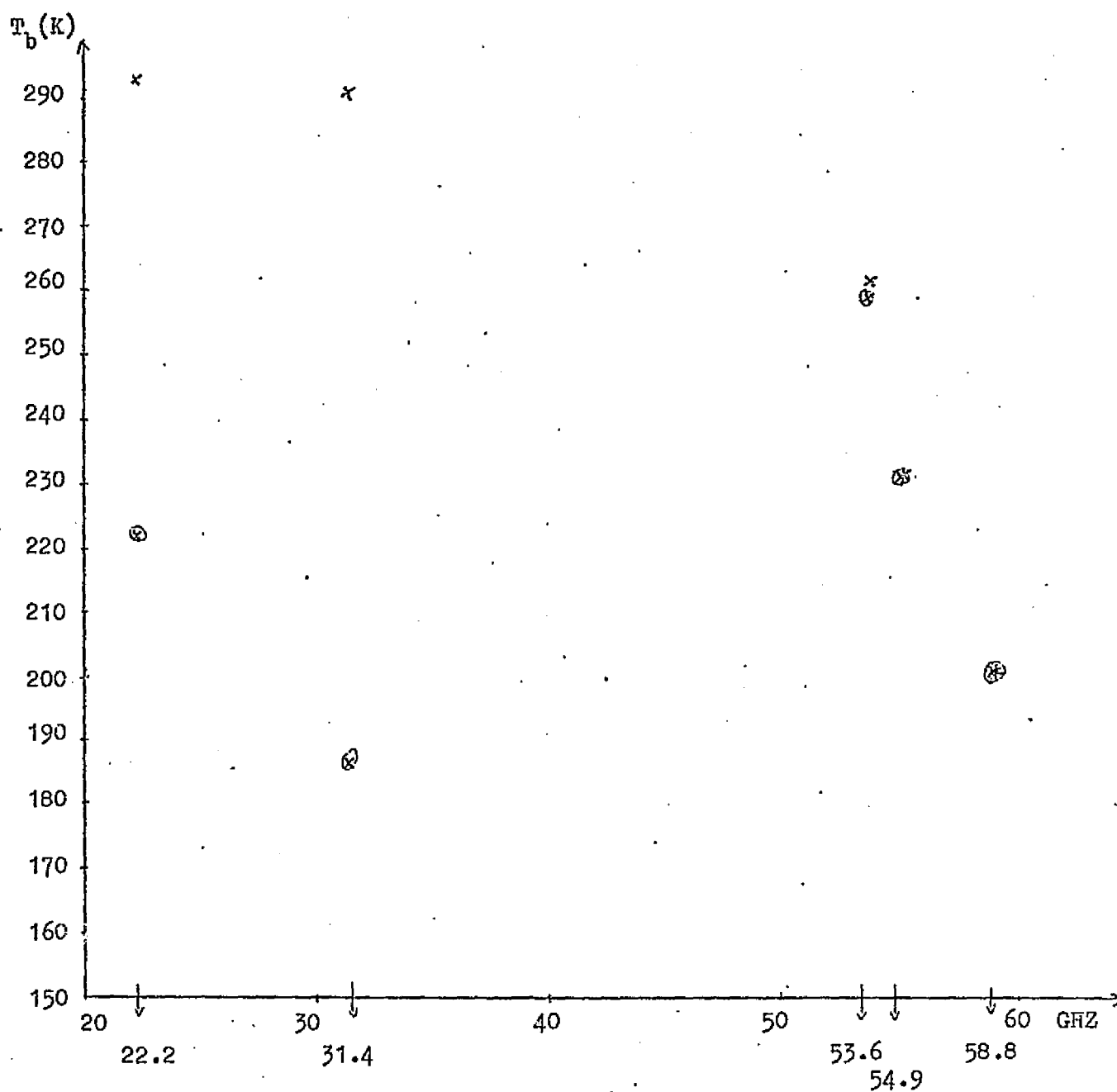


location(4)- ⊗

location(5)- x

(21Jan-30Jan)

1973

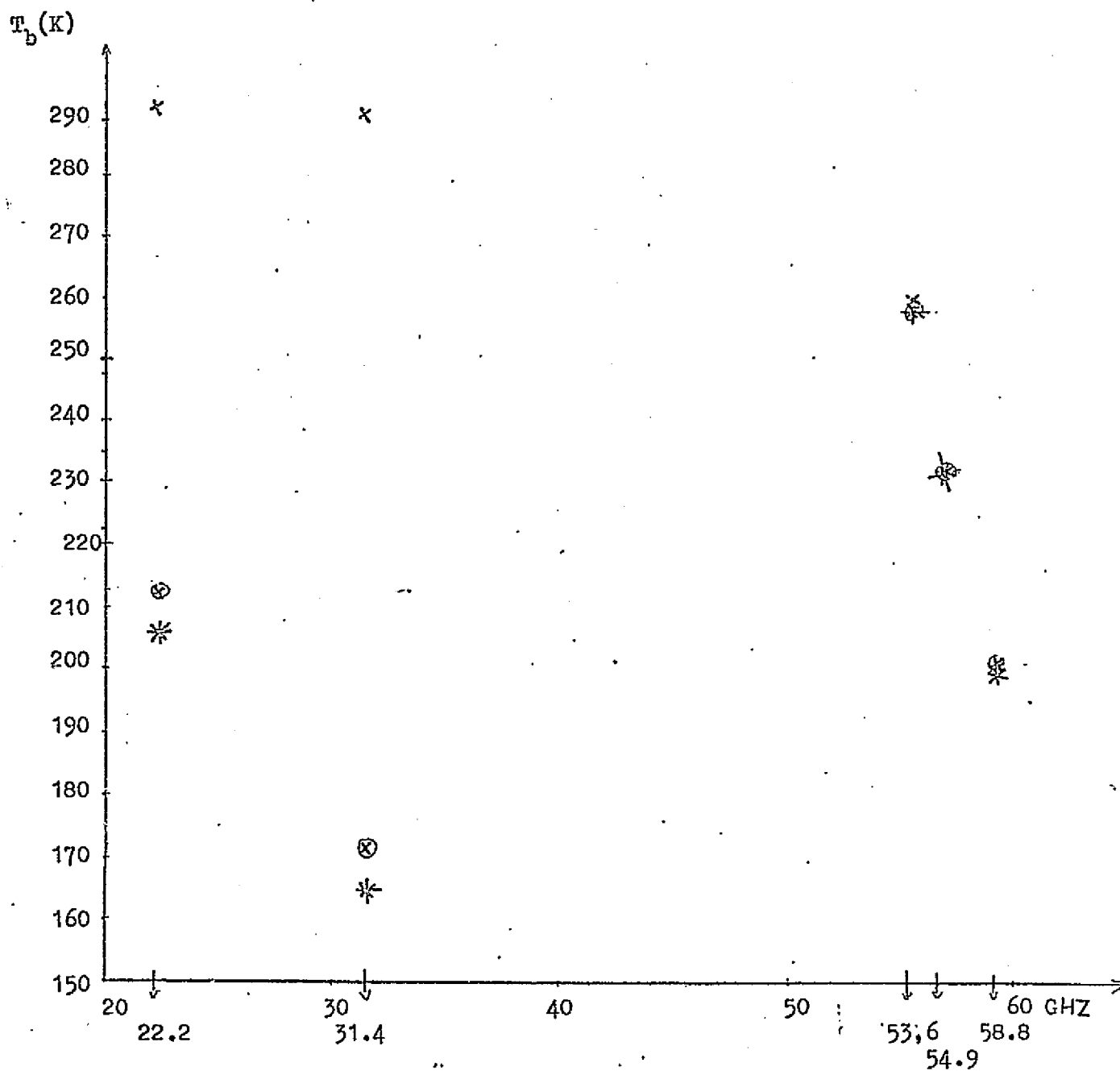


location(1)- \otimes

location(2)- \times

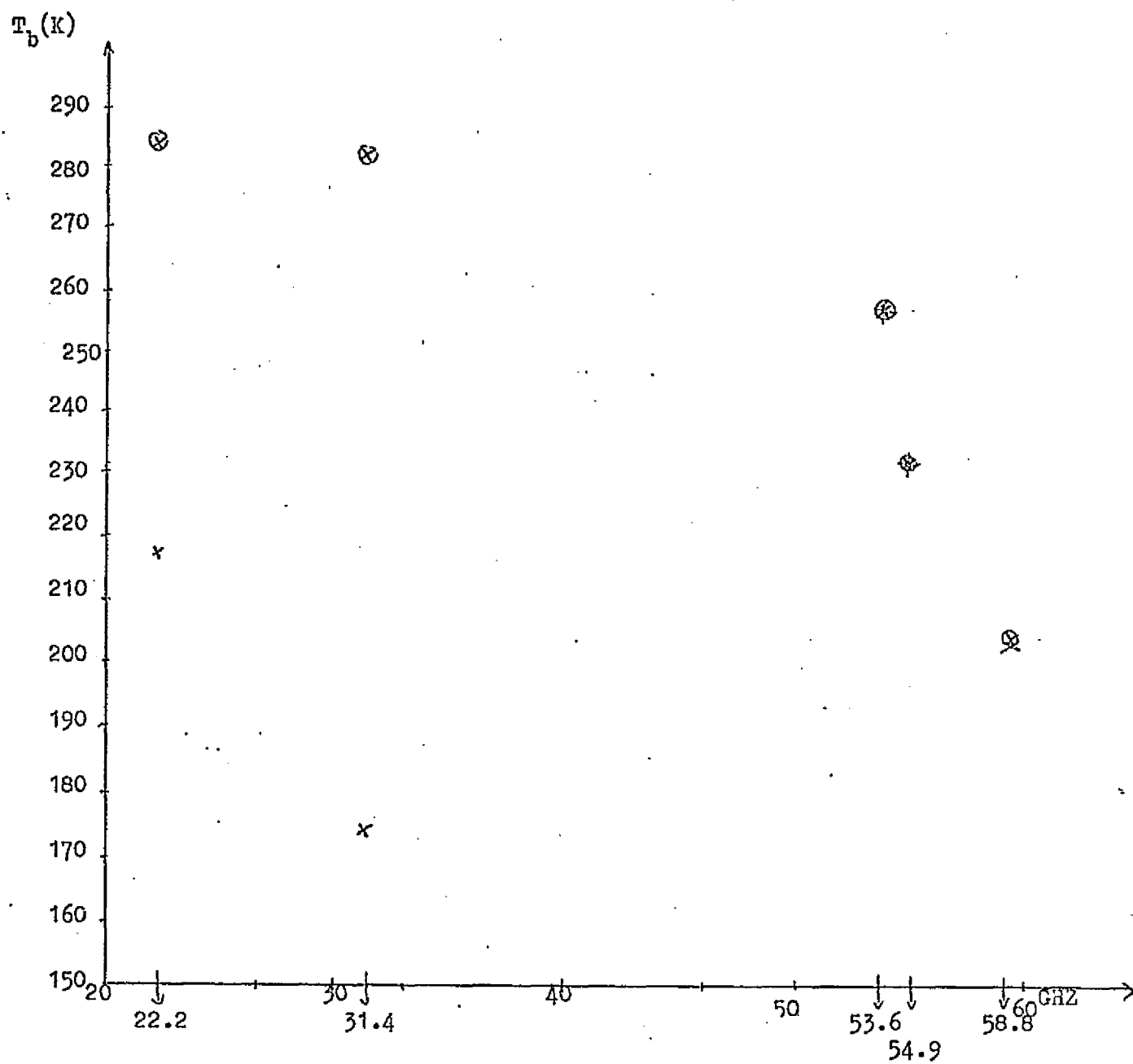
(22Feb-26Feb)

1973



location(3) - ⊗
location(4) - x
location(5) - *

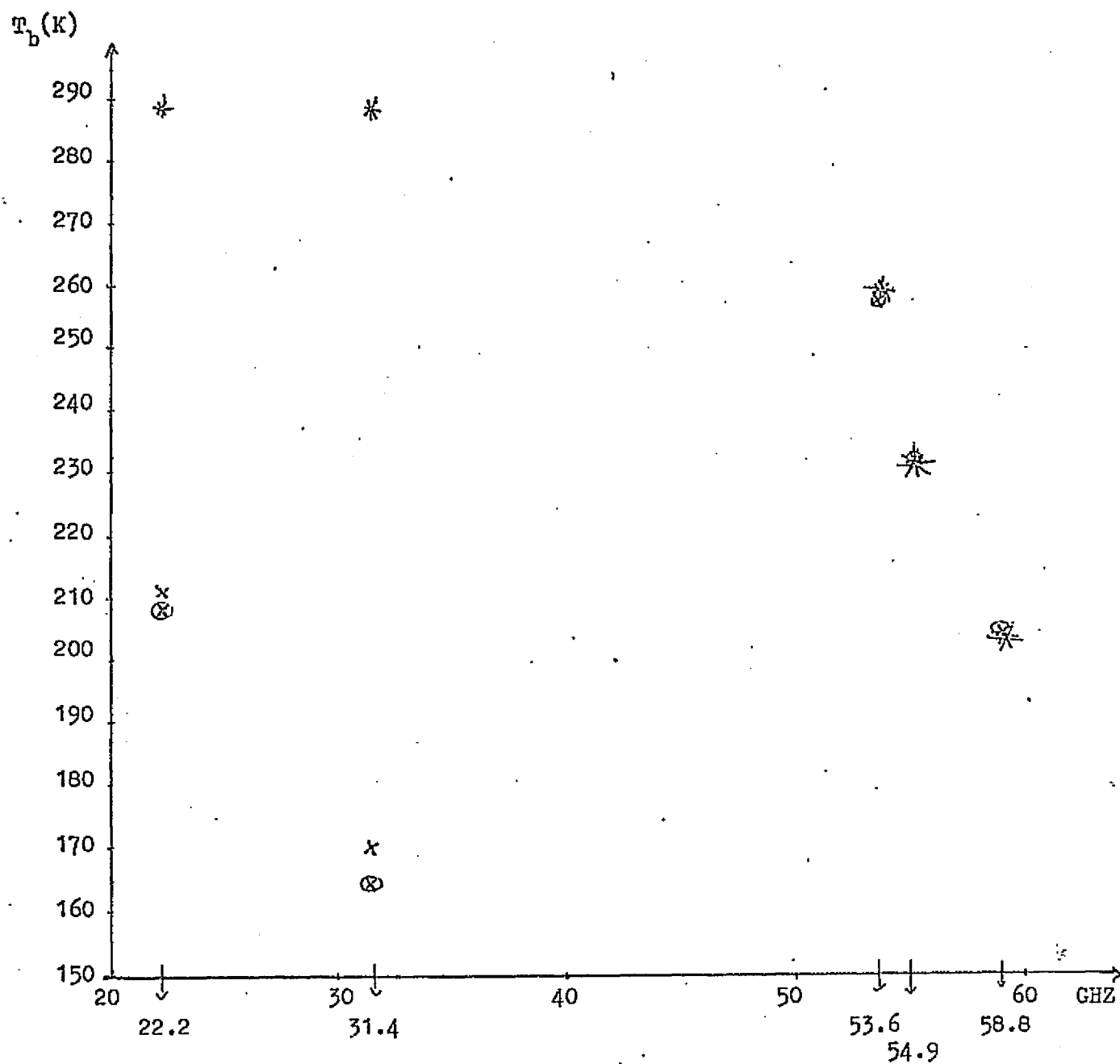
(22Feb-26Feb) 1973



location(1)- ⊗

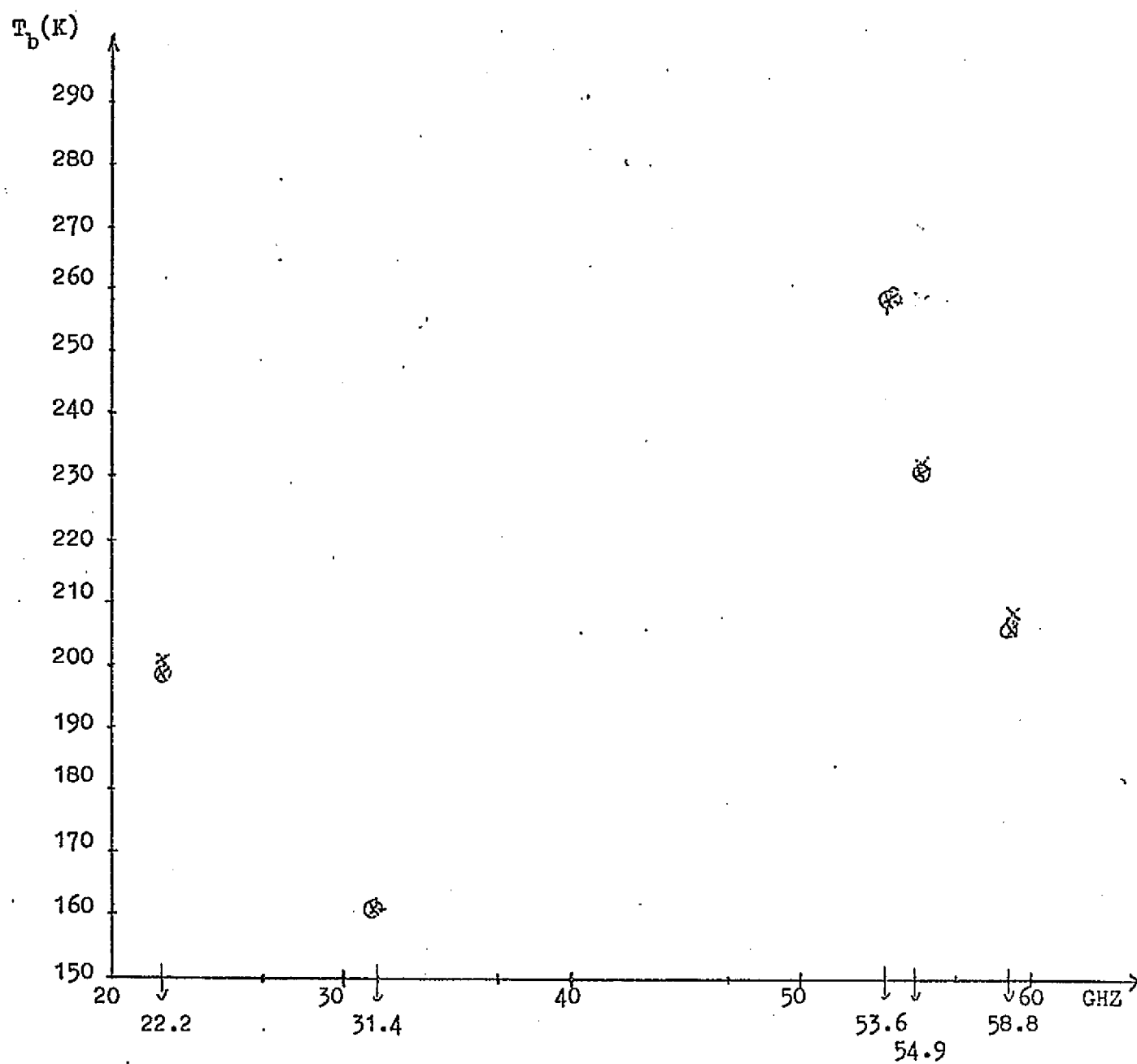
location(2)- x

(16Apr-25Apr) 1973



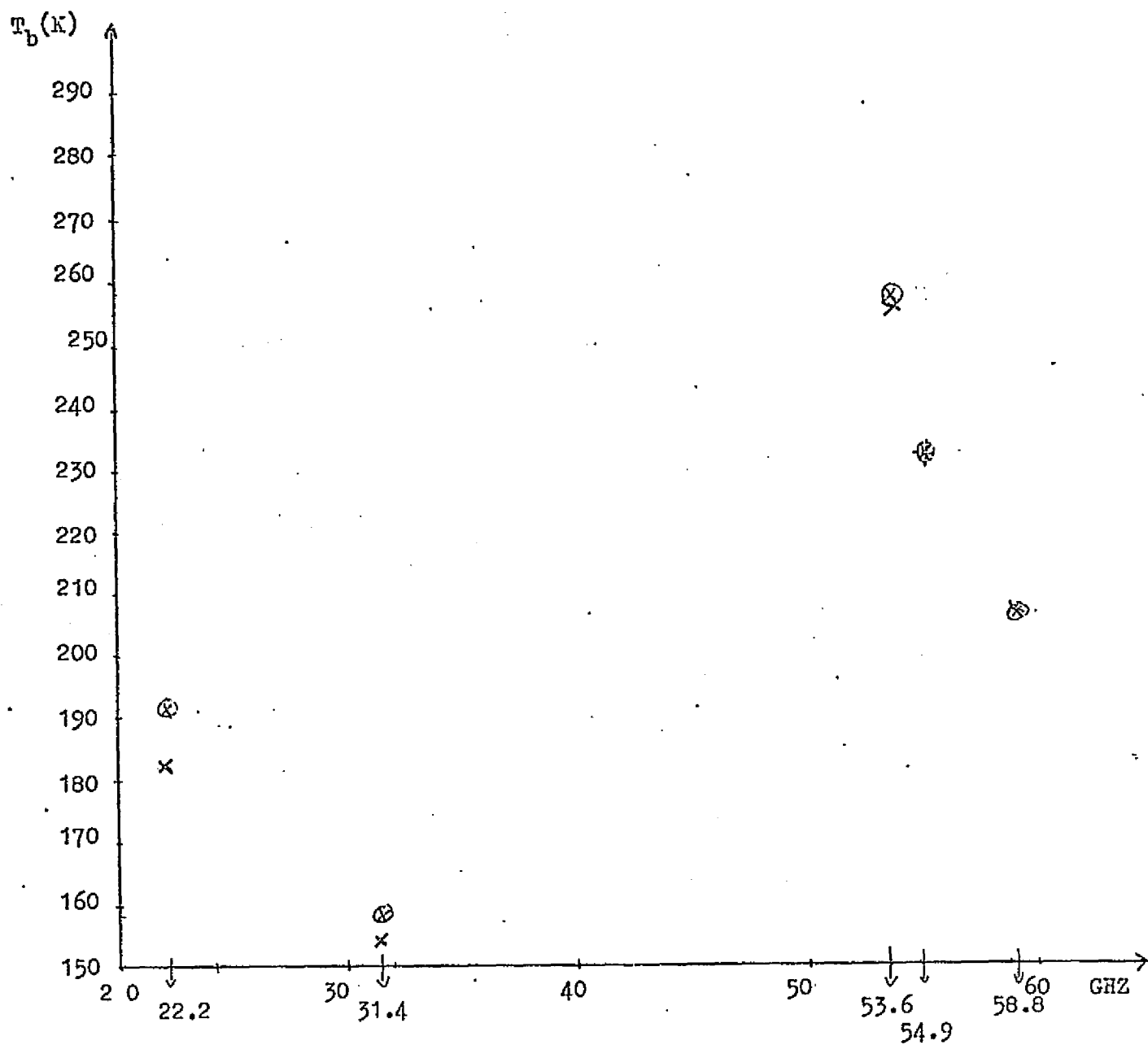
location(3)- ⊗
 location(4)- x
 location(5)- *

(16Apr-25Apr) 1973



location(2)- ⊗
location(3)- X

(17Jun-20Jun) 1973



location(4)- ⊗
location(5)- x

(17Jun-20Jun) 1973

Data Set II.

The five locations considered are:

	(1)	(2)	(3)	(4)	(5)
<u>Latitude:</u>	17 ± 0.5	17 ± 0.5	17 ± 0.5	17 ± 0.5	17 ± 0.5
<u>Longitude:</u>	$12 \pm 2W$	$4 \pm 2W$	$4 \pm 2E$	$12 \pm 2E$	$20 \pm 2E$

Measurements were all taken between 10:00 am and 12:30 pm. CHANNEL 1 and CHANNEL 2 correspond to 22.2 GHz and 31.4 GHz respectively. Even though only months are listed, they were all taken in the same period as those in Data Set II. Sometimes no data was found for our locations of interest.

Location (1)

	CHANNEL (1)	CHANNEL (2)
December	281	281
January	279	279
February	280	279
April	290	290
June	295	295

Location (2)

	CHANNEL (1)	CHANNEL (2)
December	277	276
January	-	-
February	278	278
April	-	-
June	293	292

Location (3)

	CHANNEL (1)	CHANNEL (2)
December	-	-
January	277	278
February	281	281
April	-	-
June	298	298

Location (4)

	CHANNEL (1)	CHANNEL (2)
December	280	280
January	272	271
February	284	284
April	286	286
June	-	-

Location (5)

	CHANNEL (1)	CHANNEL (2)
December	-	-
January	-	-
February	-	-
April	285	286
June	-	-

Table 2.

Frequency (GHz)	kw'	kw''
0.3	77.5	1.2
1.0	76.5	7.5
2.0	75.5	8.7
4.0	75.0	15.0
10.0	46.0	36.2
22.2	29.8	33.8
31.4	21.0	30.0

Dielectric Constant of Water at
the Frequencies of Interest

```

$JOE          EOUCLAR
1      REAL  Z,HS,CF,FF(100),Y(100),ZI,RF(7)
2      REAL  F(7),EM(7),FREQ(7)
3      COMPLEX  ZJ,U,KS(7),KW(7),RTEM(7)
4      COMPLEX  K(100),EX(100),R(100),S(99),Q(100),CON(100),CSQRT,
1 CEXP,CONJG
5      5      FORMAT(2F4.1,3X,2F5.3,3X,F4.1,I2)
6      READ(5,5) (KW(JI),KS(JI),FREQ(JI),F(JI),JI=1,7)
7      DO 111 JI=1,7
8      HS=0.84
9      CF=0.26
10     Z=0.07
11     N=10
12     ZJ=(0.0,1.0)
13     ZI=1.0
14     S(1)=Z+CF
15     N11=N-1
16     DO 50 M=2,N11
17     S(M)=S(M-1)+Z
18     50     CONTINUE
19     U=(KW(JI)+F(JI))/(KS(JI)+F(JI))
20     Y(1)=((HS/S(1))**2/2)*(-1)
21     FF(1)=((1-EXP(Y(1)))-0.19)*0.56
22     N11=N-1
23     DO 55 ML=2,N11
24     Y(ML)=((HS/S(ML))**2/2)*(-1)
25     FF(ML)=((1-EXP(Y(ML)))-0.19)*0.56
26     55     CONTINUE
27     DO 300 J=2,N
28     JN=J-1
29     Q(J)=((KS(JI)*U)+(FF(N-JN)*(KW(JI)-(KS(JI)*U))))/(U+FF(N-JN)
1*(1-U))
30     300     CONTINUE
31     K(1)=0.209*FREQ(JI)
32     DO 777 IL=2,N
33     K(IL)=0.209*FREQ(JI)*CSQRT(Q(IL))
34     777     CONTINUE
35     L=N-1
36     R(1)=K(1)-K(2)
37     R(1)=R(1)/(K(1)+K(2))
38     EX(1)=(0.0,0.0)
39     DO 525 I=2,L
40     R(I)=K(I)-K(I+1)
41     R(I)=R(I)/(K(I)+K(I+1))
42     EX(I)=2.0*K(I)*(S(I)-S(I-1))
43     525     CONTINUE
44     CON(L)=(0.0,0.0)
45     IF (AIMAG(EX(L)).GT.30.0) GO TO 89
46     CON(L)=CEXP((0.0,1.0)*EX(L))*R(L)
47     89     CONTINUE
48     LL=L-1
49     IF (LL.EQ.1) GO TO 378
50     JKL=LL-1
51     DO 526 JK=1,JKL
52     I=L-JK
53     CON(I)=(0.0,0.0)

```

REPRODUCIBILITY OF THE
ORIGINAL PAGE IS POOR

```

54      IF (AIMAG(EX(I)).GT.30.0) GO TO 88
55      CON(I)=CEXP(ZJ*EX(I))*(R(I)+CON(I+1))/(ZI+R(I)*CON(I+1))
56      88  CONTINUE
57      526 CONTINUE
58      378 CON(1)=(R(1)+CON(2))/(ZI+R(1)*CON(2))
59      RTE4(JI)=CON(1)
60      RF(JI)=(CABS(RTE4(JI)))**2
61      EM(JI)=1-RF(JI)
62      111 CONTINUE
63      10  FORMAT(' ',7F6.2)
64      WRITE(6,10) (EM(JJ),JJ=1,7)
65      STOP
66      END

```


References

- [1] Von Hippel, "Dielectric Materials and Applications", M.I.T. Press, p. 19, 1966.

- [2] P. Hoekstra and A. Delaney, "Dielectric Properties of Soils at UHF and Microwave Frequencies", Journal of Geophysical Research, Volume 79, No. 11, pp. 1700-1703, April 10, 1974.

- [3] P. Hoekstra and A. Delaney, "Dielectric Properties of Soils at UHF and Microwave Frequencies", Journal of Geophysical Research, Volume 79, No. 11, pp. 1703-1706, April 10, 1974.

- [4] E. I. Parkhomenko, "Electrical Properties of Rocks", translated from Russian by G. V. Keller, Plenum Press, New York, p. 8, 1967.

- [5] G. Poe, A. Stogryn, and A. T. Edgerton, "Determination of Soil Moisture Content using Microwave Radiometry", Final Technical Report, 1648R-1, Aerojet-General Corp., El Monte, California, Contract No. 0-35239, June 1971.

REPRODUCIBILITY OF THE
ORIGINAL PAGE IS POOR

- [6] E. I. Parkhomenko, "Electrical Properties of Rocks", translated from Russian by G. V. Keller, Plenum Press, New York, p. 16, 1967.
- [7] D. H. Staelin, "Remote Sensing of Atmospheric and Surface Temperatures with Microwaves", Proceedings of the Fifth Symposium on Temperature, Instrument Society of America, Pittsburgh, 1972.
- [8] K. Tomiyasu, "Remote Sensing of the Earth by Microwaves", Proceedings of the IEEE, Volume 62, No. 1, January 1974.
- [9] W. Peake, "Interaction of Electromagnetic Waves with Some Natural Surfaces", IRE Trans. on Antennas and Propagation, AP-7, p. 8324-8329, 1959.
- [10] K. F. Kunzi, A. D. Fisher, D. H. Staelin, and J. Waters, "Snow and Ice Surfaces Measured by the Nimbus 5 Microwave Spectrometer", to be published in Journal of Geophysical Research, 1975.
- [11] A. Stogryn, "The Brightness Temperature of a Vertically Structured Medium", Radio Science, Volume 5, No. 12, pp. 1397-1406, December 1970.

- [12] G. Poe and A. T. Edgerton, "Soil Moisture Mapping by Ground and Airborne Microwave Radiometry", Report, Microwave Division, Aerojet-General Corp., El Monte, California, 1972.
- [13] T. Schmugge, P. Gloersen, T. Wilheit, and F. Geiger, "Remote Sensing of Soil Moisture with Microwave Radiometers", Journal of Geophysical Research, Volume 79, No. 2, January 1974.
- [14] T. W. Lambe, "Capillary Phenomena in Cohesionless Soils", Ph. D. Thesis, M. I. T., 1948.
- [15] J. A. Kong, "Theory of Electromagnetic Waves", Chapter 4, Wiley Interscience, 1975.
- [16] Von Hippel, "Table of Dielectric Constants", Dielectric Materials and Applications, M. I. T. Press, p. 314, 1966.
- [17] P. W. Rosenkrantz, F. T. Barath, J. C. Blinn III, and E. J. Johnson, W. B. Lenoir, D. H. Staelin, and J. W. Waters, "Microwave Radiometric Measurements of Atmospheric Temperature and Water from an Aircraft", Journal of Geophysical Research, Volume 77, No. 30, October 20, pp. 5837-5838, 1972.

- [18] T. Schmugge, P. Gloersen, T. Wilheit, and F. Geiger, "Remote Sensing of Soil Moisture with Microwave Radiometers", Journal of Geophysical Research, Volume 79, No. 2, January 10, pp: 319-320, 1974.
- [19] G. Rummey, "Climatology and the World's Climates", Climates of Africa, Volume 10, MacMillan, New York, 1968.
- [20] R. Maignien, "Review of Research on Laterites", United Nations Educational, Scientific and Cultural Organization, 1966.

The Brightness Temperature of a Half-Space Random
Medium with Nonuniform Temperature Profile*

L. Tsang and J. A. Kong

Department of Electrical Engineering and
Computer Science and Research Laboratory
of Electronics

Massachusetts Institute of Technology
Cambridge, Massachusetts 02139

Abstract

The problem of microwave thermal emission from a half-space random medium with a nonuniform temperature distribution is solved with the radiative transfer approach. For constant absorption and scattering coefficients, the brightness temperature is determined by a simple close form formula. Physical interpretations and numerical results are illustrated and discussed for the various cases.

* This work was supported by the NASA Contract 953524 and the Joint Services Electronics Program (Contract DAAB07-74-C-0630).

I. Introduction

In passive remote sensing of the earth with microwaves, the brightness temperature reading of a radiometer depends on its angle of observation and on the microwave emissive properties of the observed area. Using the model of a half-space dielectric medium, various theories have been developed for interpretation of data collected from satellite and spacecraft. It is well appreciated that in snow, ice, or desert areas the subsurface temperature profile, absorption, and scattering are dominant factors in the surface brightness temperature [Kunzi et al 1975]. Assuming uniform temperature distribution, Gurvich et al [1973] derived expressions for the brightness temperatures of a half-space random medium with a laminar structure. Using a radiative transfer approach, England [1974] considered nonuniform temperature profile and assumed isotropic scattering phase function. Stogryn examined the brightness temperature of a vertically structured medium with no scattering [1970]. He also studied scattering by random dielectric constant fluctuations in the low frequency limit using a perturbational approach [1974]. In this paper we propose to solve the problem of microwave thermal emission from a half-space medium with a laminar structure and non-uniform temperature profile.

REPRODUCIBILITY OF THE
ORIGINAL PAGE IS POOR

II. Formulation

Consider a half-space random medium characterized by a random permittivity

$$\epsilon_t = \epsilon_m + \epsilon_f(z) \quad (1)$$

$$\epsilon_m = \epsilon_m' + i \epsilon_m''(z) \quad (2)$$

where ϵ_m' is a constant and ϵ_f and ϵ_m'' are functions of z only. Assume that $\epsilon_m'' \ll \epsilon_m'$ and that $\epsilon_f(z)$ denotes the randomly fluctuating part whose ensemble average is zero. The medium also possesses a nonuniform temperature distribution $T(z)$. A radiometer is sensing at an angle θ_0 from nadir. The result of the brightness temperature is dependent on the polarization and the observation angle θ_0 . Let I_u and I_d denote intensities for the upward and downward radiation inside the medium which make angle θ with the nadir (Figure 1). The angles θ and θ_0 are related by Snell's law. In what follows all results are expressed in terms of θ .

The radiative transfer equations are written as

$$\cos \theta \frac{d I_u}{dz} = -\kappa_e I_u + \kappa_a B_T + \kappa_s J_u \quad (3)$$

$$\cos \theta \frac{d I_d}{dz} = \kappa_e I_d - \kappa_a B_T - \kappa_s J_d \quad (4)$$

with

$$J_u = \frac{P_f}{2} I_u + \frac{P_d}{2} I_d$$

$$J_d = \frac{P_f}{2} I_d + \frac{P_f}{2} I_u$$

subject to the boundary condition

$$I_d \Big|_{z=0} = r_{ot} I_u \Big|_{z=0} \quad (5)$$

where r_{ot} is the Fresnel reflectivity at the boundary which depends on θ , θ_o , polarization, and the properties of the medium. In (3) and (4)

$$B_T = \frac{2\kappa}{\lambda^2} \frac{\epsilon_m'}{\epsilon_o} T(z) \quad (6)$$

where $T(z)$ is the temperature distribution, κ is the Boltzmann constant, and λ is the free space wavelength. Equation (3) describes the change in radiation intensity I_u as it propagates for a distance of dz . It decays by $\kappa_e I_u dz$ and is reinforced by the thermal source $\kappa_a B_T dz$ and the scattering source $\kappa_s J_u dz$. A similar interpretation applies to (4). In (3) and (4), κ_a is the loss per unit length of intensity due to absorption

$$\kappa_a = 2 \kappa_m'' \quad (7)$$

where $k_m'' = \text{Im}(k_m) = \text{Im} \sqrt{\omega^2 \mu \epsilon_m}$, and κ_e is the total extinction per unit length caused by absorption and scattering.

$$\kappa_e = \kappa_a + \kappa_s \quad (8)$$

The scattering loss per unit length κ_s and the scattering phase functions P_f and P_b are derived in Appendix A for the TE and TM waves; TE waves are polarized with electric field vector perpendicular to the plane of incidence and TM waves have polarization parallel to the plane of incidence. The results are

(1) For TE Waves

$$\kappa_s = \frac{k_m^2 \Delta \ell}{\cos \theta} \left\{ \frac{1 + 2k_m^2 \ell^2 \cos^2 \theta}{1 + 4k_m^2 \ell^2 \cos^2 \theta} \right\} \quad (9)$$

$$P_f = \frac{1 + 4k_m^2 \ell^2 \cos^2 \theta}{1 + 2k_m^2 \ell^2 \cos^2 \theta} \quad (10)$$

$$P_b = \frac{1}{1 + 2k_m^2 \ell^2 \cos^2 \theta} \quad (11)$$

(2) For TM Waves

REPRODUCIBILITY OF THE
ORIGINAL PAGE IS POOR

$$\kappa_s = \frac{k_m^2 \Delta \ell}{2 \cos \theta} \left\{ \frac{1 + 4k_m^2 \ell^2 \cos^2 \theta + \cos^2 2\theta}{1 + 4k_m^2 \ell^2 \cos^2 \theta} \right\} \quad (12)$$

$$P_f = \frac{2(1 + 4k_m^2 \ell^2 \cos^2 \theta)}{1 + 4k_m^2 \ell^2 \cos^2 \theta + \cos^2 2\theta} \quad (13)$$

$$P_b = \frac{2\cos^2 2\theta}{1 + 4k_m^2 \ell^2 \cos^2 \theta + \cos^2 2\theta} \quad (14)$$

In (9) - (14), ℓ denotes the correlation length of an exponential correlation function and Δ the variance of the fluctuation in dielectric constant.

The task now is to solve Equations (3) - (5) for given medium properties. Once the upward intensity is obtained, the brightness temperature T_B as measured by a radiometer is given by

$$T_B = \frac{\lambda^2 \epsilon_0}{2\kappa \epsilon_m'} (1 - r_{ot}) I_u \Big|_{z=0} \quad (15)$$

For the general case when κ_a and κ_s are functions of space coordinates, Equations (3) - (5) can be cast in the form of integral equations and solved by an iterative approach. The formulation is presented in Appendix B where a solution to first order in κ_s is obtained to check with that derived from exact solutions as presented in the following section.

III. Half-Space Medium with Constant Absorption and Scattering Coefficients

When κ_a and κ_s of the half-space medium are constants independent of space coordinates, (3) and (4) become two first order differential equations with constant coefficients. We assume a nonuniform temperature profile of the type

$$T(z) = T_o + T_h e^{\gamma z}. \quad (16)$$

The solution is found to be

$$I_d = P e^{\alpha z / \cos \theta} + B_o + \frac{\alpha^2 + \kappa_a \gamma \cos \theta}{\alpha^2 - \gamma^2 \cos^2 \theta} B_h e^{\gamma z} \quad (17)$$

$$I_u = \frac{\alpha - \kappa_a}{\alpha + \kappa_a} P e^{\alpha z / \cos \theta} + B_o + \frac{\alpha^2 - \kappa_a \gamma \cos \theta}{\alpha^2 - \gamma^2 \cos^2 \theta} B_h e^{\gamma z} \quad (18)$$

where

$$\alpha = \kappa_e \sqrt{(1 - \omega) \left[1 - \left(\frac{\omega}{2} P_f \right) + \left(\frac{\omega}{2} P_b \right) \right]} \quad (19)$$

$$P = - \frac{(\alpha + \kappa_a)}{(\alpha + \kappa_a) - r_{ot}(\alpha - \kappa_a)} \left[(1 - r_{ot}) B_o + \frac{(\alpha^2 + \kappa_a \gamma \cos \theta) - r_{ot}(\alpha^2 - \kappa_a \gamma \cos \theta)}{\alpha^2 - \gamma^2 \cos^2 \theta} B_h \right] \quad (20)$$

$$B_h = 2\kappa \epsilon_m' T_h / \epsilon_o \lambda^2, \quad (21)$$

$$B_o = 2\kappa \epsilon_m' T_o / \epsilon_o \lambda^2, \quad (22)$$

and the scattering albedo

$$\tilde{\omega} = \kappa_s / \kappa_e. \quad (23)$$

The first terms in (17) - (18) are the homogeneous solution to the differential equations and the second and third terms are the particular solutions.

The brightness temperature is determined from (15),

$$T_B = \frac{2\kappa_a(1 - r_{ot})}{(\alpha + \kappa_a) - r_{ot}(\alpha - \kappa_a)} \left\{ T_o + \frac{\alpha}{\alpha + \gamma \cos \theta} T_h \right\} \quad (24)$$

Physical interpretations of this simple result are explored in the next section.

IV. Numerical Results and Discussions

We now examine several special cases. (a) For medium with uniform temperature distribution and no scattering, $T_h = 0$, $\kappa_s = 0$, and $\alpha = \kappa_a$. Thus

$$T_B = (1 - r_{ot}) T_o. \quad (25)$$

The emissivity is seen to be given by $1 - r_{ot}$. This result also agrees with that obtained by reciprocity arguments.

(b) For medium with no scattering, $\kappa_s = \tilde{\omega} = 0$, the result is

$$T_B = (1 - r_{ot}) \left(T_o + \frac{\kappa_a T_h}{\kappa_a + \gamma \cos \theta} \right). \quad (26)$$

As a numerical example, we consider the subsurface temperature distribution of the Amundsen-Scott station in Antarctic [Lettau, 1971]. The temperature profile is first fitted with exponentials. We find that for December 31st,

$$T_1(z) = 222 + 34 e^{0.81z}$$

for August 31st,

$$T_2(z) = 222 - 10 e^{0.37z},$$

and for April 1st,

$$T_3(z) = 222 + 81 e^{0.51z} - 88 e^{0.66z}.$$

The unit for temperature is in degree Kelvin. The temperature profiles are shown in Figure 2. The brightness temperatures as a function of frequency at nadir are shown in Figure 3 for $\epsilon_m = 1.8(1 + i 0.003)\epsilon_o$. It is seen that at very low frequencies T_B is determined by the temperature at greater depth which is essentially a constant $T_o = 222^\circ K$ with emissivity of ice surface approximately equal to $e = 0.978$. As frequency increases, the subsurface temperature becomes more important. At very high frequencies the brightness temperature approaches the value $e(T_o + T_h)$, as seen from (26).

It is interesting to note that (24) also reduces to (26) when $P_b = 0$ which corresponds to very high frequency. For when $P_f = 2$, $\alpha = \kappa_a$.

(c) For medium with scattering and uniform temperature distribution, $T_h = 0$, and we find

$$T_B = \frac{2\kappa_a(1 - r_{ot})}{(\alpha + \kappa_a) - r_{ot}(\alpha - \kappa_a)} T_o. \quad (27)$$

Numerical results are presented in Figures 4 and 5 and compared with that obtained by Gurvich et al [1973]. We see that for the Shelf

REPRODUCIBILITY OF THE
ORIGINAL PAGE IS POOR

glacier [Figure 4], higher brightness temperatures are predicted with our model. This is because their results are applicable to low scattering cases while the scattering albedo for the Shelf glacier is rather high. In the case of continental glacier [Figure 5] where the scattering albedo is quite small, both models agree quite well except at resonance where the scattering is largest

(d) In the case of uniform temperature distribution and small scattering albedo, we expand (27) to first order in $\tilde{\omega}$ by noting that

$$\alpha \approx \kappa_e (1 - \tilde{\omega} P_f/2) \quad (28)$$

and

$$\kappa_a = \kappa_e (1 - \tilde{\omega}). \quad (29)$$

The result is casted in a form to compare with that obtained by Gurvich et al [1973].

$$T_B = (1 - r_{ot}) \left(1 - \frac{(1 - r_{ot}) k_m^2 \Delta \ell^2}{8 k_m^2 \cos \theta (1 + 4 k_m^2 \ell^2 \cos^2 \theta)} \right) T_o. \quad (30)$$

This expression differed from their result in which there is a $\cos \theta_o$ in the numerator instead of a $\cos \theta$ in the denominator as shown in (30). An alternative derivation by using the wave approach is given in Appendix C which confirms (30).

Numerical results are given in Figure 6 to compare TE and TM waves as a function of radiometer viewing angle θ_o . Clearly, scattering lowers the brightness temperature at all viewing angles.

For nonuniform temperature distribution, expanding (24) to first order in $\tilde{\omega}$ yields

$$T_B = (1 - r_{ot}) \left\{ T_o \left[1 - \frac{\tilde{\omega} P_b}{4} (1 - r_{ot}) \right] + \frac{T_h}{1 + \gamma \cos \theta / \kappa_e} \right. \\ \left. \left[1 - \frac{\gamma \cos \theta / \kappa_e}{1 + \gamma \cos \theta / \kappa_e} \frac{\tilde{\omega} P_f}{2} - \frac{\tilde{\omega} P_b}{4} (1 - r_{ot}) \right] \right\}. \quad (31)$$

This result is checked with the iteration approach as presented in Appendix B.

(e) Finally, we plot T_B for the temperature profile for the Amundsen-Scott Station by using the exact formula in (24). The results are shown in Figure 7. The radiometer is viewing from nadir.

Conclusions

The problem of a half-space random medium with nonuniform temperature distribution has been solved with the radiative transfer approach. For constant absorption and scattering coefficients, the result in (24) is very simple and admit direct physical interpretation. It is interesting to note by comparing (24) and (26) that α corresponds to an effective absorption coefficient in the presence of scattering. Various special cases are discussed. For medium with inhomogeneous absorption and scattering coefficients, an iterative approach can be used. In Appendix B, such an approach is illustrated and shown to give identical results in the limit of constant κ_a and κ_s . The theory and results are compared with previous approaches. To check the results that we obtained, the wave approach is used (Appendix C). It is a straightforward matter to extend the radiative transfer approach to multi-layer models.

Appendix A

In this appendix, we derive the scattering loss per unit length κ_s and the forward and backward scattering phase functions P_f and P_b as given in (9) - (14). The scattered electric field \vec{E}^s of an incident field \vec{E}_i can be expressed in terms of total field \vec{E} by the wave equation

$$\nabla \times \nabla \times \vec{E}^s(\vec{r}) - k_m^2 \vec{E}^s(\vec{r}) = \omega^2 \mu \epsilon_f(\vec{r}) \vec{E}(\vec{r}). \quad (A-1)$$

In terms of the dyadic Green's function we have

$$\vec{E}^s(\vec{r}) = -i\omega \int d^3r' \vec{G}(\vec{r}, \vec{r}') \cdot \epsilon_f(\vec{r}') \vec{E}(\vec{r}'). \quad (A-2)$$

Inside the integrand in (A-2) we write

$$\vec{E}(\vec{r}') \approx \vec{E}_i(\vec{r}') = \hat{A}_0 E_0 e^{i\vec{k} \cdot \vec{r}'} \quad (A-3)$$

where \vec{k} is the incident wave vector, and \hat{A}_0 is a unit vector denoting the polarization of the incident wave. Using far-field approximation, we obtain

$$\vec{E}^s(\vec{r}) = (\vec{I} - \hat{k}_s \hat{k}_s) \cdot \hat{A}_0 \frac{\omega^2 \mu e^{ikr}}{4\pi r} \int d^3r' \epsilon_f(\vec{r}') e^{i(\vec{k} - \vec{k}_s) \cdot \vec{r}'} \quad (A-4)$$

and

$$\langle |\bar{E}^S(\bar{r})|^2 \rangle = \sin^2 \chi \frac{k_m^4 E_0^2}{16\pi^2 \epsilon_m^2 r^2} \int d^3 r_1 d^3 r_2 \langle \epsilon_f(\bar{r}_1) \epsilon_f^*(\bar{r}_2) \rangle e^{i(\bar{k} - \bar{k}_s) \cdot (\bar{r}_1 - \bar{r}_2)} \quad (A-5)$$

where χ is the angle between the incident polarization \hat{A}_0 and the scattered direction \hat{k}_s . Letting $\bar{\rho} = \bar{r}_1 - \bar{r}_2$ and

$$\langle \epsilon_f(\bar{r}_1) \epsilon_f^*(\bar{r}_2) \rangle = \Delta \epsilon_m^2 b(\bar{r}_1 - \bar{r}_2) \quad (A-6)$$

we find the bistatic scattering cross section per unit volume to be

$$q(\bar{k}, \bar{k}_s) = \sin^2 \chi \frac{k_m^4 \Delta}{16 \pi^2} \int d^3 \rho b(\bar{\rho}) e^{i(\bar{k} - \bar{k}_s) \cdot \bar{\rho}} \quad (A-7)$$

This result checks with that obtained by Gurvich (1973) and Tatarski (1961) when we identify $\Delta = 4 \sigma_{no}^2$.

To calculate scattering loss per unit length, we consider the case where

$$b(\bar{\rho}) = e^{-|\bar{\rho}|/\ell} \quad (A-8)$$

Let the plane of incidence be the $\hat{x} - \hat{z}$ plane. We write

$$\bar{k} = \hat{x} k_m \sin \theta + \hat{z} k_m \cos \theta \quad (A-9)$$

$$\bar{k}_s = \hat{x} k_m \sin \theta_s \cos \phi_s + \hat{y} k_m \sin \theta_s \sin \phi_s + \hat{z} k_m \cos \theta_s \quad (A-10)$$

The scattering loss per unit length κ_s is

$$\begin{aligned} \kappa_s &= \int d\Omega_s \alpha(\vec{k}, \vec{k}_s) \\ &= \int_0^{2\pi} d\phi_s \int_0^\pi d\theta_s \sin \theta_s \sin^2 \chi \frac{k_m^2 \Delta}{4} \frac{2\ell}{1 + k_m^2 (\cos \theta - \cos \theta_s)^2 \ell^2} \\ &\quad \delta(k_m \sin \theta - k_m \sin \theta_s \cos \phi_s) \delta(k_m \sin \theta_s \sin \phi_s). \end{aligned}$$

(A-11)

Within the range of integration, the Dirac delta functions give non-zero results at (1) $\phi_s = 0$ and $\theta_s = \theta$ which corresponds to forward scattering and (2) $\phi_s = \pi$ and $\theta_s = \pi - \theta$ which corresponds to backward scattering. This finding is essentially dictated by phase matching for the laminar structure [Kong, 1975].

The integral in (A-11) is evaluated by changing variables

$$u = k_m \sin \theta_s \cos \phi_s - k_m \sin \theta \quad (A-12)$$

$$v = k_m \sin \theta_s \sin \phi_s \quad (A-13)$$

which gives the Jacobian $1/|k_m^2 \sin \theta_s \cos \theta_s|$.

(1) For TE waves, $\chi = \pi/2$, and

$$\kappa_s = \frac{k_m^2 \Delta \ell}{2 \cos \theta} \left\{ 1 + \frac{1}{1 + 4k_m^2 \ell^2 \cos^2 \theta} \right\}. \quad (A-14)$$

The first term is from forward scattering and the second term from backward scattering. Equation (9) follows from (A-14). Equations (10) - (11) are obtained from (A-14) by noting that $P_f + P_b = 2$ and $P_f/P_b = 1 + 4 k_m^2 \ell^2 \cos^2 \theta$.

(2) For TM waves, we have for forward scattering, $\chi = \pi/2$ and for backward scattering $\sin^2 \chi = \cos^2 2\theta$. The scattering loss per unit length is calculated to be

$$\kappa_s = \frac{k_m^2 \Delta \ell}{2 \cos \theta} \left\{ 1 + \frac{\cos^2 2\theta}{1 + 4k_m^2 \ell^2 \cos^2 \theta} \right\}. \quad (\text{A-15})$$

Again the first term is from forward scattering and the second term from backward scattering. Equations (12) - (14) are direct consequences of (A-15).

REPRODUCIBILITY OF THE
ORIGINAL PAGE IS POOR

Appendix B

In general, Equations (3) to (5) can be solved by an iteration approach. First we cast the Equations into integral form

$$I_u(z) = B_0 e^{-\int_{-\infty}^z dz' \kappa'_e(z')} + \int_{-\infty}^z dz' (\kappa'_a(z') B_T(z') + \kappa'_s(z') J_u(z')) e^{-\int_{z'}^z dz'' \kappa'_e(z'')} \quad (B-1)$$

$$I_d(z) = \int_z^0 dz' (\kappa'_a(z') B_T(z') + \kappa'_s(z') J_d(z')) e^{-\int_z^{z'} dz'' \kappa'_e(z'')} + r_{ot} \int_{-\infty}^0 dz' (\kappa'_a(z') B_T(z') + \kappa'_s(z') J_u(z')) e^{-\int_z^0 dz'' \kappa'_e(z'')} - \int_{z'}^0 dz'' \kappa'_e(z'') \quad (B-2)$$

where $\kappa'_s = \kappa_s / \cos \theta$, $\kappa'_a = \kappa_a / \cos \theta$, $\kappa'_e = \kappa_e / \cos \theta$. For iteration we assume κ'_s is small and write

$$I_u(z) = I_u^{(0)}(z) + I_u^{(1)}(z) + I_u^{(2)}(z) + \dots \quad (B-3)$$

$$I_d(z) = I_d^{(0)}(z) + I_d^{(1)}(z) + I_d^{(2)}(z) + \dots \quad (B-4)$$

Substituting in (B-1) to (B-2) and equating the appropriate orders, we obtain, for $m = 0, 1, 2, \dots$

$$I_u^{(m+1)} = \int_{-\infty}^z dz' \kappa'_s(z') J_u^{(m)}(z') e^{-\int_{z'}^z dz'' \kappa'_e(z'')} \quad (B-5)$$

$$\begin{aligned} I_d^{(m+1)} = & \int_z^0 dz' \kappa'_s(z') J_d^{(m)}(z') e^{-\int_z^{z'} dz'' \kappa'_e(z'')} \\ & + r_{ot} \int_{-\infty}^0 dz' \kappa'_s(z') J_u^{(m)}(z') e^{-\int_z^0 dz'' \kappa'_e(z'')} - \int_{z'}^0 dz'' \kappa'_e(z'') \end{aligned} \quad (B-6)$$

with

$$I_u^{(0)} = B_o e^{-\int_{-\infty}^z dz' \kappa'_e(z')} + \int_{-\infty}^z dz' \kappa'_a(z') B_T(z') e^{-\int_{z'}^z dz'' \kappa'_e(z'')} \quad (B-7)$$

$$\begin{aligned} I_d^{(0)} = & \int_z^0 dz' \kappa'_a(z') B_T(z') e^{-\int_z^{z'} dz'' \kappa'_e(z'')} \\ & + r_{ot} \int_{-\infty}^0 dz' \kappa'_a(z') B_T(z') e^{-\int_z^0 dz'' \kappa'_e(z'')} - \int_{z'}^0 dz'' \kappa'_e(z'') \end{aligned} \quad (B-8)$$

Consider the special case when κ'_e and κ'_s are independent

of z . Assume a nonuniform temperature profile of the type

$$T(z) = T_0 + T_h e^{\gamma z}. \quad (B-9)$$

We find from (B-7)

$$I_u^{(0)}(z) = \frac{\kappa'_a B_0}{\kappa'_e} + \frac{\kappa'_a B_h}{\kappa'_e + \gamma} e^{\gamma z} \quad (B-10)$$

B_h and B_0 are given by (21) and (22).

From (B-8),

$$I_d^{(0)}(z) = \frac{\kappa'_a B_0}{\kappa'_e} + \frac{\kappa'_a B_h}{\kappa'_e - \gamma} e^{\gamma z} + \left[- \left(\frac{\kappa'_a B_0}{\kappa'_e} + \frac{\kappa'_a B_h}{\kappa'_e - \gamma} \right) + r_{ot} \left(\frac{\kappa'_a B_0}{\kappa'_e} + \frac{\kappa'_a B_h}{\kappa'_e + \gamma} \right) \right] e^{\kappa'_e z}. \quad (B-11)$$

Introducing (B-10) and (B-11) in (B-5), we obtain

$$I_u^{(1)} \Big|_{z=0} = \frac{\omega \kappa'_a B_0}{\kappa'_e} + \frac{\kappa'_s P_f}{2} \frac{\kappa'_a B_h}{(\kappa'_e + \gamma)^2} + \frac{\kappa'_s P_b}{2} \frac{\kappa'_a B_h}{\kappa_e'^2 - \gamma^2} + \frac{\omega P_b}{4} \left[- \left(\frac{\kappa'_a B_0}{\kappa'_e} + \frac{\kappa'_a B_h}{\kappa'_e - \gamma} \right) + r_{ot} \left(\frac{\kappa'_a B_0}{\kappa'_e} + \frac{\kappa'_a B_h}{\kappa'_e + \gamma} \right) \right]. \quad (B-12)$$

The brightness temperature is then given by

$$T_B = \frac{\lambda^2 (1 - r_{ot}) \epsilon_0}{2\kappa\epsilon_m} (I_u^{(0)}(0) + I_u^{(1)}(0))$$

which gives (31).

Appendix C

For uniform temperature distribution with constant T_o , the brightness temperature is given by

$$T_b = T_o (1 - r_{ot} - s) \quad (C-1)$$

where s denotes contributions from scattering. Consider a plane TE wave incident upon the half-space medium at the incident angle θ .

$$E_{yi} = E_o e^{i(k_x x - k_z z)} \quad (C-2)$$

The equations that govern the electric fields in the upper and lower regions are

$$\left(\frac{d^2}{dz^2} + k_z^2 \right) E_y = 0 \quad (C-3)$$

$$\left(\frac{d^2}{dz^2} + k_{mz}^2 \right) E_{yt} = -\omega^2 \mu \epsilon_f(z) E_{yt} \quad (C-4)$$

where $k_x^2 + k_z^2 = k^2$, $k_x^2 + k_{mz}^2 = k_m^2$, and E_{yt} is the electric field in the half-space medium.

We first solve the Green's function for (C-3) and (C-4) and then use Born approximation to calculate the scattered fields.

The Green's functions in the two regions are governed by

$$\left(\frac{d^2}{dz^2} + k_z^2 \right) G_{ot}(z, z') = 0 \quad (C-5)$$

$$\left(\frac{d^2}{dz^2} + k_{mz}^2 \right) G_{tt}(z, z') = \delta(z - z'). \quad (C-6)$$

Imposing the following boundary conditions at $z = 0$:

$$G_{ot} = G_{tt} \quad (C-7)$$

$$\frac{d G_{ot}}{dz} = \frac{d G_{tt}}{dz} \quad (C-8)$$

and the radiation condition at $z \rightarrow \pm \infty$, we find

$$G_{ot}(z, z') = \frac{1 - R_{ot}}{2i k_{mz}} e^{ik_z z - ik_{mz} z'} \quad (C-9)$$

where R_{ot} is the Fresnel TE reflection coefficient between two media with permittivities ϵ and ϵ_m . The Green's function in region t $G_{tt}(z, z')$ is given by a more complicated expression.

The Born approximation to the scattered field in region 0 is

$$E_Y^s(z) = - \int_{-\infty}^0 dz' G_{ot}(z, z') \omega^2 \mu \epsilon_f(z') E_{ty}(z'). \quad (C-10)$$

The zeroth order field amplitude in region t is given by

$$E_{ty}^0(z') = (1 + R_{ot}) E_0 e^{-ik_{mz} z'} \quad (C-11)$$

Using the correlation function in (A-8), we obtain

$$\begin{aligned} \langle |E^S|^2 \rangle &= E_0^2 \frac{(1 - R_{ot}^2)^2 \Delta k_m^4}{4 |k_{mz}^2|} \int_{-\infty}^0 dz_1 \int_{-\infty}^0 dz_2 \\ &\quad e^{-i2k_{mz} z_1 + i2k_{mz}^* z_2} e^{-|z_1 - z_2|/\ell} \\ &= E_0^2 \frac{(1 - r_{ot})^2 \Delta k_m^4}{8 |k_{mz}^2| k_{mz}''} \frac{\ell}{1 + 4k_{mz}^2 \ell^2} \\ &\approx E_0^2 \frac{(1 - r_{ot})^2 \Delta k_m^2 \ell}{8 k_m'' \cos \theta (1 + 4k_{mz}^2 \ell^2)} \quad (C-12) \end{aligned}$$

in view of the fact that $k_{mz}' k_{mz}'' = k_m' k_{m'}''$, $k_m' \approx k_m$ and $k_{mz}' \approx k_{mz} \approx k_m \cos \theta$. Equation (C-12) gives the second term in (30).

REPRODUCIBILITY OF THE
ORIGINAL PAGE IS POOR

References

- [1] England, A. W. (1974), Thermal Microwave Emission from a Halfspace Containing Scatterers, Radio Sci., 9, 447-454.
- [2] Gurvich, A. S., V. I. Kalinin, and D. T. Matveyev (1973), Influence of the Internal Structure of Glaciers on Their Thermal Radio Emission, Atm. and Oceanic Phys., 9, 712-717.
- [3] Kong, J. A. (1975), Theory of Electromagnetic Waves, Wiley-Interscience, New York.
- [4] Kunzi, K. F., D. H. Staelin, and J. W. Waters (1974), Earth Surface Emission Measured with the Nimbus 5 Microwave Spectrometer, Proc. of the URSI Commission II Specialist Meeting on Microwave Scattering and Emission from the Earth, Sept. 24, p. 113.
- [5] Lettau, H. (1971), Antarctic Atmosphere as a Test Tube for Meteorological Theories, pp. 443-475, in Research in the Antarctic, Washington: Am. Assn. for the Adv. of Sci.
- [6] Stogryn, A. (1970), The Brightness Temperature of a Vertically Structured Medium, Radio Sci., 5, 1397-1406.

- [7] Stogryn, A. (1974), Electromagnetic Scattering by Random Dielectric Constant Fluctuations in a Bounded Medium, Radio Sci., 5, 509-518.
- [8] Tatarskii, V. I. (1961), Wave Propagation in a Turbulent Medium, McGraw-Hill, New York.

Figure Captions

- Figure 1. Geometry of the problem.
- Figure 2. Subsurface temperature distributions at the Amundsen-Scott Station in Antarctic.
- Figure 3. Brightness temperature (without scattering) as a function of frequency for the three temperature distributions shown in Figure 2.
- Figure 4. Brightness temperature for shelf glacier and compared with that obtained by Gurvich et al and depicted in broken lines.
- Figure 5. Brightness temperature for Continental Glacier and compared with that obtained by Gurvich et al and depicted in broken lines.
- Figure 6. Brightness temperature as a function of viewing angle for TE and TM waves.
- Figure 7. Brightness temperature as a function of frequency for different scattering media for the three different temperature distributions in Figure 2.

Figure 1.

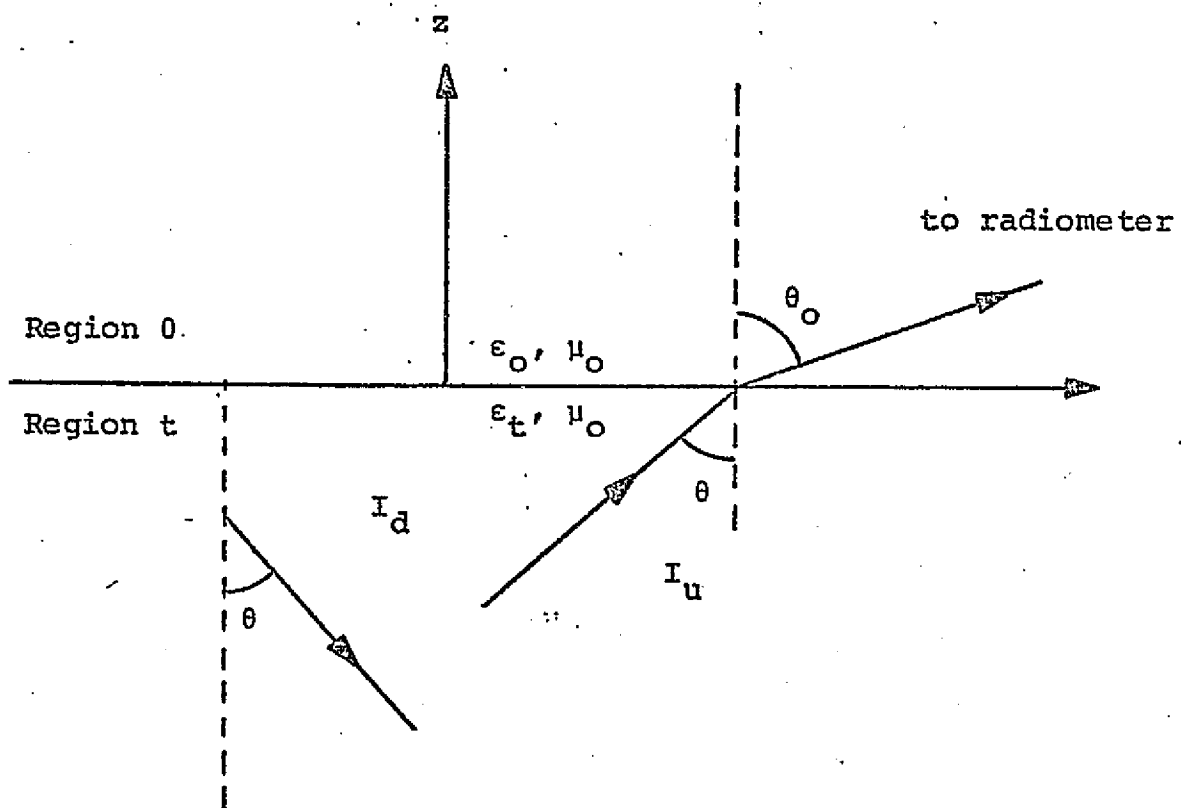


Figure 2.

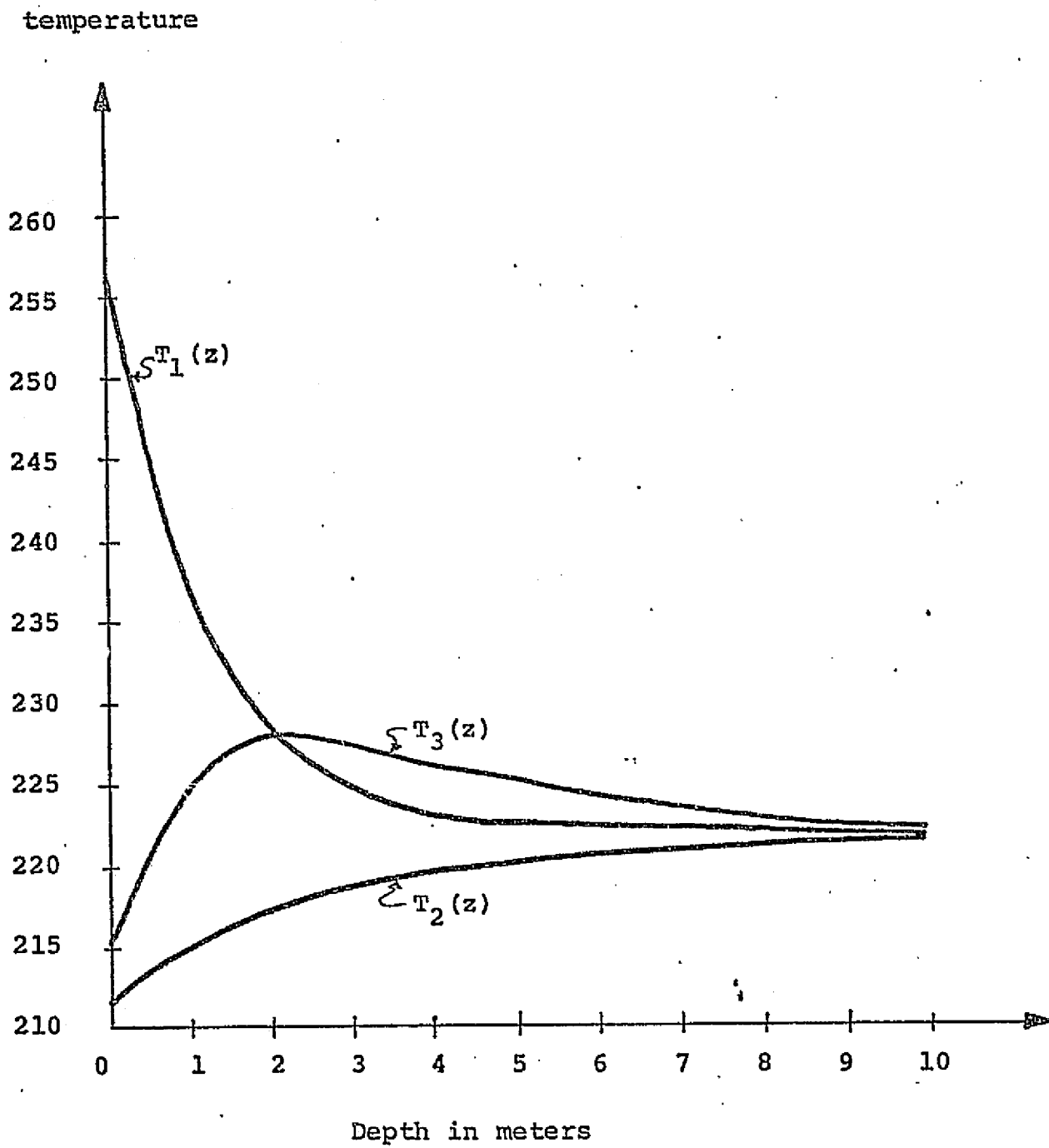


Figure 3.

Brightness temperature

$$\epsilon_m' = 1.8$$

$$\epsilon_m'' = -0.00054$$

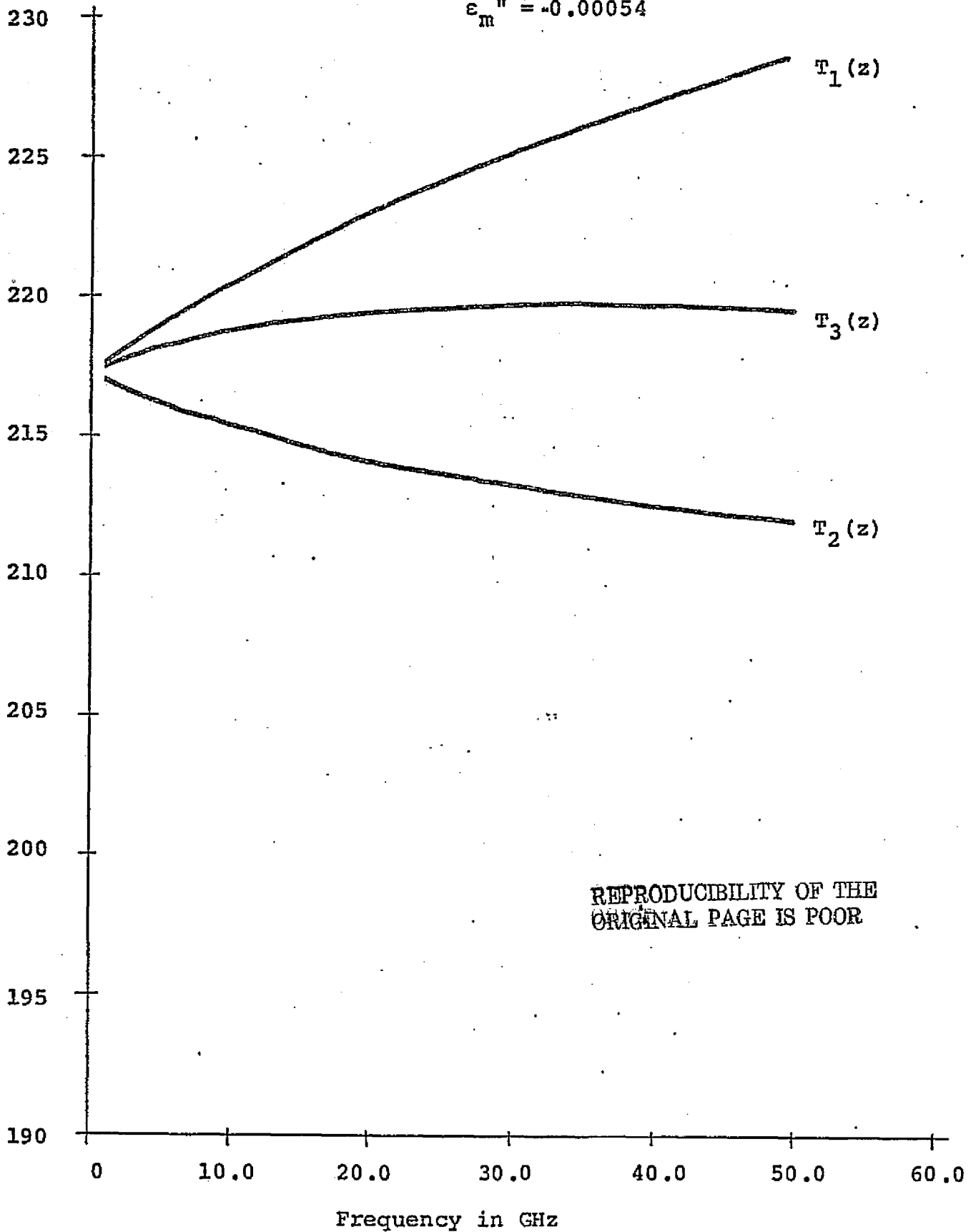


Figure 4.

Shelf Glacier

(Gurvich's Notations)

$$\epsilon_m' = 1.8$$

$$\epsilon_m'' = 6.7 \times 10^{-4}$$

$$n_i = 2.5 \times 10^{-4}$$

$$\Delta = 0.002$$

$$l = 2 \text{ mm.}$$

$$z_o = 2 \text{ mm.}$$

$$T_o = 258^\circ\text{K}$$

$$P = 2.7$$

Brightness temperature

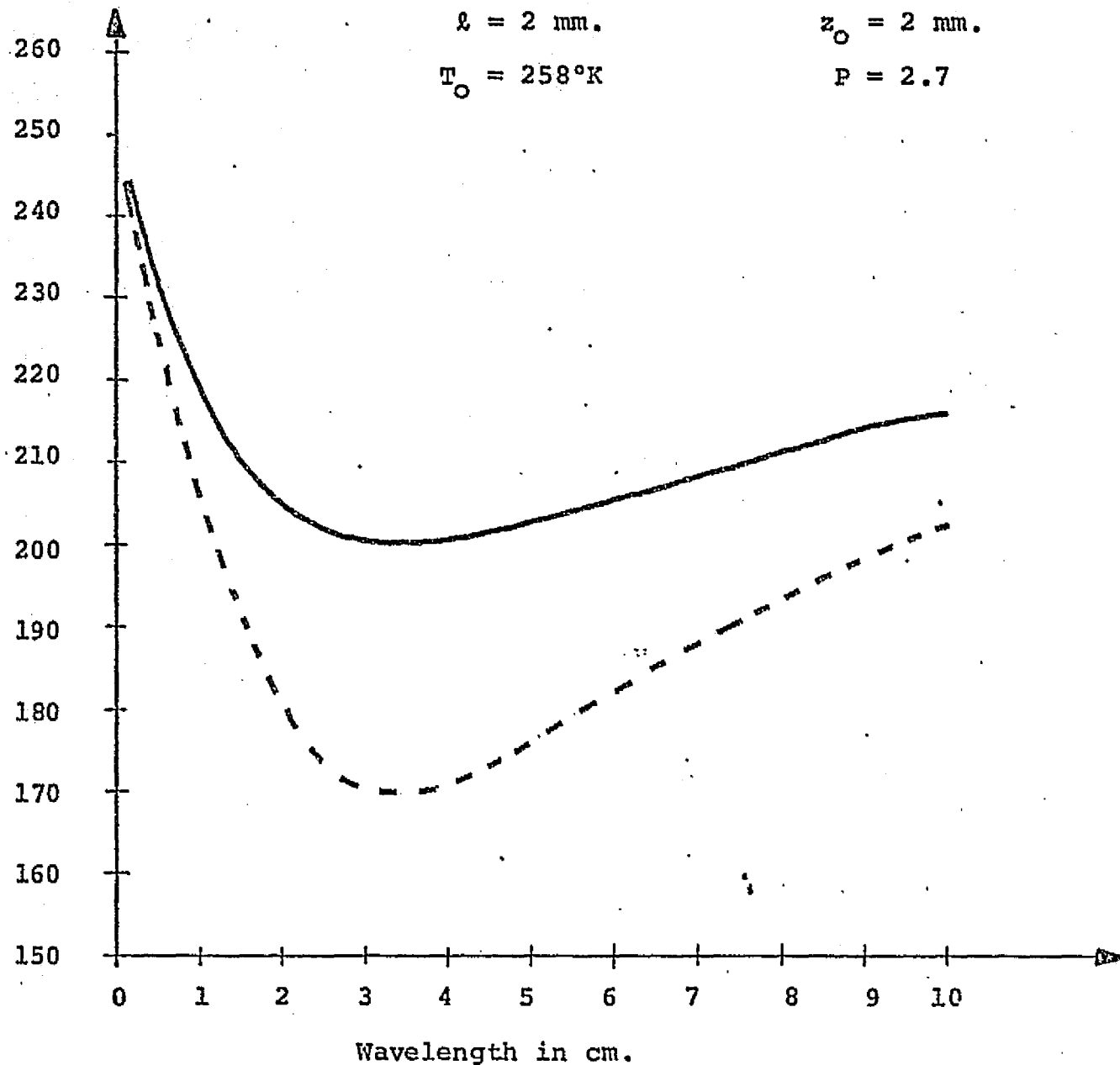


Figure 5.

Brightness Temperature

Continental Glacier (Gurvich's Notations)

$$\epsilon_m' = 1.8$$

$$\epsilon_m'' = 5.4 \times 10^{-4}$$

$$\Delta = 0.0006$$

$$n_i = 2 \times 10^{-4}$$

$$l = 0.6 \text{ mm.}$$

$$z_o = 0.6 \text{ mm.}$$

$$T_o = 233^\circ\text{K}$$

$$P = 1$$

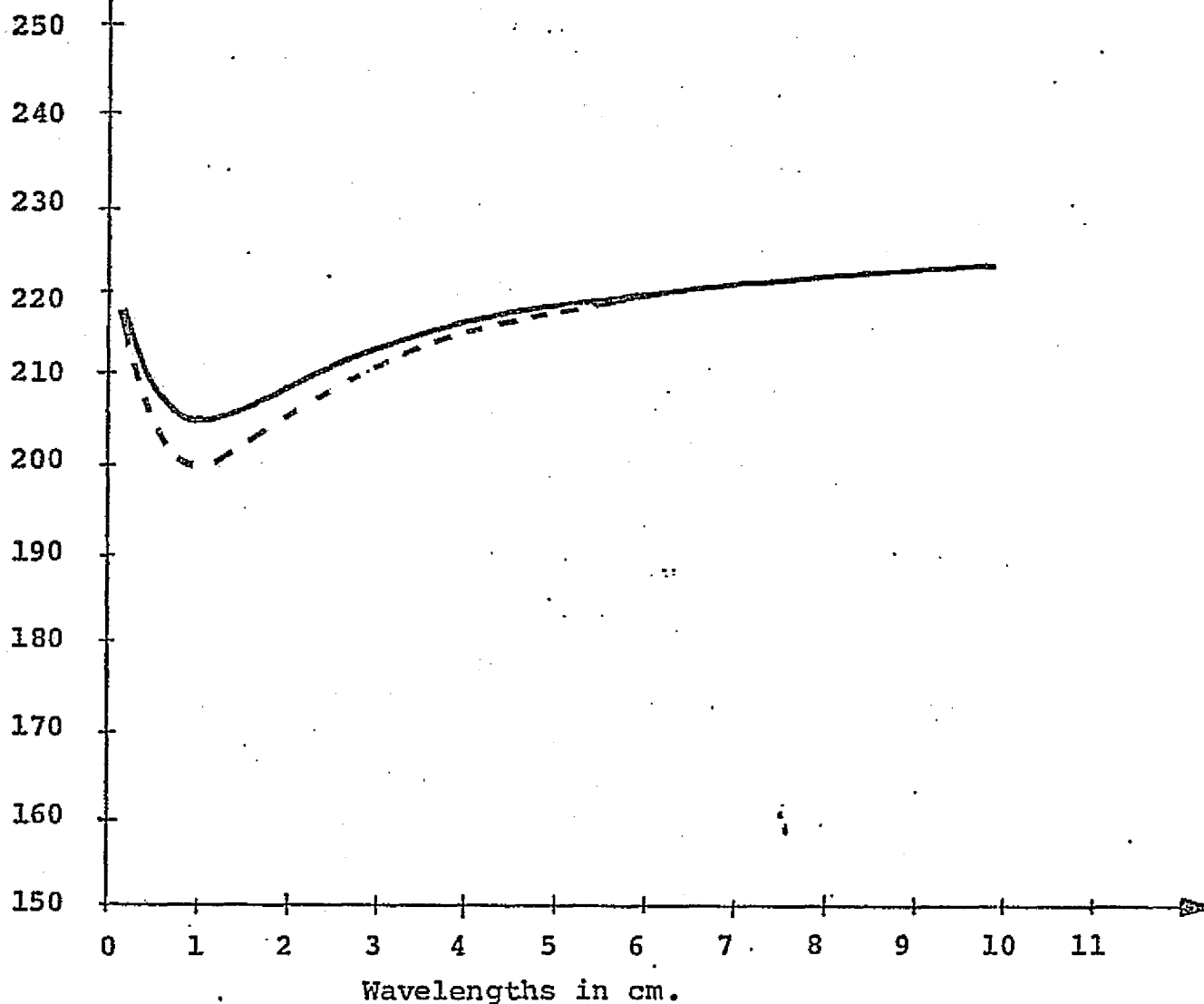


Figure 6.

Frequency = 20 GHz

$$\epsilon_m' = 1.8$$

$$\epsilon_m'' = 0.00054$$

$$l = 2 \text{ mm.}$$

$$T = T_1(z)$$

Brightness Temperature

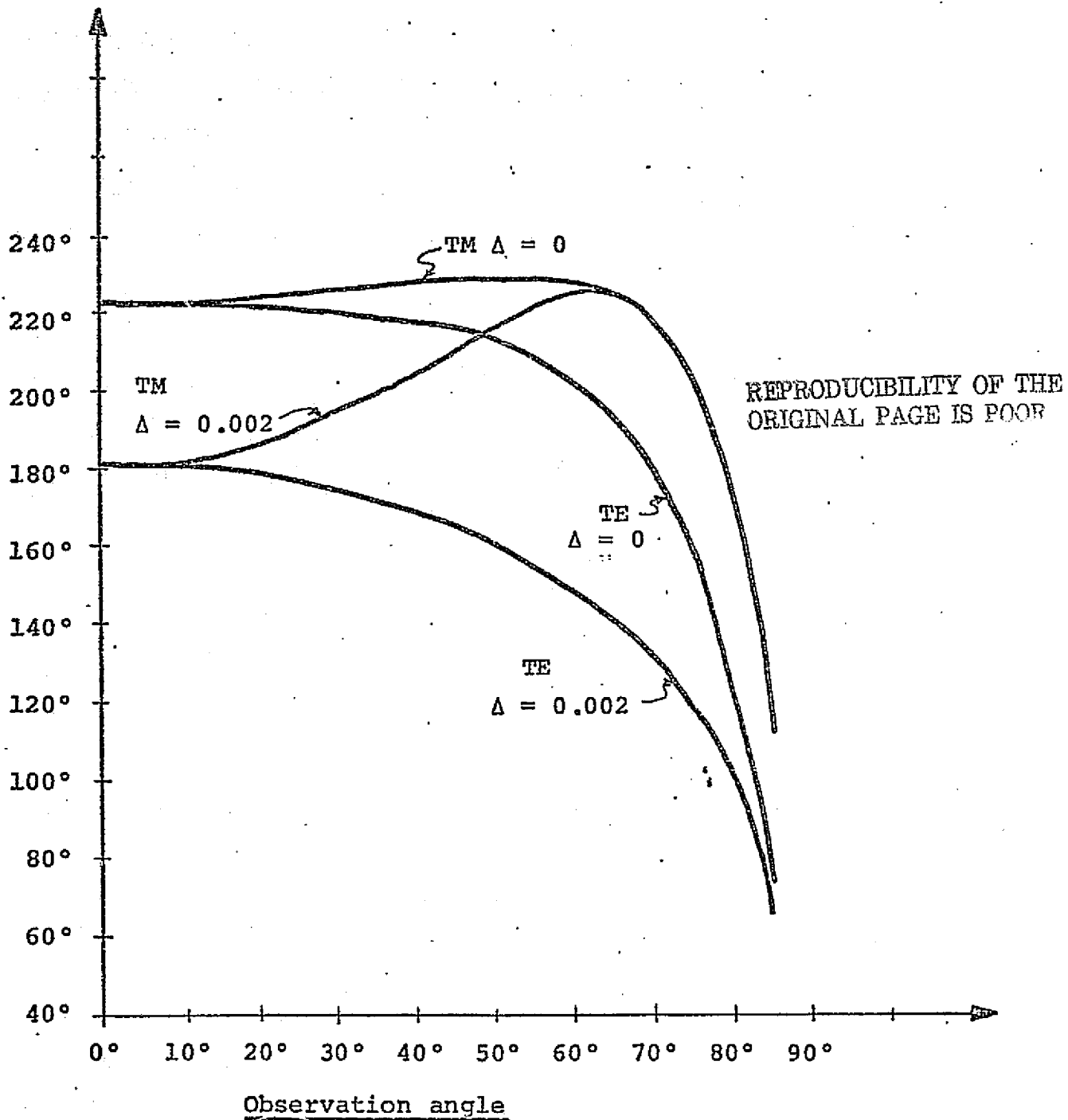


Figure 7a.

Brightness Temperature

$$\epsilon_m' = 1.8$$

$$\epsilon_m'' = 0.00054$$

$$l = 2 \text{ mm.}$$

$$T = T_1(z)$$

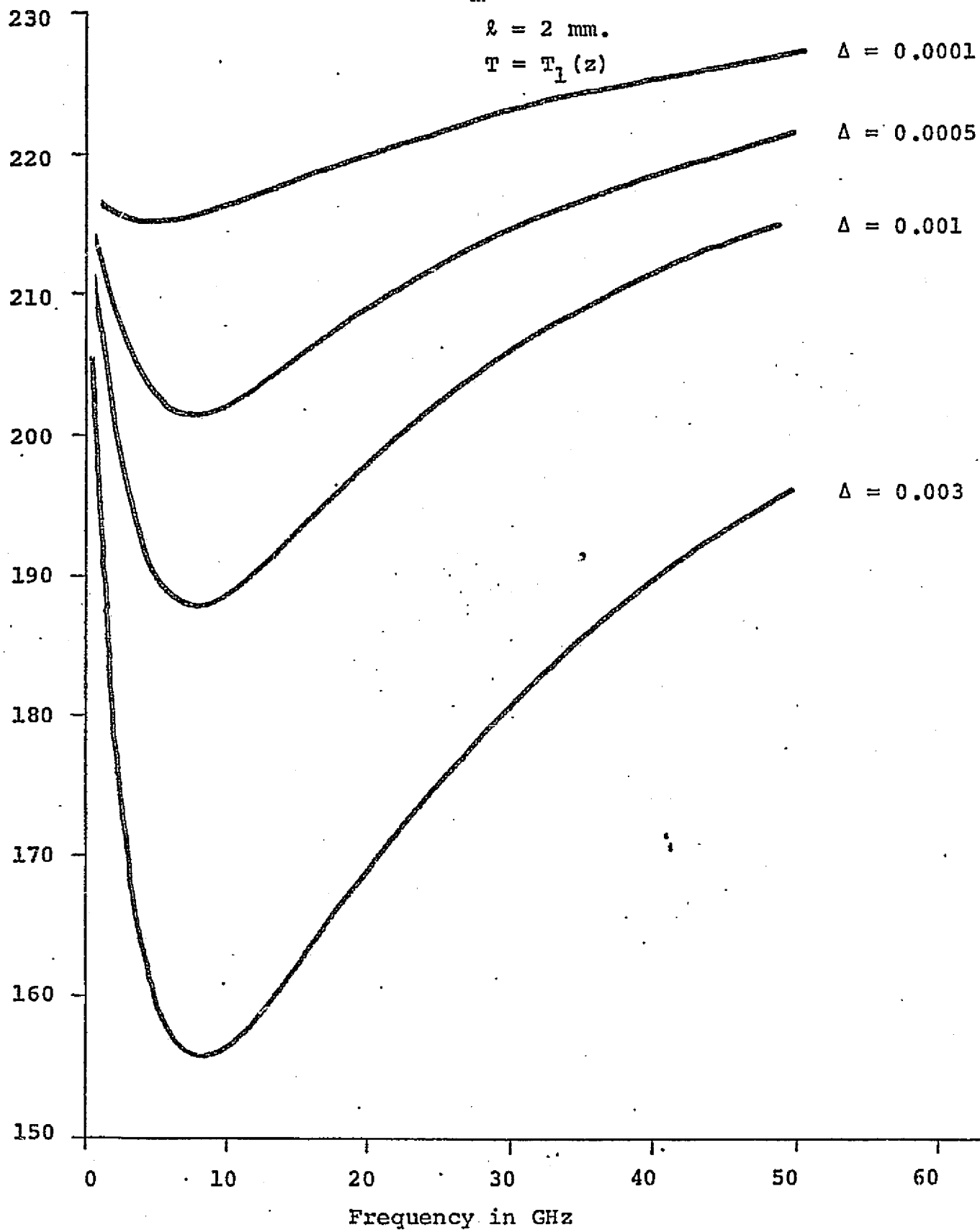


Figure 7b.

Brightness Temperature

$$\epsilon_m' = 1.8$$

$$\epsilon_m'' = 0.00054$$

$$l = 2 \text{ mm.}$$

$$T = T_2(z)$$

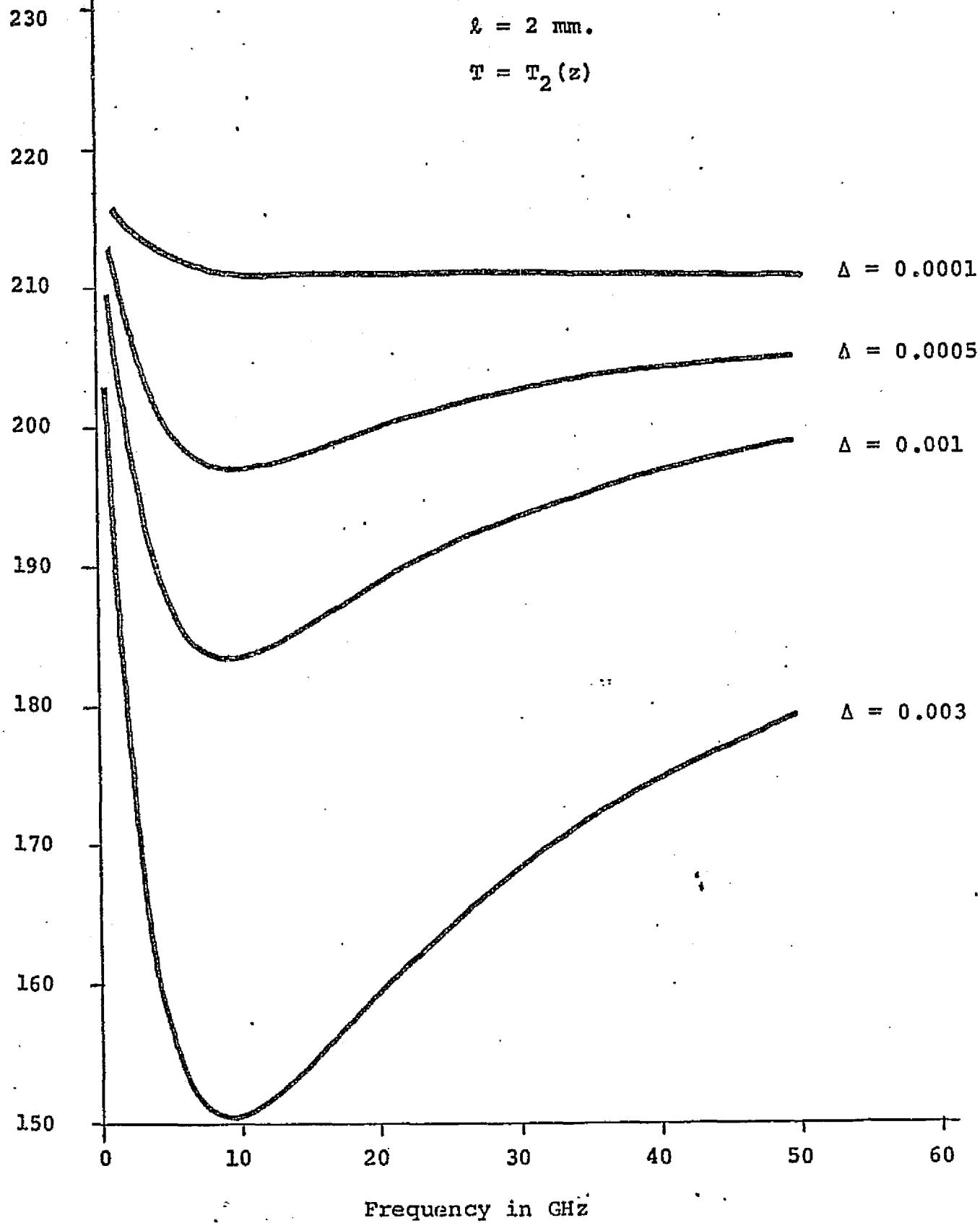


Figure 7c.

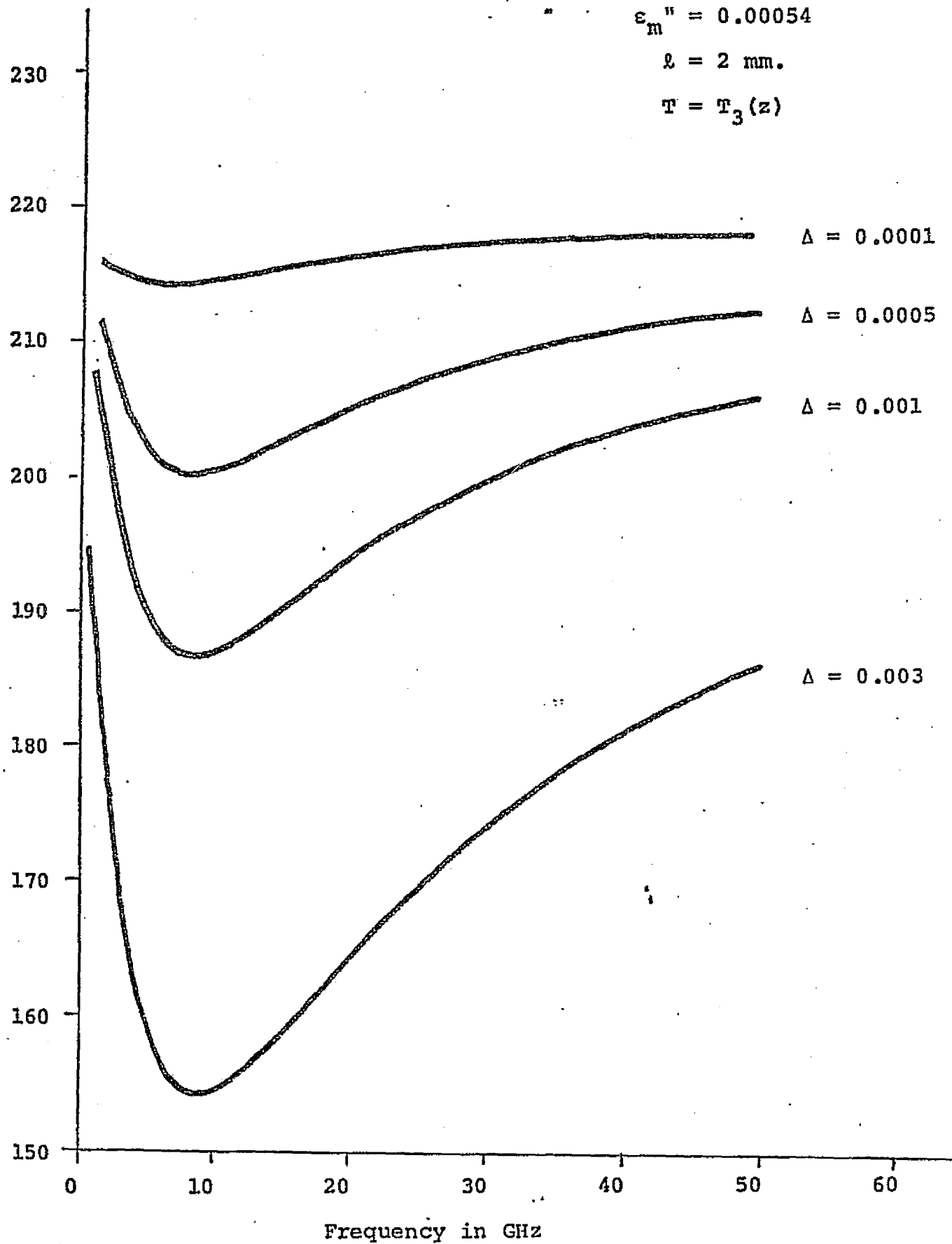
Brightness Temperature

$$\epsilon_m' = 1.8$$

$$\epsilon_m'' = 0.00054$$

$$l = 2 \text{ mm.}$$

$$T = T_3(z)$$



Microwave Remote Sensing of a Two-Layer Random Medium*

by

L. Tsang and J. A. Kong

Department of Electrical Engineering and

Computer Science and Research Laboratory

of Electronics

Massachusetts Institute of Technology

Cambridge, Massachusetts 02139

Abstract

Modified radiative transfer (MRT) equations are derived for a two-layer random medium from the Dyson equation by using the nonlinear approximation and from the Bethe-Salpeter equation by using the ladder approximation. The MRT equations yield simple and useful solutions which are applicable to both active and passive microwave remote sensing.

* This work was supported by the Joint Services Electronics Program (Contract DAAB07-74-C-0630) and the NASA Contract 953524.

I. Introduction

In microwave remote sensing of the earth or other planets, theoretical models are essential to the interpretation of the collected data. The effects of absorption and scattering have long been recognized as dominant factors in both active and passive sensing. Using the model of a half-space random medium with laminar structure, Gurvich, Kalinin and Matveyev^[1] investigated thermal radio emission in Antarctic areas. The problem of scattering by a medium with a small random fluctuating part in permittivity was studied by Stogryn^[2]. Assuming a half-space containing random distributed scatterers embedded in a low loss dielectric, England^[3] examined emission darkening caused by scatterers with a radiative transfer approach.

The problem of random media can be treated with the radiative transfer method which deals with energy fluxes and with the renormalization method which deals directly with field quantities. The renormalization method gives rise to the Dyson equation for the mean field and the Bethe-Salpeter equation for the covariance of the field.^[3,4] In solving the equations, the bilocal approximation is usually applied to the Dyson equation which is then solved by mathematical techniques such as the Fourier transform method. A ladder approximation is made on the Bethe-Salpeter equation which is then solved by the method of iteration.^[4,5] In the case of multiple wave scattering, the method of iteration involves solving many integrals and leads to complicated results after one of two

iterations. Under the assumption of far field interaction and incoherence among waves in different directions, radiative transfer equations have been derived from Bethe-Salpeter equations to study multiple scattering. [6-11]

In this paper we investigate the problem of scattering and emission of microwaves by a slab random medium with a laminar structure and bounded by different dielectric on each side. We employ the nonlinear approximation [13-14] rather than the more popular bilocal approximation to the Dyson equation. A two variable expansion technique [15] is applied to obtain the mean Green's function, which is then used to derive a set of modified radiative transfer (MRT) equations. They are modified because in our derivation we include coherent effects which are important in the case of bounded medium. The MRT equations are then solved and illustrated.

II. Formulation

Consider a two-layer medium with boundaries at $z = 0$ and $z = -d$ (Figure 1). The slab between the two boundaries is a random medium with a permittivity

$$\epsilon_1 = \epsilon_{1m} + \epsilon_{1f}(z) \quad (1)$$

$$\langle \epsilon_{1f}(z) \rangle = 0. \quad (2)$$

The mean permittivity ϵ_{1m} is independent of depth. The random part of the permittivity $\epsilon_{1f}(z)$ is real and has a zero ensemble average as indicated by (2). The variance of the fluctuating part of the permittivity is also assumed to be small.

A monochromatic plane wave is normally incident upon the two layer medium

$$E_i = \exp(-i k_o z). \quad (3)$$

The time dependent factor $\exp(-i\omega t)$ has been suppressed. The governing equations are the one-dimensional wave equations in each region.

$$\left(\frac{d^2}{dz^2} + k_o^2 \right) E_o = 0 \quad (4)$$

in region 0,

$$\left(\frac{d^2}{dz^2} + k_{1m}^2 \right) E_1 = f(z) E_1 \quad (5)$$

in region 1, and

$$\left(\frac{d^2}{dz^2} + k_2^2 \right) E_2 = 0 \quad (6)$$

in region 2, where

$$k_{1m}^2 = \frac{\epsilon_{1m}}{\epsilon_0} k_0^2 \quad (7)$$

$$f(z) = - \frac{\epsilon_{1f}(z)}{\epsilon_0} k_0^2 \quad (8)$$

$$k_2^2 = \frac{\epsilon_2}{\epsilon_0} k_0^2. \quad (9)$$

We separate the fields in each region into two parts; one part is the mean field, the other accounts for fluctuation

$$E = E_m + \mathcal{E}$$

with $\langle E \rangle = E_m$ and $\langle \mathcal{E} \rangle = 0$. The field intensity is

$$\langle EE^* \rangle = |E_m|^2 + \langle \mathcal{E} \mathcal{E}^* \rangle.$$

The Dyson equation can be obtained for the mean field in region 1 [4-5].

$$\left(\frac{d^2}{dz^2} + k_{1m}^2\right) E_{1m}(z) = \int_{-d}^0 dz_1 Q(z, z_1) E_{1m}(z_1) \quad (10)$$

where $Q(z, z_1)$ is the mass operator which is an infinite series of the unperturbed Green's functions $G_{11}^0(z, z_1)$ and the correlation functions $B_f(z, z_1) = \langle f(z) f(z_1) \rangle$. Writing in terms of the mean Green's function $G_{11m}(z, z_1)$, the Dyson equation becomes

$$\begin{aligned} \left(\frac{d^2}{dz^2} + k_{1m}^2\right) G_{11m}(z, z') &= \int_{-d}^0 dz_1 Q(z, z_1) G_{11m}(z_1, z') \\ &+ \delta(z - z'). \end{aligned} \quad (11)$$

In writing the Green's function, we use the first subscript to denote the region in which the observation point is located and the second subscript to denote the region in which the source is located. For the covariance, the Bethe-Salpeter equations takes the form

$$\begin{aligned} \langle \mathcal{E}_1(z) \mathcal{E}_1^*(z') \rangle &= \int_{-d}^0 dz_1 \int_{-d}^0 dz_2 \int_{-d}^0 dz_1' \int_{-d}^0 dz_2' G_{11m}(z, z_1) \\ &G_{11m}^*(z', z_1') I(z_1, z_2, z_1', z_2') [E_{1m}(z_2) E_{1m}^*(z_2')] \\ &+ \langle \mathcal{E}_1(z_2) \mathcal{E}_1^*(z_2') \rangle \end{aligned} \quad (12)$$

where $I(z_1, z_2, z_1', z_2')$ is the intensity operator^[4-5]. Thus we see that the Dyson equation must be solved before one can solve the Bethe-Salpeter equation.

Both the Dyson equation and the Bethe-Salpeter equation are exact equations. However, the mass operator and the intensity operator are in the form of infinite series. Two types of approximations, the bilocal approximation^[4-5] and the nonlinear approximation^[13-14] are used in solving these equations. In the following sections, we apply the nonlinear approximation. As we shall see, this approximation preserves the principle of conservation of energy and enables us to derive the modified radiative transfer equations for bounded medium.

III. Mean Green's Function

In order to solve for the mean Green's function, we impose the nonlinear approximation on the mass operator in (11)

$$Q(z, z_1) \approx Q_n(z, z_1) = G_{1lm}(z, z_1) B_f(z, z_1). \quad (13)$$

The correlation function $B_f(z, z_1)$ is assumed to take the form

$$B_f(z, z_1) = \langle f(z) f(z_1) \rangle = \delta k_{1m}^4 e^{-|z - z_1|/\ell} \quad (14)$$

where δ is the variance and ℓ is the correlation length of the fluctuating part of the permittivity.

Before proceeding to the solutions, we define some parameters and specify their ranges of interest to us. Let $k_{1m} = k_{1m}' + i k_{1m}''$ with k_{1m}' and k_{1m}'' both real (we use prime and double prime to denote the real and imaginary parts of a quantity respectively), we require $k_{1m}'' \ll k_{1m}'$. The absorption wave number κ_a and the absorption length ℓ_a are defined to be

$$\kappa_a = 2k_{1m}'' \quad (15a)$$

$$\ell_a = 2\pi/\kappa_a. \quad (15b)$$

The scattering wave number κ_s and the scattering length ℓ_s are defined to be

$$\kappa_s = \delta l k_{lm}^{\prime 2} \quad (16a)$$

$$l_s = 2\pi/\kappa_s.$$

The wavelength inside medium 1 is taken to be $\lambda_{lm} = 2\pi/k_{lm}'$.

The range of interest to us is for $l_a, l_s \ll \lambda_{lm}, l$.

The Dyson equation under the nonlinear approximation becomes

$$\left(\frac{d^2}{dz^2} + k_{lm}^2 \right) G_{llm}(z, z') = \delta k_{lm}^4 \int_{-d}^0 dz_1 G_{llm}(z, z_1) e^{-|z - z_1|/l} G_{llm}(z_1, z') + \delta(z - z'). \quad (17)$$

This equation can be solved by using the two variable expansion procedures. [15] We define long distance scales $\xi = \delta z$, $\xi' = \delta z'$, and $\xi_1 = \delta z_1$. From $\xi = \delta z$ it follows that

$$\frac{d^2}{dz^2} = \frac{\partial^2}{\partial z^2} + 2\delta \frac{\partial^2}{\partial z \partial \xi} + \delta^2 \frac{\partial^2}{\partial \xi^2}. \quad (18)$$

The mean Green's function is expanded in perturbation series

$$G_{llm}(z, \xi; z', \xi') = G_{llm0}(z, \xi; z', \xi') + \delta G_{llm1}(z, \xi; z', \xi') + \dots \quad (19)$$

Substituting (18) and (19) in (17), we find that on balancing terms to zeroth order in δ ,

$$\left(\frac{\partial^2}{\partial z^2} + k_{1m}^2 \right) G_{11mo}(z, \xi; z', \xi') = \delta(z - z') \quad (20)$$

and to first order in δ

$$\begin{aligned} \left(\frac{\partial^2}{\partial z^2} + k_{1m}^2 \right) G_{11ml}(z, \xi; z', \xi') = & -2 \frac{\partial^2}{\partial z \partial \xi} G_{11mo}(z, \xi; z', \xi') \\ & + k_{1m}^4 \int_{-d}^0 dz_1 G_{11mo}(z, z_1) e^{-|z - z_1|/\ell} G_{11mo}(z_1, z'). \end{aligned} \quad (21)$$

The solution to (20) is written as

$$\begin{aligned} G_{11mo}(z, \xi; z', \xi') = & [A(\xi) e^{ik_{1m}z} + B(\xi) e^{-ik_{1m}z}] \\ & [U(\xi') e^{ik_{1m}z'} + W(\xi') e^{-ik_{1m}z'}] \end{aligned} \quad (22a)$$

for $z > z'$ and

$$\begin{aligned} G_{11mo}(z, \xi; z', \xi') = & [A(\xi') e^{ik_{1m}z'} + B(\xi') e^{-ik_{1m}z'}] \\ & [U(\xi) e^{ik_{1m}z} + W(\xi) e^{-ik_{1m}z}] \end{aligned} \quad (22b)$$

for $z < z'$. In (22), note the symmetry property of the Green's function.

Following the two variable expansion procedure, we substitute (22) in (21) and eliminate secular terms. We observe that $A(\xi_1)$, $B(\xi_1)$, $U(\xi_1)$ and $W(\xi_1)$ as variables in the integrand are varying on the ℓ_a and ℓ_s scale. They vary much more slowly than $\exp(-|z - z_1|/\ell)$ which is 1 at $z = z_1$ and decays on the ℓ scale. These terms can be taken out of the integral sign and substituted with their values at $\xi_1 = \xi$. We find that in order to eliminate the secular terms, the following equations must be satisfied:

$$\frac{dA(\xi)}{d\xi} + g A(\xi) \left[B(\xi)U(\xi) \left(\frac{2 + i3k_{1m}\ell}{1 + i2k_{1m}\ell} \right) + A(\xi)W(\xi) \left(\frac{1 - ik_{1m}\ell}{1 - i2k_{1m}\ell} \right) \right] = 0 \quad (23)$$

$$\frac{dB(\xi)}{d\xi} - g B(\xi) \left[A(\xi)W(\xi) \left(\frac{2 - i3k_{1m}\ell}{1 - i2k_{1m}\ell} \right) + B(\xi)U(\xi) \left(\frac{1 + ik_{1m}\ell}{1 + i2k_{1m}\ell} \right) \right] = 0 \quad (24)$$

$$\frac{dU(\xi)}{d\xi} + g U(\xi) \left[B(\xi)U(\xi) \left(\frac{1 + ik_{1m}\ell}{1 + i2k_{1m}\ell} \right) + A(\xi)W(\xi) \left(\frac{2 - i3k_{1m}\ell}{1 - i2k_{1m}\ell} \right) \right] = 0 \quad (25)$$

$$\frac{dW(\xi)}{d\xi} - g W(\xi) \left[A(\xi)W(\xi) \left(\frac{1 - ik_{1m}\ell}{1 - i2k_{1m}\ell} \right) + B(\xi)U(\xi) \left(\frac{2 + i3k_{1m}\ell}{1 + i2k_{1m}\ell} \right) \right] = 0 \quad (26)$$

where

$$g = ik_{1m}^3 \ell. \quad (27)$$

Combining (23) with (26), and (24) with (25), we obtain

$$W(\xi) \frac{dA(\xi)}{d\xi} + A(\xi) \frac{dW(\xi)}{d\xi} = 0 \quad (28)$$

and

$$B(\xi) \frac{dU(\xi)}{d\xi} + U(\xi) \frac{dB(\xi)}{d\xi} = 0. \quad (29)$$

Thus

$$A(\xi)W(\xi) = L_1 \quad (30)$$

$$B(\xi)U(\xi) = L_2 \quad (31)$$

where L_1 and L_2 are constants independent of ξ . Substituting (30)-(31) in (23) and (24), we can solve for $A(\xi)$, $B(\xi)$, $U(\xi)$, and $W(\xi)$.

$$A(\xi) = C_1 e^{-g(M_2 + M_1)\xi} \quad (32)$$

$$B(\xi) = C_2 e^{g(N_1 + N_2)\xi} \quad (33)$$

$$U(\xi) = \frac{L_2}{C_2} e^{-g(N_1 + N_2)\xi} \quad (34)$$

$$W(\xi) = \frac{L_1}{C_1} e^{g(M_2 + M_1)\xi} \quad (35)$$

where

$$M_1 = L_1 \left(\frac{1 - ik_{1m}l}{1 - i2k_{1m}l} \right) \quad (36)$$

$$M_2 = L_2 \left(\frac{2 + i3k_{1m}l}{1 + i2k_{1m}l} \right) \quad (37)$$

$$N_1 = L_1 \left(\frac{2 - i3k_{1m}l}{1 - i2k_{1m}l} \right) \quad (38)$$

$$N_2 = L_2 \left(\frac{1 + ik_{1m}l}{1 + i2k_{1m}l} \right) \quad (39)$$

Substituting in (22) yields

$$G_{11mo}(z, z') = \{ C e^{-g(M_2 + M_1)\delta z} e^{ik_{1m}z} + e^{g(N_1 + N_2)\delta z} e^{-ik_{1m}z} \} \\ \{ L_2 e^{-g(N_1 + N_2)\delta z'} e^{ik_{1m}z'} + \frac{L_1}{C} e^{g(M_2 + M_1)\delta z'} e^{-ik_{1m}z'} \} \quad (40)$$

for $z > z'$ and

$$G_{11mo}(z, z') = \{ C e^{-g(M_2 + M_1)\delta z'} e^{ik_{1m}z'} + e^{g(N_1 + N_2)\delta z'} e^{-ik_{1m}z'} \} \\ \{ L_2 e^{-g(N_1 + N_2)\delta z} e^{ik_{1m}z} + \frac{L_1}{C} e^{g(M_2 + M_1)\delta z} e^{-ik_{1m}z} \} \quad (41)$$

for $z < z'$, where $C = C_1/C_2$ in (40) and (41) is a constant to be determined together with L_1 and L_2 by the boundary conditions.

The Green's functions in (40) and (41) are continuous at $z = z'$. By (20) we must also have $[dG_{11mo}/dz]_{z=z'_+} - [dG_{11mo}/dz]_{z=z'_-} = 1$ which gives

$$L_1 - L_2 = 1/i2k_{1m}. \quad (42)$$

We next match the continuity of G_{11mo} and dG_{11mo}/dz at $z = 0$ and at $z = -d$. At $z = 0$, we have

$$C = 1/R_{10} \quad (43)$$

where R_{10} is the reflection coefficient at $z = 0$. At $z = -d$ we have

$$\frac{C L_2}{L_1} e^{g[N_1 + N_2 + M_1 + M_2]\delta d} = R_{12} e^{i2k_{1m}d} \quad (44)$$

where R_{12} is the reflection coefficient at $z = -d$.

$$R_{10} = \frac{k_{1m} - k_0}{k_{1m} + k_0} = -R_{01}; \quad (45a)$$

$$R_{12} = \frac{k_{1m} - k_2}{k_{1m} + k_2}. \quad (45b)$$

We define

$$\eta_1 \equiv \eta_1' + i \eta_1'' = k_{1m}(1 - k_{1m}^2 \delta \ell (M_1 + M_2)) \quad (46a)$$

$$\eta_2 \equiv \eta_2' + i \eta_2'' = k_{1m}(1 - k_{1m}^2 \delta \ell (N_1 + N_2)). \quad (46b)$$

In view of (36)-(39) and (42)-(44), we find

$$\eta_1 - \eta_2 = i \frac{\kappa_s}{2} \quad (47)$$

$$\begin{aligned} \eta_1 + \eta_2 = & 2k_{1m} - k_{1m}^3 \delta \ell L_1 \left\{ \frac{3 - i4k_{1m}\ell}{1 - i2k_{1m}\ell} \right. \\ & \left. + R_{10} R_{12} \left(\frac{3 + i4k_{1m}\ell}{1 + i2k_{1m}\ell} \right) e^{i(\eta_1 + \eta_2)d} \right\}. \end{aligned} \quad (48)$$

From (42) and (44), we find

REPRODUCIBILITY OF THE
ORIGINAL PAGE IS POOR

$$L_1 = \frac{1}{i2k_{1m}(1 - R_{10} R_{12} e^{i(\eta_1 + \eta_2)d})}. \quad (49)$$

Thus the zeroth order mean Green's function as determined from (40) and (41) reads

$$G_{11mo}(z, z') = L_1 (e^{i\eta_2 z} + R_{10} e^{-i\eta_1 z}) (R_{12} e^{i(\eta_1 + \eta_2)d + i\eta_1 z'} + e^{-i\eta_2 z'}) \quad (50)$$

for $z > z'$ and

$$G_{11mo}(z, z') = L_1 (e^{i\eta_2 z'} + R_{10} e^{-i\eta_1 z'}) (R_{12} e^{i(\eta_1 + \eta_2)d + i\eta_1 z} + e^{-i\eta_2 z}) \quad (51)$$

for $z < z'$. From (47) and (48) we see that the effective propagation constants η_1 and η_2 depend on the boundary conditions as well as the properties of the media.

The two variable expansions technique can similarly be applied to the Dyson equation for the mean field

$$\left(\frac{d^2}{dz^2} + k_{1m}^2 \right) E_{1m}(z) = \delta k_{1m}^4 \int_{-d}^0 dz_1 G_{11m}(z, z_1) e^{-|z - z_1|/\ell} E_{1m}(z_1) \quad (52)$$

under the nonlinear approximation (13). The zeroth order solution is

$$E_{lmo}(z) = i2k_{lm} L_1 T_{01} (e^{-i\eta_2 z} + R_{12} e^{i(\eta_1 + \eta_2)d + i\eta_1 z})$$

(53)

where $T_{01} = 1 + R_{01}$. We also define $T_{10} = 1 + R_{10}$, where $R_{10} = -R_{01}$.

IV. Modified Radiative Transfer (MRT) Equations

We now proceed to derive modified radiative transfer equations from the Bethe-Salpeter equation (12).

We apply the ladder approximation to the Bethe-Salpeter equation (12).

$$I(z_1, z_2; z_1', z_2') \approx B_f(z_1, z_1') \delta(z_1 - z_2) \delta(z_1' - z_2'). \quad (54)$$

Under the ladder approximation (54), (12) becomes

$$\begin{aligned} \langle \mathcal{E}_1(z) \mathcal{E}_1^*(z') \rangle &= \delta k_{1m}^4 \int_{-d}^0 dz_1 \int_{-d}^0 dz_2 G_{11m}(z, z_1) G_{11m}^*(z', z_2) \\ &\quad e^{-|z_1 - z_2|/\ell} \{E_{1m}(z_1)E_{1m}^*(z_2) + \langle \mathcal{E}_1(z_1) \mathcal{E}_1^*(z_2) \rangle\}. \end{aligned} \quad (55)$$

The fluctuating part of the field is written as a summation of upward and downward propagating waves,

$$\mathcal{E}_1(z) = \mathcal{E}_{1u}(z) e^{ik_{1m}'z} + \mathcal{E}_{1d}(z) e^{-ik_{1m}'z}. \quad (56)$$

We then have

$$\begin{aligned}
\langle \mathcal{E}_1(z) \mathcal{E}_1^*(z') \rangle = & J_u(z, z') e^{ik'_{1m}(z - z')} + J_d(z, z') e^{-ik'_{1m}(z - z')} \\
& + J_{c_1}(z, z') e^{ik'_{1m}(z + z')} + J_{c_2}(z, z') e^{-ik'_{1m}(z + z')}
\end{aligned}
\tag{57}$$

where

$$J_u(z, z') = \langle \mathcal{E}_{1u}(z) \mathcal{E}_{1u}^*(z') \rangle \tag{58a}$$

$$J_d(z, z') = \langle \mathcal{E}_{1d}(z) \mathcal{E}_{1d}^*(z') \rangle \tag{58b}$$

$$J_{c_1}(z, z') = \langle \mathcal{E}_{1u}(z) \mathcal{E}_{1d}^*(z') \rangle \tag{58c}$$

$$J_{c_2}(z, z') = \langle \mathcal{E}_{1d}(z) \mathcal{E}_{1u}^*(z') \rangle. \tag{58d}$$

J_{c_1} and J_{c_2} represent the correlation between the upward and downward propagating waves.

We wish to derive radiative transfer equations that govern the behavior of intensities

$$I_u(z) = J_u(z, z) \tag{59}$$

REPRODUCIBILITY OF THE
ORIGINAL PAGE IS POOR

$$I_d(z) = J_d(z, z) \tag{60}$$

$$I_c(z) = J_{c_1}(z, z) = J_{c_2}^*(z, z). \tag{61}$$

We restrict the separation of z and z' to be on the wavelength scale which is much less than ℓ_a and ℓ_s scale, $|z - z'| \sim O(\lambda_{1m}) \ll \ell_a, \ell_s$. We also require that $|z|, |z'|, |z + d|, |z' + d|, d \gg \lambda_{1m}$, namely both z and z' are far away from the two boundaries on the wavelength scale and the correlation length scale. However, both z and z' can be close to the boundary on the ℓ_a, ℓ_s scale, and so are J_u, J_d, J_{c_1} and J_{c_2} . Without loss of generality we consider (55) for $z > z'$, balance terms by their phase factors and then let $z' \rightarrow z$. After considerable algebra (Appendix I), we find

$$I_u(z) = e^{-\kappa_2 z} I_1(z, z) + r_{12} e^{-(\kappa_1 + \kappa_2)d - \kappa_1 z} I_4(z, z) \quad (62)$$

$$I_d(z) = r_{01} e^{\kappa_1 z} I_1(z, z) + e^{\kappa_2 z} I_4(z, z) \quad (63)$$

$$I_c(z) e^{i2k_{1m}^* z} = -R_{01}^* e^{i(\eta_2 + \eta_1^*)z} I_1(z, z) + R_{12} e^{i(\eta_1 + \eta_2)d + i(\eta_1 + \eta_2^*)z} I_4(z, z) \quad (64)$$

where

$$\kappa_1 = 2\eta_1'' = \kappa_a + \frac{\kappa_s}{2} + \frac{\kappa_s}{2} \frac{D_1}{|D|^2} \frac{(3 + 8k_{1m}^2 \ell^2)}{(1 + 4k_{1m}^2 \ell^2)} \quad (65)$$

$$\kappa_2 = 2\eta_2'' = \kappa_a - \frac{\kappa_s}{2} + \frac{\kappa_s}{2} \frac{D_1}{|D|^2} \frac{(3 + 8k_{1m}^2 \ell^2)}{(1 + 4k_{1m}^2 \ell^2)} \quad (66)$$

$$D = 1 + R_{01} R_{12} e^{i(\eta_1 + \eta_2)d} \quad (67a)$$

$$D_1 = 1 - r_{01} r_{12} e^{-(\kappa_1 + \kappa_2)d} \quad (67b)$$

$$\begin{aligned} I_1(z, z) = & \frac{\delta k_{1m}^2}{4|D|^2} \int_{-d}^z dz_1 \left\{ \frac{|T_{01}|^2}{|D|^2} [g_b r_{12}^2 e^{-2(\kappa_1 + \kappa_2)d - 2\kappa_1 z_1} \right. \\ & + 4g_f r_{12} e^{-(\kappa_1 + \kappa_2)d - \kappa_1 z_1 + \kappa_2 z_2} + g_b e^{2\kappa_2 z_1}] \\ & + g_b r_{12} I_u(z_1) e^{-(\kappa_1 + \kappa_2)d - \kappa_1 z_1} + g_b I_d(z_1) e^{\kappa_2 z_1} \\ & + g_f r_{12} I_d(z_1) e^{-(\kappa_1 + \kappa_2)d - \kappa_1 z_1} + g_f I_u(z_1) e^{\kappa_2 z_1} \\ & + g_f R_{12}^* I_c(z_1) e^{-i(\eta_1^* + \eta_2^*)d + i(2k_{1m}' - \eta_1^* - \eta_2)z_1} \\ & \left. + g_f R_{12} I_c^*(z_1) e^{i(\eta_1 + \eta_2)d + i(\eta_1 + \eta_2 - 2k_{1m}')z_1} \right\} \end{aligned}$$

(68)

$$\begin{aligned}
I_4(z, z) = & \frac{\delta k_{1m}^2}{4|D|^2} \int_z^0 dz_1 \left\{ \frac{|T_{01}|^2}{|D|^2} [g_b r_{12} e^{-(\kappa_1 + \kappa_2)d - (\kappa_1 + \kappa_2)z_1} \right. \\
& + g_f(1 + r_{01} r_{12} e^{-(\kappa_1 + \kappa_2)d}) + g_b r_{01} e^{(\kappa_1 + \kappa_2)z_1} \\
& - g_f(R_{01} R_{12} e^{i(\eta_1 + \eta_2)d} + R_{01}^* R_{12}^* e^{-i(\eta_1^* + \eta_2^*)d})] \\
& + (g_b I_u(z_1) + g_f I_d(z_1)) e^{-\kappa_2 z_1} \\
& + r_{01}(g_f I_u(z_1) + g_b I_d(z_1)) e^{\kappa_1 z_1} \\
& - g_f R_{01} I_c(z_1) e^{i(2k_{1m}' - \eta_1 - \eta_2^*)z_1} \\
& \left. - g_f R_{01}^* I_c^*(z_1) e^{i(\eta_2 + \eta_1^* - 2k_{1m}')z_1} \right\} \quad (69)
\end{aligned}$$

$$g_f = 2\ell$$

REPRODUCIBILITY OF THE
ORIGINAL PAGE IS POOR

(70)

$$g_b = \frac{2\ell}{1 + 4k_{1m}^2 \ell^2}$$

(71)

and $r_{01} = |R_{01}|^2$, $r_{12} = |R_{12}|^2$. From (64), we can express I_c in terms of I_u and I_d .

$$\begin{aligned}
 I_c e^{i(2k_{1m} - \eta_2 - \eta_1^*)z} &= \frac{1}{D_1} \{- R_{01}^* I_u(z) e^{\kappa_2 z} \\
 &\quad - R_{12} r_{01} I_u(z) e^{i(\eta_1 + \eta_2)d + \kappa_2 z} \\
 &\quad + R_{01}^* r_{12} I_d(z) e^{-(\kappa_1 + \kappa_2)d - \kappa_1 z} \\
 &\quad + R_{12} I_d e^{i(\eta_1 + \eta_2)d - \kappa_1 z}\}. \quad (72)
 \end{aligned}$$

We note that in view of (62)-(63) and (68)-(69),

$$I_d(0) = r_{01} I_u(0) \quad (73a)$$

$$I_u(-d) = r_{12} I_d(-d). \quad (73b)$$

These are the boundary conditions satisfied by the intensities I_u and I_d .

Writing the integral equations (62)-(63) in differential form, we obtain

$$\begin{aligned}
\frac{dI_u}{dz} = & -\kappa_e I_u + \frac{K_s}{2} (p_f I_u + p_b I_d) \\
& + \frac{|T_{01}|^2}{|D|^2} \left[\frac{K_s p_b}{2} e^{\kappa_2 z} + \right. \\
& \left. \left(K_s p_f + \frac{K_s p_f}{2} \right) r_{12} e^{-(\kappa_1 + \kappa_2)d - \kappa_1 z} \right]
\end{aligned} \tag{74}$$

$$\begin{aligned}
\frac{dI_d}{dz} = & \kappa_e - \frac{K_s}{2} (p_f I_d + p_b I_u) \\
& - \frac{|T_{01}|^2}{|D|^2} \left[r_{12} \frac{K_s p_b}{2} e^{-(\kappa_1 + \kappa_2)d - \kappa_1 z} \right. \\
& \left. + \left(K_s p_f - \frac{K_s p_f}{2} \right) e^{\kappa_2 z} \right]
\end{aligned} \tag{75}$$

where

$$k_s = \frac{\kappa_s (1 + 2k_{1m}^2 \ell^2)}{1 + 4k_{1m}^2 \ell^2} \tag{76}$$

$$K_s = \frac{D_1}{|D|^2} k_s \tag{77}$$

$$\kappa_e = \kappa_a + K_s \tag{78}$$

$$p_f = \frac{1 + 4k_{1m}^2 \ell^2}{1 + 2k_{1m}^2 \ell^2} \quad (79)$$

$$p_b = \frac{1}{1 + 2k_{1m}^2 \ell^2}.$$

Equations (74) and (75) together with the boundary conditions in (73) are the modified radiative transfer equations derived from the Bethe-Salpeter equation under the ladder approximation.

In the case of a half-space random medium, we let $d \rightarrow \infty$ and the modified radiative transfer equations reduce to

$$\frac{dI_u}{dz} = -\kappa_e I_u + \frac{k_s}{2} (p_f I_u + p_b I_d) + \frac{k_s p_b}{2} |T_{01}|^2 e^{\kappa_e z} \quad (76)$$

$$\frac{dI_d}{dz} = \kappa_e I_d - \frac{k_s}{2} (p_f I_d + p_b I_u) - \frac{k_s p_f}{2} |T_{01}|^2 e^{\kappa_e z}. \quad (77)$$

We remark that the principle of energy conservation is perserved with the use of the nonlinear approximation for the mean Green's function instead of using the more popular bilocal approximation. This is shown in Appendix II.

V. Solution to the MRT Equations

The modified radiative transfer equations (74) and (75) are simply two simultaneous first order differential equations with constant coefficients. They are readily solved and written in the following form:

$$I_d = \frac{|T_{01}|^2}{|D|^2} (P e^{\alpha z} + Q f_2 e^{-\alpha(z + 2d)} - e^{\kappa_2 z}) \quad (78)$$

$$I_u = \frac{|T_{01}|^2}{|D|^2} (P f_2 e^{\alpha z} + Q e^{-\alpha(z + 2d)} - r_{12} e^{-\kappa_1 z - (\kappa_1 + \kappa_2)d}) \quad (79)$$

where

$$P = \frac{(1 - f_2 r_{12}) D_1}{(1 - f_2 r_{01})(1 - f_2 r_{12}) - (f_2 - r_{01})(f_2 - r_{12}) e^{-2\alpha d}} \quad (80)$$

$$Q = -P \frac{f_2 - r_{12}}{1 - f_2 r_{12}} \quad (81)$$

REPRODUCIBILITY OF THE
ORIGINAL PAGE IS POOR

$$f_2 = \frac{2(\kappa_e - \alpha) - K_s P_f}{K_s P_b} \quad (82)$$

$$\alpha = \kappa_e (1 - \omega)^{1/2} \left(1 - \frac{\omega}{2} P_f + \frac{\omega}{2} P_b\right)^{1/2} \quad (83)$$

and $\tilde{\omega} = K_s / \kappa_e$ is the albedo.

To calculate emissivity e of the two layer medium, we note that by reciprocity

$$e = 1 - r \quad (84)$$

where r is the reflectivity. The field in region 0 can be written as

$$E_0 = e^{-ik_0 z} + \Gamma e^{ik_0 z}. \quad (85)$$

The reflectivity is $r = \langle \Gamma \Gamma^* \rangle$. We observe that $\langle E_0 E_0^* \rangle = \langle E_1 E_1^* \rangle$ and $|E_{0m}(0)|^2 = |E_{1m}(0)|^2$ at the boundary $z = 0$. By (53) and (85), we have

$$\langle \Gamma \rangle = \frac{R_{01} + R_{12} e^{i(\eta_1 + \eta_2)d}}{D} \quad (86a)$$

$$\langle E_0 E_0^* \rangle = 1 + \langle \Gamma \rangle + \langle \Gamma^* \rangle + \langle \Gamma \Gamma^* \rangle. \quad (86b)$$

By (57) and (62)-(64) we have

$$\begin{aligned} \langle E_1 E_1^* \rangle_{z=0} &= |E_{1m}(0)|^2 + \langle \mathcal{E}_1 \mathcal{E}_1^* \rangle_{z=0} \\ &= 1 + \langle \Gamma \rangle + \langle \Gamma^* \rangle + |\langle \Gamma \rangle|^2 + I_u(0) + I_d(0) + I_c(0) + I_c^*(0) \\ &= 1 + \langle \Gamma \rangle + \langle \Gamma^* \rangle + |\langle \Gamma \rangle|^2 + I_u(0) |T_{10}|^2. \end{aligned} \quad (87)$$

Equating (86) and (87) we obtain

$$r = \langle \Gamma \Gamma^* \rangle = |\langle \Gamma \rangle|^2 + I_u(0) |T_{10}|^2 = \frac{|R_{01} + R_{12} e^{i(\eta_1 + \eta_2)d}|^2}{|D|^2} + \frac{t_{01}^2}{|D|^2}$$

$$\left\{ \frac{(1 - f_2 r_{12})(f_2 - r_{12} e^{-(\kappa_1 + \kappa_2)d}) - (f_2 - r_{12})(1 - f_2 r_{12} e^{-(\kappa_1 + \kappa_2)d}) e^{-2\alpha d}}{(1 - f_2 r_{01})(1 - f_2 r_{12}) - (f_2 - r_{01})(f_2 - r) e^{-2\alpha d}} \right\}$$

(88a)

where

$$t_{01} = 1 - r_{01}. \quad (88b)$$

We now consider several special cases:

1. A half space random medium. We let $d \rightarrow \infty$, and (88) becomes

$$r = r_{01} + \frac{t_{01}^2 f_2}{1 - r_{01} f_2} \quad (89)$$

which is identical to that derived from a phenomenological radiative transfer approach.

2. The second layer is perfect conductor. We have $R_{12} = -1$ and $r_{12} = 1$. Equation (88) becomes

$$r = \left| \frac{R_{01} - e^{i(\eta_1 + \eta_2)d}}{1 - R_{01} e^{i(\eta_1 + \eta_2)d}} \right|^2 + \frac{t_{01}^2 \{ f_2 - e^{-(\kappa_1 + \kappa_2)d} + (1 - f_2 e^{-(\kappa_1 + \kappa_2)d}) e^{-2\alpha d} \}}{\{ 1 - f_2 r_{01} + (f_2 - r_{01}) e^{-2\alpha d} \} |1 - R_{01} e^{i(\eta_1 + \eta_2)d}|^2} \quad (90)$$

It is interesting to note that as $\tilde{\omega} \rightarrow 1$, we have $\alpha \rightarrow 0$, $f_2 \rightarrow 1$ and from (90) $r \rightarrow 1$. Thus all the incident power is reflected.

VI. Conclusions

In this paper modified radiative transfer equations are derived from the Bethe-Salpeter equations. The nonlinear approximation is applied to the Dyson equation and a two variable expansion technique is used to find the mean Green's function. The modified radiative transfer equations accomodate coherent effects which are essential to bounded media and appear in observed data. The MRT equations are solved and the results are presented in Equation (88). In Figure 2 and 3 we illustrate the emissivity for a half-space random medium and a slab random medium with $\delta = 0.1$ and 0.2 . We see that in the half-space case the null in emissivity due to scattering occurs at $4k_{lm}^2 \ell^2 = 1$. In the slab case scattering dampens the interference pattern and decreases emissivity in general. The existence of the interference patterns depends on the location of the subsurface and the extinction loss of the random medium.

Appendix I.

On substituting equations (50) and (51) into the right hand side of equation (55), we find that

$$\begin{aligned}
 \langle \xi_1(z) \xi_1^*(z') \rangle = & \{ e^{i\eta_2 z - i\eta_2^* z'} + r_{01} e^{-i\eta_1 z + i\eta_1^* z'} \\
 & - R_{01}^* e^{i\eta_2 z + i\eta_1^* z'} - R_{01} e^{-i\eta_1 z - i\eta_2^* z'} \} I_1(z, z') \\
 & + \{ R_{12}^* e^{-i(\eta_1^* + \eta_2^*)d + i\eta_2 z - i\eta_1^* z'} \\
 & - R_{01} e^{-i\eta_1 z + i\eta_2^* z'} + e^{i\eta_2 z + i\eta_2^* z'} \\
 & - R_{01} R_{12} e^{-i(\eta_1^* + \eta_2^*)d - i\eta_1 z - i\eta_1^* z'} \} I_2(z, z') \\
 & + \{ R_{01} e^{i(\eta_1 + \eta_2)d + i\eta_1 z - i\eta_2^* z'} - R_{01}^* e^{-i\eta_2 z + i\eta_1^* z'} \\
 & + e^{-i\eta_2 z - i\eta_2^* z'} - R_{01}^* R_{12} e^{i(\eta_1 + \eta_2)d + i\eta_1 z + i\eta_1^* z'} \} \\
 & I_3(z, z') + \{ r_{12} e^{-(\kappa_1 + \kappa_2)d + i\eta_1 z - i\eta_1^* z'}
 \end{aligned}$$

$$\begin{aligned}
& + e^{-i\eta_2 z + i\eta_2^* z'} + R_{12} e^{i(\eta_1 + \eta_2)d + i\eta_1 z + i\eta_2^* z'} \\
& + R_{12}^* e^{-i(\eta_1^* + \eta_2^*)d - i\eta_2 z - i\eta_1^* z'} \} I_4(z, z') \quad (A.1)
\end{aligned}$$

where

$$\begin{aligned}
I_1(z, z') &= \frac{\delta k_{1m}^2}{4|D|^2} \int_{-d}^z dz_1 \int_{-d}^{z'} dz_2 [R_{12} e^{i(\eta_1 + \eta_2)d + i\eta_1 z_1} + e^{-i\eta_2 z_1}] \\
& [R_{12}^* e^{-i(\eta_1^* + \eta_2^*)d - i\eta_1^* z_2} + e^{i\eta_2^* z_2}] \exp\left(-\frac{|z_1 - z_2|}{\ell}\right) \\
& [E_{1m}(z_1) E_{1m}^*(z_2) + \langle \mathcal{E}_1(z_1) \mathcal{E}_1^*(z_2) \rangle] \quad (A.2)
\end{aligned}$$

$$\begin{aligned}
I_2(z, z') &= \frac{\delta k_{1m}^2}{4|D|^2} \int_{-d}^z dz_1 \int_{z'}^0 dz_2 (e^{-i\eta_2^* z_2} - R_{01}^* e^{i\eta_1^* z_2}) \\
& (R_{12} e^{i(\eta_1 + \eta_2)d + i\eta_1 z_1} + e^{-i\eta_2 z_1}) \exp\left(-\frac{|z_1 - z_2|}{\ell}\right) \\
& [E_{1m}(z_1) E_{1m}^*(z_2) + \langle \mathcal{E}_1(z_1) \mathcal{E}_1^*(z_2) \rangle] \quad (A.3)
\end{aligned}$$

$$I_3(z, z') = \frac{\delta k_{1m}^2}{4|D|^2} \int_z^0 dz_1 \int_{-d}^{z'} dz_2 (e^{i\eta_2 z_1} - R_{01} e^{-i\eta_1 z_1})$$

$$(R_{12}^* e^{-i(\eta_1^* + \eta_2^*)d - i\eta_1^* z_2} + e^{i\eta_2^* z_2}) \exp\left(-\frac{|z_1 - z_2|}{\ell}\right)$$

$$[E_{1m}(z_1) E_{1m}^*(z_2) + \langle \mathcal{E}_1(z_1) \mathcal{E}_1^*(z_2) \rangle] \quad (A.4)$$

$$I_4(z, z') = \frac{\delta k_{1m}^2}{4|D|^2} \int_z^0 dz_1 \int_{z'}^0 dz_2 (e^{i\eta_2 z_1} - R_{01} e^{-i\eta_1 z_1})$$

$$(e^{-i\eta_2^* z_2} - R_{01}^* e^{i\eta_1^* z_2}) \exp\left(-\frac{|z_1 - z_2|}{\ell}\right)$$

$$[E_{1m}(z_1) E_{1m}^*(z_2) + \langle \mathcal{E}_1(z_1) \mathcal{E}_1^*(z_2) \rangle]. \quad (A.5)$$

We next substitute (53) and (57) into (A.2) to (A.5). In the integrands in (A.2) to (A.5), since $J_u(z_1, z_2)$, $J_d(z_1, z_2)$, $J_{c_1}(z_1, z_2)$ and $J_{c_2}(z_1, z_2)$ are slowly varying on the ℓ scale, we replace them by $I_u(z_1)$, $I_d(z_1)$, $I_c(z_1)$, and $I_c^*(z_1)$ respectively.

Because of the range restriction on z and z' , most of the contributions of the integrals in (A.2) to (A.5) come from terms with constructive interference. We conclude then that $I_2(z, z')$

and $I_3(z, z')$ are small compared with $I_1(z, z')$ and $I_4(z, z')$.

Balancing terms on both sides of equation (A.1), by their respective phases, we arrive at the following equations

$$e^{ik'_{1m}(z - z')} :$$

$$\begin{aligned} J_u(z, z') e^{ik'_{1m}(z - z')} &= e^{in_2 z - in_2^* z'} I_1(z, z') \\ &+ r_{12} e^{-(n_1 + n_2)d + in_1 z - in_1^* z'} I_4(z, z') \end{aligned} \quad \text{A.6a}$$

$$e^{-ik'_{1m}(z - z')} :$$

$$\begin{aligned} J_d(z, z') e^{-ik'_{1m}(z - z')} &= r_{01} e^{-in_1 z + in_1^* z_1} I_1(z, z') \\ &+ e^{-in_2 z + in_2^* z'} I_4(z, z') \end{aligned} \quad \text{(A.6b)}$$

$$e^{ik'_{1m}(z + z')} :$$

$$J_{c_1}(z, z') e^{ik'_{1m}(z + z')} = -R_{01}^* e^{in_2 z + in_1^* z'} I_1(z, z')$$

$$+ R_{12} e^{i(\eta_1 + \eta_2)d + i\eta_1 z + i\eta_2^* z'} I_4(z, z') \quad (A.6c)$$

$$e^{-ik'_{lm}(z + z')} :$$

$$J_{c_2}(z, z') e^{-ik'_{lm}(z + z')} = -R_{01} e^{-i\eta_1 z - i\eta_2^* z'} I_1(z, z')$$

$$+ R_{12}^* e^{-i(\eta_1^* + \eta_2)d - i\eta_1^* z' - i\eta_2 z} I_4(z, z'). \quad (A.6d)$$

Setting $z' = z$ in equation (A.6), we obtain equations (62) to (64).

Appendix II.

Because the fluctuating part of the permittivity is real, we can obtain from equation (6) the energy conservation relationship

$$E_1^* \frac{d^2}{dz^2} E_1 - E_1 \frac{d^2}{dz^2} E_1^* + 2i(k_{1m}^2)'' |E_1|^2 = 0. \quad (A.7)$$

We use superscript double prime to denote imaginary part of a quantity.

Taking the ensemble average of (A.7), we have

$$\begin{aligned} y_1 &\equiv E_{1m}^* \frac{d^2}{dz^2} E_{1m} - E_{1m} \frac{d^2}{dz^2} E_{1m}^* \\ &+ \lim_{z' \rightarrow z} \left\{ \frac{d^2}{dz^2} \langle \mathcal{E}_1(z) \mathcal{E}_1^*(z') \rangle - \frac{d^2}{dz^2} \langle \mathcal{E}_1^*(z) \mathcal{E}_1(z') \rangle \right\} \\ &+ 2i(k_{1m}^2)'' \{ |E_{1m}|^2 + \langle |\mathcal{E}_1(z)|^2 \rangle \} = 0. \end{aligned} \quad (A.8)$$

Taking the integration of y_1 over region 1, we define

$$y_2 \equiv \int_{-d}^0 dz y_1 = 0. \quad (A.9)$$

For our purpose of energy conservation to the zeroth order, we require that both y_1 and y_2 to be of order $0(\delta)$. We remark that y_1 being of $0(\delta)$ does not imply y_2 is of $0(\delta)$. For instance, the integration of y_1 from $z = -\infty$ to 0 , which is the case for a half-space medium, may yield a significant value for y_2 . We thus require that there be no constructive interference terms of $0(\delta)$ in y_1 . This condition then is sufficient to guarantee that y_2 is of $0(\delta)$.

From (52), we obtain

$$\begin{aligned}
 & E_{1m}^* \frac{d^2}{dz^2} E_{1m} - E_{1m} \frac{d^2}{dz^2} E_{1m}^* \\
 &= -2i(k_{2m}^2)'' |E_{1m}|^2 \\
 &+ 2i \left[\int_{-d}^0 G_{11m}(z, z_1) B_f(z, z_1) E_{1m}^*(z) E_{1m}(z_1) dz_1 \right]'' . \quad (A.10)
 \end{aligned}$$

In view of (55) and (17),

$$\begin{aligned}
 & \lim_{z \rightarrow z'} \frac{d^2}{dz^2} \left\{ \langle \mathcal{E}(z) \mathcal{E}^*(z') \rangle - \langle \mathcal{E}^*(z) \mathcal{E}(z') \rangle \right\} \\
 &= -2i(k_{1m}^2)'' \langle |\mathcal{E}_1(z)|^2 \rangle + 2i \left\{ \int_{-d}^0 dz_1 G_{11m}^*(z, z_1) B_f(z, z_1) \right.
 \end{aligned}$$

$$\left[E_{1m}(z) E_{1m}^*(z_1) + \langle \mathcal{E}_1(z) \mathcal{E}_1^*(z_1) \rangle \right] + 2i \left\{ \int_{-d}^0 dz_1 G_{11m}(z, z_1) B_f(z, z_1) \langle \mathcal{E}(z_1) \mathcal{E}^*(z) \rangle \right\}. \quad (A.11)$$

Substituting (A.10) into (A.11), we find that $y_1 = O(\delta^2)$. Thus energy is conserved to the required order.

If we had used the bilocal approximation to Dyson's equation, rather than the nonlinear approximation, i.e. instead of (13), we use

$$Q(z, z_1) = G_{11m}^0(z, z_1) B_f(z, z_1) \quad (A.12)$$

where $G_{11m}^0(z, z_1)$ is the Green's function for the unperturbed problem, we would have obtained

$$y_1 = 2i \left\{ \int_{-d}^0 dz_1 (G_{11m}^0(z, z_1) - G_{11m}^b(z, z_1)) B_f(z, z_1) \right. \\ \left. [E_{1m}^{b*}(z) E_{1m}^b(z_1) + \langle \mathcal{E}_1^*(z) \mathcal{E}_1(z_1) \rangle] \right\}. \quad (A.13)$$

We use superscript b to denote bilocal quantities. If for $|z - z_1| \leq O(\delta)$,

$$G_{11m}^0(z, z_1) - G_{11m}^b(z, z_1) = O(\delta), \quad (A.14)$$

then y_1 as given by (A.13) is of $O(\delta^2)$. Equation (A.14) is in general true for unbounded medium but not for bounded medium. We also remark that if we use bilocal quantities in the derivation, the MRT equations so obtained, even for half space medium, lack symmetry and do not conserve energy.

References

- [1] Gurvich, A. S., V. I. Kalinin, and D. T. Matveyev,
"Influence of the internal structure of glaciers on
their thermal radio emission," Atm. and Oceanic Phys.,
9, 712-717, 1973.

- [2] Stogryn, A., "Electromagnetic scattering by random
dielectric constant fluctuations in a bounded medium,"
Radio Science, 5, 509-518, 1974.

- [3] England, A. W., "Thermal microwave emission from a half-
space containing scatterers," Radio Science, 9, 447-454,
1974.

- [4] Frisch, V., "Wave propagation in random medium," Probabilis-
tic Methods in Applied Mathematics, 1, edited by Bharuche-
Reid, 76-198, Academic Press, 1968.

- [5] Tatarskii, V. I., "Propagation of electromagnetic waves in
a medium with strong dielectric constant fluctuations,"
Sov. Phys. JETP, 19, 946-953, 1964.

- [6] Sancer, M. I., and Varvatsis, A. S., "An investigation of
the renormalization and Rytov methods as applied to pro-
pagation in a turbulent medium," NCL 69-28R, Northrop Corp.
Laboratories, 1969.

- [7] Barabanenkov, Y. N. and Finkelberg, V. M., "Radiative transport equation for correlated scatterers," Sov. Phys. JETP, 26, 587-591, 1968.
- [8] Stott, P., "A transport theory for the multiple scattering of electromagnetic wave by a turbulent plasma," J. Phys. A, 1, 675-689, Dec. 1968.
- [9] Watson, K., "Multiple scattering of electromagnetic waves in an underdense plasma," J. Math. Phys., 10, 688-702, April 1969.
- [10] Fante, R. L., "Propagation of electromagnetic waves through turbulent plasma using transport theory," IEEE Trans. on Antennas and Propagation, AP-21, no. 9, 750-755, Sept. 1973.
- [11] Gurvich, A. S., and Tatarskii, V. I., "Coherence and intensity fluctuations of light in the turbulent atmosphere," Rad. Sci., 10, no. 1, 3-14, Jan. 1975.
- [12] Ishimaru, A., "Correlation function of a wave in a random distribution of stationary and moving scatterers," Rad. Sci., 10, no. 1, 45-52, Jan. 1975.
- [13] Dence, D., and Spence, J. E., "Wave propagation in random anisotropic media," Probabilistic Methods in Applied Mathematics, 3, edited by A. T. Bheruche-Reid, Academic Press, 1973.

- [14] Rosenbaum, S., "The mean Green's function: a non-linear approximation," Radio Science, 6, 379-386, 1971.
- [15] Cole, J. D., Perturbation Methods in Applied Mathematics, Grim Blaisdell, Waltham, Mass., 79-119, 1968.

Figure Captions

Figure 1. Geometrical configuration of the problem.

Figure 2. Emissivity of a half-space medium with $\epsilon_1' = 3.2\epsilon_0$,
 $\epsilon_1'' = .16\epsilon_0$, $l = 2$ mm.

Figure 3. Emissivity of a two layer random medium with $\epsilon_1' = 3.2\epsilon_0$,
 $\epsilon_1'' = .16\epsilon_0$, $l = 2$ mm., $\epsilon_2 = 81\epsilon_0$, and $d = 20$ cm.

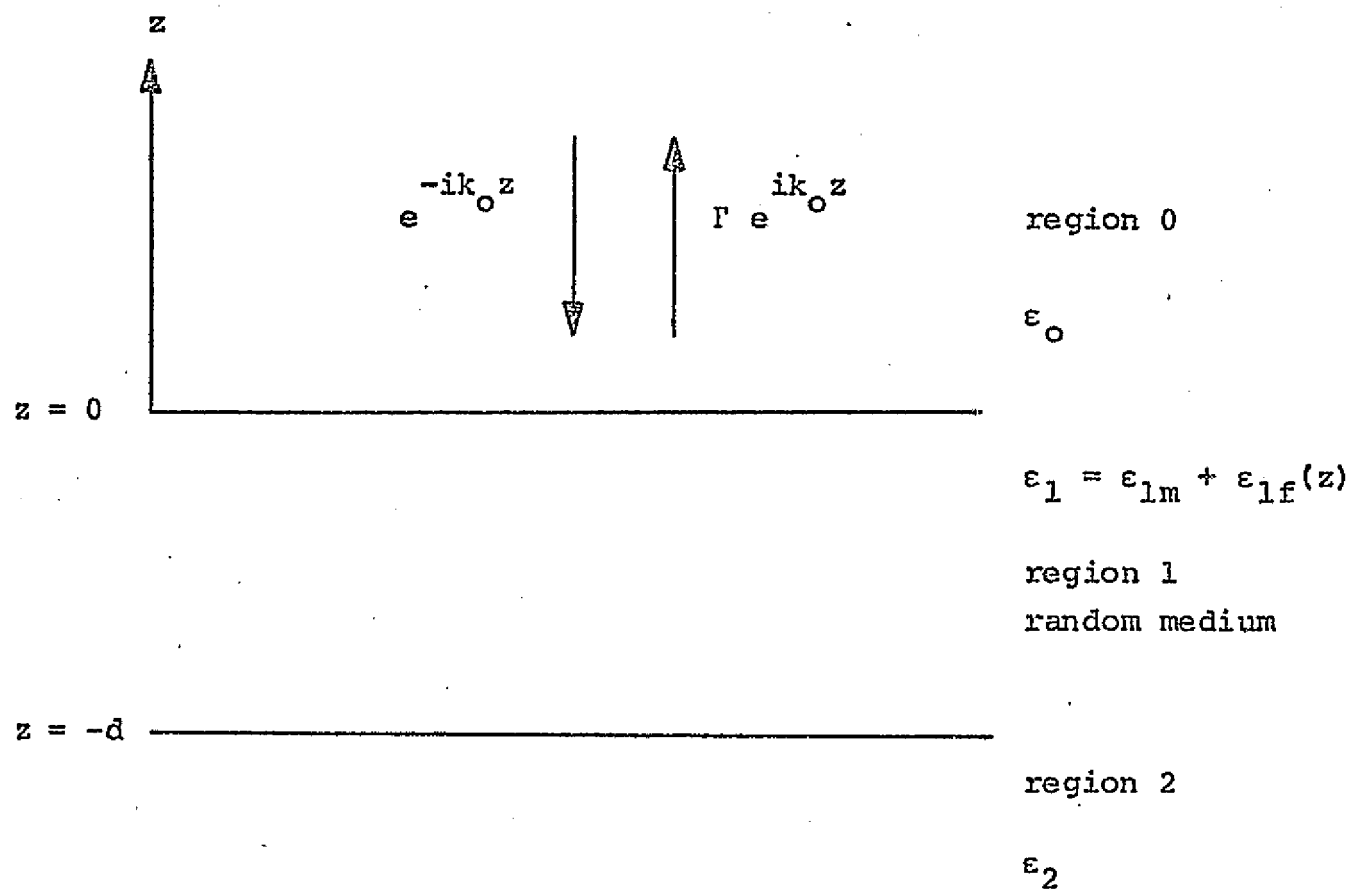


Figure 1.

Figure 2

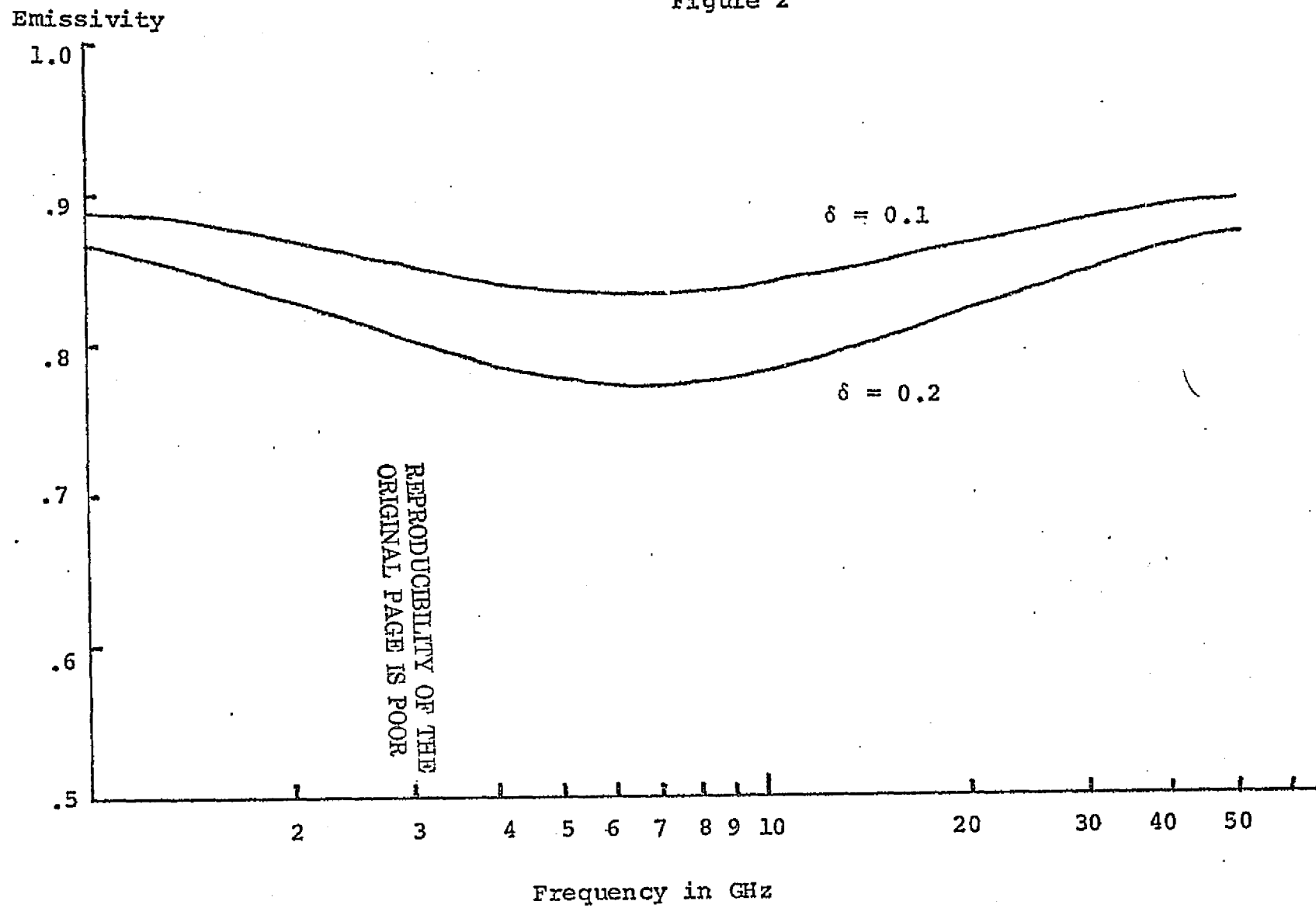
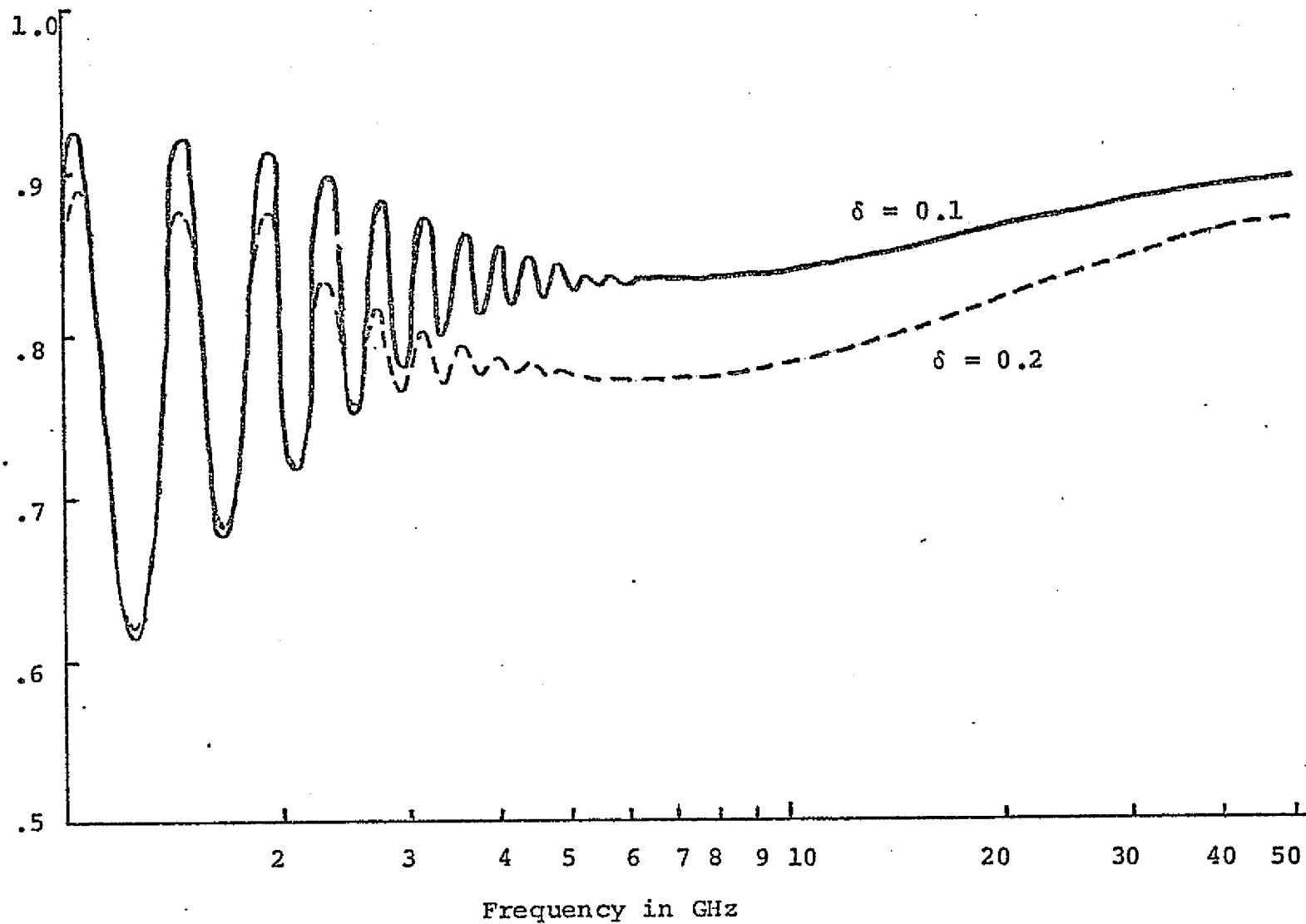


Figure 3

Emissivity



APPENDIX VI

Microwave Thermal Emission from a Stratified Medium with Nonuniform Temperature Distribution*

by

L. Tsang, E. Njoku, and J. A. Kong

Department of Electrical Engineering and
Computer Science and Research Laboratory
of Electronics

Massachusetts Institute of Technology

Cambridge, Massachusetts 02139

Abstract:

Using the dissipation-fluctuation approach, the brightness temperature of a stratified medium with inhomogeneous permittivities and nonuniform temperature profiles are solved. The solution is expressed in closed form ready for machine computation. Numerical results are illustrated and compared with closed form analytical solutions and results obtained from the WKB method for simple profiles.

* This work was supported by the NASA Contract 953524 and the Joint Service Electronics Program Contract DAAB07-74-C-0630.

I. Introduction

In microwave passive remote sensing of the earth, the brightness temperature is determined by the geometrical configuration, the medium properties, and the temperature distributions of the area under observation. With the model of a vertically structure medium Stogryn^[1] used the fluctuation-dissipation theorem^[2] and formulated the solution for the brightness temperature in terms of a two-point boundary value problem by solving a second-order ordinary differential equation, together with the evaluation of an integral. In this paper we extend the propagation matrix formulation^[3] and solve for the brightness temperature of a stratified medium. The problem is an important one because inhomogeneous permittivities and nonuniform temperature profiles can be conveniently approximated by a stratified medium. On the other hand analytical results can only be obtained for very few media with simple profiles. The solutions for the stratified medium are expressed in closed forms and numerical examples are given for different temperature and permittivity profiles. The results are compared with the well-known exact solutions for simple profiles and with those obtained with the WKB method.

II. Dyadic Green's Functions for a Stratified Medium

Consider a stratified medium consisting of N layers and with planes of stratification perpendicular to the z -axis (Figure 1). Let there be a point source in region 0. In order to calculate field vectors in any region l , we first consider dyadic Green's function $\bar{\bar{G}}(\bar{r}, \bar{r}')$ in the absence of the stratified medium,

$$\bar{E}(\bar{r}, \omega) = \int d^3r' \bar{\bar{G}}(\bar{r}, \bar{r}') \cdot \bar{J}(\bar{r}'). \quad (1)$$

The dyadic Green's function $\bar{\bar{G}}(\bar{r}, \bar{r}')$ is governed by the equation

$$\nabla \times \nabla \times \bar{\bar{G}}(\bar{r}, \bar{r}') - \omega^2 \mu \epsilon \bar{\bar{G}}(\bar{r}, \bar{r}') = i\omega \mu \bar{I} \delta(\bar{r} - \bar{r}'). \quad (2)$$

By the method of scattering superposition^[4], we obtain (from Appendix A where dyadic Green's functions are derived for uniaxial media)

$$\bar{\bar{G}}(\bar{r}, \bar{r}') = \begin{cases} -\frac{\omega \mu}{8\pi^2} \iint_{-\infty}^{\infty} dk_x dk_y \frac{1}{k_z} \{ \hat{e}(k_z) \hat{e}(k_z) + \hat{h}(k_z) \hat{h}(k_z) \} e^{i\bar{k} \cdot (\bar{r} - \bar{r}')} & z' \leq z \\ -\frac{\omega \mu}{8\pi^2} \iint_{-\infty}^{\infty} dk_y dk_y \frac{1}{k_z} \{ \hat{e}(-k_z) \hat{e}(-k_z) + \hat{h}(-k_z) \hat{h}(-k_z) \} e^{i\bar{k} \cdot (\bar{r} - \bar{r}')} & z \leq z' \end{cases} \quad (3)$$

REPRODUCIBILITY OF THE
ORIGINAL PAGE IS POOR

where

$$k_z = (\omega^2 \mu \epsilon - k_x^2 - k_y^2)^{1/2} \quad (4)$$

$$\hat{e}(k_z) = \frac{1}{(k_x^2 + k_y^2)^{1/2}} \{\hat{x} k_y - \hat{y} k_x\} \quad (5)$$

$$\hat{h}(k_z) = \frac{1}{k} \{\hat{e} \times \bar{k}\} \quad (6)$$

$$k = (k_x^2 + k_y^2 + k_z^2)^{1/2} \quad (7)$$

$$\bar{k} = \hat{x} k_x + \hat{y} k_y + \hat{z} k_z \quad (8)$$

$$\bar{k} = \hat{x} k_x + \hat{y} k_y - \hat{z} k_z. \quad (9)$$

We see that $\hat{e}(k_z)$ is a unit vector perpendicular to the plane of incidence determined by \bar{k} and \hat{z} and \hat{h} is a unit vector parallel to the plane of incidence.

For the stratified medium, dyadic Green's functions are

written as

$$\begin{aligned} \bar{G}_{00}(\bar{r}, \bar{r}') = & - \frac{\omega\mu}{8\pi^2} \iint_{-\infty}^{\infty} dk_x dk_y \frac{1}{k_z} \{ (R^{TE} \hat{e}(k_z) e^{i\bar{k} \cdot \bar{r}} \\ & + \hat{e}(-k_z) e^{i\bar{k} \cdot \bar{r}}) \hat{e}(-k_z) e^{-i\bar{k} \cdot \bar{r}'} + (R^{TM} \hat{h}(k_z) e^{i\bar{k} \cdot \bar{r}} \\ & + \hat{h}(-k_z) e^{i\bar{k} \cdot \bar{r}}) \hat{h}(-k_z) e^{-i\bar{k} \cdot \bar{r}'} \} \end{aligned} \quad (10)$$

for $z \leq z'$ in region 0,

$$\begin{aligned} \bar{G}_{l0}(\bar{r}, \bar{r}') = & - \frac{\omega\mu}{8\pi^2} \iint_{-\infty}^{\infty} dk_x dk_y \frac{1}{k_z} \{ (A_l \hat{e}_l(k_{lz}) e^{i\bar{k}_l \cdot \bar{r}} \\ & + B_l \hat{e}_l(-k_{lz}) e^{i\bar{k}_l \cdot \bar{r}}) \hat{e}_l(-k_z) e^{-i\bar{k} \cdot \bar{r}'} + (C_l \hat{h}_l(k_{lz}) e^{i\bar{k}_l \cdot \bar{r}} \\ & + D_l \hat{h}_l(-k_{lz}) e^{i\bar{k}_l \cdot \bar{r}}) \hat{h}_l(-k_z) e^{-i\bar{k} \cdot \bar{r}'} \} \end{aligned} \quad (11)$$

in region l, and

$$\begin{aligned} \bar{G}_{to}(\bar{r}, \bar{r}') = & -\frac{\omega\mu}{8\pi^2} \iint_{-\infty}^{\infty} dk_x dk_y \frac{1}{k_z} \{ T^{TE} \hat{e}_t(-k_{tz}) e^{i\bar{k}_t \cdot \bar{r}} \hat{e}(-k_z) e^{-i\bar{k} \cdot \bar{r}'} \\ & + T^{TM} \hat{h}_t(-k_{tz}) e^{i\bar{k}_t \cdot \bar{r}} \hat{h}(-k_z) e^{-i\bar{k} \cdot \bar{r}'} \} \end{aligned} \quad (12)$$

in region t . In writing the dyadic Green's functions, we use the first subscript to denote the region in which the observation point is located and the second subscript to denote the region in which the source is located. The coefficients A_ℓ , B_ℓ , C_ℓ , D_ℓ , and the reflection and transmission coefficients for TE and TM waves R^{TE} , R^{TM} , T^{TE} and T^{TM} are determined by matching boundary conditions and related to one another by propagation matrices^[3]. In this case, the TE and TM quantities are both for electric field vectors and are not dual to each other. The TE quantities are found in reference 3. The TM quantities are given in Appendix B.

III. Brightness Temperature of the Stratified Medium

To find the brightness temperature of the stratified medium, we apply the fluctuation-dissipation theorem^[2]. The thermal sources in region l is denoted by $\bar{J}_l(\bar{r}, \omega)$. The expectation value of $\langle \bar{J}_l \bar{J}_l^* \rangle$ is

$$\langle \bar{J}_l(\bar{r}, \omega) \bar{J}_l^*(\bar{r}', \omega') \rangle = \frac{4}{\pi} \omega \epsilon_l'' K T_l(\bar{z}) \bar{I} \delta(\omega - \omega') \delta(\bar{r} - \bar{r}') \quad (13)$$

where K is the Boltzman constant, $T_l(z)$ the temperature distribution in the l th region, and \bar{I} the identity matrix. Equation (13) is true under the assumption $\hbar\omega \ll KT$ which is valid at microwave frequencies.

The brightness temperature at angular frequency ω is defined as^[1]

$$T_B^{TE}(\hat{k}, \omega) = \frac{(2\pi)^3}{K} (c/\omega)^2 \frac{1}{2} c \epsilon_0 \int_0^\infty d\omega' \int_0^\infty k^2 dk \int_{-\infty}^\infty d^3k' \{ \hat{e} \cdot \langle \bar{E}(\bar{k}, \omega) \bar{E}^*(\bar{k}', \omega') \rangle \cdot \hat{e} e^{i(\bar{k} - \bar{k}') \cdot \bar{r} - i(\omega - \omega')t} \} \quad (14a)$$

for the horizontal polarization or TE waves and

$$T_B^{TM}(\hat{k}, \omega) = \frac{(2\pi)^3}{K} (c/\omega)^2 \frac{1}{2} c \epsilon_0 \int_0^\infty d\omega' \int_0^\infty k^2 dk \int_{-\infty}^\infty d^3k' \{ \hat{h} \cdot \langle \bar{E}(\bar{k}, \omega) \bar{E}^*(\bar{k}', \omega') \rangle \cdot \hat{h} e^{i(\bar{k} - \bar{k}') \cdot \bar{r} - i(\omega - \omega')t} \} \quad (14b)$$

for the vertical polarization or TM waves. In order to determine the electric field intensity $\bar{E}(\bar{k}, \omega)$, we note that

$$\bar{E}(\bar{r}, \omega) = \sum_{\ell=1}^t \int_{-\infty}^{\infty} dx' \int_{-\infty}^{\infty} dy' \int_{-d_{\ell}}^{-d_{\ell}-1} dz' \bar{G}_{0\ell}(\bar{r}, \bar{r}') \cdot \bar{J}_{\ell}(\bar{r}') \quad (15)$$

where $t = N + 1$ and $d_t \rightarrow \infty$. By the symmetric properties of dyadic Green's functions, $\bar{G}_{0\ell}(\bar{r}, \bar{r}') = \bar{G}_{0\ell}^t(\bar{r}', \bar{r})$, where the superscript t denotes transpose. In view of (11), we find

$$\begin{aligned} \bar{G}_{0\ell}(\bar{r}, \bar{r}') = & -\frac{\omega\mu}{8\pi^2} \int_{-\infty}^{\infty} d^3k \delta(k_z - \sqrt{\omega^2\mu\epsilon - k_x^2 - k_y^2}) \frac{e^{i\bar{k} \cdot \bar{r}}}{k_z} \\ & \{ \hat{e}(k_z) [A_{\ell} \hat{e}_{\ell}(-k_{\ell z}) e^{-i\bar{k}_{\ell} \cdot \bar{r}'} + B_{\ell} \hat{e}_{\ell}(k_{\ell z}) e^{-i\bar{k}_{\ell} \cdot \bar{r}'}] \\ & + \hat{h}(k_z) [C_{\ell} \hat{h}_{\ell}(-k_{\ell z}) e^{-i\bar{k}_{\ell} \cdot \bar{r}'} + D_{\ell} \hat{h}_{\ell}(k_{\ell z}) e^{-i\bar{k}_{\ell} \cdot \bar{r}'}] \}. \quad (16) \end{aligned}$$

A change of variable of integration from k_x, k_y to $-k_x$ and $-k_y$ is made in arriving at (16). Introducing (16) in (15), we obtain

$$\begin{aligned} \bar{E}(\bar{r}, \omega) = & -\frac{\omega\mu}{8\pi^2} \sum_{\ell=1}^t \iint_{-\infty}^{\infty} dx' dy' \int_{-d_{\ell}}^{-d_{\ell}-1} dz' \delta(k_z - \sqrt{\omega^2\mu\epsilon - k_x^2 - k_y^2}) \\ & \frac{1}{k_z} \{ \hat{e}(k_z) [A_{\ell} \hat{e}_{\ell}(-k_{\ell z}) e^{-i\bar{k}_{\ell} \cdot \bar{r}'} + B_{\ell} \hat{e}_{\ell}(k_{\ell z}) e^{-i\bar{k}_{\ell} \cdot \bar{r}'}] + \hat{h}(k_z) \\ & [C_{\ell} \hat{h}_{\ell}(-k_{\ell z}) e^{-i\bar{k}_{\ell} \cdot \bar{r}'} + D_{\ell} \hat{h}_{\ell}(k_{\ell z}) e^{-i\bar{k}_{\ell} \cdot \bar{r}'}] \} \cdot \bar{J}_{\ell}(\bar{r}'). \quad (17) \end{aligned}$$

Using (13) and (14) we find the brightness temperature to be

$$T_B^{TE}(\hat{k}, \omega) = k^3 \cos \theta \sum_{\ell=1}^t \frac{\epsilon_{\ell}''}{\epsilon_0} \int_{-d_{\ell}}^{-d_{\ell+1}} dz' T_{\ell}(z')$$

$$\left| \frac{1}{k_z} [A_{\ell} \hat{e}_{\ell}(-k_{\ell z}) e^{ik_{\ell z} z'} + B_{\ell} \hat{e}_{\ell}(k_{\ell z}) e^{-ik_{\ell z} z'}] \right|^2 \quad (18a)$$

$$T_B^{TM}(\hat{k}, \omega) = k^3 \cos \theta \sum_{\ell=1}^t \frac{\epsilon_{\ell}''}{\epsilon_0} \int_{-d_{\ell}}^{-d_{\ell+1}} dz' T_{\ell}(z')$$

$$+ \frac{1}{k_z} [C_{\ell} \hat{h}_{\ell}(-k_{\ell z}) e^{ik_{\ell z} z'} + D_{\ell} \hat{h}_{\ell}(k_{\ell z}) e^{-ik_{\ell z} z'}] \right|^2. \quad (18b)$$

In the derivation of (18), we use the relation $\delta[k_z - \sqrt{\omega^2 \mu \epsilon - k_x^2 - k_y^2}] = U(k_z) \cos \theta \delta(k - \omega \sqrt{\mu \epsilon})$, where $U(k_z) = 1$ for $k_z > 0$ and $U(k_z) = 0$ for $k_z < 0$.

The calculation of the integral in (18) is straightforward. Without loss of generality, we let the plane of observation be the $x - z$ plane and set $k_y = 0$. The temperature $T_{\ell}(z')$ is a constant in region ℓ , (the case of non-constant temperature can be generalized easily) we find that for horizontal polarization

$$\begin{aligned}
T_B^{TE}(\theta) = & \frac{k}{\cos \theta} \frac{N}{\sum_{l=1}^N} \frac{\epsilon_l'' T_l}{\epsilon_0} \left\{ \frac{|A_l e^{-ik_{lz} d_l}|^2}{2k_{lz}''} (1 - e^{2k_{lz}''(d_l - 1 - d_l)}) \right. \\
& - \frac{|B_l e^{ik_{lz} d_l}|^2}{2k_{lz}''} (1 - e^{-2k_{lz}''(d_l - 1 - d_l)}) \\
& - \frac{(A_l e^{-ik_{lz} d_l})(B_l e^{ik_{lz} d_l})^*}{2ik_{lz}'} (1 - e^{-i2k_{lz}'(d_l - 1 - d_l)}) \\
& \left. + \frac{(A_l e^{-ik_{lz} d_l})^*(B_l e^{ik_{lz} d_l})}{2ik_{lz}'} (1 - e^{i2k_{lz}'(d_l - 1 - d_l)}) \right\} \\
& + \frac{k}{\cos \theta} \frac{\epsilon_t'' T_t}{\epsilon_0} \frac{|T^{TE}|^2 e^{-2k_{tz}'' d_n}}{2k_{tz}''} \quad (19)
\end{aligned}$$

Similarly, for vertical polarization, we obtain

REPRODUCIBILITY OF THE
ORIGINAL PAGE IS POOR

$$\begin{aligned}
T_B^{TM}(\theta) = & \frac{k}{\cos \theta} \sum_{\ell=1}^N \frac{\epsilon_\ell'' T_\ell}{\epsilon_0 |k_\ell|^2} (|k_{\ell z}|^2 + k_x^2) \left\{ \frac{|C_\ell e^{-ik_{\ell z} d_\ell}|^2}{2k_{\ell z}''} \right. \\
& (1 - e^{-2k_{\ell z}''(d_\ell - d_\ell - 1)}) - \frac{|D_\ell e^{ik_{\ell z} d_\ell}|^2}{2k_{\ell z}''} (1 - e^{2k_{\ell z}''(d_\ell - d_\ell - 1)}) \\
& + \frac{|k_{\ell z}|^2 - k_x^2}{|k_{\ell z}|^2 + k_x^2} \left[\frac{(C_\ell e^{-ik_{\ell z} d_\ell})(D_\ell e^{ik_{\ell z} d_\ell})^*}{2ik_{\ell z}'} (1 - e^{i2k_{\ell z}'(d_\ell - d_\ell - 1)}) \right. \\
& \left. \left. - \frac{(C_\ell e^{-ik_{\ell z} d_\ell})^*(D_\ell e^{ik_{\ell z} d_\ell})}{2ik_{\ell z}'} (1 - e^{-i2k_{\ell z}'(d_\ell - d_\ell - 1)}) \right] \right\} \\
& + \frac{k}{\cos \theta} \frac{\epsilon_t'' (|k_{tz}|^2 + k_x^2) T_t}{\epsilon_0 |k_t|^2} |T^{TM}|^2 \frac{e^{-2k_{tz}'' d_n}}{2k_{tz}''} . \quad (20)
\end{aligned}$$

For homogeneous half-space with constant temperature, we find

$$T_B^{TE} = (1 - r^{TE}) T_t \quad (21)$$

and

$$T_B^{TM} = (1 - r^{TM}) T_t. \quad (22)$$

In the derivation of (21) and (22), we made use of the identities $2k_{tz}' k_{tz}'' = \omega^2 \mu \epsilon_t''$ and $|k_{tz}|^2 + k_x^2 = \omega^2 \mu (\epsilon_t' k_{tz}' + \epsilon_t'' k_{tz}'') / k_{tz}'$.

In Figure 2 we examine the angular dependence of the brightness temperature. At 1 GHz, T_B^{TE} and T_B^{TM} are plotted as a function of observation angle for the following profiles:

$$\frac{\epsilon_1(z)}{\epsilon_0} = 9.0(1 + i 0.3) - (5.5 + i 2.5) e^{az} \quad (23a)$$

$$\epsilon_t = \epsilon_1(-d) \quad (23b)$$

$$T(z) = T_0 + \Delta T e^{bz} \quad (23c)$$

$$T_t = T(-d) \quad (23d)$$

with $a = 0.02 \text{ cm}^{-1}$, $b = 0.05 \text{ cm}^{-1}$, $d = 30 \text{ cm}$, and $\Delta T = \pm 20^\circ\text{K}$.

It is interesting to observe a maximum for vertical polarizations similar to the Brewster angle for a uniform half space medium.

In Figure 3, we plot the brightness temperature of a radio-meter looking from nadir as a function of frequency for the following permittivity and temperature profiles:

$$\frac{\epsilon_1(z)}{\epsilon_0} = 9.0(1 + i 0.3) - (5.5 + i 2.5) e^{az} \quad (24a)$$

$$\epsilon_t = \epsilon_1(-d) \quad (24b)$$

$$T = T_0 + \Delta T e^{bz} \quad (24c)$$

$$T_t = T(-d) \quad (24d)$$

with $a = 0.02 \text{ cm}^{-1}$, $d = 30 \text{ cm}$, $T_0 = 280^\circ\text{K}$, $\Delta T = \pm 20^\circ\text{K}$, and $b = 0.05 \text{ cm}^{-1}$ and 0.1 cm^{-1} . In the calculations the temperature and the permittivity profiles are stratified into 350 layers from 0 to $z = -d$. We see that at low frequencies the subsurface temperature affects T_B more than at high frequencies. At very low frequencies the brightness temperatures for different parameters of a and b approach the same value dictated by T_0 and the effective emissivity of the medium.

In Figure 4 the brightness temperature as observed from nadir is plotted as a function of frequency for the following profiles:

$$\epsilon_1(z)/\epsilon_0 = 9.0(1 + i 0.1) - (5.5 + i 0.83) e^{az} \quad (25a)$$

$$\epsilon_t(z \leq -20 \text{ cm})/\epsilon_0 = 9.0(1 + i 0.05) \quad (25b)$$

$$T(z) = T_0 + \Delta T e^{bz} \quad (25c)$$

$$T_t = T(z = -20 \text{ cm}) \quad (25d)$$

with $a = 0.02 \text{ cm}^{-1}$, $b = 0.1 \text{ cm}^{-1}$, $T_0 = 280^\circ\text{K}$, and $\Delta T = \pm 20^\circ\text{K}$. Note that there is an abrupt change in the permittivity profile at $z = -20 \text{ cm}$. At low frequencies, we see interference effects.

For higher frequencies, the brightness temperature is determined by $T_0 \pm \Delta T$ times the effective surface emissivity of the medium.

The interference effect at low frequencies is not characteristic of the abrupt change of the permittivity profile. For a continuous permittivity profile the interference is illustrated in Figure 5, where

$$\epsilon_1(z)/\epsilon_0 = (2.88 + i 0.34) e^{-az} \quad (26a)$$

$$\epsilon_t = \epsilon_1(z = -1 \text{ m}) \quad (26b)$$

$$T(z) = 300 - 20 e^{bz}, \quad -\infty < z < 0, \quad (26c)$$

$a = 2 \text{ m}^{-1}$ and $b = 3 \text{ m}^{-1}$. In the calculations, the region from $z = 0$ to $z = -1 \text{ m}$ is stratified into 350 layers. The temperature profile from $z = -1 \text{ m}$ to $-\infty$ is not stratified because (18) can be readily integrated. For this profile the exact solutions are presented in Appendix C. The result calculated with the stratified model is found to agree very well with that calculated with the exact formulas.

IV. WKB Solution

When the permittivity of the stratified medium can be written in terms of a continuous function $\epsilon(z)$ for $z < 0$, we follow an approach parallel to that used by Stogryn and find the brightness temperature for the horizontal and vertical polarizations to be

$$T_B^{TE} = \frac{k^2}{k_z} \int_{-\infty}^0 dz T(z) \epsilon_r''(z) |\psi(z)|^2 \quad (27)$$

and

$$T_B^{TM} = \frac{1}{k_z} \int_{-\infty}^0 dz T(z) \epsilon_r''(z) \left\{ \left| \frac{1}{\epsilon_r(z)} \frac{d\phi(z)}{dz} \right|^2 + \left| \frac{k_x \phi(z)}{\epsilon_r(z)} \right|^2 \right\} \quad (28)$$

where

$$\epsilon_r(z) = \epsilon_r'(z) + \epsilon_r''(z) = \epsilon(z)/\epsilon_0 \quad (29)$$

is the dielectric constant. The functions $\psi(z)$ and $\phi(z)$ in (27) and (28) are governed by the following equations:

$$\frac{d^2 \psi(z)}{dz^2} + [\epsilon_r(z)k^2 - k_x^2] \psi(z) = 0 \quad (30a)$$

$$\epsilon_r(z) \frac{d}{dz} \left[\frac{1}{\epsilon_r(z)} \frac{d\phi(z)}{dz} \right] + [\epsilon_r(z)k^2 - k_x^2] \phi(z) = 0. \quad (31a)$$

The boundary conditions are

$$1 + R_h = \psi(0) \quad (30b)$$

$$k_z(1 - R_H) = i \left(\frac{\partial \psi}{\partial z} \right)_{z=0} \quad (30c)$$

$$1 + R_V = \phi(0) \quad (31b)$$

$$\epsilon_r(0) k_z(1 - R_V) = i \left(\frac{\partial \phi}{\partial z} \right)_{z=0} \quad (31c)$$

Approximate solutions to these equations are easily determined with the WKB method.

Consider an equation of the following form

$$\frac{d^2 \chi}{dz^2} + [g(z)]^2 \chi = 0. \quad (32)$$

The WKB solution for an outgoing wave is

$$\chi(z) \sim \frac{C}{\sqrt{g(z)}} e^{-i \int_0^z dz g(z)} \quad (33)$$

Provided

$$g \gg \frac{1}{g} \frac{dg}{dz} \gg \frac{1}{\sqrt{g}} \frac{d^2}{dz^2} (1/\sqrt{g}). \quad (34)$$

Comparing (30) and (31) with (32), we see that

$$\frac{d^2 \chi}{dz^2} + [g_e(z)]^2 \chi = 0 \quad (35)$$

$$[g_e(z)]^2 = \epsilon_r(z) k^2 - k_x^2 \quad (36)$$

and

REPRODUCIBILITY OF THE
ORIGINAL PAGE IS POOR

$$\frac{d^2}{dz^2} [\phi/\sqrt{\epsilon_r}] + [g_m(z)]^2 [\phi/\sqrt{\epsilon_r}] = 0 \quad (37)$$

$$[g_m(z)]^2 = [g_e(z)]^2 - \sqrt{\epsilon_r} (d^2/dz^2) (1/\sqrt{\epsilon_r}). \quad (38)$$

The condition (24) is met if the medium is slowly varying such that

$$\frac{1}{\sqrt{\epsilon_r}} \frac{d}{dz} (\sqrt{\epsilon_r}) \ll g_e(z). \quad (39)$$

Under this assumption,

$$[g_m(z)]^2 \approx [g_e(z)]^2 = \epsilon_r k^2 - k_x^2. \quad (40)$$

After matching boundary conditions at $z = 0$ and making use of (27) and (28), we obtain

$$T_B^{TE} = (1 - r^{TE}) \int_{-\infty}^0 dz \, 2T(z) \frac{|g(0)|}{|g(z)|} \frac{g'(z)}{g'(0)} g''(z) e^{2 \int_0^z ds g''(s)} \quad (41)$$

$$T_B^{TM} = (1 - r^{TM}) \int_{-\infty}^0 dz \, 2T(z) \frac{f(z)}{f(0)} \frac{|g(0)|}{|g(z)|} \frac{g'(z)}{g'(0)} g''(z) e^{2 \int_0^z ds g''(s)} \quad (42)$$

where

$$f(z) = \frac{|g(z)|^2 + k_x^2}{|\epsilon_r(z)|} \quad (43a)$$

$$r^{TE} = \left| \frac{k_z - g(0)}{k_z + g(0)} \right|^2 \quad (43b)$$

$$r^{TM} = \left| \frac{k_z \epsilon_r(0) - g(0)}{k_z \epsilon_r(0) + g(0)} \right|^2 \quad (43c)$$

It is interesting to see that under the assumption that g'' is very small such that $|g(z)| \approx g'(z)$, (41) and (42) reduce to

$$T_B = (1 - r) \int_{-\infty}^0 2T(z) g''(z) e^{2 \int_0^z ds g''(s)} \quad (44)$$

which is a well-known result in the radiative transfer theory.

To illustrate the use of (41) and (42), we plot the WKB result in Figure 5 to compare with that obtained from the stratified model. We note that the WKB result is quite accurate in the high frequency side. For low frequencies, the WKB fails to predict interference effects. This is due to the fact that the reflectivity is a constant for the WKB approach, whereas for the stratified model, the reflectivity exhibits the interference effect. The reflectivities are plotted in Figure 6. The CPU time in using the IBM 370 for calculation of the brightness temperature in Figure 5 is approximately 0.12 minutes for the stratified model, 0.10 minutes for the exact solution, and 0.03 minutes for the WKB approach. This implies that WKB is useful in the frequency range where its results are valid.

V. Discussions

In this paper we apply the dissipation-fluctuation approach to find the brightness temperature of a stratified medium with inhomogeneous permittivities and nonuniform temperature profiles. The results are expressed in closed form. The solution to this problem is an important one because only very few special profiles can be approximated and solved in analytical forms. Even then the solution is in the form of special functions and requires perhaps as much computer time to calculate numerically. Numerical results to the stratified medium model are illustrated. They are also compared with the exact solutions and the results obtained from WKB approximation. At high frequency limit, profiles that can be treated with the WKB method may require less computer time. However when the frequency gets higher than microwave frequency, the approach proposed in this paper becomes inaccurate^[5]. Also in the calculations we omit the contributions to the brightness temperature arising from reflections of sky radiation and cosmic background, which can be easily accounted for by adding to the above results.

References

- [1] A. Stogryn, The Brightness Temperature of a Vertically Structured Medium, Radio Science, 12, 1397-1406, 1970.
- [2] L. Landau and E. Lifshitz, Electrodynamics of Continuous Media, Pergamon Press, London, 1960.
- [3] J. A. Kong, Theory of Electromagnetic Waves, Wiley-Interscience, New York, 1975.
- [4] C. T. Tai, Dyadic Green's Functions in Electromagnetic Theory, Chapter 8, Intex Comp., 1971.
- [5] A. Stogryn, A Note on Brightness Temperature at Millimeter Wavelength, IEEE Transactions on Geoscience Electronics, GE-13, 81-84, 1975.

Figure Captions

- Figure 1. Geometrical configuration of stratified isotropic medium.
- Figure 2. Brightness temperature as a function of observation angle for TE and TM waves at 1 GHz.
- Figure 3. Brightness temperature as a function of frequency for profiles in Equation (24).
- Figure 4. Brightness temperature as a function of frequency for profiles in Equation (25).
- Figure 5. Brightness temperature calculated with the stratified model and the exact formula compared with that calculated with the WKB method.
- Figure 6. Reflectivities calculated for the stratified medium and for the WKB method.

Appendix A.

In this section we derive dyadic Green's function for a uniaxial medium with optic axis parallel to the z axis. Dyadic Green's functions for uniaxial media are governed by the following equation

$$(\bar{\nabla} \cdot \bar{\mu}^{-1} \cdot \bar{\nabla} - \omega^2 \bar{\epsilon}) \cdot \bar{G}(\bar{r}, \bar{r}') = i\omega \bar{I} \delta(\bar{r} - \bar{r}') \quad (\text{A.1})$$

where

$$\bar{\mu}^{-1} = \begin{bmatrix} 1/\mu & 0 & 0 \\ 0 & 1/\mu & 0 \\ 0 & 0 & 1/\mu_z \end{bmatrix} \quad (\text{A.2})$$

is the inverse permeability tensor,

$$\bar{\epsilon} = \begin{bmatrix} \epsilon & 0 & 0 \\ 0 & \epsilon & 0 \\ 0 & 0 & \epsilon_z \end{bmatrix} \quad (\text{A.3})$$

is the permittivity tensor, \bar{I} denotes the identity matrix, and $\bar{\nabla}$ is defined by $\bar{\nabla} \cdot \bar{A} = \nabla \times \bar{A}$ for any vector \bar{A} . Equation (A.1) follows directly from Maxwell's equations.

We write the Fourier transform pair of dyadic Green's function as

$$\bar{G}(\bar{k}, \bar{r}') = \int_{-\infty}^{\infty} d^3r \bar{G}(\bar{r}, \bar{r}') e^{-i\bar{k} \cdot \bar{r}} \quad (A.4)$$

$$\bar{G}(\bar{r}, \bar{r}') = \frac{1}{8\pi^3} \int_{-\infty}^{\infty} d^3k \bar{G}(\bar{k}, \bar{r}') e^{i\bar{k} \cdot \bar{r}}. \quad (A.5)$$

Substituting (A.5) in (A.1) yields

$$\bar{G}(\bar{k}, \bar{r}') = -i\omega [\bar{k} \cdot \bar{\mu}^{-1} \cdot \bar{k} + \omega^2 \bar{\epsilon}]^{-1} e^{i\bar{k} \cdot \bar{r}'} \quad (A.6)$$

where

$$\bar{k} = \begin{bmatrix} 0 & -k_z & k_y \\ k_z & 0 & -k_x \\ -k_y & k_x & 0 \end{bmatrix}. \quad (A.7)$$

After introducing (A.2), (A.3), and (A.7) into (A.6) and performing the matrix inversion, we obtain

$$\begin{aligned}
\bar{G}(\bar{k}, \bar{r}') = & -\frac{i}{\omega \epsilon_z} e^{i\bar{k} \cdot \bar{r}'} \left\{ -\frac{\omega^2 \mu \epsilon_z}{(k_x^2 + k_y^2) D_1(\bar{k})} \begin{bmatrix} k_y^2 & -k_x k_y & 0 \\ -k_x k_y & k_x^2 & 0 \\ 0 & 0 & 0 \end{bmatrix} \right. \\
& + \frac{1}{D_2(\bar{k})} \left. \begin{bmatrix} \frac{k_x^2 + k_y^2 - \omega^2 \mu \epsilon_z}{k_x^2 + k_y^2} k_x^2 & \frac{k_x^2 + k_y^2 - \omega^2 \mu \epsilon_z}{k_x^2 + k_y^2} k_x k_y & k_x k_z \\ \frac{k_x^2 + k_y^2 - \omega^2 \mu \epsilon_z}{k_x^2 + k_y^2} k_y k_x & \frac{k_x^2 + k_y^2 - \omega^2 \mu \epsilon_z}{k_x^2 + k_y^2} k_y^2 & k_y k_z \\ k_z k_x & k_z k_y & k_z^2 \end{bmatrix} \right\}
\end{aligned}
\tag{A.8}$$

where

$$D_1(\bar{k}) = k_z^2 + \frac{\mu}{\mu_z} (k_x^2 + k_y^2 - \omega^2 \mu_z \epsilon) \tag{A.9}$$

$$D_2(\bar{k}) = k_z^2 + \frac{\epsilon}{\epsilon_z} (k_x^2 + k_y^2 - \omega^2 \mu \epsilon_z). \tag{A.10}$$

To evaluate the integration over k_z in (A.5), we find that the

poles of the integrand occur at the zeros of $D_1(\bar{k})$ and $D_2(\bar{k})$, corresponding to $k_z = \pm k_z^m$ and $k_z = \pm k_z^e$ where

$$k_z^m = \sqrt{k^2 - \mu(k_x^2 + k_y^2)/\mu_z} \quad (\text{A.11})$$

and

$$k_z^e = \sqrt{k^2 - \epsilon(k_x^2 + k_y^2)/\epsilon_z}. \quad (\text{A.12})$$

They correspond to the type I and type II characteristic waves [3] in the medium. Assuming the medium is slightly lossy, then we find

$$\bar{G}(\bar{r}, \bar{r}') = \begin{cases} -\frac{\omega\mu}{8\pi^2} \iint_{-\infty}^{\infty} dk_x dk_y \left[\frac{1}{k_z^m} \hat{e}\hat{e} e^{i\bar{k}_m \cdot (\bar{r} - \bar{r}')} + \frac{1}{k_z^e} \hat{h}(k_z^e) \hat{h}(k_z^e) e^{i\bar{k}_e \cdot (\bar{r} - \bar{r}')} \right], & \text{for } z' < z \\ -\frac{\omega\mu}{8\pi^2} \iint_{-\infty}^{\infty} dk_x dk_y \left[\frac{1}{k_z^m} \hat{e}\hat{e} e^{i\bar{k}_m \cdot (\bar{r} - \bar{r}')} + \frac{1}{k_z^e} \hat{h}(-k_z^e) \hat{h}(-k_z^e) e^{i\bar{k}_e \cdot (\bar{r} - \bar{r}')} \right], & \text{for } z < z' \end{cases} \quad (\text{A.13})$$

where

$$\bar{k}_e = \hat{x} k_x + \hat{y} k_y + \hat{z} k_z^e \quad (\text{A.14})$$

$$\bar{k}_m = \hat{x} k_x + \hat{y} k_y + \hat{z} k_z^m \quad (\text{A.15})$$

$$\bar{k}_e = \hat{x} k_x + \hat{y} k_y - \hat{z} k_z^e \quad (\text{A.16})$$

$$\bar{k}_m = \hat{x} k_x + \hat{y} k_y - \hat{z} k_z^m \quad (\text{A.17})$$

$$\hat{e} = \frac{1}{\sqrt{k_x^2 + k_y^2}} (\hat{x} k_y - \hat{y} k_x) \quad (\text{A.18})$$

$$\hat{h}(k_z^e) = \frac{1}{k} [\hat{e} \times \bar{k}_e] \quad (\text{A.19})$$

$$\hat{h}(-k_z^e) = \frac{1}{k} [\hat{e} \times \bar{k}_e] \quad (\text{A.20})$$

and $k = \omega\sqrt{\mu\epsilon}$. We see that \hat{e} is a unit vector in the direction of the electric field for TE waves and \hat{h} is in the direction of the electric field for TM waves. Equation (A.13) reduces to Eq. (3) when the medium is isotropic.

Appendix B.

The TM reflection coefficient in continued fraction form is

$$\begin{aligned}
 R^{TM} = & \frac{1}{S_{01}} + \cfrac{\left(1 - \frac{1}{S_{01}^2}\right) e^{-i2k_{1z}d_1}}{\frac{1}{S_{01}} e^{-i2k_{1z}d_1}} + \frac{1}{S_{12}} + \cfrac{\left(1 - \frac{1}{S_{12}^2}\right) e^{-i2k_{2z}(d_2 - d_1)}}{\frac{1}{S_{12}} e^{-i2k_{2z}(d_2 - d_1)}} \\
 & + \dots + \frac{1}{S_{(n-1)n}} + \cfrac{\left(1 - \frac{1}{S_{(n-1)n}^2}\right) e^{-i2k_{nz}(d_n - d_{n-1})}}{\frac{1}{S_{(n-1)n}} e^{-i2k_{nz}(d_n - d_{n-1})}} + S_{nt}
 \end{aligned}$$

where

$$S_{\ell(\ell+1)} = \frac{\epsilon_{\ell+1} k_{\ell z} - \epsilon_{\ell} k_{(\ell+1)z}}{\epsilon_{\ell+1} k_{\ell z} + \epsilon_{\ell} k_{(\ell+1)z}}$$

is the TM Fresnel reflection coefficient at each boundary.

The wave amplitudes C_{ℓ} and D_{ℓ} in each layer are related by propagation matrices.

$$\begin{bmatrix} C_{\ell+1} e^{-ik(\ell+1)z d_{\ell+1}} \\ D_{\ell+1} e^{ik(\ell+1)z d_{\ell+1}} \end{bmatrix} = \bar{V}_{(\ell+1)\ell}^{TM} \begin{bmatrix} C_{\ell} e^{-ik_{\ell}z d_{\ell}} \\ D_{\ell} e^{ik_{\ell}z d_{\ell}} \end{bmatrix}$$

where:

$$\bar{V}_{(\ell+1)\ell}^{TM} = \frac{1}{2} \frac{\mu(\ell+1) k_{\ell}}{\mu_{\ell} k(\ell+1)} \left[1 + \frac{\epsilon_{\ell+1} k_{\ell} z}{k(\ell+1) z} \right]$$

$$\begin{bmatrix} e^{-ik(\ell+1)z(d_{\ell+1} - d_{\ell})} & S_{(\ell+1)\ell} e^{-ik(\ell+1)z(d_{\ell+1} - d_{\ell})} \\ S_{(\ell+1)\ell} e^{ik(\ell+1)z(d_{\ell+1} - d_{\ell})} & e^{ik(\ell+1)z(d_{\ell+1} - d_{\ell})} \end{bmatrix}$$

Appendix C.

In this appendix, we present the exact solutions of the brightness temperature of the medium with permittivity profile

$$\epsilon_1(z) = (\epsilon_1' + i \epsilon_1'') e^{-az},$$

$$\epsilon_t(z) = \epsilon_1(z = -d)$$

and temperature profile

$$T(z) = T_0 + (\Delta T) e^{bz}.$$

In terms of Bessel functions, the brightness temperature as observed from nadir is equal to

$$T_B = k \int_{-d}^0 d\xi T(\xi) \frac{\epsilon''(\xi)}{\epsilon_0} \left| \alpha J_0 \left(2 \frac{k_1}{a} e^{-\frac{a\xi}{2}} \right) + \beta N_0 \left(2 \frac{k_1}{a} e^{-\frac{a\xi}{2}} \right) \right|^2$$

$$+ T_0 \frac{k_t'}{k} \left| \alpha J_0(\eta_d) + \beta N_0(\eta_d) \right|^2 \left\{ 1 + \frac{2k_t''}{(b + 2k_t'')} \left(\frac{\Delta T}{T_0} \right) e^{-bd} \right\}$$

where

$$\alpha = \frac{\pi \eta_0}{2} [G_Y^+(\eta_0) + R G_Y^-(\eta_0)]$$

REPRODUCIBILITY OF THE
ORIGINAL PAGE IS POOR

$$\beta = -\frac{\pi\eta_0}{2} [G_J^+(\eta_0) + R G_J^-(\eta_0)]$$

$$\eta_0 = \frac{2k_1}{a}$$

$$\eta_d = 2 \frac{k_1}{a} e^{ad/2}$$

$$R = \frac{G_Y^+(\eta_0) G_J^+(\eta_d) - G_Y^+(\eta_d) G_J^+(\eta_0)}{G_Y^+(\eta_d) G_J^-(\eta_0) - G_Y^-(\eta_0) G_J^+(\eta_d)}$$

$$G_J^+(\eta_0) = J_0'(\eta_0) - i \frac{k}{k_1} J_0(\eta_0)$$

$$G_J^+(\eta_d) = J_0'(\eta_d) - i J_0(\eta_d)$$

$$G_Y^+(\eta_0) = Y_0'(\eta_0) - i \frac{k}{k_1} Y_0(\eta_0)$$

$$G_Y^+(\eta_d) = Y_0'(\eta_d) - i Y_0(\eta_d)$$

$$G_J^-(\eta_0) = J_0'(\eta_0) + i \frac{k}{k_1} J_0(\eta_0)$$

$$G_Y^-(\eta_0) = Y_0'(\eta_0) + i \frac{k}{k_1} Y_0(\eta_0)$$

Figure 1.

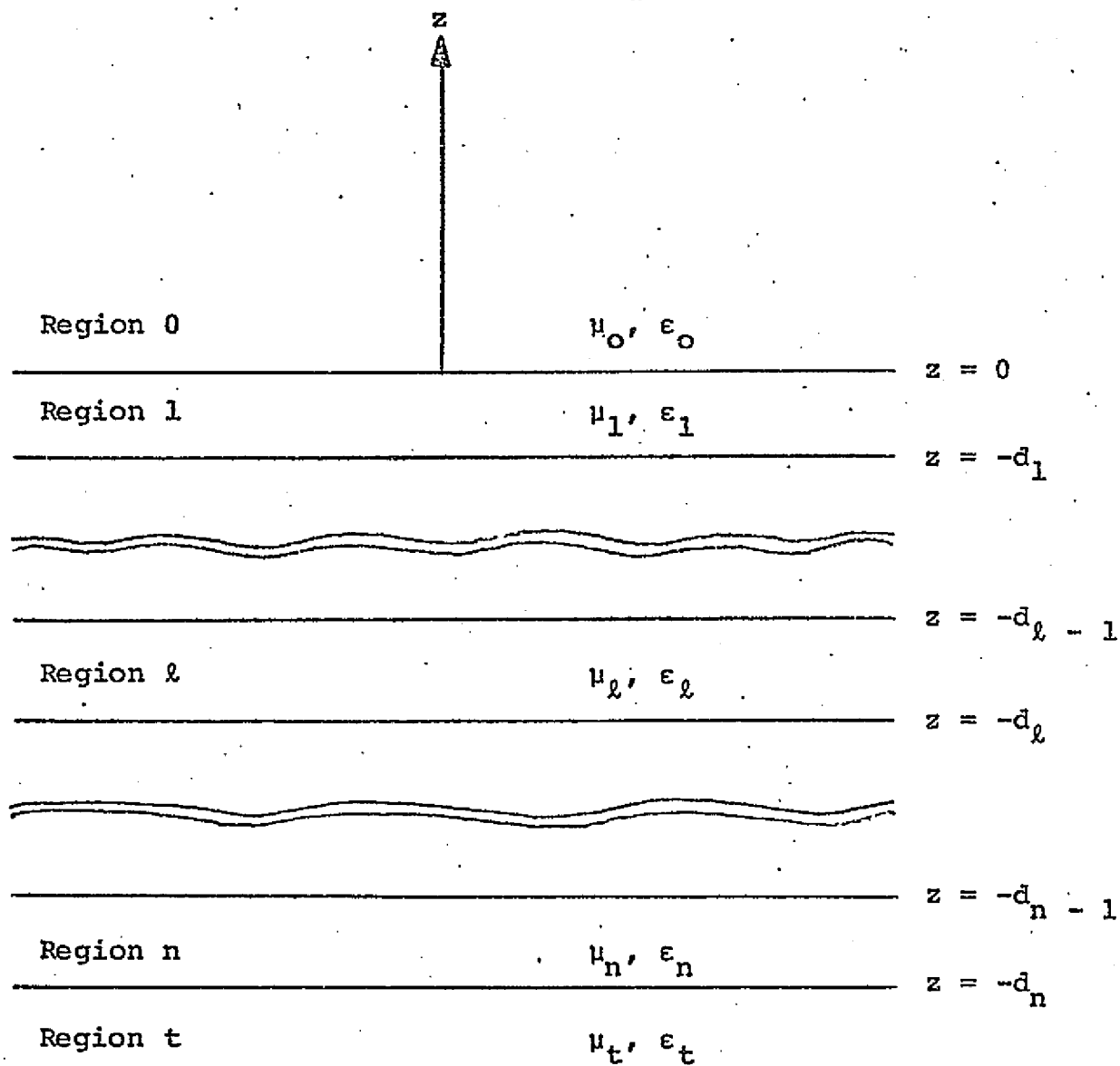


Figure 2.

REPRODUCIBILITY OF THE
ORIGINAL PAGE IS POOR

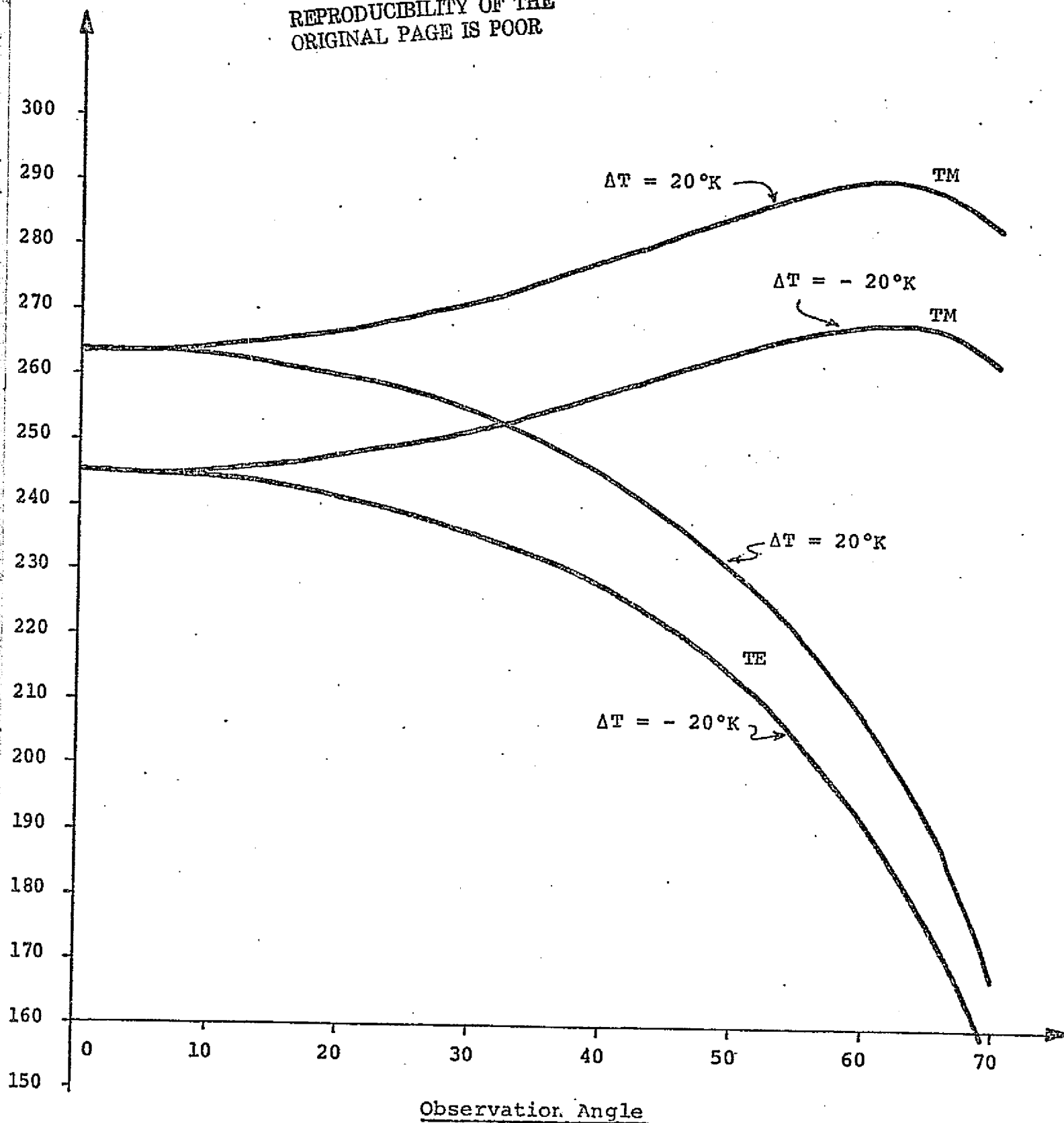


Figure 3.

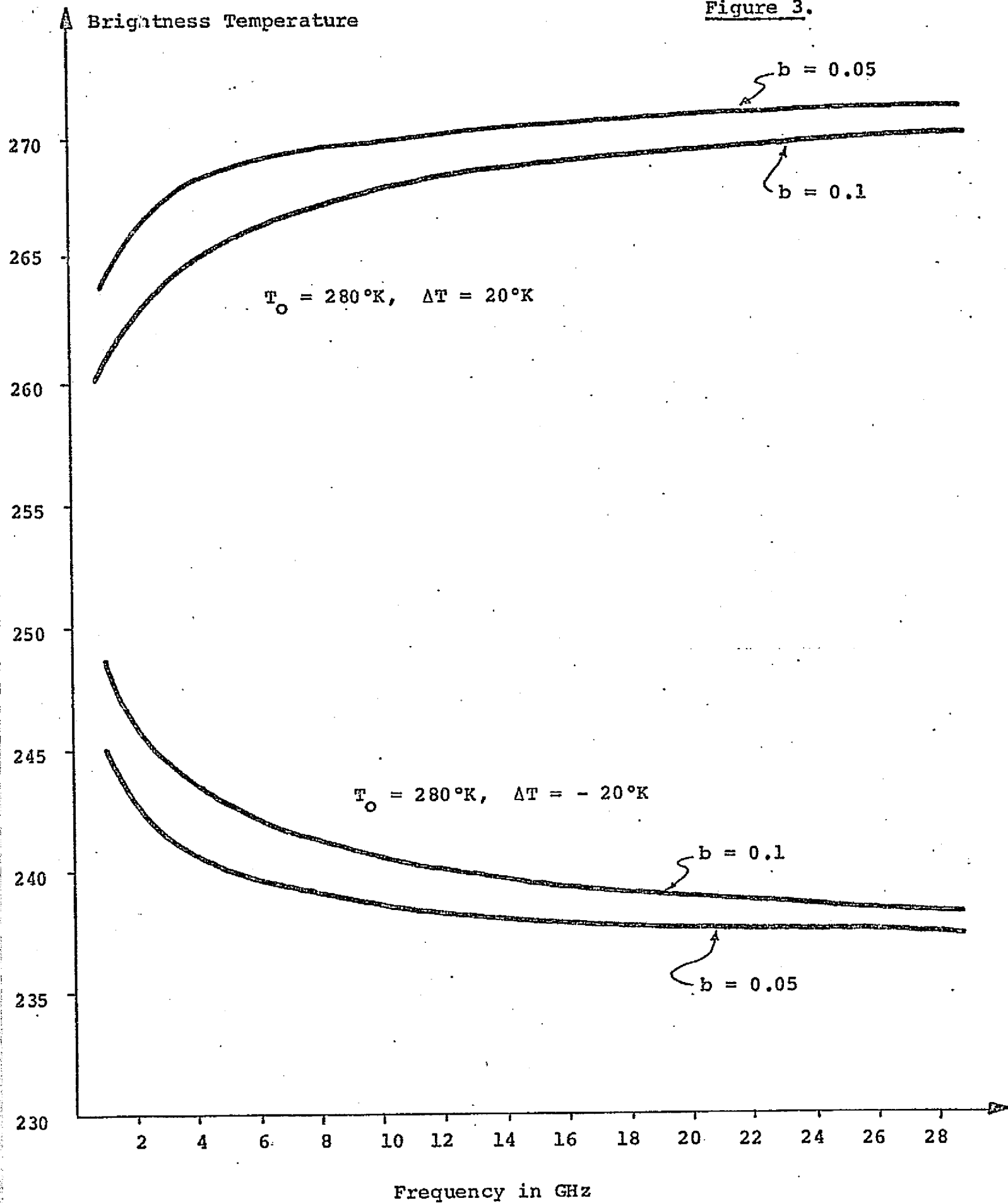


Figure 4.

REPRODUCIBILITY OF THE
ORIGINAL PAGE IS POOR

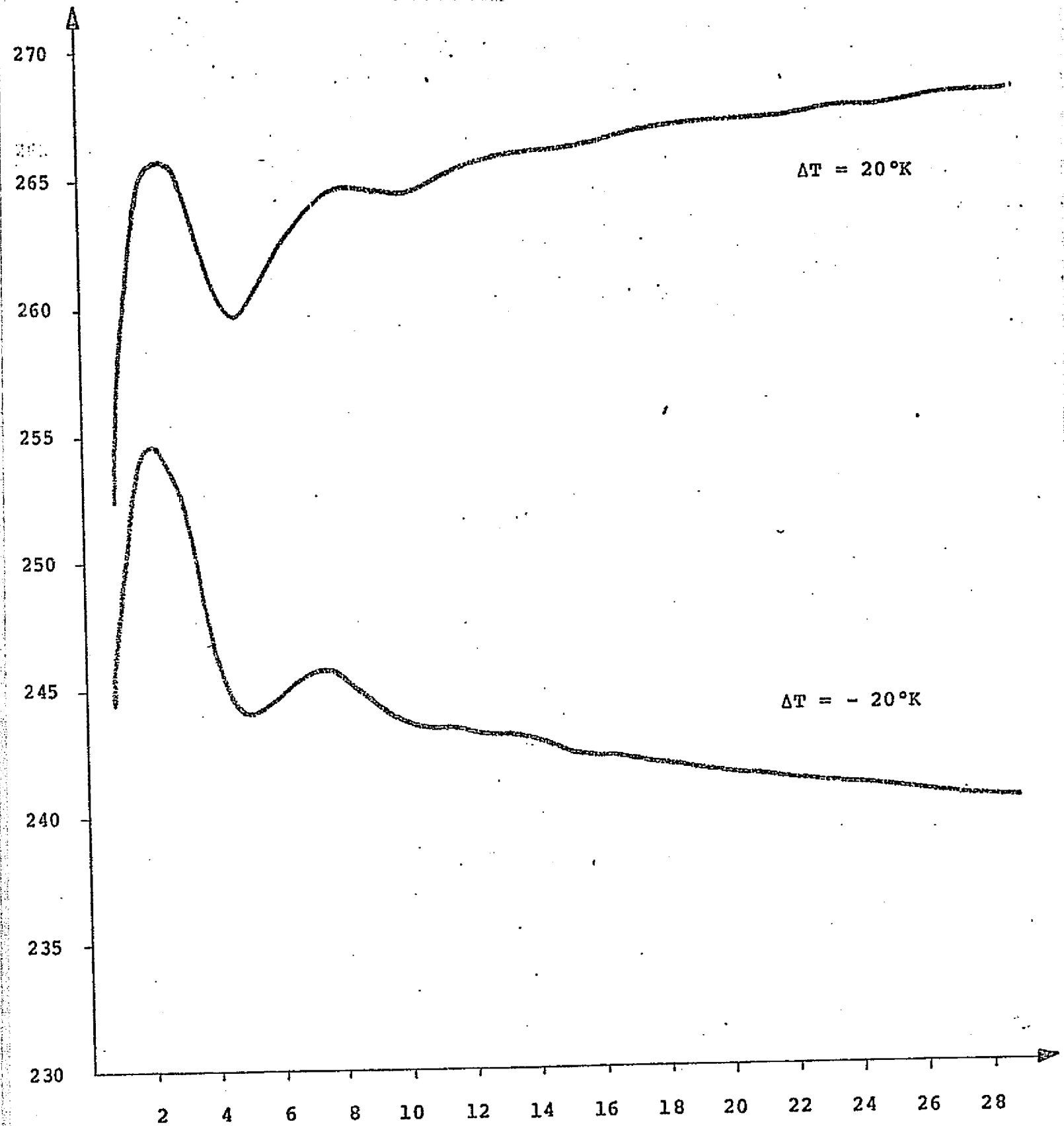


Figure 5.

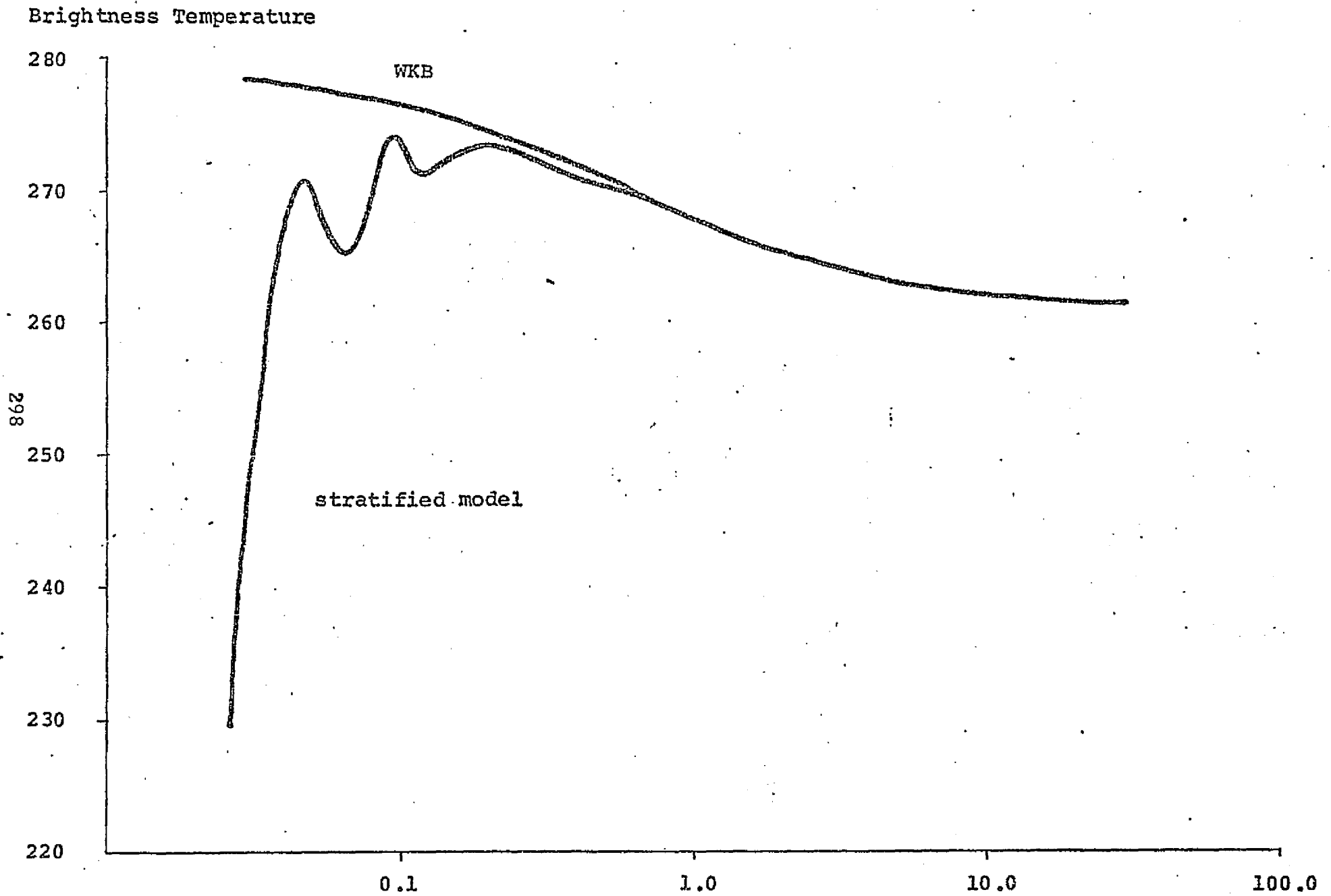


Figure 6.

